FINITE ELEMENT MODELLING AND TESTING OF FILAMENT-WOUND ORTHOTROPIC COMPONENTS

by

Eur Ing **Ivor Arthur Jones** BSc BEng CEng MIMechE

Thesis submitted to the University of Nottingham for the degree of Doctor of Philosophy, October 1993

CONTENTS

ABSTRACT

Existing software for CNC filament winding of fibre reinforced plastics has been linked to typical finite element codes by automating the generation of finite element models of filament wound components. The algorithms required for this process have been created and encoded as computer programs. The program FILFEM I generates models of components manufactured using the CADFIL I CAD/CAM system for the filament winding of axisymmetric components. The suite of programs named FILFEM II achieves the same objective for non-axisymmetric components manufactured using CADFIL II although its method of operation is quite different from that of FILFEM I. FILFEM I has been tested by automatically generating models of a pinched cylindrical filament-wound tube manufactured from glass-reinforced polyester resin. The results from these models generally compared well with results obtained from experiments and from an analytical solution extended by the author from work by Calladine. However, the validity of a comparison with experiment depends upon the accuracy of the material properties assumed in the analyses.

The material property values required for the analyses were investigated experimentally. Tests based upon pinched rings and a modified split-disc method are described together with more conventional tests of material properties. A method is presented for the determination of unidirectional material properties from the experimentally-measured properties of laminates. Difficulties in obtaining consistent results were attributed to problems with the quality of the specimens, inadequacies in the orthotropic model of material behaviour, and to material damage occurring during the experiments.

In order to provide a test component for FILFEM II, a number of filament wound elbows were manufactured although some problems with winding quality remain. The fibre paths files used in manufacturing the elbows were used to test the operation of FILFEM II and further work including experimental verification is proposed.

ACKNOWLEDGEMENTS

The author wishes to thank his academic advisors, Professor M.J. Owen and Dr V. Middleton, for their advice and encouragement throughout the project. The author is also extremely grateful to the Head of Department, Professor B.R. Clayton, for the use of the facilities of the Department of Mechanical Engineering and for the opportunity to study for a doctorate whilst employed as a member of academic staff.

The author has had a great deal of support from friends and colleagues throughout the project. At risk of neglecting any individuals not identified by name, he wishes to extend his gratitude to the following people:

to Mr H.D. Rees for his advice and expertise on the filament winding process and to Messrs M. Sloman, G. Tomlinson, B. Foster and R. Smith and the staff of the Engineering Faculty Workshop for their practical assistance;

to the staff of Crescent Consultants Limited (Mr S.V. Middleton, Mr A.P. Priestley and Dr E.V. Rice) for their advice and expertise on the CADFIL filament winding software and for the use of the Apollo computer facilities;

to Dr J.J. Webster, Dr A.A. Becker and Dr E.V. Rice for their advice on finite element analysis;

to Professor T.H. Hyde for his guidance in the early stages of the project;

to Mr K.F. Hutcheon for reading and commenting on the penultimate draft of the thesis;

to Mr P.D.W. Soden and Professor S.R. Reid for the opportunity to make use of laboratory facilities at UMIST, and to Mr M. Readman for his practical help;

and to Miss B.C. Sandford for her advice on typesetting and for typing two sections of the thesis.

The author would like especially to thank his parents for their unfailing support particularly during the time of this project.

NOMENCLATURE

Because of the considerable variety of types of engineering analysis covered in this thesis, a number of symbols take different meanings depending upon context. Such symbols are also identified locally within each context to avoid ambiguity. Separate lists of nomenclature are given in Appendices A and F owing to the specialised nature of the theory contained in those appendices.

Conventions

a, A	scalar values
$\{A\}$	a column vector or array with elements A_i
$[A]$	a matrix with elements A_{ij}
$[A]^T$	transpose of matrix $[A]$ where $A^T_{ji} = A_{ij}$
$[A]^{-1}$	inverse of matrix $[A]$
$\begin{bmatrix} [A] & [B] \\ [C] & [D] \end{bmatrix}$	Matrix partitioned into sub-matrices $[A]$, $[B]$, $[C]$ and $[D]$
$[0]$	null matrix
$f(x)$	a function of x
$f'(x), f''(x)$	first and second derivatives of $f(x)$ with respect to x
$\bar{x}$	mean value of x
$[\bar{S}]$	off-axis property matrix

Co-ordinate and axis systems

x, y, z	right-handed orthogonal Cartesian co-ordinates; reference directions for a laminate lying in the x-y plane
x, θ, z	reference directions for a cylindrical laminated shell (axial, circumferential and through-thickness)
x, r, θ	cylindrical polar co-ordinates
ξ, η	parametric co-ordinates of an isoparametric finite element
X, Y, Z	linear axes of filament winding machine
A, B, C	rotational axes of filament winding machine
1, 2	material principal directions (axes parallel and perpendicular to fibre direction within a lamina)

Symbols

a	radius of a cylindrical shell
b	bandwidth (width of fibre tow laid on mandrel)
c	constant in a linear equation; constant in Ting and Yuan's solution to the pinched cylinder problem: $c = [3(1-\nu^2)]^{1/4}(a/t)^{1/2}$
d	diameter of mandrel
e	takes its usual mathematical meaning ≈ 2.718
f_i	difference between theoretical and measured value of Young's modulus for specimen i
i, j	integer indices
k	modulus of an elastic foundation or of an analogous system; an integer index
l	length of a curved member
m	an integer; band pattern number; order of highest valid term in a series
n	an integer; number of a harmonic in a Fourier series; number of plies
p	pressure
q	force distributed around a circumferential line
r	radius; radial position; correlation coefficient
s	curvilinear distance
t	thickness
u_x, u_r etc.	nodal displacements of a finite element
w	radial deflection of a cylindrical shell; deflection of a beam; width
$\{w\}$	system of deflections and slopes of a beam
w_{edge}	width of edge region of a shell
w_v, w_h	vertical and horizontal radial deflections of a cylindrical shell subjected to a vertical pinching load
z	through-thickness position within a laminate measured from mid-surface
A	cross-sectional area; a scalar constant
$[A],[B],[D]$	sub-matrices (partitions) of laminate stiffness matrix
B	flexural rigidity of a beam or analogous system; a scalar constant
C	a scalar constant
$[C]$	flexibility matrix of an elastic system
D	flexural rigidity of an isotropic shell $= Et^3/[12(1-\nu^2)]$

D_x	flexural rigidity of an orthotropic shell
E	Young's modulus
F.R.	flexural rigidity of a member
F.M.R.	fibre mass ratio (proportion by mass of fibre in a composite)
F	sum of squares of f_i; concentrated force on a beam or analogous system
$\{F\}$	system of forces and moments applied to a system
G	shear modulus
H	scalar constant
K_1, K_2	constants ensuring consistency of units in equations (C.3)–(C.5)
$[K]$	stiffness matrix of an elastic system
L_1, L_2	distances of ends of a cylindrical shell measured from load position
M	bending moment
$\{M\}$	system of bending and twisting stress couples applied to a laminate (moment per unit of laminate width)
N	tensile force; number of items in a set or series
$\{N\}$	system of direct and shear stress resultants applied to a laminate (force per unit of laminate width)
P	pinching load
Q	dummy force
$[Q]$	on-axis stiffness matrix of a composite lamina under plane stress
$[\bar{Q}]$	off-axis stiffness matrix of a composite lamina under plane stress
R	radius of a ring or curved beam
S_{xx}, S_{yy}, S_{xy}	statistical quantities e.g. $S_{xx} = \Sigma x^2 - N\bar{x}^2$
$[S]$	on-axis compliance of a composite lamina under plane stress
$[\bar{S}]$	off-axis compliance of a composite lamina under plane stress
$[T]$	matrix used in the off-axis transformation of $[S]$ and $[Q]$
U	strain energy of an elastic system
V	volume; shear force
V_f	volume fraction of fibre in a composite
W	vessel weight
$\mathscr{E}$	function for calculating Young's modulus of a many-layered laminate
$[\alpha]$, $[\beta]$, $[\beta]^T$, $[\delta]$	sub-matrices (partitions) of laminate compliance matrix $\begin{bmatrix} [\alpha] & [\beta] \\ [\beta]^T & [\delta] \end{bmatrix} = \begin{bmatrix} [A] & [B] \\ [B] & [D] \end{bmatrix}^{-1}$

δ_h	horizontal diameter change of a vertically-pinched ring
ε, γ	direct and shear strains (engineering definition of shear strain)
$\{\varepsilon^0\}$	system of mid-surface strains of a laminate
$\{\kappa\}$	system of curvatures and twists of a laminate
θ	angular position; winding angle; slope of a beam
λ	decay parameter for beam on elastic foundation or analogous system
ν	Poisson's ratio of an isotropic material
ν_{12}	Poisson's ratio of an orthotropic material = $-\varepsilon_2/\varepsilon_1$
ξ, η	parametric co-ordinates; constants in the Halpin-Tsai equations (5.1)(a-d)
ρ	density
σ, τ	direct and shear stresses
ϕ	ply angle; nodal rotation
ψ	angular position around a quadrant
Δ	gradient of a line
Π	total potential energy

Superscripts

0	relating to the mid-surface of a laminate

Subscripts (where not explicitly defined above)

x, y, z	relating to global Cartesian directions; relating to reference directions on a laminate lying in the x-y plane (similarly for axis systems 1-2, x-θ-z etc.)
6	relating to in-plane shear
i, j, k	subscripts of an array, matrix or set of values
e	relating to an element in an elastic system
i	inside
f	relating to fibre material
m	relating to matrix material
o	outside

Other subscripts in the form of text are assumed to be self-explanatory.

GLOSSARY

ABAQUS — A finite element analysis system marketed by Hibbitt, Karlsson and Sorensen Inc.[100]

anisotropic — Having material properties (e.g. Young's modulus) which are different in all directions in which they are measured.

band pattern number — A value related to the manner in which an axisymmetric component is wound with a repeating pattern. If successive windings of fibre are laid immediately adjacent to each other, the band pattern number is unity. If, for example, every third winding of fibre lies adjacent to the original fibre, the band pattern number would be three (Fig. 2.4 (a)-(c)).

bandwidth — Width of fibre tow when laid onto mandrel during winding.

CAD/CAM — Computer aided design/computer aided manufacture.

CADFIL I, CADFIL II® — A pair of CAD/CAM systems for filament winding based upon work by Young[7] and Shearing[10] and marketed by Crescent Consultants Limited, Nottingham. CADFIL® is a registered trade mark of this consultancy. CADFIL I is applicable to axisymmetric filament-wound components, and CADFIL II is applicable to non-axisymmetric components.

CLT Classical lamination theory. A mathematical model relating to plates assembled from rigidly-connected layers or laminae made from orthotropic materials.

CNC Computer numerical control. A description applied to a machine tool (including a filament winding machine) where the movements of the slides are controlled by a dedicated microcomputer. The instructions are supplied in the form of a file of commands and co-ordinate data known as a part-program.

filament winding A manufacturing process for fibrous composite materials in which a continuous tow or roving of fibre is impregnated with resin and wound onto a mandrel. The resin is then cured.

FILFEM I, FILFEM II A pair of programs for linking the CADFIL I and CADFIL II filament winding systems to finite element analysis systems such as PAFEC and ABAQUS.

finite element analysis A computer-based technique used primarily for the structural analysis of complex components by discretising them into simpler entities known as elements.

FORTRAN, FORTRAN77 An abbreviation of FORmula TRANslation. A high-level computer language for mathematical applications, widely used by engineers and scientists. FORTRAN77 is the version of the language standardised in 1977 and is for practical purposes the standard version in use in 1993.

GRP Glass reinforced plastic. One of the most common types of composite material. It is readily manufactured by filament winding.

mandrel A former onto which the fibre is wound. It may be removable (e.g. a smooth cylinder), may form a permanent part of the filament-wound structure (e.g. it may be the metallic liner of a pressure vessel) or may be destroyed *in situ* by washing or dissolving to leave a hollow filament-wound component.

NAG Numerical Algorithms Group. This organisation maintains several libraries of subroutines including the NAG FORTRAN library[115], which consists of several thousand ready-written FORTRAN subroutines for achieving specific mathematical, statistical or numerical tasks e.g. matrix inversion or equation solution.

orthotropic Having material properties which are symmetrical about three orthogonal planes. Orthotropy is a special case of anisotropy. Special orthotropy is the situation where the principal directions of the material correspond to the reference directions of the specimen e.g. the loading directions. General orthotropy is the situation where the material is arbitrarily orientated with respect to the reference directions and the symmetry in the behaviour is not therefore immediately apparent.

PAFEC Program for Automatic Finite Element Calculations. A finite element analysis system originally developed within the Department of Mechanical Engineering at the University of Nottingham. It is now marketed by PAFEC Limited[59].

part-program A data file of machine control instructions for a CNC machine tool.

ply A layer in a laminate.

ply angle The angle of the fibre direction within a ply to a specified reference direction on the specimen.

progression factor A scale factor applied to the angular positions of points defining the payout eye path around an axisymmetric mandrel so that successive windings of fibre are laid side-by-side in an orderly manner.

QuickBasic A structured version of BASIC (a language intended primarily for microcomputers) with some similarities to FORTRAN. It is designed for use with IBM-compatible personal computers and is produced by Microsoft Ltd. It includes facilities to communicate with interfaces such as data collection cards, and unlike many versions of BASIC it can be compiled to produce machine code.

roving A bundle or string of continuous filaments.

tow The resin-impregnated fibre which is laid onto the mandrel during winding.

voidage The presence and degree of gaps in the composite material caused by incomplete impregnation of the fibres by the resin.

winding angle The angle of the fibre to a meridian on the mandrel (equal to the angle to the axis of a cylindrical mandrel).

CHAPTER 1: INTRODUCTION

1.1 Background and overview of thesis

Polymeric-matrix fibre composites have become an important family of engineering materials, particularly because they provide the opportunity to tailor the material properties to suit the application by careful choice of fibre, matrix and manufacturing method. One of the commonest composite materials encountered in engineering is glass-reinforced polyester resin. Although in its hand-manufactured randomly reinforced form it has relatively little strength or stiffness, more sophisticated manufacturing techniques such as filament winding result in a directional composite with a high fibre content and advantageous strength and stiffness in the direction of the fibres.

In the filament winding process, a continuous roving or bundle of glass fibre filaments is impregnated with a liquid resin before being wound under tension onto a former or mandrel (Fig. 1.1). A practical limitation upon the process is that to avoid slippage the fibre must be laid on, or close to, a geodesic path; in other words it must follow the shortest possible route over the surface of the mandrel. The fibre is placed by means of a payout eye for which the path must be carefully chosen to lie on a series of tangents extended from the fibre path (Fig. 1.2). When complete coverage of the mandrel has been achieved, the resin is cured to form a laminated composite with a high proportion of fibres. The properties of this composite are highly directional (anisotropic) within the plane of the laminate and are highly dependent upon the details of the manufacturing process. Structures with advantageous strength-to-weight and stiffness-to-weight ratios can be manufactured if the fibres are placed in a suitable direction to withstand the applied loads, although manufacturing considerations greatly restrict the choice of feasible winding patterns.

Filament winding has been established for many years. One of the earliest applications was in pressure vessels for rocketry, the development work for which began in the 1940s[1]. A brief literature review on the history of the process is included in Chapter 2. Filament winding was traditionally performed using machines controlled by a variety of mechanical linkages and mechanisms[5]. However, the advent of computer numerical control (CNC) technology has resulted in the development of machines with much greater flexibility, opening up the possibility of manufacturing components with complex shapes. Accurate specification of payout eye movement in terms of a CNC part-program is necessary and manual teaching of this data is extremely tedious for complex fibre paths. However, CAD/CAM software (e.g. CADFIL) has been developed at the University of Nottingham and elsewhere to generate the CNC part-program data from theoretically-computed fibre paths. This technology is now well established for the manufacture of axisymmetric components such as pressure vessels. For the manufacture of non-axisymmetric components such as tee-pieces and cranked arms, user-specific development work is still required when developing new components. A more detailed description of the CNC filament winding process is included in Chapter 2.

It has already been mentioned that the composite material produced by filament winding is both anisotropic and highly dependent upon the manufacturing process. More accurately, it consists of an orthotropic laminate whose thickness, lamination sequence and ply directions vary continuously over the surface of the mandrel. A photograph of a simple filament-wound test component is given in Fig. 1.3(a) and the alternating lamination sequence is highlighted in Fig. 1.3(b). This alternation is caused by the interweaving of successive windings of fibre, giving an over-and-under pattern which is repeated every time the mandrel is given a complete coverage of fibre. It may therefore be clearly seen that the actual structure of even a simple component is somewhat complex, making structural analysis a difficult task. In certain simple situations it is feasible to perform a structural analysis of a filament-wound component using classical methods, and Chapter 3 includes a review of the literature in this area as well as an overview of the mechanics of directional composite materials. The complex geometries of many practical components, together with the

complexity of material properties and their inhomogeneity, makes classical analysis impractical in many situations. Thus it is often necessary to resort to numerical methods such as finite element analysis if the designer is to be able to carry out a satisfactory assessment of his chosen design.

Finite element (FE) methods have evolved in parallel with the development of digital computers, and have been regarded as an established engineering tool since the 1970s. Numerous commercially available finite element codes now exist, and most general-purpose FE codes include facilities for the analysis of laminated orthotropic materials. The problem in applying these systems to filament-wound components, especially those of complex geometry, is that the amount of input data required is extremely large. Much of this data relates to the laminate structure, i.e. to the material directions, thicknesses and lamination sequences. Various mesh generation packages are available but these are intended for modelling conventional isotropic components and do not include facilities for generating the data defining the laminate structure. For relatively simple components it is feasible to create a finite element model manually and Chapter 4 includes a review of publications relating to work of this kind. Also included in Chapter 4 are an overview of the finite element method, a discussion on the availability of FE codes for the analysis of composites, and some details of the finite element types used in this thesis.

Although the volume of data required for the FE analysis of a complex filament wound structure is very large, most of it can be calculated from the data created within the fibre path generation and CNC part-program generation processes. Little work has been published on this data conversion/model generation process, and it is the principal aim of this thesis to describe the creation of a useful link between CNC filament winding and finite element analysis. This takes the form of a pair of FE model generation systems dedicated to filament wound structures. The challenge in this area of the project lay in devising suitable logic for automatically constructing a model adequately representing the complex filament-wound structure based upon the available data. The kinds of data defining the axisymmetric and non-axisymmetric structures were quite different, especially regarding the volume of data involved. The

algorithms required to create the two types of FE models were therefore entirely dissimilar in philosophy. Both of these systems have been successfully encoded and a more detailed description of the operation of these will be given in Chapter 6. The system for axisymmetric structures (FILFEM I) has been developed to a reasonable degree of completion; experience gained in its use is outlined in Chapter 7 and will be referred to again in this chapter. The equivalent system for non-axisymmetric structures (FILFEM II) has been completed to a basic level of operation, laying the foundations for a substantial programme of further development and testing work.

Although reliable values of material properties were required for use in conjunction with the automatically-generated FE models, it was found that no such information was readily available for the material under consideration. It was therefore necessary to undertake a programme of materials testing in an attempt to characterise the behaviour of the glass-polyester composite commonly manufactured by filament winding. A full account of this experimental programme is given in Chapter 5. This programme included the development of two simple tests to provide independent measurements of the elastic properties of samples cut from filament-wound cylindrical components. The errors made in modelling both of these load cases have been examined in detail. Difficulties were encountered in obtaining consistent results especially for the properties of angle-wound specimens. This was attributed to the fact that the linear elastic orthotropic material model assumed both by classical theory and the FE systems provides an adequate representation of the composite's behaviour only under ideal conditions of small strain. In an attempt to overcome this problem, a technique was developed for working backwards and fitting the apparent unidirectional properties of the material to the observed laminate behaviour. Some of the unidirectional properties thus obtained were clearly unrealistic in value but calculations performed with them gave excellent prediction of component stiffness when applied to a nominally axisymmetric component.

In order to gain practical experience of the model generation system for axisymmetric components, and to assess the usefulness of the results obtained, a simple specimen and loadcase were use as the basis for the comparison of experimental and FE results.

The test case consisted of a modification of the well-known pinched cylinder problem, made more complex by the use of a laminated tube with varying winding angle and lamination sequence over its surface. Various FE models were tested against the experimental behaviour of the component by measuring diametral deflections per unit load. As already mentioned, the FE results obtained using the best-fitted unidirectional properties showed excellent agreement with experimental data, although caution is recommended in the interpretation of these results because of the difficulties encountered in obtaining satisfactory material property data for the analysis. The experiment, the FE models and the results are all presented in Chapter 7. To provide further data for comparison, an existing analytical solution to the pinched cylinder problem was extended to cover the problem in hand by assuming various simplifications to the true structure of the cylinder. This analytical solution is outlined in Chapter 7 and presented in more detail in Appendix J. Excellent agreement was obtained between the analytical results and those for the most closely comparable FE model.

The creation of a system for the automatic finite element modelling of non-axisymmetric structures has already been described, and Chapter 8 lays the foundations for further work to develop this system in the light of experimental results. An elbow-shaped pipe was chosen to form a suitable non-axisymmetric test component, and existing filament winding CNC technology was extended to make it possible to create part-programs for the manufacture of this component. A number of elbows were made and although there is still scope for improvement in manufacturing techniques the basis of the procedure is now well established. The fibre paths used for winding these elbows were used as the input data during the initial testing of the FILFEM II model generation system.

It will be observed by the reader that although both finite element analysis and filament winding are established technology and have been applied together for many years, the main objective of this thesis is the construction of a firm link between the appropriate automated systems where such links were previously few and tenuous. In more general terms the purpose of this thesis is to establish interfaces between

existing items of work in the areas of mechanics of solids, computational methods, manufacturing engineering and materials testing, and to bridge gaps in available knowledge and technology by means of new work where appropriate.

1.2 Summary of objectives

The objectives of this investigation have been discussed in general terms, and it is instructive at this stage to present a more specific list of the areas of work to be addressed.

1.2.1 To develop approaches, logic and mathematical techniques to achieve automatic finite element model generation for filament wound structures manufactured with the aid of the CADFIL CAD/CAM systems for filament winding.

1.2.2 To encode the techniques specified in section 1.2.1 as programs so as to form practical engineering design tools. The input to these programs should be data obtained from CADFIL defining the filament wound structure, and the output should be a file defining the finite element model in a form suitable for analysis by an existing finite element code e.g. PAFEC.

1.2.3 To characterise the elastic properties of a typical filament-wound composite material. This stage may include the development of new tests and analysis techniques.

1.2.4 To obtain experience of using the design tools specified in section 1.2.2 and, where possible, to perform experiments upon components for comparison with the results obtained from the automatically-generated finite element models. This will involve the design and manufacture of appropriate filament wound components and will make use of the material property data discussed in section 1.2.3.

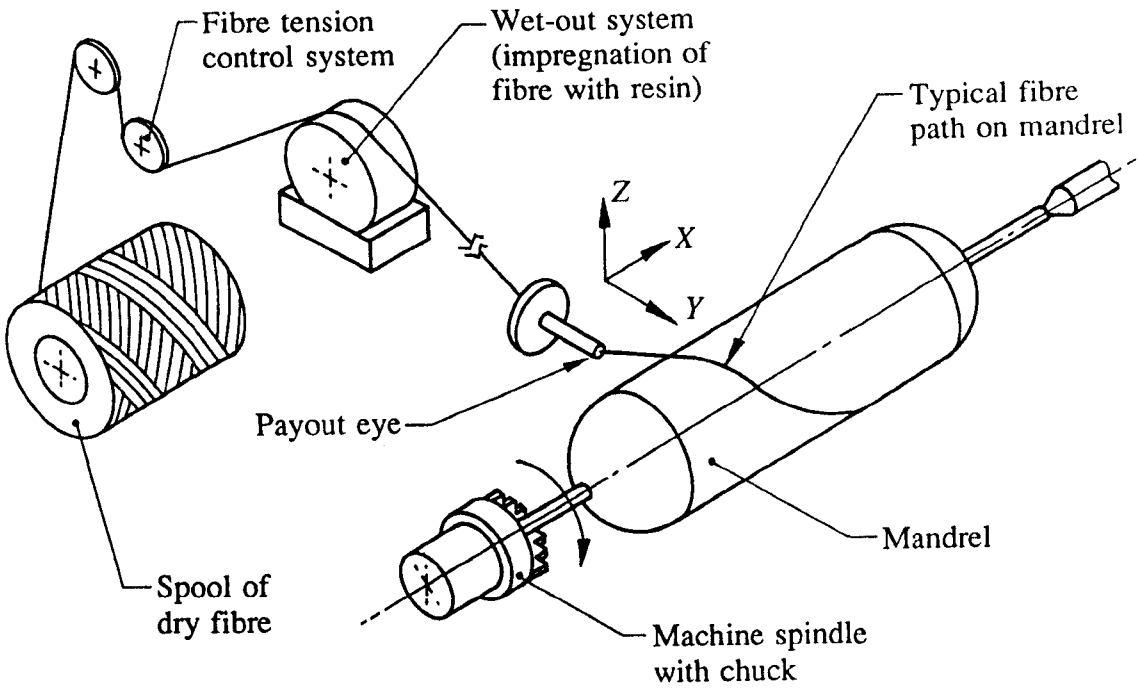

Fig. 1.1: Schematic diagram of CNC filament winding process. (Machine slides providing *X*-*Y*-*Z* movement of payout eye are omitted for clarity).

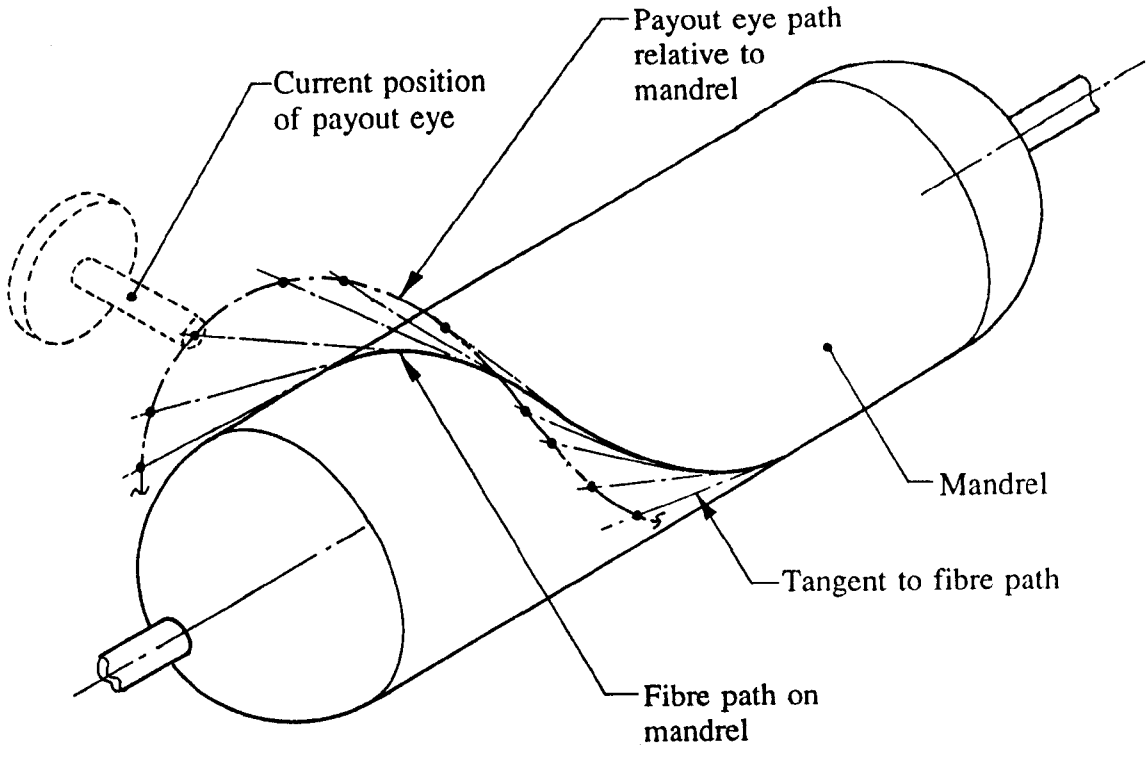

Fig. 1.2: Determination of payout eye path. Tangents to the fibre path are extended clear of the mandrel by an appropriate distance to give payout eye position; the locus of such points give the payout eye path relative to the mandrel.

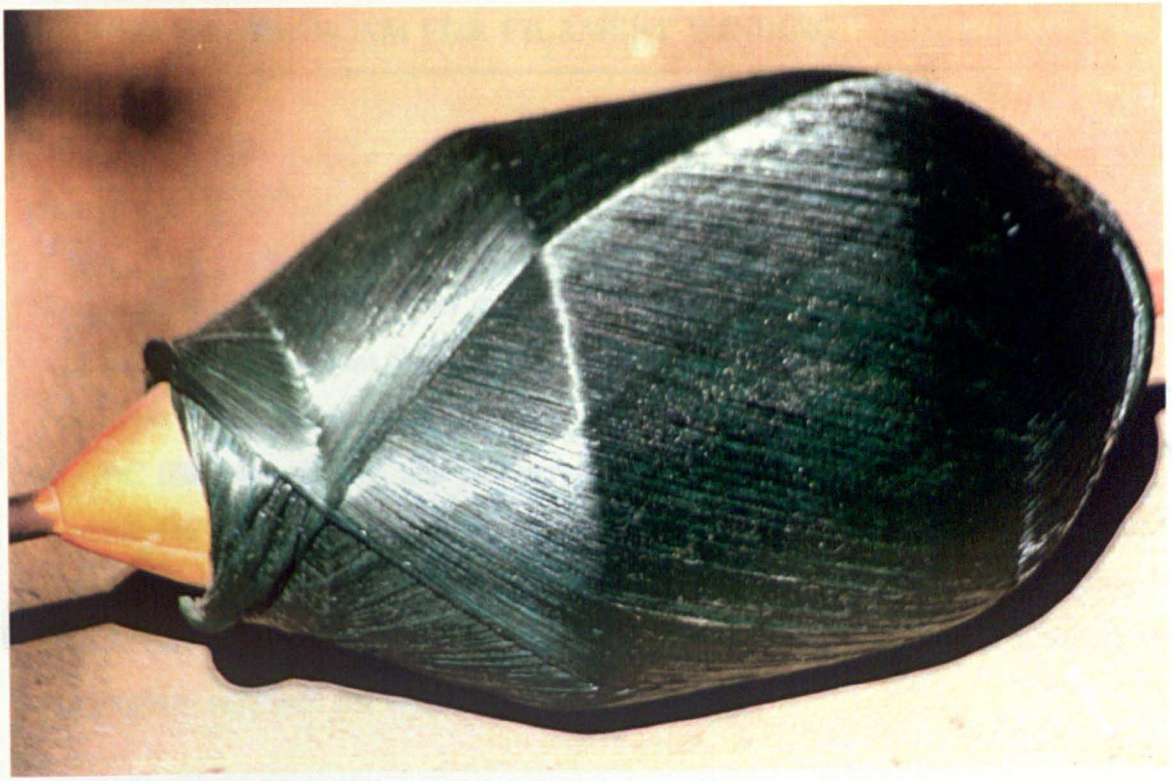

(a) Photograph of filament-wound demonstration component

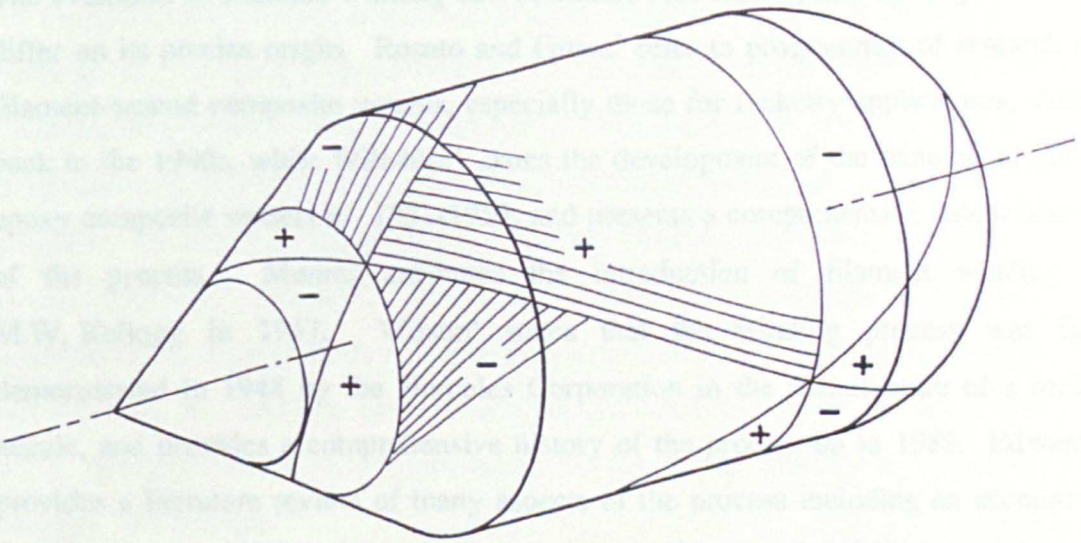

(b) Diagram highlighting the alternating lamination sequence visible in (a) above

Fig. 1.3: Alternating lamination sequence on a nominally-axisymmetric filament-wound component

CHAPTER 2 : CAD/CAM FOR FILAMENT WINDING

2.1 Introduction

This chapter begins with a brief overview of the literature on the history of filament winding including recent literature not included in earlier surveys referenced. A description of the filament winding process is presented from the particular viewpoint of CNC filament winding, and an overview is given of the CADFIL systems which generate the CNC machine data for axisymmetric and non-axisymmetric components. It is these systems which have formed the foundation for the work to be described later in this thesis. A brief description of the filament winding facilities available at Nottingham conclude the chapter.

2.2 A brief history of filament winding

The evolution of filament winding can be traced over many years although accounts differ on its precise origin. Rosato and Grove[1] refer to programmes of research on filament-wound composite vessels, especially those for rocketry applications, dating back to the 1940s, while Wiltshire[2] dates the development of the winding of glass-epoxy composite vessels to 1951-1953, and presents a comprehensive patent history of the process. Munro[3] attributes the introduction of filament winding to M.W. Kellogg in 1947. Wilson[4] states that the winding process was first demonstrated in 1948 by the Hercules Corporation in the manufacture of a rocket nozzle, and provides a comprehensive history of the process up to 1989. Edwards[5] provides a literature review of many aspects of the process including an account of its history up to 1985, making particular use of references 1 and 2 and including a considerable amount of literature on the commercial aspects of the process. This literature review will not be further duplicated here. Munro[3] provides a survey of more recent developments with particular reference to the kind of CNC techniques which are to be described in this chapter and to robotic filament winding.

Traditional filament winding methods were implemented using winding machines whose operation was based on the use of mechanical linkages and mechanisms[5] to create the required winding paths. Such methods still provide a simple and effective means of manufacture of high-volume components with simple winding patterns[6]. These production methods restricted the application of filament winding to axisymmetric components such as pressure vessels[6]. However, Rosato and Grove illustrate a winding machine controlled by punched tape, and by the late 1970s CNC technology was being applied to filament winding machines[4]. This made feasible the construction of machines where the payout eye was no longer constrained in its movements by the limitations of mechanical linkages. This freedom made it possible to consider the manufacture of complex non-axisymmetric components using filament winding.

During 1982-1985 Edwards[5] conducted a feasibility study into the manufacture of complex components using CNC filament winding. Although his attempts to manufacture highly complex components (such as an automobile wishbone) were unsuccessful, numerous simpler geometries were successfully wound. This study laid the foundations for subsequent work on CNC filament winding at the University of Nottingham. Young[7] developed a CAD/CAM program (AXCAD) for the computational prediction of geodesic and friction-controlled paths on axisymmetric components of arbitrary shape and the processing of these paths to give CNC part-programs; this software has since been further developed and marketed under licence as the CADFIL® system[8,9]. Shearing[10] further developed the computation of geodesic and friction-controlled paths for application to non-axisymmetric components; this software has similarly been developed and marketed under the name CADFIL II®[8,11]. Related studies have concentrated on the use of robotics in the winding of complex components[12,13].

The University of Nottingham has not been alone in developing CAD systems for filament winding. CADFIBER[14,15], CADMAC[16,17,18] and ARIANNA[19] all appear to have similar capabilities to the CADFIL systems although only limited information has been published on the application of these packages to the

manufacture of real components. Vogt and Taylor[20] describe the creation of geodesic and nearly-geodesic (friction-controlled) fibre paths on axisymmetric and non-axisymmetric components, the latter being defined by spline surfaces. Other work has been published on the analytical determination of winding paths for complex components[21].

2.3 Outline of the CNC filament winding process

Rosato and Grove[1] provide a thorough background to the filament winding process but it is instructive to outline the CNC implementation of the technique. A typical CNC filament winding machine is shown in diagrammatic form in Fig. 2.1, and the process is represented in simplified form in Fig. 1.1.

Dry fibre is supplied in the form of spools which are mounted within a system which unwinds the fibre rovings so as to maintain a constant tension. Closed-loop feedback control of the tension is usually provided. The fibre is drawn through a wet-out system which impregnates it with liquid resin. The fibre then passes through a payout eye which moves in a path clear of the rotating mandrel onto which the fibre is to be wound. If the fibre is to remain on the mandrel without slipping it must be laid along the shortest distance over the surface of the mandrel, known as a geodesic path: to achieve this pattern it is necessary to move the payout eye in such a path that the fibre is always tangential to the desired geodesic path at the point where it contacts the mandrel (Fig. 1.2). In practice it is possible to depart slightly from the true geodesic path by making use of the friction between the fibre and the mandrel surface.

Where the machine is controlled using CNC technology, up to six axes of movement (*X*, *Y*, *Z*, *A*, *B* and *C*, illustrated in Fig. 2.1) are normally available for numerical control. One of these (*A*) is normally the mandrel rotation, and the payout eye is usually given two or three translational axes (*X*-*Z*). Usually, rotation of the payout eye is restricted to one axis (*B*) but a wrist-like action (*C*) is occasionally encountered. Control of the machine is usually achieved by using a standard CNC controller for machine tool applications.

2.4 Review of the capabilities of the CADFIL systems

2.4.1 *CADFIL for axisymmetric components (henceforward referred to as CADFIL I)*[22]

The CADFIL I system is designed to run on an IBM-compatible personal computer and is used for creating the fibre paths (and hence the CNC machine control data) for the manufacture of axisymmetric filament-wound components. The system consists of two main programs each of which carries out a number of tasks. The first of these carries out fibre path and payout eye generation and covers the following tasks.

(a) Mandrel definition. The geometry of the axisymmetric mandrel is defined in terms of a series of points which form its generator (meridional section). The co-ordinates of these points are stored in a file. They are used to create a surface model of the mandrel using triangular facets.

(b) Fibre path generation. A starting position and starting angle for the fibre are defined by the user and the fibre path is projected over the surface under the control of the user. The default setting is that the fibre follows a geodesic path over the surface, but a variable amount of frictional steering is available so that significant departures may be made from the geodesic path assuming fibre slippage does not occur in reality. The path is stored in a data file as a sequence of co-ordinate positions. A typical fibre path created in CADFIL I is illustrated in Fig. 2.2.

(c) Payout eye path generation. The required clearance of the payout eye from the mandrel is entered, and the path of the payout eye is computed from the fibre path. For each point on the payout eye path, this is achieved by extending the line defining the direction of a typical region of the fibre from its point of tangency with the mandrel to the point where it clears the mandrel by the appropriate distance (Fig. 1.2). The payout eye path is the locus of a series of such points, and the co-ordinates of

these are stored in a file. A typical payout eye path created within CADFIL I, plotted in relation to the mandrel, is given in Fig. 2.3. In practice the mandrel rotates and the payout eye path moves back and forth to trace this path around the mandrel.

The second program carries out the post-processing of the payout eye paths and includes the following tasks.

(a) Closure of payout eye path. In principle, the payout eye path is modified to give a regularly-repeating fibre path for which successive windings will lie side by side (Fig. 2.4 (a) and (b)). This is achieved by scaling the rotational movement of the mandrel relative to the payout eye, the scale factor being a value close to unity known as the progression factor. In practice, the mismatch between successive fibre paths may be such that it is preferable instead for every third winding (for example) to lie adjacent to the original one (Fig. 2.4(c)). This procedure is adopted to avoid excessive alteration to the original fibre path and hence to minimise the risk of fibre slippage. The resulting order of rotational symmetry in the fibre path and laminate structure is known as the band pattern number; in these examples it is 1 and 3 respectively.

(b) Generation of CNC control data. This stage must take account of the absolute position of the machine's co-ordinate datum, the units of measurement employed by the machine, and the axes of the machine (displacement of payout eye and rotation of mandrel and payout eye) which are available and required. The resulting set of data is expressed as a file of CNC control commands known as a part-program.

2.4.2 *CADFIL II*[23]

The process of generating filament winding data for non-axisymmetric components is considerably more complex than for axisymmetric components. The software has been developed primarily as a consultancy tool rather than as

a marketable product and hence some customisation of the coding is required for particular applications. The larger volume of data involved also means that greater computing power is required to implement the program: workstations such as the Apollo are recommended. The stages of operation of the system are as follows:

(a) Mandrel surface definition. The geometry of the mandrel is discretised into plane facets defined in terms of corner co-ordinates which are stored in a data file. The generation of this data generally requires the user to write a short special-purpose program.

(b) Fibre path generation. This is achieved in two stages. A "template" fibre is created as a geodesic or friction-steered path, and this is used to create a "family" of fibres which are spaced an equal distance apart on the surface of the mandrel. The fibre family is stored as a sequence of point co-ordinates in a file.

(c) Replication and linking. Each fibre family may be replicated by reflection in any planes of symmetry which exist on the mandrel. These fibre paths must then be assembled into an appropriate sequence (with appropriate transition paths to link the ends of the fibre paths) so that they can be wound without breaking the fibre.

(d) Payout eye path generation. The payout eye is constrained to move on a surface explicitly defined in terms of geometrical entities (cylinders, cones, ellipsoids, spheres etc.) which stands clear of the mandrel and is known as a control surface.

(e) CNC control data generation. The payout eye data is post-processed to give the machine co-ordinate data required to achieve the laying of the fibre onto the mandrel. This set of data is stored as a CNC part-program.

Chapter 8 describes the manufacture of a non-axisymmetric filament-wound component using CADFIL II and may be regarded as a case study illustrating the above process.

2.4.3 *Definition of structures produced using CADFIL*

It is noteworthy that, in the case of both CADFIL systems, the component structure is almost completely defined by the information contained in the winding data files, provided that full details of the material (constitutive properties and the cross-sectional area of the impregnated roving) are available. However, the extraction of this component definition had not been attempted until now, and it is the objective of this thesis to establish a procedure for achieving this task so that numerical modelling of the filament-wound structure for stress/strain analysis now becomes feasible.

2.5 Filament winding facilities

A Pultrex Modwind 1S-5NC 5-axis CNC filament winding machine fitted with a GE FANUC 11M control system is available to the author. This machine is illustrated in Fig. 2.5 and its main features may be identified from Fig. 2.1. A data link to an IBM-compatible personal computer enables CNC part-programs to be loaded from diskette into controller memory. A variety of tooling has been built up for this machine including payout eyes and mandrels. A comprehensive description of the machine was given by Edwards[5]; although the current FANUC controller was fitted after this account was written the remainder of the description is valid and repetition here is unnecessary.

A smaller, 3-axis machine described by Brown[13] was originally built for use in a robotic filament winding cell; it is currently being used for development work by Haq[24]. Although this machine will be ideally suited to the manufacture of small axisymmetric components, manufacture of specimens for this investigation was carried out the Pultrex machine which may be regarded as a fully-developed and established system similar to many industrial installations.

2.6 Conclusions

It has been demonstrated that the filament winding process is long-established and the CNC implementation of the process is now mature technology for simple (axisymmetric) components. Software for generating the data required for CNC filament winding is well-established for axisymmetric components. Equivalent software for non-axisymmetric components is also available. An important feature of programs of this kind is their ability to produce accurate definitions of the fibre paths with which a component is wound. This ability to define fibre path data is crucial to the automatic finite element modelling of filament-wound components and this connection will be explored in detail in Chapter 6.

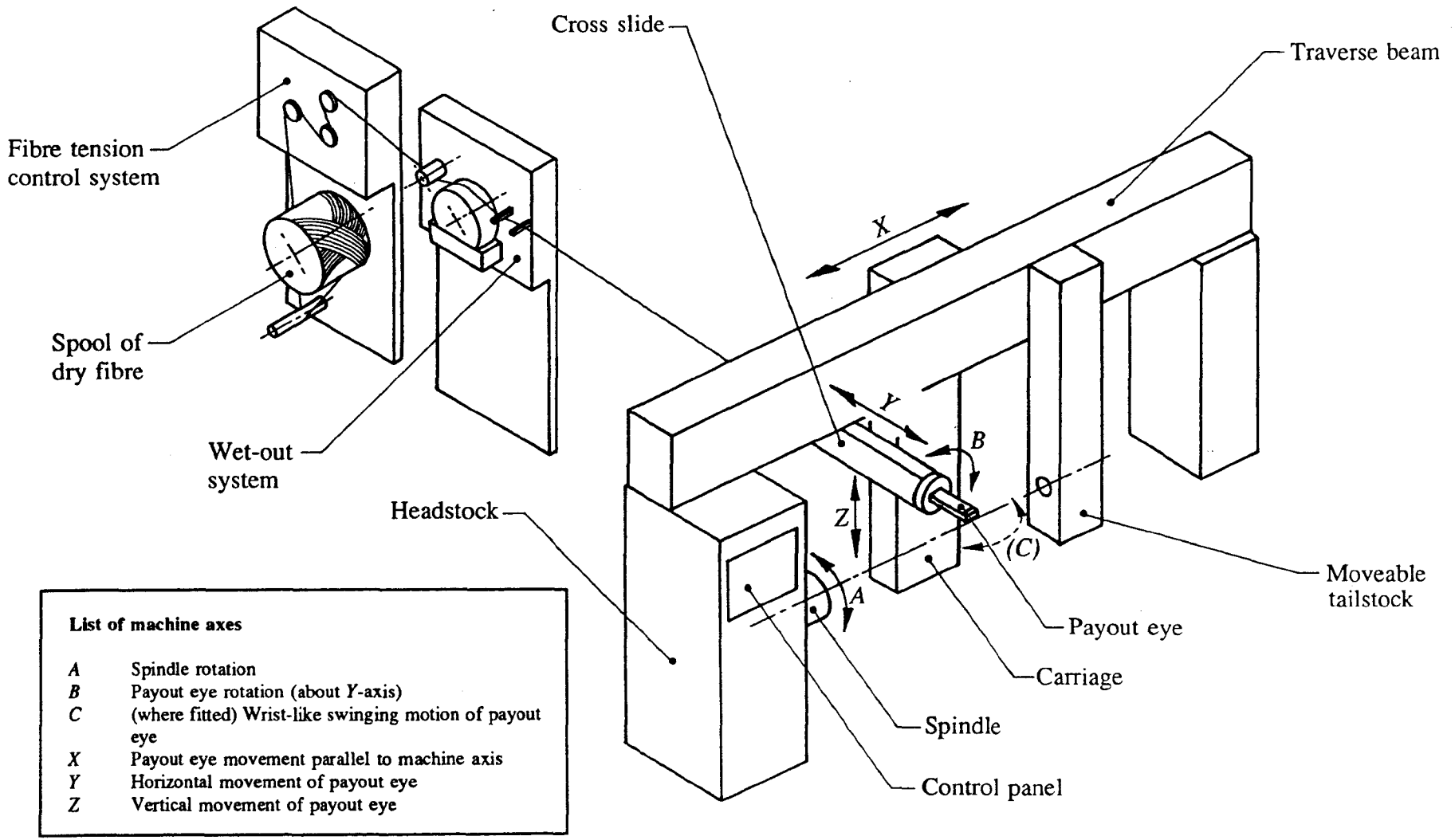

Fig. 2.1: Schematic diagram of a typical CNC filament winding machine (Pultrex Modwind 1S-5NC; drawing adapted from Edwards[5])

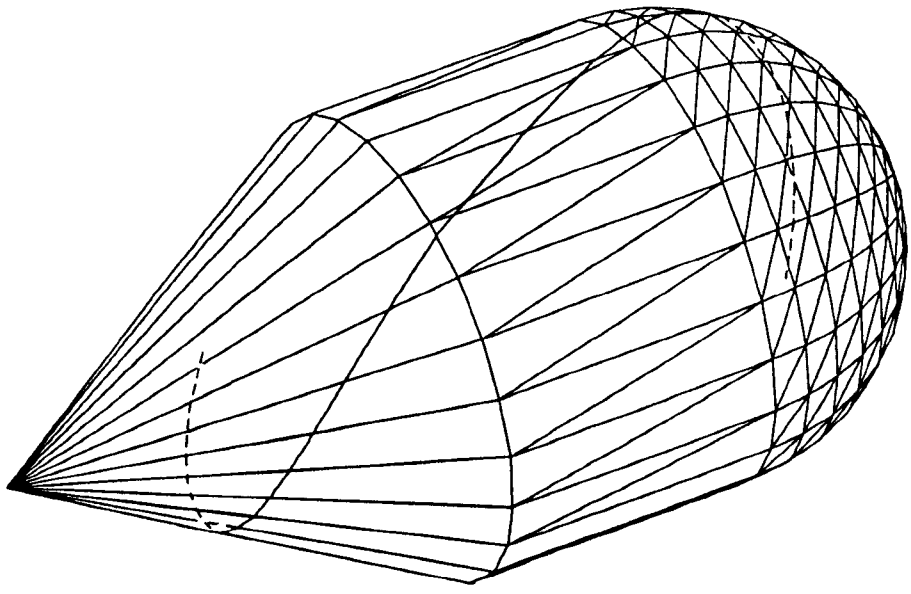

Fig. 2.2: Typical fibre path created using CADFIL I

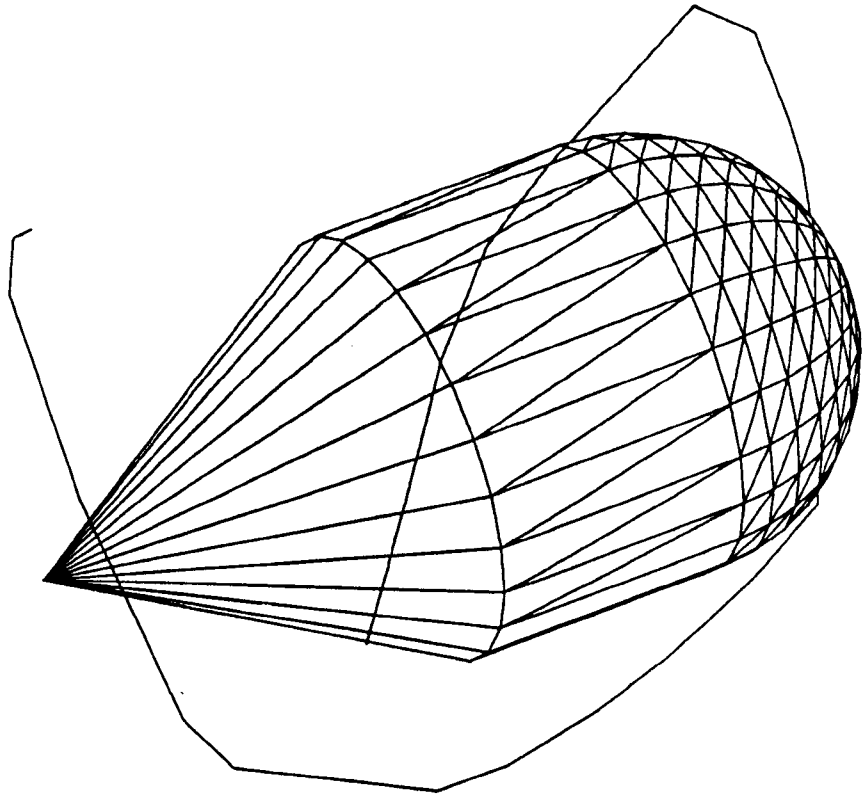

Fig. 2.3: Payout eye path required to lay fibre shown in Fig. 2.2
(Payout eye movement is shown relative to mandrel).

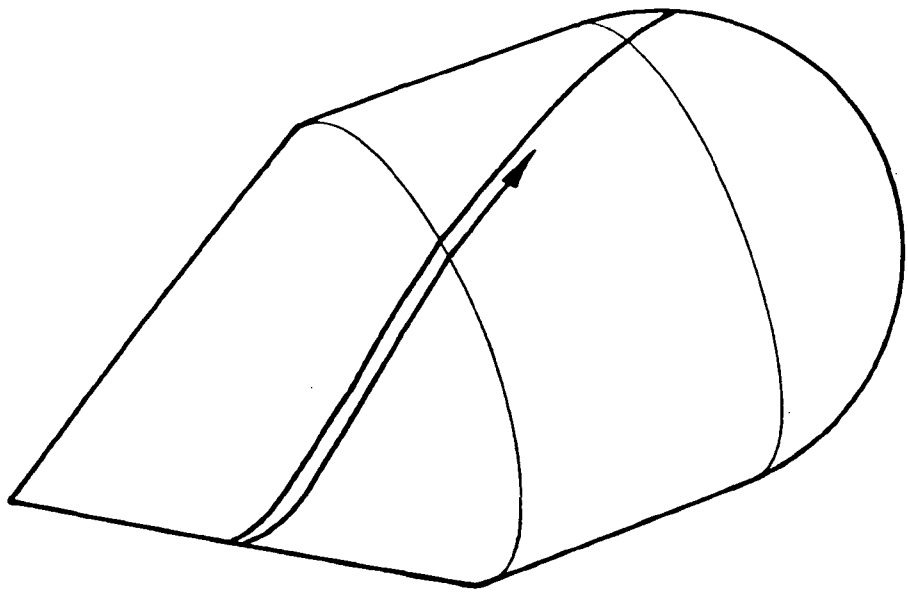

(a) Laying of successive windings of fibre adjacent to each other
(diagram simplified for clarity: only left-to-right path of fibre is shown)

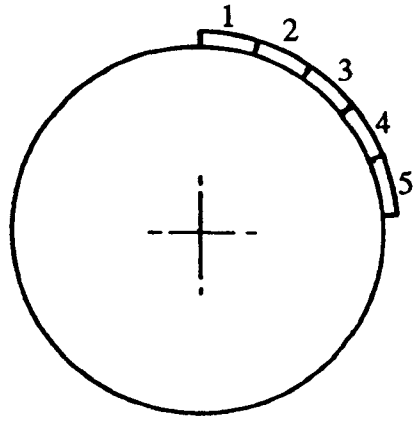

(b) Section through (a): winding sequence for a band pattern number of 1

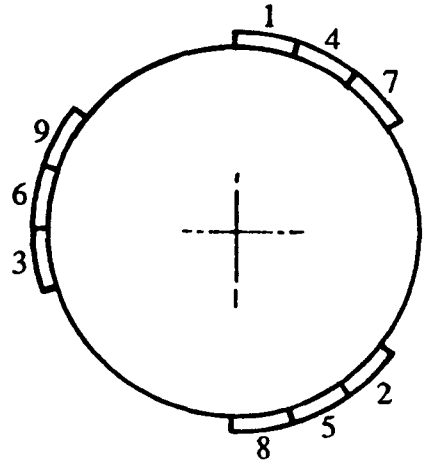

(c) One possible winding sequence for a band pattern number of 3

Fig. 2.4: Use of various winding sequences to achieve a smooth build-up of fibre
(adapted from reference 22)

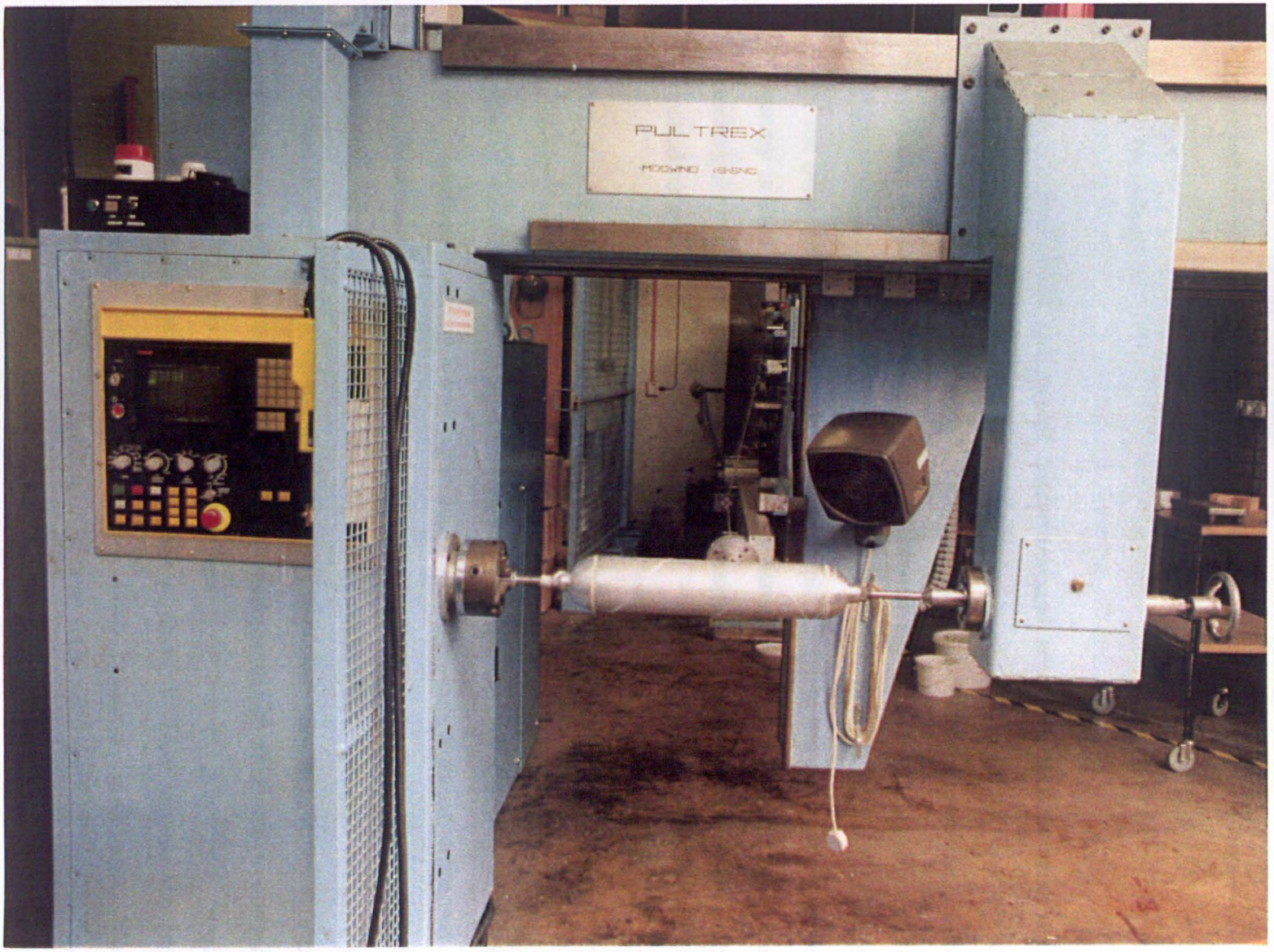

Fig. 2.5: Pultrex Modwind 1S-5NC filament winding machine

CHAPTER 3: CLASSICAL STRESS ANALYSIS OF FILAMENT-WOUND STRUCTURES

3.1 Introduction

The accurate stress analysis of filament-wound structures is both necessary and potentially difficult. One reason for the difficulty is the orthotropic behaviour of the filament-wound material from which they are made. Another reason is the continuous variation of the material thickness, orientation and lamination sequence over the surface of the structure. The need for stress analysis is discussed, and an overview of the behaviour of anisotropic and orthotropic materials and laminates is given. A survey is then presented which describes some of the classical structural analysis techniques which have been applied to composite laminates in general and to filament-wound structures in particular.

3.2 The need for accurate stress analysis of filament-wound structures

One of the primary advantages of filament-wound structures is that they can exhibit very favourable strength-to-weight and stiffness-to-weight ratios compared with conventional all-metallic structures. These properties can only be fully exploited if methods of structural analysis are available to allow the tailoring of the component design to service duty, taking account of the important constraint of manufacturing feasibility. It is necessary to avoid either unacceptable risk of failure or, conversely, over-engineering so as to negate the advantages of the material properties. Structural analysis of filament-wound components is a particular problem because the material generally behaves in an anisotropic (or, more precisely, orthotropic) manner; techniques for modelling this behaviour are well established and it is essential to gain an understanding of these before attempting the analysis of orthotropic components.

3.3 Modelling of orthotropic materials and laminates

Composite materials, especially filament-wound fibre-reinforced plastics, differ from conventional engineering materials (such as metals) in possessing material properties which are not isotropic. Whereas the elastic behaviour of isotropic materials can be described using only two elastic constants (the Young's modulus and the Poisson's ratio), a truly anisotropic material requires (in general) 21 independent elastic constants to form the symmetric square matrix which relates the six components of stress to the six components of strain. This model represents the most general case and in many practical situations the structure of the material (which may, for instance, be made from unidirectionally-aligned fibres) will possess one or more planes of symmetry. The most common assumption is that the material is symmetrical about three mutually perpendicular planes, and such a material (which is said to be orthotropic) can be described in terms of nine independent elastic constants. Furthermore, a subset of orthotropy known as transverse isotropy can be defined using only five independent constants. This applies to a material whose properties are uniform within a specified plane, typically that normal to the fibre direction. The full constitutive relations which describe anisotropy and its subsets form standard bookwork for which numerous references (e.g. Jones[25]) exist.

For thin shell applications (such as those to be considered in this thesis) it is often useful to simplify the three-dimensional stress-strain relationships to consider only a plane-stress state. There are now only four independent elastic constants; these four independent quantities can be expressed in various forms namely the terms in the compliance matrix $[S]$, the terms in the material stiffness matrix $[Q]=[S]^{-1}$, or as orthotropic engineering constants. Hooke's law for a plane-stress situation may be expressed as:

$$\begin{Bmatrix} \varepsilon_1 \\ \varepsilon_2 \\ \gamma_{12} \end{Bmatrix} = \begin{bmatrix} S_{11} & S_{12} & 0 \\ S_{12} & S_{22} & 0 \\ 0 & 0 & S_{66} \end{bmatrix} \begin{Bmatrix} \sigma_1 \\ \sigma_2 \\ \tau_{12} \end{Bmatrix} \quad \text{where:} \quad S_{11} = \frac{1}{E_1}; \quad S_{22} = \frac{1}{E_2}$$

$$S_{12} = -\frac{\nu_{12}}{E_1} = -\frac{\nu_{21}}{E_2} \qquad (3.1)$$

$$S_{66} = \frac{1}{G_{12}}$$

or alternatively:

$$\begin{Bmatrix}\sigma_1\\ \sigma_2\\ \tau_{12}\end{Bmatrix} = \begin{bmatrix}Q_{11} & Q_{12} & 0\\ Q_{12} & Q_{22} & 0\\ 0 & 0 & Q_{66}\end{bmatrix}\begin{Bmatrix}\varepsilon_1\\ \varepsilon_2\\ \gamma_{12}\end{Bmatrix}$$

where: $Q_{11} = \dfrac{E_1}{1-\nu_{12}\nu_{21}}$; $\quad Q_{22} = \dfrac{E_2}{1-\nu_{12}\nu_{21}}$

$$Q_{12} = \frac{\nu_{12}E_2}{1-\nu_{12}\nu_{21}} = \frac{\nu_{21}E_1}{1-\nu_{12}\nu_{21}}$$

$$Q_{66} = G_{12} \qquad (3.2)$$

These equations have been expressed in terms of engineering definitions of strain and use the contracted subscript notation commonly used by engineers rather than the full tensorial notation sometimes used in mathematical discussions.

The above relationships apply where the (1,2) axis system for the stresses and strains corresponds to the principal axes of the material. Where the stresses and strains are expressed in an x-y axis system orientated at angle ϕ to the material's axis system, the off-axis compliance and stiffness matrices $[\bar{S}]$ and $[\bar{Q}]$ are obtained by the fourth-rank tensor transformation of $[S]$ and $[Q]$ respectively:

$$\begin{Bmatrix}\varepsilon_x\\ \varepsilon_y\\ \gamma_{xy}\end{Bmatrix} = \begin{bmatrix}\bar{S}_{11} & \bar{S}_{12} & \bar{S}_{16}\\ \bar{S}_{12} & \bar{S}_{22} & \bar{S}_{26}\\ \bar{S}_{16} & \bar{S}_{26} & \bar{S}_{66}\end{bmatrix}\begin{Bmatrix}\sigma_x\\ \sigma_y\\ \tau_{xy}\end{Bmatrix} = [\bar{S}]\begin{Bmatrix}\sigma_x\\ \sigma_y\\ \tau_{xy}\end{Bmatrix}, \text{ similarly } \begin{Bmatrix}\sigma_x\\ \sigma_y\\ \tau_{xy}\end{Bmatrix} = [\bar{Q}]\begin{Bmatrix}\varepsilon_x\\ \varepsilon_y\\ \gamma_{xy}\end{Bmatrix} \qquad (3.3)\ (a\&b)$$

where:

$$[\bar{S}] = [T]^T[S][T] \quad (a)$$

$$[\bar{Q}] = [T]^{-1}[S][T]^{-T} \quad (b)$$

and: $$[T] = \begin{bmatrix}\cos^2\phi & \sin^2\phi & 2\sin\phi\cos\phi\\ \sin^2\phi & \cos^2\phi & -2\sin\phi\cos\phi\\ -\sin\phi\cos\phi & \sin\phi\cos\phi & \cos^2\phi-\sin^2\phi\end{bmatrix} \qquad (3.4)$$

The term *generally orthotropic* is sometimes used to describe the off-axis behaviour of an orthotropic material, to distinguish from its *specially orthotropic* behaviour when the loading axis system coincides with the material principal directions.

Structures made from composite materials often consist of laminates assembled from layers with off-axis principal directions, and these generally exhibit coupling between

different modes of deformation. The behaviour of laminates is frequently modelled using classical lamination theory (CLT). This gives a relationship between the mid-surface strains $\{\varepsilon^0\}$ and curvature and twist $\{\kappa\}$ of a laminated orthotropic plate and the forces $\{N\}$ and couples $\{M\}$ per unit of plate width required to cause these deformations. CLT for a laminate with n layers, referred to a global x-y co-ordinate system may be expressed as:

$$\begin{Bmatrix} N_x \\ N_y \\ N_{xy} \\ M_x \\ M_y \\ M_{xy} \end{Bmatrix} = \begin{bmatrix} A_{11} & A_{12} & A_{16} & B_{11} & B_{12} & B_{16} \\ A_{12} & A_{22} & A_{26} & B_{12} & B_{22} & B_{26} \\ A_{16} & A_{26} & A_{66} & B_{16} & B_{26} & B_{66} \\ B_{11} & B_{12} & B_{16} & D_{11} & D_{12} & D_{16} \\ B_{12} & B_{22} & B_{26} & D_{12} & D_{22} & D_{26} \\ B_{16} & B_{26} & B_{66} & D_{16} & D_{26} & D_{66} \end{bmatrix} \begin{Bmatrix} \varepsilon_x^0 \\ \varepsilon_y^0 \\ \gamma_{xy}^0 \\ \kappa_x \\ \kappa_y \\ \kappa_{xy} \end{Bmatrix} \quad \text{or:} \quad \begin{Bmatrix} \{N\} \\ \{M\} \end{Bmatrix} = \begin{bmatrix} [A] & [B] \\ [B] & [D] \end{bmatrix} \begin{Bmatrix} \{\varepsilon^0\} \\ \{\kappa\} \end{Bmatrix} \tag{3.5}$$

where:

$$A_{ij} = \sum_{k=1}^{n} (\bar{Q}_{ij})_k (z_k - z_{k-1}), \quad B_{ij} = \sum_{k=1}^{n} \tfrac{1}{2} (\bar{Q}_{ij})_k (z_k^2 - z_{k-1}^2), \quad C_{ij} = \sum_{k=1}^{n} \tfrac{1}{3} (\bar{Q}_{ij})_k (z_k^3 - z_{k-1}^3)$$

and where z is the position of the top or bottom surface of each layer measured with respect to the mid-surface of the laminate.

$$\text{Similarly:} \begin{Bmatrix} \varepsilon^0 \\ \kappa \end{Bmatrix} = \begin{bmatrix} [\alpha] & [\beta] \\ [\beta]^T & [\delta] \end{bmatrix} \begin{Bmatrix} [N] \\ [M] \end{Bmatrix} \quad \text{where:} \begin{bmatrix} [\alpha] & [\beta] \\ [\beta]^T & [\delta] \end{bmatrix} = \begin{bmatrix} [A] & [B] \\ [B] & [D] \end{bmatrix}^{-1} \tag{3.6}$$

Of particular interest within this thesis are regular antisymmetric angle-ply laminates. These have an even number of similar plies or layers. The orientation of each ply in the sequence (measured relative to the axis of the specimen of laminate) alternates in sign but remains constant in value. This is the laminate structure which is laid during the filament winding of an axisymmetric component, provided that a single winding pattern is used for the whole process. As discussed in Chapter 1, the lamination sequence varies over the surface of the component (Figs. 1.3(a) and (b)). For an antisymmetric laminate, A_{16}=A_{26}=B_{11}=B_{12}=B_{22}=B_{66}=D_{16}=D_{26}=0, i.e. there is no coupling between tension and shear, bending and tension, shearing and twisting or bending and twisting. Coupling does exist between other pairs of modes. For example, coupling between tension and twisting is illustrated in Fig. 3.1(a) and (b)); this effect tends to zero as the number of layers becomes large (Fig. 3.1(c)).

The derivation of CLT[25] makes the Kirchhoff-Love assumption that normal sections through the shell thickness remain normal and undeformed, whereas there will in practice be transverse shear stresses and strains including interlaminar shear stresses. Additionally, the through-thickness stress has been assumed to be negligible but in extreme situations of bending such stresses can cause delamination[26]. For the purpose of calculating strains and deflections, CLT provides a useful and relatively simple first approximation which is sufficient for many practical engineering situations, but considerable work has been performed to model the true behaviour of laminated plates and shells more accurately. For instance, Ambartsumyan[27], Kaprellian, Rogers and Spencer[28], and Pipes and Pagano[26,29,30] present analyses of laminated flat plates; some of these references include the determination of stresses not obtainable from CLT. Spencer et al[31], Whitney and Sun[32], Reddy[33], Widera et al[34,35] and Cai et al[36,37] all present analyses of cylindrical or doubly curved laminated shells. These theories are generally extremely complex and are listed above for completeness. Since this kind of work is of limited relevance to the main objective of the thesis, no attempt has been made to incorporate these theories into the analysis of the simple loadcases presented here. All these complex theories assume the composite material to be linear elastic in behaviour, and rigorous theoretical models based upon these theories would still be subject to disagreement with experimental results if the behaviour of the real composite material were to depart significantly from the ideal.

3.4 **Classical stress analysis of filament-wound components**

Finite element solutions are becoming increasingly important in engineering and FE is the only realistic approach to the stress analysis of filament-wound components of complex geometry. However, it is instructive to examine the stress analysis techniques applied to spherical, spheroidal and cylindrical geometries and to compare these with the finite element approaches to similar problems described in Chapter 4. These analytical methods demonstrate the kind of analytical techniques applied by engineers to filament-wound structures and make use of design, optimisation and failure criteria which may be applicable to finite element analyses. In addition to

providing important background information for the designer of filament-wound vessels and structures, these papers provide alternatives to a full FE analysis which may be useful to verify such an analysis or avoid the need for it.

3.4.1 *Spherical and spheroidal structures*

The most significant work in this area appears to be due to Gerstle[38] who examined the case of a filament-wound internally-pressurised spherical vessel. This consisted of a thin ductile metal bladder or liner wound with an elastic composite material in a pattern assumed to give quasi-isotropic (transversely isotropic) material properties. The on-axis stiffness properties of the composite were predicted using the rule-of-mixtures[25] for E_1 and ν_{12} and using equations due to Whitney[39] and Foye[40]. These properties were then integrated around all possible orientations to give averaged tensile and shear properties for a quasi-isotropic laminate. Equilibrium and compatibility, as applied by Love[41] to a sphere, were used to determine the behaviour of the vessel as the bladder passed through the stages of elasticity and partial and full yield. The strength of the assembly was assessed using three failure criteria: maximum stress, maximum strain, and two versions of a criterion based upon radial and tangential strength due to Norris and Ashkenazi[42]. It was concluded that good radial compressive strength and a high volume fraction of fibre were important in obtaining a vessel with a high burst pressure.

Comparison of theoretical results with experimental data[43] showed excellent correlation (within a few percent or better) for strain vs. pressure during a burst test, but relatively poor correlation (not quantified) for bursting pressure calculated theoretically from the material strength properties. However, it was found that the maximum stress and maximum strain at failure were both, for a given material, largely independent of vessel geometry. It was suggested therefore that such experimentally determined values of strain at failure should be used with the maximum strain criterion. The analysis was then extended to include a design optimisation of "vessel efficiency" = pV/W (where p=pressure, V=volume, W=vessel weight) as a function of design proportions, enabling the

designer to choose the best configuration for a given bladder/composite material combination.

Gerstle and Moss[44] applied the theory outlined above to thick-walled spherical vessels designed to withstand very high pressures, and demonstrated the benefits of using two distinct materials for the composite wrapping: a strong but compliant composite (e.g. Kevlar/epoxy) over-wound with a stiffer, slightly weaker material (e.g. carbon fibre/epoxy).

Gerstle's model[38] was applied by Guess[45] to a practical problem, a spherical pressure vessel manufactured from a thin seamless electroformed copper liner with a stainless steel filling tube and overwrapped with a quasi-isotropic Kevlar 49/epoxy composite. The calculations were performed in two stages: Gerstle's model was used to calculate nominal values of stress and strain, and a finite element model was used to take account of the stress concentrations around the filling stem. The calculated values of stress and strain were found to be in good agreement when considering the region of the vessel away from the filling tube. Details of the material properties and finite element formulations are not given.

Lewis[46] presents a literature survey on manufacturing methods and strength analysis for lined spherical pressure vessels. He describes and gives the properties for the materials used for the liner and the wrapping, and describes current manufacturing techniques including the choice of winding patterns (uniaxial multiangular and delta-axisymmetric) and the various types of removable mandrel. Some applications of filament-wound pressure vessels are listed. The spherical elastic-plastic shell theory due to Gerstle[38] and Love[41] is quoted. The strength and life-prediction aspects of the vessels are then examined and it is stated that such a vessel may initially withstand the applied stress but eventually fail in a stress-rupture or creep-rupture mode. Finally, the subject of damage measurement is examined and a number of damage accumulation models of spherical pressure vessels are described. These are compared with experimental results and are found to give generally good correlation.

Martin[47] describes a method of optimising the geometry of a filament-wound pressure vessel, given prescribed values of two important dimensions of the vessel (radius of the polar opening and length of the vessel). The objective function for this optimisation was again pV/W and the constraints included the use of the Tsai-Hill failure criterion[42]. The shape of the meridian of the vessel was approximated by a B-spline curve, and the fibre stresses were evaluated using membrane theory and laminate theory. The thickness distribution due to the winding pattern was taken into account. Considerable weight savings were achieved with the optimised design compared with the original shape, the weight/volume ratio being reduced by a factor of six during the optimisation.

3.4.2 *Cylindrical structures*

In most of the above analyses, the behaviour of the composite material was assumed to be quasi-isotropic because the chosen winding pattern gave a uniform distribution of fibre directions over the surface. This is not generally the case with cylindrical structures where a helical path is normally used, resulting in an antisymmetric angle-ply laminate. Netting analysis[48] is often used to show that the optimal winding angle for a closed-ended cylinder under internal pressure is ±54.7°. However, for situations where such simplifications are inappropriate (such as thick-walled cylinders and situations involving edge-moment effects), conventional thin- and thick-shell theory must be extended to this orthotropic situation.

Moss[49] extended Gerstle's[38] analysis of metallic-lined composite spheres to cover filament-reinforced cylindrical tubes. Plane-strain analysis was employed, the Tresca yield criterion was used for the metallic liner (assumed to be elastic-perfectly plastic) and the maximum strain failure criterion was used for the filament-wound composite wrapping.

Hoa, Ouelette and Sankar[50] used classical lamination theory (simplified by the omission of bending terms) applied to membrane stress resultants to predict the strains in the cylindrical portion of a ±54.7° filament-wound vessel. Agreement

between theory and experiment was variable, errors being typically a few percent but much more serious (approaching 40%) in the worst case. No results were predicted or quoted in this paper for the non-cylindrical portions of the vessel.

A more complete analysis of the behaviour of axisymmetric vessels is offered by Padovec[51], who follows the conventional route of considering discontinuity bending stresses in shells of revolution in addition to membrane stresses. The vessel is assumed to consist of a cylindrical barrel with a domed end-closure, there being five alternative shapes presented for the latter. These five do not, surprisingly, include a torispherical end. Padovec begins by outlining the tensile and flexural behaviour of an antisymmetric angle-ply laminate using (in a different notation from that familiarly employed) the principles underlying orthotropic transformation and classical lamination theory. He then analyses the membrane stresses and strains in the cylindrical barrel and in the alternative patterns of end-closure. The bending theory for the cylindrical shell is an orthotropic version of the theory presented by Hetenyi[52], and that for the domed end is similarly based upon the work of Geckeler[53]. The incompatibility between the deflections and slopes of the cylinder and dome under membrane action alone is counteracted by the presence of shear forces and bending moments at the discontinuity in the vessel geometry.

A similar kind of analysis is performed by Highton and Soden[54] to understand the behaviour of a flange-ended test specimen design for characterising the multiaxial strength characteristics of filament-wound GRP. Once again the structure is analyzed using an orthotropic extension of the cylindrical shell theory presented by Hetenyi[52], treating the filament-wound composite as either a homogeneous orthotropic material of averaged properties, or as a laminate. The specimen took the form of a thin filament-wound tube, the central portion (the gauge length) of which had a constant wall thickness. The ends were reinforced with a thick layer of circumferential windings which tapered to zero thickness towards the central portion of the tube. At the ends of the specimen, split cast aluminium alloy flanges were assembled around the reinforced tube and bonded

in place. The stress distribution in the specimen was modelled using orthotropic shell theory in two different ways:

(a) The structure was considered as a series of long, rigidly-connected (contiguous) tubes of sufficient length that the discontinuity stresses at their junctions did not interact. The aim of this exercise was to obtain a rate of change of wall thickness which would not result in excessive direct axial or interlaminar shear stress. The flanges and hubs were treated as rings with rigid cross-sections and were designed with just sufficient flexibility to avoid high stresses in the reinforced GRP tube due to rigid clamping.

(b) Once a design had been chosen, it was checked using a more rigorous computer-based analysis which split the specimen into a series of finite-length tubes, each of which was treated as a short beam on an elastic foundation. In this case, classical lamination theory was used to obtain the properties of each tube cross-section.

For a simple isotropic test case, model (b) was found to be in good agreement with established theory[55] relating to tapered flanged joints, and in reasonable agreement (errors of typically 30%) with the approximate analysis (a) when comparing values of shear force and bending moment. The models were then applied to the specimen geometry and some minor modifications were made to the gauge length/reinforcement transition to avoid high values of discontinuity stress.

It may be observed that the method used by Padovec[51] and Highton and Soden[54] for calculating the laminate flexural rigidity differs slightly from that suggested by the author in Chapter 5 and Appendix B (section B.3.2.) These authors take the flexural rigidity of a laminated shell D_x in the x-direction to be $D_{11} - B_{11}^2/A_{11}$. This calculation of D_x ignores the tendency of an antisymmetrically laminated cylinder to undergo shear strain (and hence twisting as if under torsion) when subjected to an axisymmetric edge moment. The present author has a personal

preference for the following alternative, since it avoids the artificial constraint on this mode of deformation:

$$D_x = \frac{\delta_{22}}{\delta_{11}\delta_{22} - \delta_{12}^2} \tag{3.7}$$

In practice the difference in numerical values is likely to be small for many-layered laminates. Typical cases examined were an 8-layered antisymmetric laminate with ply angles of ±30°, ±45° and ±60°. The values of D_x obtained from equation (3.7) were smaller by 1.9%, 1.75% and 0.95% respectively†.

3.5 Discussion: usefulness and limitations of classical analysis

The work reviewed in this chapter illustrates the kind of analysis that can be achieved using classical techniques. In particular it introduces some of the approaches adopted in the analysis of cylinders and rings in Chapter 5, especially the orthotropic extensions[51,54] to the well-known cylindrical shell theory presented by Hetenyi[52]. The work of Gerstle, Guess and Moss[38,43,44,45,49] would be of particular use for the validation of techniques for modelling metallic-lined spherical and cylindrical vessels before the application of such techniques to more complex geometries.

---

† 2.8 mm thick, 8-layered antisymmetric laminate with the following unidirectional material properties: E_1 = 46000 MNm^{-2}, E_2 = 8000 MNm^{-2}, G_{12} = 5000 MNm^{-2}, ν_{12} = 0.3. Summary of results:

Ply angle	Flexural rigidity D_x (N)		Percentage difference
	$D_x=D_{11} - B_{11}^2/A_{11}$	$D_x=\delta_{22}/(\delta_{11}\delta_{22}-\delta_{12}^2)$	
±30°	575480	564610	-1.889
±45°	364650	358260	-1.753
±60°	222380	220270	-0.949

The references reviewed relate primarily to the analysis of filament-wound vessels of very simple geometry, taking account of the orthotropic or anisotropic behaviour of the composite material and the elastic-plastic behaviour of the liner where used. Even in this apparently simple situation the analysis becomes very complex and it would be quite impractical to regard the derivation of such analyses as a routine approach to engineering stress analysis problems. It would be almost impossible to write equations to carry out accurately the stress analysis of filament-wound components of complex geometries such as elbows and tee-pieces. It is therefore necessary to consider alternative methods of stress analysis which are both more accessible to the practical engineer and more suitable for complex geometries and winding patterns. Finite element analysis is such a tool and will be described next, both in general terms and with particular reference to filament-wound components.

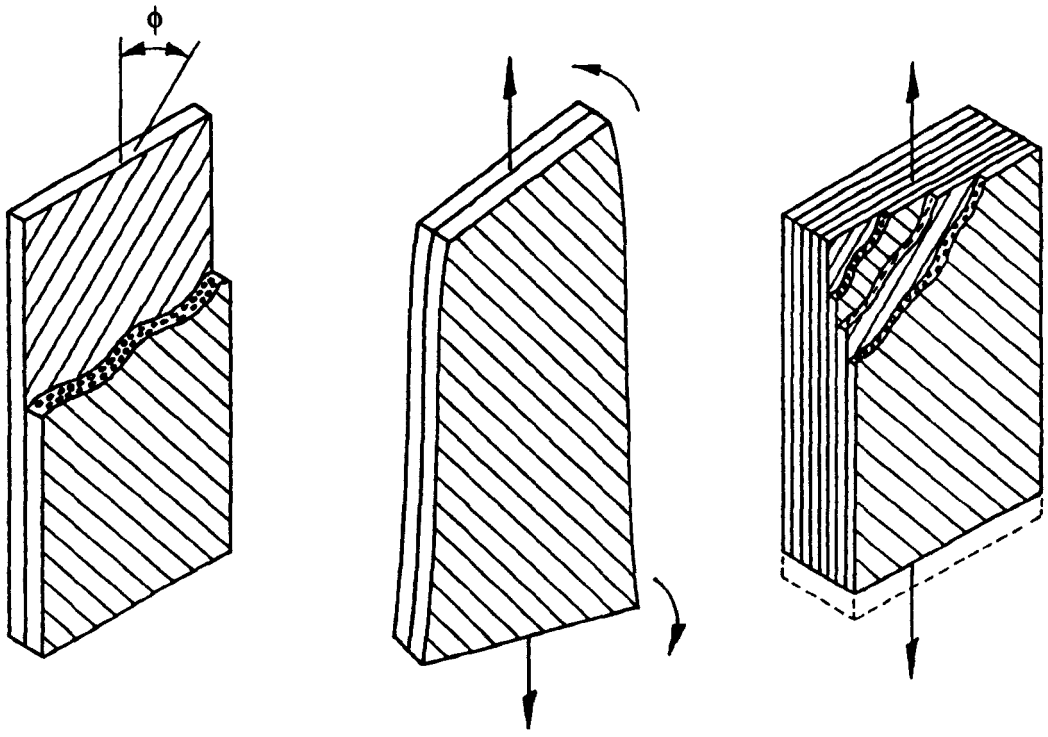

(a) Two-layered antisymmetric angle-ply laminate

(b) Laminate twists in uniaxial tension, i.e. there is coupling between tension and twisting

(c) As number of layers becomes large, tension/twist coupling vanishes and laminate acts as homogeneous orthotropic material

Fig. 3.1: The phenomenon of coupling between tension and twisting

CHAPTER 4: THE FINITE ELEMENT METHOD AND ITS APPLICATION TO FILAMENT-WOUND STRUCTURES

4.1 Introduction

The complex geometries encountered in engineering components prohibit the use of exact analytical solutions to provide numerical answers. The finite element method is a powerful numerical technique for solving engineering problems in the field of structural mechanics by discretising a continuous system into a large number of finite regions. Each region is easily modelled mathematically breaking the initial calculation down into many simpler problems. The simultaneous solution of these problems requires the use of a digital computer. The FE method utilises various branches of engineering mathematics dating back over 200 years. Its evolution can be traced back to aeronautical applications of matrix methods in the 1940s, but has only been developed as a system since 1960 as the facilities for its implementation have become available. Various historical accounts of the method may be consulted[56,57]. From the mid-1970s onwards the number of commercially-available FE systems has proliferated and the method has become generally accepted as an engineering tool. Two of these systems (PAFEC and ABAQUS) are available within the Department of Mechanical Engineering.

Finite element theory has evolved into a complex branch of engineering mathematics and computing and it would be quite inappropriate to include a comprehensive account of the technique here. A number of such accounts are available, notably that by Zienkiewicz and Taylor[58]. The approach adopted in this chapter is to present a largely descriptive statement of the finite element method. For further reference, a detailed statement of the mathematical framework used for elements using an isoparametric formulation[59,60] is given in Appendix A. A review of two areas of literature is presented. Firstly the application of FE stress analysis to filament-wound structures, particularly pressure vessels, is described. Secondly, a review is presented of the published formulations of laminated orthotropic elements suitable for analysis

of filament-wound structures. Mention is made of the practical capabilities of commercially-available FE systems in the analysis of filament-wound structures. Finally, descriptive outlines are presented for four types of element used in the work described in this thesis.

4.2 Brief overview of finite element theory: isoparametric elements

The finite regions or elements, which approximate to the true component geometry, take different forms depending upon the geometry of the component to be modelled. Of particular interest in this thesis are thin shell and axisymmetric elements. Each element is defined in terms of points in space (nodes) which are linked in a specified pattern or order (the topology of the element). Each node possesses certain degrees of freedom (DOFs); in the context of structural analysis these are linear and rotational displacements. These displacements are related to the forces applied to the element by a stiffness matrix which may be calculated from element geometry and material properties. The stiffness matrices for the elements may then be used to assemble the stiffness matrix for the structure.

This thesis makes particular use of elements based on an isoparametric formulation[59,60]. This means that the polynomial functions (known as shape functions) used to interpolate both the co-ordinate positions and the variables (e.g. displacements) over the element are of the same form as each other. These functions also relate the true geometry of the element to that of a fictitious parent element by means of a mapping (Fig. 4.1) and it is within the domain of the parent element that the calculation of the element stiffness matrix takes place. This is achieved by integrating the strain energy over the volume of the element using Gaussian quadrature[61]. This is a form of numerical integration consisting of the weighted summation of the integrand evaluated at Gauss points. These are sampling points whose positions are inherently defined within the integration method. Differentiating the strain energy with respect to displacement gives the element stiffness. The concepts of shape functions, isoparametric mapping and integration of strain energy are outlined in section A.2 of Appendix A. The contribution of each element to the stiffness of the system is added

during the assembly of the global stiffness matrix. This matrix is used to calculate the displacements of the structure from the applied forces and the restraints.

4.3 Finite element stress analysis of filament-wound structures

FE analysis of filament-wound structures has been performed since the advent of the method. Most of the available literature relates to traditional applications of filament winding such as pressure vessels.

4.3.1 *Filament-wound spheres with metallic liners*

Chen and Clewlow[62] describe the finite element analysis of a metallic spherical pressure vessel reinforced with filament-wound Kevlar/epoxy. The liner is assumed to have a bilinear (elastic/strain hardening) characteristic, is designed to yield or autofrettage during initial overpressurisation, and is intended to carry a portion of the pressure load. The design criteria therefore include the requirements that the compressive stress in the liner after autofrettage should not exceed the value necessary to cause buckling, and should not exceed the yield stress to avoid low cycle fatigue failure. The filament-wound material is assumed to consist of angle-wound orthotropic laminae rigidly coupled in balanced pairs so that the coupling between tension and shear (as observed in the global directions) is eliminated. This analysis is extended to cover balanced multi-layer composites.

The geometrical expressions relating equatorial winding angles to thickness and local winding angle are stated, and were used as the basis for determining the fibre buildup and hence the vessel thickness profile. However, no attempt was made to force the finite element boundaries to coincide with the fibre layer boundaries when generating the FE mesh. Indeed, for reasons of limited program capacity, it was necessary for groups of elements in the membrane-loaded parts of the structure to be assigned average material properties. A particular feature of this analysis was that slip elements were incorporated between the composite and the liner to simulate non-adhesion.

The structural analysis was carried out by means of an in-house FE program AB5U (particular to Aerojet Manufacturing Company of California, USA) for axisymmetric bodies having cylindrically anisotropic material properties, and the data for this program was generated using three pre-processors. The results of the FE analysis were post-processed to calculate the residual stresses in the liner and the operating strain range of the liner, and to predict the burst pressure. The failure criterion used was that of maximum effective strain.

Knight[63] gives a detailed account of the use of a finite element program to analyze the stresses in a metallic sphere reinforced with Kevlar 49/epoxy wound in the delta-axisymmetric pattern. An existing FE program written by Wilson[64,65] was modified to cope with three-dimensionally orthotropic material properties and to increase its element capacity. As with the analysis by Chen and Clewlow[62], the material properties of each pair of laminae (of opposite orientation) are modelled by considering the equivalent properties of a material formed by closely coupling the two laminae. No attempt was made to generate a mesh for which the element boundaries coincided with the boundaries between the layers of windings. Lamina stresses were found by transforming the strains calculated by the FE package to the local directions of the fibres. The results from a typical case study are presented; it is claimed that the predicted burst pressure (based upon the maximum fibre stress criterion) was within 4% of the experimental average burst pressure.

In a later paper, Knight[66] applies the Weibull statistical failure theory[67] to filament-reinforced spheres. This failure criterion is especially suited to brittle materials. The finite element analysis was used in conjunction with this criterion to predict the failure pressure of two vessels described by Gerstle and Guess[68]. The predicted failure pressure of 400 MPa agreed well with the measured failure pressures of 365 MPa and 370 MPa.

Leavesley and Knight[69,70] describe a finite element model of the loss of strength caused in a filament-wound structure by the buckling during manufacture

of the fibres in the inner layers under the compressive influence of the outer layers. Unlike Knight's earlier models this involved the positioning of the element boundaries to coincide with the boundaries of the different layers. The filament winding process is simulated by the progressive "switching-on" of the material properties of each successive layer. This is achieved by changing the modulus of the element in two stages from an initial very small value, via an intermediate value during the winding process, to the true value of the composite material. When the average strain along a fibre path becomes compressive, it is judged that the layer will have lost much of its strength and stiffness; when the stress in an element becomes compressive its material properties are changed to an isotropic set of values which ignore the longitudinal reinforcement effect of the fibre (i.e. the transverse stiffness properties are applied to all directions). It should be observed that the elements used in this analysis appear to be highly distorted in many cases. Axisymmetric quadrilateral isoparametric elements were used, with the thickness transitions using these same elements collapsed to triangular form.

4.3.2 *Finite element analysis of filament-wound cylindrical vessels, tubes and miscellaneous structures*

Knoell[71] describes the COMTANK system, intended as a user-friendly and largely foolproof method of designing filament-wound vessels. This takes basic design shape data and wrap angles and performs a simple netting analysis to provide a first estimate of the required number of fibre wraps. The design is then automatically encoded as a finite element model. COMTANK is dedicated to two basic shapes, oblate spheroids and dome-ended cylinders. The stresses in each ply of the laminate are found from the stress resultants that exist at a point in the vessel wall. The vessel is modelled as an orthotropic laminated thin shell of revolution[72], and the material properties are stored in tabular form for linear interpolation between values of wrap angle. It was stated that no experimental data was available for comparison with the computed results.

Rizzo and Vicario[73] used finite element analysis to examine the influence of specimen dimensions upon the accuracy of tests using filament-wound tubes to characterise laminate properties. Various quantitative conclusions were drawn regarding the effects of thickness/diameter and length/diameter ratios and the helix angle upon stress distributions and test accuracy. The finite element program used was unusual in its ability to take account of general anisotropy in an axisymmetric situation.

Hardy and Malik[74] describe an optimisation procedure for laminated structural members. The structual analysis within this procedure is based upon the PAFEC finite element system and the optimisation algorithm is defined in the paper. The objective function and constraints for the optimisation can be defined as appropriate. It is not clear from the paper precisely how the execution of the FE program was coupled to that of the optimisation program, but a description is given of how the data is transferred by means of files. The optimisation program generates the FE data input file by means of a package-specific pre-processor routine, and the FE package output routines are modified to create output in a standard format. Two simple case studies are presented to illustrate this procedure.

A later paper[75] by the above authors applies a similar philosophy to the optimal design of filament-wound dome-ended cylindrical pressure vessels consisting of a metallic liner overwrapped with planar-wound and hoop-wound composite. Axisymmetric finite elements was used. Again, PAFEC was used as the finite element system and the optimisation was performed using a NAG[122] subroutine. The data generation routines included a simulation of the filament winding process to establish material directions, thicknesses and properties, although it is not stated that any manufacturing data was produced. The objective (as with the vessel optimisations described earlier) was to maximise the vessel efficiency, the variables in this case being the thicknesses of the composite and the metallic liner and the choice of materials. A typical case study is presented, although no experimental results are included for comparison.

Li et al[76] describe the modelling of a filament-wound tube made from glass-epoxy subjected to transverse crushing by a spherical indenter. Large-deflection analysis was implemented using ABAQUS and load-deflection characteristics were obtained which agreed within 15-20% with experimental data. No attempt was made to model the alternating lamination sequence of the tube since this was stated to be a difficult task.

Eckold and Wells[16,18] describe the finite element analysis of some simple axisymmetric filament-wound components. The components were analysed using data prepared automatically from the CADMAC filament winding system. In both cases, the FE results are compared with strains measured experimentally, revealing differences ranging from a few percent to 100% or more. Overall stiffness of a filament-wound bellows was overestimated by 50% although this result was considered to be a reasonably good comparison. These two papers provide the only evidence of a link being established between a filament winding CAD/CAM system and a finite element analysis system. The need for this kind of link is explored in section 4.5 and is discussed in greater detail in Chapter 6.

4.3.3 *Discussion of literature on the analysis of filament-wound structures*

It may be seen that the application of finite element analysis to filament-wound structures is far from new, and that a substantial quantity of work has been published on the subject. Because details of each analysis are generally specific to the FE code used by a particular establishment and because a complete specification of the analysis would be voluminous, most of the papers described do not present a sufficiently complete definition of the solution to enable an outsider to replicate the results. The main benefit of this literature is therefore in demonstrating what can be achieved and in providing guidance on the approaches which have been found to be useful. It should be noted however that computing power has developed to a very large degree since much of this work was performed, greatly easing the restrictions upon the size and complexity of analysis task which is feasible.

4.4 Finite element formulations suitable for filament-wound structures

A number of authors have described the formulation of finite elements for the analysis of laminated and orthotropic composites. These are usually developments of formulations for isotropic elements[63,77]. Although all the elements used in this investigation are those commercially available within the ABAQUS and PAFEC FE codes, it is instructive to examine the variety of element formulations which have been published to address the need for the analysis of structures such as those manufactured by filament winding.

An example is the element presented by Knight[63] which is closely based upon an axisymmetric element formulation described in an early paper by Wilson[64]. In their original form, these elements are stated by Knight to have modelled a material with transverse isotropy in the radial/meridional plane, although Knight extended the elements to allow full orthotropy.

Dong[72] presents the formulation for a simple laminated shell of revolution element capable of modelling non-axisymmetric loadcases constructed from Fourier series. A number of comparisons with analytical solutions show excellent agreement.

Panda and Natarajan[77] describe the formulation of a finite element capable of modelling doubly-curved laminated shells of revolution. The element is based upon an isotropic superparametric element formulated by Ahmad, Irons and Zienkiewicz[78]. This element has four degrees of freedom at each node (three translations and one rotation, the latter being in the axial-radial plane). The assumptions made include Kirchhoff's hypothesis that normal stress through the thickness of the element is negligible. Gaussian integration is used to find the contribution to element stiffness of each layer in the laminate. Numerical tests of the element against exact solutions to cylindrical shell problems by Pagano and Whitney[79] give results which are at worst about 7% in error and in other cases indistinguishable from the exact solution.

Natarajan, Hoa and Sankar[80] build upon this work to formulate an element designed primarily for examining the strain and stress patterns near the nozzle-cylinder shell intersections of filament-reinforced plastic vessels. A 20-noded 3-dimensional finite element is used for this purpose. Gaussian integration on a layer-by-layer basis is again used. A note of caution is sounded against the careless use of symmetry in modelling filament-wound structures; this is illustrated using the example of a filament-wound cylinder which was helically symmetric rather than axisymmetric, and tended to twist under axisymmetric loading. If such a structure is modelled as a quadrant the calculated results will be incorrect. The same formulation of element is presented in greater detail using different notation and with slightly altered verification examples in a paper by Hoa, Yu and Sankar[81]. Such an element would be of use in modelling a complex structure such as a thick-walled filament-wound tee-piece if suitable elements are not commercially available.

Knight and Rogers[82,83,84] describe the formulation and use of a finite element which covers the entire thickness of a filament-wound axisymmetric structure by using several integration points in each layer. Linear variation of displacement is assumed in the in-plane direction, while the polynomial order modelling the through-thickness variation of displacements is selected by the user and may be high to model variation through different layers. Since Gaussian quadrature is not suitable for this situation, rectangular integration is used. This type of element is claimed to reduce by 75% the amount of computer time required to solve a typical problem. The authors explore the accuracy of the element when applied to the modelling of a number of single-layer and multi-layer isotropic and orthotropic cylinders, and show that the accuracy is in the order of ±3%[84].

A number of laminated orthotropic elements have been formulated by Chen, Yang et al[85,86,87] for use on a microcomputer. These consist of a symmetrically laminated beam element, a symmetrically laminated plate element, and three laminated plate elements.

A recent book by Ochoa and Reddy[88] on the FE analysis of composite laminates provides an overview of the mechanics of composite materials and describes a variety of FE formulations including comparisons with benchmark results. The practical problems of modelling filament-wound structures are not addressed, however.

4.5 Commercial availability of finite element systems for stress analysis of composites

Many of the above references were written when finite element packages were at an early stage of development. There is now a proliferation of powerful finite element packages available for lease or purchase; some of these are general purpose packages, others have specific capabilities in specialised areas. Most of the general purpose FE systems have the capability to model laminated orthotropic components with varying degrees of sophistication, and a number of reviews of the available software for this application have been conducted. In 1982 Griffin[89] presented a list of selection criteria and described the capabilities of eleven packages then available but did not make any particular recommendations. The packages reviewed included PAFEC and ABAQUS.

More recently (1992) Taig has presented a report on the capabilities of a sample of commercial FE packages for analysis of laminated composites. He gives a detailed review of the requirements of such systems and makes particular reference to the difficulties of setting up accurate FE models of filament-wound components and laminated structures[90]; this is because the thickness and fibre orientation are heavily dependent upon the practicalities of the manufacturing process. He concludes that none of the packages tested takes these constraints into consideration; however, it is the writer's opinion that the FILFEM system to be described in this thesis provides many of the capabilities to overcome the shortcomings outlined by Taig. In addition to the software review, Taig proposes a number of benchmark problems with which composite capabilities in FE packages may be evaluated, and presents the test results obtained from the various packages tested. Surprisingly, these packages included PAFEC but not ABAQUS. No specific recommendations are made regarding the

optimum package, although P/COMPOSITE and ANSYS appear to fare best in his review.

4.6 Finite element types used in this thesis

Four main types of elements have been used in this investigation and will be described in outline. The first three are implemented in the PAFEC finite element system; the last is implemented in the ABAQUS system. As a practical example of the isoparametric concept, the full formulation of the first of these elements is presented in Appendix A (Section A.3).

4.6.1 *Axisymmetric isoparametric quadrilateral Fourier element available in PAFEC*[91]

This may be visualised as an annulus consisting of the solid of revolution of a quadrilateral with curvilinear sides (defined using 8 nodes). In their simplest form these elements are subjected to axisymmetric loading and have two translational degrees of freedom u_x and u_r per node (Fig. 4.2). However, an interesting and useful variation on this element is that which permits the use of loads which vary in a sinusoidal manner around the circumference of the structure. By this means any loadcase which varies arbitrarily around the circumference may be synthesised using a Fourier series of sinusoidally varying loads. The elements for this application are of similar geometry but possess 3 degrees of freedom u_x u_r and u_θ per node. The formulation of this version of the element is given in Section A.3 of Appendix A. It is understood that elements with similar capability have been coded for the ABAQUS system but problems with their non-linear capabilities mean that only the low-order Fourier elements have been released at the time of writing.

4.6.2 *Ahmad's eight-noded thick shell element implemented in PAFEC*[92,93,94]

This element models a region (of curvilinear quadrilateral shape) of a doubly curved shell of significant thickness as an assembly of infinitely thin isoparametric membranes which are constrained to shear in a uniform manner at

the nodes. The element may alternatively be regarded as a 20-noded brick element with the surplus degrees of freedom eliminated by constraints. Three translational degrees of freedom u_x, u_y and u_z and two out-of-plane rotations (about uniquely defined local directions) exist at each node. The assumption of uniform shear through the element thickness clearly disobeys equilibrium locally (shear stress at the top and bottom surfaces must actually be zero) and hence the element stiffness matrix includes a correction factor of 1.2 on the through-thickness shear stiffness terms. A six-noded curvilinear triangle is also available.

The Ahmad thick-shell element is given orthotropic capability in PAFEC, and it is necessary to transform the orthotropic properties of each layer to give the (off-axis) orthotropic properties in terms of the element's local axis system. This is performed at each Gauss integration point, although the transformation is only defined once for each element. Therefore if the element's curvature is severe the transformed material axes will not be even approximately coplanar with the element surface at the Gauss points, and in practice warnings will be flagged by PAFEC.

4.6.3 *The semi-Loof thin shell element implemented in PAFEC*

This element also models an eight-noded region of a doubly curved shell but through-thickness shear deformation is neglected. Three translational degrees of freedom are defined per node. Eight additional nodes are defined within the element coding and are placed part way along each side of the element (actually at the integration points required for 2-point Gaussian integration along an element side). These are termed Loof nodes in honour of H.W. Loof who first used such nodes. A central node is also internally defined. At each Loof node a single rotation (about an axis along the element edge) is defined. The reduced number of degrees of freedom is obtained by the application of various constraints to the complete system of degrees of freedom. These include the use of discrete Kirchhoff constraints (constraint to zero shear at a set of specific points) at the Loof nodes.

The formulation of the semi-Loof element is complex. The definitive account of its evolution and formulation is given by its originator Irons[95], and a full listing of one version of his coding for this element is available[96]. A triangular version of the semi-Loof element also exists[97]. It is worth mentioning that the PAFEC system makes use of Irons's original FORTRAN code with little modification other than that of suitable interfacing to the PAFEC architecture[98]. PAFEC extends the capability of the elements to cover laminated orthotropic shells.

It should be mentioned that although the user of the element within the PAFEC package need not be concerned with the existence or location of the Loof nodes, it is necessary to be aware of the manner in which the rotational degrees of freedom are represented within PAFEC's data structure. They are arbitrarily assigned to the ϕ_x and ϕ_y freedoms at the mid-side nodes, although they are in no way to be regarded as rotations about the x or y axes. This means that great care must be taken in assigning rotational constraints to the mid-side nodes. A side effect of the arrangement of the rotational degrees of freedom is that there is no rotational connectivity of corner nodes[95]; therefore there will be a spurious localised hinging effect where a normal load is applied to a corner node (Fig. 4.3).

It is noted from the PAFEC Data Preparation Manual[99] that this element can give over-stiff results in inextensional situations (i.e. where bending is the predominant form of deformation). An example of such a situation is the pinching of a thin cylindrical tube. This poor behaviour can be largely overcome by the use of reduced integration.

4.6.4 *Thin shell elements used in ABAQUS*[100]

A number of doubly-curved thin shell finite elements are used in ABAQUS, of which two are used in this thesis. One of these is a three-noded triangular shell element (type STRI35). This is a "true" (classical) thin shell in which the (discrete) Kirchhoff assumption of non-deformable normals is applied algebraically, in this case along element boundaries. The other element is a four-

noded quadrilateral which is one of a family of shear flexible shell elements based upon an isoparametric formulation. The four-noded quadrilateral uses reduced integration. The discrete Kirchhoff constraint is applied numerically at points within or at the edge of the element (for instance at points on the element edge spaced as Gauss points) using penalty methods; this makes the elements suitable for thin shell applications without risk of numerical problems. In the case of both of these elements, Simpson's rule is used for the through-thickness integration (five-point integration is the default for single layer shells, three points per layer are the default for laminated shells). The formulations of both types of elements are very complex and will not be summarised here; in addition to the mathematical description in the ABAQUS theory manual[101] a more descriptive outline of the elements and their applications is available[102].

Although the formulations of the two types of elements are based upon different philosophies their method of use, and the active degrees of freedom they possess, are identical. At each node there are five DOFs. These consist of three displacements and two out-of-plane rotations. Six degrees of freedom are activated where necessary, i.e. where rotational restraints are specified, where moment loads are applied, where 6-DOF elements are attached, where non-unique normals exist (i.e. shells meet at a cusp) or where multi-point constraints are applied.

4.7 Conclusions

The finite element method has been described and a considerable variety of its existing applications to filament-wound structures have been reviewed. Besides the literature on actual analyses, several papers on the formulations of suitable finite elements have been examined. The availability of relevant commercial FE codes has also been discussed. Mention has been made of a recent review of the finite element analysis of composites which has reinforced the need for a link between the FE data input process and the manufacturing processes for laminated composites. One example of such a link has been found. Finally, the discussion of FE methods and

codes has been put into context by introducing the elements which will be encountered in Chapters 6 and 7; these chapters describe the automatic generation of FE meshes and the results obtained from them.

Although the nature of many of the papers reviewed makes it difficult to draw firm conclusions or extract specific items of theory, it is clear that much ingenious work has been performed in the application of finite element analysis to filament-wound composites. While these analyses extend in complexity far beyond the simple linear elastic test case described in Chapter 7, they illustrate the kind of advanced analyses for which the meshes automatically generated by FILFEM I and possibly FILFEM II might eventually be used.

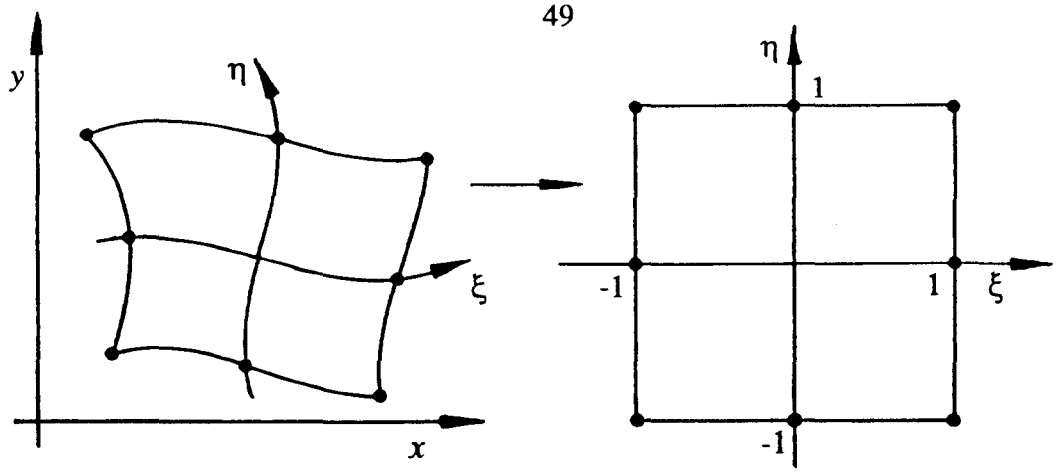

Fig. 4.1: Isoparametric mapping from x-y to ξ-η co-ordinate systems

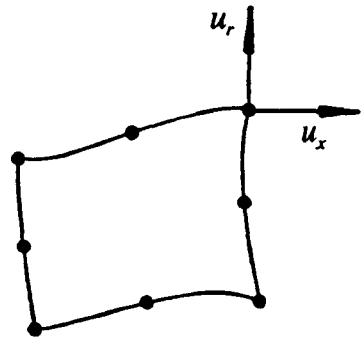

Fig. 4.2: Axisymmetric isoparametric element showing degrees of freedom at one node

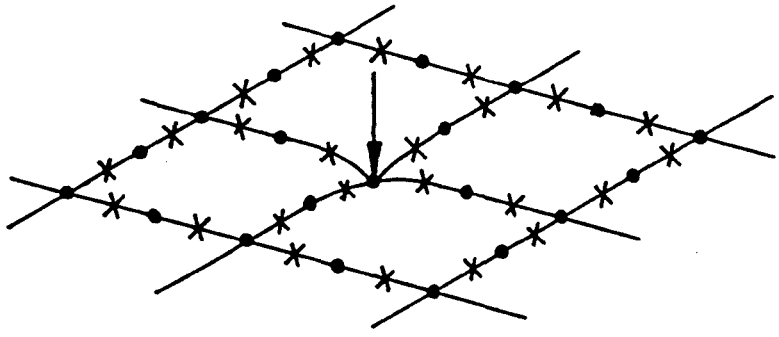

Fig. 4.3: Lack of slope continuity at corner nodes in semi-Loof elements: slope continuity exists only at Loof nodes (×) (after Irons[95])

CHAPTER 5: EXPERIMENTAL DETERMINATION OF ELASTIC PROPERTIES OF FILAMENT-WOUND GRP

5.1 Overview of chapter

This chapter begins with a brief review of some of the methods available for both the theoretical calculation and the experimental determination of the elastic properties of composite materials. The need is highlighted for a simple, cost-effective test of material properties and two such tests are described with results, along with the results of two more conventional tests for comparison. All four tests were found to give results for angle-ply laminate behaviour which differ by varying amounts from those predicted from conventional orthotropic theories. The most satisfactory explanation proposed for these differences is that the orthotropic material model is of limited accuracy despite its usefulness as a simple approximation. In particular, very significant non-linearities and permanent changes in properties are observed in some laminates when strains of 2000$\mu\varepsilon$ are exceeded. Finally, an attempt is made to obtain the unidirectional orthotropic material properties from the laminate properties by a best-fitting procedure, and the resulting properties are found to predict accurately the observed stiffness of the filament-wound laminate despite being at variance with typical estimates of the unidirectional properties.

5.2 Background

If a structural analysis of a filament-wound component is to be undertaken, it is essential that the material properties are satisfactorily understood. The properties of directional composites such as those produced by filament winding have already been examined from a theoretical viewpoint in Chapter 3, with particular reference to the linear elastic orthotropic model of material behaviour. The properties which define the behaviour of such a material may either be evaluated experimentally from specimens of the composite material, or predicted theoretically from the properties of the fibre and matrix and the proportions in which they are combined in the composite.

Jones[25] reviews the theoretical methods of predicting properties of composites and makes particular reference to the Halpin-Tsai equations. These are simple empirical equations which are fitted to more complex analytical models of the structure of fibres within the composite, and may be stated as follows.

$$
\begin{aligned}
E_1 &= E_f V_f + E_m(1 - V_f) \qquad (a)\\
\nu_{12} &= \nu_f V_f + \nu_m(1 - V_f) \qquad (b)\\
\text{and:}\quad \frac{M}{M_m} &= \frac{1 + \xi\eta V_f}{1 - \eta V_f} \qquad (c)\\
\text{where:}\quad \eta &= \frac{(M_f/M_m) - 1}{(M_f/M_m) + \xi} \qquad (d)
\end{aligned}
\tag{5.1}
$$

in which M = E_2, G_{12} or ν_{12} for composite

M_f = fibre property E_f, G_f or ν_f

M_m = matrix property E_m, G_m or ν_m

V_f = fibre volume fraction
(proportion of composite by volume)

The constant ξ takes different values for the calculations of E_2, G_{12} and ν_{23}. For E_2 and G_{12} the values of 2 and 1 are often used respectively although the values of ξ may be chosen to fit empirical data.

Eckold[103] presents a comprehensive literature survey on the failure criteria for composite materials and also includes a review of available methods of predicting and measuring the elastic properties of orthotropic materials. Experimental methods such as those described by Whitney[104] and Kavanagh[105] are of interest. Jones[25] discusses the problems associated with the testing of composite materials and discusses some experimental techniques with particular reference to the measurement of shear moduli. Weatherby[106] presents an experimental investigation into the elastic properties and strength of glass-reinforced polyester, including much data on elastic properties of angle-ply laminates and a review of failure criteria. This data exhibited a great deal of scatter in the measured values. Weatherby concentrated on the measurement of elastic properties of flat laminates which were wound onto a flat plate and cured in a press. A variety of experimental methods was used for testing these specimens. The methods included the use of tensile and compressive tests on flat

coupons and use of the two-rail shear test[25]. One of the problems of Weatherby's approach is that the manufacturing method of the specimens does not closely represent the manufacturing method of the actual components, since the latter rely upon the tension in the fibre to achieve a compacted laminate structure during winding and cure. By contrast, hydrostatic methods of testing oil-filled filament-wound tubes enable uniaxial and biaxial loading to be achieved in a genuine filament-wound structure but are messy and require the availability of hydraulic test equipment. Suitable equipment is not readily available to the author and as a result, two simple cost-effective tests were developed which require a minimum of apparatus other than the use of standard materials-testing equipment.

5.3 The pinched ring or proving ring test

This test arose from a suggestion by Dr V. Middleton and is intended as a means of obtaining the flexural properties of a laminate. Reddy and Reid[107] have used the concept of a pinched ring for the determination of the yield stress in metals and it is understood that a similar test has also been applied by these researchers to the determination of failure-related properties in composites[108]. However, the author believes it provides a very simple method of measuring elastic properties and the following discussion includes an analysis of its capabilities and sources of error. The experimental basis behind the method is that a thin ring of the specimen material is compressed diametrally between two flat plates and the change in its transverse diameter is measured and related to the compressing force.

5.3.1 *Theory*

In its simplest form the analysis of a pinched ring is a textbook application of Castigliano's method. If the ring is very thin compared with its radius R, the only significant mode of deformation is flexure (the effects of shear deformation and longitudinal compression being negligible). It may be shown that for small deflections caused by a load P, the change in diameter perpendicular to the loading direction (Fig. 5.1) is given by:

$$\delta_h = \frac{PR^3}{\text{F.R.}}\left(\frac{2}{\pi} - \frac{1}{2}\right) \tag{5.2}$$

If the ring section is narrow compared with its thickness t its flexural rigidity may be calculated using beam theory, i.e. flexural rigidity F.R. = EI. A more complete analysis, taking account of the effects of compression and shear and the effects of beam curvature, yields the following formula (of which Equation (5.2) is a simplification):

$$\delta_h = \frac{PR^3}{EI}\left(\frac{2}{\pi} - \frac{1}{2}\right) + \frac{PR}{2AE}\left(1 - \frac{8}{\pi} + \frac{4I}{\pi AR^2}\right) + \frac{1.2PR}{2GA} \tag{5.3}$$

In practical cases it is prudent to make the ring wide enough that edge imperfections may be neglected, and this leads to a problem in applying the above formulae. This is because the ring is too wide to ignore the self-restraint (which occurs in wide plates and shells) against anticlastic curvature but not wide enough to be considered infinite. The following method of correction was suggested by Dr J.J. Webster. The results obtained for the isotropic case are identical to those due to Lamb[109]. However, this derivation was carried out independently of that by Lamb, is much simpler and is easily extended to model the orthotropic situation. At the edges of the ring, the absence of restraining moment (which would prevent anticlastic curvature) may be considered as the superposition of a negative moment onto the restraining moment existing away from the edges. According to classical cylindrical shell theory[110] this effect will die away over a distance related to the constant $\lambda = (k/4D)^{1/4}$ where $k = Et/R^2$ is the radial stiffness per unit area of the shell and $D = Et^3/[12(1-\nu^2)]$ is its flexural rigidity per unit width. It may be shown that the contribution to circumferential moment from this decaying edge moment is the same as that due to a constant moment acting over a width w_{edge} for a ring of finite width w:

$$w_{edge} = \frac{1}{\lambda}\left[\frac{\cosh\lambda w - \cos\lambda w}{\sinh\lambda w + \sin\lambda w}\right] \tag{5.4}$$

The outermost bands of the ring of width w_{edge} are therefore assumed to have no restraint against anticlastic curvature whereas the remainder of the ring is assumed

to be subject to this restraint; the total flexural rigidity is assumed to be the sum of the rigidities of the three sections.

$$\text{F.R.} = 2w_{\text{edge}}\frac{Et^3}{12} + (w - 2w_{\text{edge}})\frac{Et^3}{12(1-\nu^2)} \tag{5.5}$$

It is convenient now to define an effective second moment of area of the ring cross-section $I_{eff} = [2w_{edge} - (w - 2w_{edge})/(1-\nu^2)]t^3/12$ which takes account of the increased flexural rigidity of the (inboard) region of the ring assumed to be fully restrained. Equation (5.5) may now be used in Equation (5.2) by expressing the flexural rigidity F.R. as EI_{eff}. It is also possible to extend the model of the edge effects to consider the more general case where the ring is assumed to be homogeneous and specially orthotropic and the following expressions are derived in Sections B.1 and B.2 of Appendix B:

$$\delta_h = \frac{PR^3}{E_\theta I_{\text{eff}}}\left(\frac{2}{\pi} - \frac{1}{2}\right) + \frac{PR}{2AE_\theta}\left(1 - \frac{8}{\pi}\right) + \frac{2PI_{\text{eff}}}{\pi A^2 E_\theta R} + \frac{1.2PR}{2G_{\theta z}A} \tag{5.6}$$

$$\text{where:} \qquad I_{\text{eff}} = \left[2w_{\text{edge}} + \frac{w - 2w_{\text{edge}}}{1 - \nu_{x\theta}\nu_{\theta x}}\right]\frac{t^3}{12} \tag{5.7}$$

with w_{edge} defined in equation (5.4) and λ for the orthotropic case defined as:

$$\lambda = \sqrt[4]{\frac{E_\theta}{E_x}\frac{3(1-\nu_{x\theta}\nu_{\theta x})}{R^2t^2}} \tag{5.8}$$

The values of E_x, E_θ, $\nu_{\theta x}$ and $\nu_{x\theta}$ (for a many-layered laminate treated as a homogeneous orthotropic material) are obtained from the off-axis compliances of the unidirectional composite using a method described in Appendix B (Section B.3):

$$E_x = \frac{\bar{S}_{66}}{\bar{S}_{11}\bar{S}_{66} - \bar{S}_{16}^2} \quad \text{(a)} \qquad E_\theta = \frac{\bar{S}_{66}}{\bar{S}_{22}\bar{S}_{66} - \bar{S}_{26}^2} \quad \text{(b)}$$

$$\nu_{x\theta} = -\frac{\bar{S}_{12}\bar{S}_{66} - \bar{S}_{16}\bar{S}_{26}}{\bar{S}_{11}\bar{S}_{66} - \bar{S}_{16}^2} \quad \text{(c)} \quad \text{and} \quad \nu_{\theta x} = -\frac{\bar{S}_{12}\bar{S}_{66} - \bar{S}_{16}\bar{S}_{26}}{\bar{S}_{22}\bar{S}_{66} - \bar{S}_{26}^2} \quad \text{(d)} \qquad (5.9)$$

where (in this instance) the angle of the fibres to the axial or meridional (x) direction is used as the transformation angle when obtaining the off-axis compliances using equation (3.4)(a).

The theory described above treats the laminated ring as being made from an equivalent homogeneous orthotropic material. An alternative approach to the calculation of F.R. for Equation (5.2) uses the same method of correction for edge effects but employs classical lamination theory. In this case the flexural rigidities (with and without restraint against anticlastic curvature) and the radial stiffness of the laminated shell are obtained directly from the laminate compliance matrix. The following results are obtained in Section B.4. of Appendix B:

$$\text{F.R.} = \frac{2w_{edge}}{\delta_{22}} + (w - 2w_{edge})\left[\frac{\delta_{11}}{\delta_{11}\delta_{22} - \delta_{12}^2}\right] \qquad (5.10)$$

where w_{edge} is obtained using Equation (5.4) from the following value of λ:

$$\lambda = \sqrt[4]{\frac{\delta_{66}(\delta_{11}\delta_{22} - \delta_{12}^2)}{4R^2\delta_{22}(\alpha_{11}\delta_{66} - \beta_{26}^2)}} \qquad (5.11)$$

and where:

$$\begin{Bmatrix} \varepsilon_x^0 \\ \varepsilon_\theta^0 \\ \gamma_{x\theta}^0 \\ \kappa_x \\ \kappa_\theta \\ \kappa_{x\theta} \end{Bmatrix} = \begin{bmatrix} \alpha_{11} & \alpha_{12} & \alpha_{16} & \beta_{11} & \beta_{12} & \beta_{16} \\ \alpha_{21} & \alpha_{22} & \alpha_{26} & \beta_{21} & \beta_{22} & \beta_{26} \\ \alpha_{61} & \alpha_{62} & \alpha_{66} & \beta_{61} & \beta_{62} & \beta_{66} \\ \beta_{11} & \beta_{21} & \beta_{61} & \delta_{11} & \delta_{12} & \delta_{16} \\ \beta_{12} & \beta_{22} & \beta_{62} & \delta_{21} & \delta_{22} & \delta_{26} \\ \beta_{16} & \beta_{26} & \beta_{66} & \delta_{61} & \delta_{62} & \delta_{66} \end{bmatrix} \begin{Bmatrix} N_x \\ N_\theta \\ N_{x\theta} \\ M_x \\ M_\theta \\ M_{x\theta} \end{Bmatrix} \quad \text{or:} \quad \begin{Bmatrix} \{\varepsilon^0\} \\ \{\kappa\} \end{Bmatrix} = \begin{bmatrix} [\alpha] & [\beta] \\ [\beta]^T & [\delta] \end{bmatrix} \begin{Bmatrix} \{N\} \\ \{M\} \end{Bmatrix}$$

$$\text{where:} \quad \begin{bmatrix} [\alpha] & [\beta] \\ [\beta]^T & [\delta] \end{bmatrix} = \begin{bmatrix} [A] & [B] \\ [B] & [D] \end{bmatrix}^{-1} \qquad (5.12)$$

and:

$$\begin{Bmatrix} N_x \\ N_\theta \\ N_{x\theta} \\ M_x \\ M_\theta \\ M_{x\theta} \end{Bmatrix} = \begin{bmatrix} A_{11} & A_{12} & A_{16} & B_{11} & B_{12} & B_{16} \\ A_{12} & A_{22} & A_{26} & B_{12} & B_{22} & B_{26} \\ A_{16} & A_{26} & A_{66} & B_{16} & B_{26} & B_{66} \\ B_{11} & B_{12} & B_{16} & D_{11} & D_{12} & D_{16} \\ B_{12} & B_{22} & B_{26} & D_{12} & D_{22} & D_{26} \\ B_{16} & B_{26} & B_{66} & B_{16} & D_{26} & D_{66} \end{bmatrix} \begin{Bmatrix} \varepsilon_x^0 \\ \varepsilon_\theta^0 \\ \gamma_{x\theta}^0 \\ \kappa_x \\ \kappa_\theta \\ \kappa_{x\theta} \end{Bmatrix} \quad \text{or:} \quad \begin{Bmatrix} \{N\} \\ \{M\} \end{Bmatrix} = \begin{bmatrix} [A] & [B] \\ [B] & [D] \end{bmatrix} \begin{Bmatrix} \{\varepsilon^0\} \\ \{\kappa\} \end{Bmatrix} \qquad (5.13)$$

It was considered instructive to examine the relative significance of the four terms on the RHS of Equation (5.6) and to compare these with the results obtained from classical lamination theory. The values of the terms were calculated for a set of laminated rings of typical dimensions† and a variety of ply angles made from material with a representative set of properties (included in Table 5.1). These results are presented in Table 5.2. This analysis is also presented graphically (Fig. 5.2) in percentage form, illustrating the relative magnitude of the errors introduced by simplifying the model of the pinched ring. The worst errors (approximately 2%) occur for ply angles (to the direction of bending) of ±25°. These errors are mainly due to the artificial restraints against coupling effects which are applied when modelling the laminate as a homogeneous material. It was considered that errors of this magnitude are likely to be acceptable when compared with the practical scatter encountered in experimental results relating to composites.

---

† Inner diameter = 112mm, thickness = 2.8mm, width = 30mm, number of plies = 8.

5.3.2 *The use of pinched rings in the determination of elastic properties*

It may be observed from Table 5.2 that, for practical filament-wound rings, the homogeneous model with edge correction (taking account only of flexural deformation) agrees closely with more complex models. It may also be observed that if an estimate of I_{eff} is calculated using Equation (5.7) together with assumed values of elastic properties, the simplified form of Equation (5.6) may be differentiated and re-arranged to give a revised estimate of the laminate circumferential Young's modulus in terms of the deflection per unit load:

$$E_\theta = \frac{R^3}{I_{eff}} \frac{\left(\frac{2}{\pi} - \frac{1}{2}\right)}{\frac{d(\delta_h)}{dP}} \qquad (5.14)$$

If an accurate value of E_θ is to be calculated it is therefore necessary that I_{eff} should be estimated accurately from the assumed values of elastic properties. A sensitivity analysis has therefore been performed to establish the significance of errors in the assumed properties. A typical set of dimensions and properties was chosen and I_{eff} was calculated for the range of ply angles 0° – 90°. The calculation was repeated with each of the elastic moduli and ν_{12} altered in turn by ±10%. The results of this sensitivity analysis are plotted in Figs. 5.3 and 5.4; it will be observed that the effects upon I_{eff} of 10% errors in estimated elastic moduli E_1 and G_{12} are typically 1–1.5%; however, the sensitivity to errors in E_2 and ν_{12} is very much less. The errors in I_{eff} caused by inaccurate estimates of elastic moduli become insignificant where the ply angle approaches 0° or 90° (unidirectional material) and are at their worst for ply angles of around ±35°–45°. Even a radical change in the estimated value of E_2 to a very low value (typical of that chosen by curve-fitting in Section 5.8) results in a change in I_{eff} of approximately 2% at worst. (Fig. 5.3). It may be concluded that if realistic values of elastic properties are estimated, the use of proving rings provides a very simple and reasonably robust method of measuring actual values of Young's moduli of unidirectional and laminated composites.

5.3.3 *Design of specimens*

The dimensions and construction of the specimens were chosen as a compromise between the assumptions that the laminate was many-layered and thin with respect to its radius, and also took account of the availability of an existing mandrel for winding. The width of the rings (approximately 30mm) was chosen to be sufficiently narrow that a number of specimens could be cut from each tube manufactured. However, it appears reasonable to assume that they are sufficiently wide that any edge imperfections would have little effect on the stiffness of the ring.

The material chosen for the experimental investigations in this project was Silenka E-Glass rovings[111] (2400 TEX) reinforced with Scott Bader Crystic 272 isophthalic polyester resin[112]. The resin was used in conjunction with Scott Bader Catalyst Powder B (dibenzoyl peroxide dispersed in di-cyclohexyl phthalate). This is by far the most common fibre/matrix combination used at Nottingham since the materials are readily available, economical and straightforward in use. It was chosen for this project for these reasons and because experimental data on its material properties had already been collected during an earlier project[106], providing a set of data for comparison with any properties measured during this investigation.

5.3.4 *Manufacture of Specimens*

Specimens were wound on the Pultrex filament winding machine to the nominal winding angles of ±30°, ±45°, ±60°, ±75° and 90°. An attempt was made to wind specimens to ±15° but it was clear that the laminate was of poor quality (twisting or spinning of the fibre was taking place resulting in a rounded rather than flat tow) and would not have been representative of the normal laminate quality.

Considerable experimentation took place in establishing a good process method. Initial attempts produced rings which were cracked, delaminated and poorly wetted-out; the final method of manufacture included the use of Melinex mould-release film (rather than PVA or Würtz[113] release agents), newer batches of resin and hardener (old materials are more viscous and appear not to permeate the

roving adequately), painting of the mandrel with a layer of resin before winding, and the use of a diamond saw (driven by an air turbine) for slicing the specimens. The resulting specimens were of greatly improved quality compared with earlier rings. However, the appearance of the composite was still milky rather than clear. While this will be due in part to the differing refractive indices of the fibre and matrix, it is suspected that other reasons may be incomplete wetting-through of the fibre bundle and/or incomplete dissolution of the protective size on the fibres. There is a certain amount of voidage in the composite which becomes apparent when it is examined under a scanning electron microscope (Fig. 5.5). It may be concluded that although the specimens used were of the best quality available to the author, there is considerable room for improvement in the integrity of the composite and work is being planned to tackle this problem.

Two different mandrels were used. All of the specimens with nominal winding angles of 90° and ±75° and some of the specimens with a nominal winding angle of ±60° specimens were wound on a split cylindrical mandrel of 112mm diameter with flanged ends. This mandrel presented no problems in winding steep angles; the small change in fibre direction required to reverse the helix direction of the fibre at the mandrel ends was easily achieved by frictional steering. For shallow winding angles (±45° or less) the large change in fibre direction would have required far more space on the mandrel than was available. For this purpose a dome-ended cylindrical mandrel of the same diameter was manufactured. The domes provide a curved surface over which a geodesic path can reverse the helix direction of the fibre without problems.

The filament winding CNC part-programs were generated using the CADFIL I system. The post-processing options were chosen to make four of the machine axes active (*X*, *Y*, *A* and *B*; see Fig. 2.1). Where possible, a band-pattern number of 1 was used for the winding pattern, since this minimises the number of times the lamination sequence alternates around the mandrel. The mandrel was given four complete sets of windings or covers. Since each cover corresponds to two layers of opposite ply orientation (corresponding in turn to the outward and return movements of the payout eye along the mandrel) the resulting structure was an

eight-layered antisymmetric laminate. The nominally circumferential (hoop) windings give a ±89.2° laminate which is very close to being a unidirectional material. A list of all sets of specimens, and the programs, winding parameters and names, is given in Table 5.3. The winding of a typical specimen with ±60° nominal winding angle is shown in Fig. 5.6.

The wet-out parameters were kept constant for all the main series of specimens; the values were: machine speed 100%, fibre back tension setting 20psi (corresponding to a tension of 10N), doctor blade setting 0.20mm.

The turnaround regions covering the domed ends of the mandrel were removed where necessary by sawing them off with a turbine-driven diamond saw, and the tube was removed from the mandrel. The tube was sliced into rings by lining with plaster (to avoid tearing on breakthrough); again the diamond saw was used (Fig. 5.7).

5.3.5 *Test apparatus*

A diagram showing the experiment is shown in Fig. 5.8 and photograph in Fig. 5.9. The basic test equipment consisted of Instron 1193 and 1195 universal testing machines modified to provide direct electrical output of load cell amplifier signal and fitted with a 50kN tension and compression load cell. This load cell was the most sensitive compression cell available. The rings were compressed between a pair of platens. To maximise the sensitivity of the machine, a Solartron digital voltmeter sensitive to 0.01 mV was used to monitor the load cell amplifier output. Sensitivity to 0.1 N was available by use of the 1kN range on the load cell amplifier in conjunction with the DVM. Further resolution was made impractical by electrical noise on the signal. Calibration was achieved electrically using features available in the load cell circuitry. Checks of the resulting accuracy using calibration weights gave varying errors of approximately 1–2%. The reading at zero load was found to drift typically by 0.3N (sometimes of up to 1N) during some tests.

Deflections were measured using dial test indicators mounted on magnetic stands. These were set to within 1mm of the centre height of the rings and aligned as accurately as possible with each other using a straightedge. Sensitivity of the gauges was 0.005mm if care was taken.

5.3.6 *Test procedure*

The apparatus was connected up, alignment of the dial gauges was checked and the apparatus switched on and allowed to warm up for at least an hour. The load cell was calibrated electrically immediately before the first test and at intervals during a laboratory session, a small amount of sensitivity drift (typically 0.1%) being apparent. Checks with calibration weights were carried out on initial setup to ensure that no significant calibration errors were present.

Cured polyester resin is believed to have a tendency to absorb moisture from the air, so every effort was made to keep the specimens in a dry atmosphere before use. Where possible they were stored in a desiccator for approximately five days, otherwise they were kept in a warm oven (40°C) for a similar period before being allowed to cool before the test.

Each ring was carefully aligned in the test rig and was initially loaded to cause around 3mm total diametral deflection in the transverse direction. The load was left in place for approximately one minute then removed; it was found that this pre-loading procedure helped to reduce the amount of hysteresis in the load-deflection graphs. For reasons that will be discussed in Section 5.7.6, the author now believes this procedure to have been misguided and if similar experiments are to be performed a monotonically increasing loading procedure is to be preferred.

The load cell circuitry was then zeroed and the load-deflection characteristics measured by incrementally increasing the load on the ring and measuring the horizontal deflections using the dial gauges. It was found that the viscoelasticity of the rings caused some time-dependent drift (typically 1N) in the readings of

load, and this was largely overcome by slightly overshooting each load setting before backing off and taking the reading. Full load varied between the different ring specifications, but generally corresponded to a diametral deflection totalling 2–3mm.

The dimensions and masses of each ring were measured. Slight variations in thickness inevitably occurred around and across each ring in addition to the surface irregularities caused by the bundled nature of the fibres. A number of measurements were therefore taken of both the peak thickness (using a micrometer with a ball anvil on the inside and a flat anvil on the outside of the ring) and the trough thickness (using a two-ball micrometer for the hoop wound specimens which had no sharp changes in thickness, and a point micrometer for the angle-wound specimens where narrow troughs did occur). The fibre content of each specimen was estimated using a burnoff procedure based upon BS2782[114].

5.3.7 *Processing of data*

To minimise the effects of experimental scatter it was considered advisable to test a substantial number of specimens, and the correspondingly large amount of experimental data justified the writing of a considerable amount of data analysis software. The function of each program is described in Section C.2 of Appendix C; it is sufficient here to state that the programs perform various calculations upon the measured dimensions and theoretical winding angle, perform a linear regression upon the displacement-load data, calculate the circumferential Young's modulus of the ring using equation (5.14), and perform a normalisation of these calculated values of Young's modulus to take account of variations in fibre content. The normalisation process makes use of the Halpin-Tsai equations[25] (equations (5.1)(a–d)) and assumes the fibre and matrix properties listed in Table 5.4. The output from this suite of programs is a list of data points (one for each specimen) of Young's modulus and ply angle.

5.3.8 *Results of pinched ring experiments*

It will be readily appreciated that the volume of results obtained from the programme of materials testing exceeds that which can reasonably be included in this thesis. Sample observations are presented in Appendix D and the results calculated from these will be summarised in this chapter.

Figs D.1 to D.5 (in Appendix D) illustrate how the transverse diameter of the rings change with varying load. It will be observed that for the rings with winding angles of ±30°, ±45° and ±60° there is significant hysteresis visible in the results, although for the rings with steeper winding angles (±75° – hoop) this is much less apparent.

The results of the pinched ring experiments are summarised in Table 5.5 and are included in Fig. 5.10 as a scatter plot of Young's modulus vs. ply angle. A word of warning is necessary here: the ply angle of the laminate, measured with respect to the loading direction, should not be confused with the winding angle measured with respect to the winding machine axis. For axially-loaded tubes they are equal; for all other specimens their sum is 90°. It will immediately be noted that for ply angles of 60° the values of Young's modulus estimated using this experimental method are very low compared with the kind of values that might have been expected from typical unidirectional properties (such as those estimated from the work of Weatherby or using the Halpin-Tsai equations (5.1)) given in Table 5.1. No satisfactory explanation was forthcoming for these results and it was decided to design another testing procedure which could be performed upon the same specimens to verify or refute the results obtained.

5.4 The roller-assisted split disc method

5.4.1 *Background*

A well-established method for determining the ultimate tensile stress of filament-wound composite materials involves the tensile testing of ring-shaped specimens using a pair of dee-shaped half-mandrels which are pulled apart.. These

specimens are often known as NOL (Naval Ordnance Laboratory) rings. This method is formalised in the standard ANSI/ASTM D2290[115], which also covers the testing of ring-shaped specimens made from thermoplastic tube. Although the method is unsuitable for the determination of stress-strain properties[116] it was realised that if friction between the ring and the two halves of the split disc (the "dees") could be reduced to a low level, such an application would be feasible.

5.4.2 *Description of method*

A partly-sectioned view of the rig is shown in Fig. 5.11, and a photograph in Fig. 5.12. The basic design of the rig closely follows that defined in the standard D2290-76[115] for the testing of thermoplastic tubes, but with an important difference. Instead of the dees being made a close fit directly into the ring, they are manufactured so that a set of needle rollers (manufactured in this instance from silver steel) may be inserted between the ring and the dees. Thus the ring becomes the outer race and the dees become the inner race of a needle roller bearing, conceptually reducing the friction between ring and dees to a negligible value. In practice it will be realised that Hertzian deformation of the rollers and surfaces (along with the fact that the composite material is not perfectly elastic), together with irregularities on the surface of the composite, will mean that the effective friction, though small, will not be as small as in a true needle roller bearing. In addition, there is of course no "rolling element" effect in the transverse direction so there may be some frictional restraint against the Poisson's ratio effect. In order to reduce frictional effects the specimens were sprayed with "Sprayflon" PTFE spray and allowed to dry before use.

The dimensions of the rings were chosen so that a satisfactory number of specimens could be obtained from tubes wound upon an existing mandrel; the diameter of the mandrel (including mould release film) was 112.1mm and the width of rings chosen was 30mm (identical to those used for the pinched ring tests).

5.4.3 *Theoretical justification and accuracy of method*

It is commonly assumed that the traditional method of inducing circumferential stress into a thin cylindrical shell (namely internal hydrostatic pressurisation, with pistons restraining the pressurised fluid) will induce an almost uniform strain throughout the thickness of the shell. This assumption was examined geometrically and it was found that, for a cylinder of the dimensions under consideration (diameter 112mm, thickness 2.8mm) the ratio of circumferential strain at the inside surface to that on the outside is 1.05 (refer to Appendix E). By contrast, the split disc method described here produces uniform circumferential strain throughout the cross-section of the ring.

It was considered necessary to calculate the localised bending effects due to the separation of the dees as the load is applied. If the curvature of the specimen is neglected, it may be considered as a beam of known flexural rigidity and subjected to a known tension, mounted on an elastic foundation consisting of the rollers which are closely spaced and in line contact with the beam. It can be shown (Appendix F) using contact mechanics[117] together with beam-on-elastic-foundation theory[118] that the errors due to localised effects will become very small over a distance of approximately 14mm from the split line, and die away to a negligible value approximately 19mm from the split line; this is borne out by the fact that over most of the circumference the burnishing effect of the rollers on the lubricant-sprayed surface appeared to be of similar degree at all points away from the split line.

The validity of the comparison between the flexural and tensile experiments should be explained in the light of the well-known tendency for antisymmetric angle-ply laminates to twist under tensile loading. This effect was discussed in Section 3.3 and illustrated in Fig. 3.1. This behaviour is described mathematically using classical lamination theory by the fact that the terms β_{16}, β_{26}, β_{61} and β_{62} are non-zero for an antisymmetric angle-ply laminate. If the laminate is subjected to restraint against twisting while being loaded (instead of being subjected to a purely tensile load) the modulus of the material will appear to be greater than that

measured without the restraint. As the number of pairs of layers becomes large, the tendency to twist (and the effect of the restraint) decreases to zero; it would be found that a laminate with very many thin layers under pure tension would give the same results as for a laminate with a few thick layers subjected to a restraint against twisting. In the roller-assisted split disc method, the specimen is held (by its own tension) into a twist-free cylindrical form; thus the laminate is fully restrained against twist and behaves as a many-layered laminate.

Under flexural loading, an antisymmetric angle-ply laminate does not exhibit any tendency to twist (δ_{16}, δ_{26}, δ_{61} and δ_{62} are all zero); it does exhibit a slight tendency to deform in an in-plane shearing mode (once again, β_{16}, β_{26}, β_{61} and β_{62} are non-zero). This degree of freedom is not restrained in the proving ring experiment and so the results are not (in theory) identical to those which would be obtained from a many-layered laminate; however calculations suggest that the effect is negligible (e.g. 1.4% difference for a ±30° laminate with typical orthotropic properties and 8 layers) compared with the kind of scatter typically observed in measurements on composite materials.

5.4.4 *Apparatus*

An Instron 1193 universal testing machine was used to provide the load; the load-measuring arrangements were identical to those used for the pinched ring tests except that a 25kN load cell (fitted with a universal joint linkage) was used.

A low-cost solution to the datalogging requirements was found by constructing a simple IBM-PC-based datalogger including data collection hardware manufactured by CIL and Amplicon. Some additional circuitry was manufactured containing the bridge completion resistors and shunt calibration resistors, and a large program (ALPHALOG) was written in Microsoft QuickBasic to provide control and data handling (Fig. 5.13). This system fulfilled all the requirements of the experiments and included facilities for programmable gauge supply voltages and very simple and rapid calibration; no problems were encountered in its use for the split disc and axial compression experiments. Throughout the

experiments, the three-wire method[119] was used to connect the gauges into quarter-bridge circuits. The bridges were balanced with high-stability 120Ω resistors. An important feature of the system was that power was supplied to the strain gauges only while a reading was being taken, minimising the heat generated within the gauge. This precaution is particularly necessary with non-metallic specimens including GRP because of their poor thermal conductivity, since large spurious readings can be caused by thermal drift.

5.4.5 *Procedure*

In all cases, the rings were stored either in a desiccator or a warm oven for several days prior to testing so as to avoid the presence of excessive moisture in the material.

Strain was measured using electrical resistance strain gauges mounted on the outer surface of the specimen. Gauges were applied both in the circumferential direction and in the meridional direction so as to be able to estimate both E_θ and $\nu_{\theta r}$. Polyester-backed gauges manufactured by TML[120] were used. Gauges of type FLA-30-11 (30mm gauge length) were used in the circumferential direction, giving sufficient length to minimise the effects of localised inhomogeneities; the transverse gauges were of type FLA-10-11 (10mm gauge length) to fit within the width of the specimen. The thermal characteristics of the gauges were arbitrarily chosen to match those of mild steel; it would not have been feasible to choose gauges to match the thermal characteristics of the variety of laminates under consideration. The effects of thermal drift were therefore minimised by energising the gauges only when necessary for reading, and by carrying out the tests in a temperature-controlled room. After considerable experimentation the decision was taken to use Loctite Multibond 330 acrylic adhesive with Loctite 738 activator[121]. Care was taken when carrying out the experiments to orientate the specimen so that the strain gauges were well away (typically 20mm) from the split line to avoid any localised bending effects.

The split disc apparatus was partially dismantled by removing the shackles and unscrewing the cover plates from one side of the dees. The specimen was then placed over the dees and a piece of card placed in the split line. The rollers were placed one-by-one in the annular gap between the dees and the specimen, the card forming a means of preventing the rollers from chasing around the annular gap. When all the rollers had been inserted the cover plates were screwed back into place and the rig assembled in its shackles.

The split disc apparatus was loaded by placing it in the Instron machine; universal joints and ball joints were used above and below the apparatus to ensure that it was loaded in pure tension without any transverse bending moments. Electrical connections to the datalogger were made at this stage.

The specimens were loaded incrementally until a maximum strain of around 3000 με was measured. Because filament-wound GRP exhibits considerable viscoelasticity, especially when wound as an angle-ply laminate, a deliberate policy was adopted of overshooting the value of load for each reading. This helped to bring the material nearer to its steady-state condition and reduce the amount of viscoelastic relaxation of the load during the reading of the gauges. The procedure adopted (which in retrospect was probably misguided) was that the rings were loaded and unloaded at least once before the readings were taken. This bedded the rings into position in the rig and also appeared to reduce the amount of hysteresis in the readings; the explanation for this will be discussed in Section 5.7.6.

5.4.6 *Results*

Typical graphs of strain vs. load are presented in Figs. D6 – D10 (Appendix D). Linear regression on the results was performed, although the points in the graphs corresponding to the taking-up of slack were ignored for the purposes of the regression. Data processing programs written in FORTRAN are described in Section C3 of Appendix C, and the results of the calculations are summarised in Table 5.6. The transverse strains are used to estimate the Poisson's ratio of the

angle-ply laminates in Table 5.7. A graph of the normalised values of Young's modulus vs. ply angle is presented in Fig. 5.14, and a graph of Poisson's ratio vs. ply angle is presented in Fig. 5.15.

5.5 Axial compression tests

5.5.1 *Description of test*

Because of the practical difficulties of manufacturing filament-wound tubes with very shallow winding angles, an alternative method of loading was devised for obtaining properties of the laminate for ply angles approaching ±90°. This involved subjecting filament-wound tubes to uniform axial compression to measure values of compressive Young's Moduli. Some overlap was provided between the ply angles covered by the split disc and axial compression to enable the estimated values of moduli to be compared. Specimens wound at nominal angles of ±60°, ±75° and 90° (hoop) were manufactured, and gauges of type FLA-30-11 were bonded to the specimen (using Loctite 330/738[121]) in an axial direction and (in the case of the hoop-wound specimens) a circumferential direction.

To ensure that the axial load was applied as concentrically as practically possible, machined end plates were manufactured which enabled the specimen to be loaded between centres, i.e. between conical anvils, in the Instron machine. A sectional view of the apparatus is shown in Fig. 5.16 and a photograph in Fig. 5.17. The specimen length (110mm) was chosen so that any transverse restraint provided by the plates would have negligible effect upon the strains observed in the central region of the specimen. Winding details are summarised in Table 5.8.

5.5.2 *Procedure and results*

The specimens were incrementally loaded to 20kN using the procedure already described for the split disc specimens; full load corresponded to strains of typically 2000–3000 με. Typical graphs of strain vs. load are presented in Appendix D (figs. D.11 – D.13). The data was processed using FORTRAN

programs described in Section C.4 of Appendix C, and the results are summarised in Table 5.9. The calculation of Poisson's ratio for the hoop wound specimens is included in Table 5.7. Young's modulus and Poisson's ratio are plotted along with the results of the split disc tests in Figs 5.14 and 5.15.

5.6 Discussion of results from direct loading tests (split disc and axial compression)

The overall trends shown by these results are in good agreement with the results obtained by Weatherby[106] and by the author in Section 5.3. However, a number of differences are may be observed. Firstly, it may be observed by comparing Figs. 5.10 and 5.14 that the Young's moduli of the split disc (tension) specimens for ply angles of ±60° have even lower values than those calculated from the pinched ring tests; by contrast, for the same ply angle the Young's moduli from the compression tests are considerably higher in value. An equally unexpected result is that the ±75° compression specimens show considerably lower values of Young's moduli than the hoop wound (90°) specimens (Fig. 5.14).

It was observed from the results from the hoop-wound specimens that a small amount of shearing appeared to have occurred between the gauges and the specimens; this was observed as slight negative "hysteresis" with the unloading curve recording smaller strains than the loading curve. This is clearly visible on Figs D.10 (a and b) in Appendix D. This effect was attributed to the use of stale adhesive but was considered to have an insignificant effect upon the gradient of the straight line fitted to the recorded points.

Some surprising results emerging from the split disc tests are those relating to the ply angles of 0° (measurement of E_1) and ±15°. The Young's Moduli (50–61 GNm^{-2}) measured for the nominal ply angle of 0° are considerably higher than the value of E_1 predicted from fibre and matrix properties via the Halpin-Tsai equations (46 GNm^{-2}). Similarly the Young's moduli measured for the ±15° laminate (43–45 GNm^{-2}) are not as far below than the predicted value of E_1 as might be expected from classical theory.

Errors in assumed fibre properties have been discounted since E-glass has consistent properties even between different manufacturers. Errors in matrix properties would have little effect upon E_1. Errors in the values of fibre fraction measured by the burnoff test appear unlikely since very similar values were estimated by independent means described in Appendix C (Section C.2.1). Experimental error remained a possibility and verification of these results using a more conventional test of E_θ appeared desirable.

At this stage the results suggested either that the tensile transverse Young's modulus of filament-wound GRP was very much lower under practical situations than conventional estimates (such as those obtained by Weatherby[106] and those obtained by direct loading in compression) would suggest, or that classical orthotropic theory provided a poor prediction of the behaviour of laminates with ply angles approaching 90°. No more rigorous explanation was found until close to the end of the investigation when the opportunity arose to perform a more conventional test of material properties, namely the open-ended pressure test. The opportunity to perform this test arose from discussions with Mr P.D.W. Soden at UMIST regarding the unexpected results obtained from the pinched ring test. The pressure test also provided an opportunity to verify some of the other unexpected results obtained.

5.7 Open-ended pressure test

5.7.1 *Description and sources of error*

The objective of this experiment is to produce within the walls of a thin tube-shaped specimen a purely circumferential stress by means of hydraulic pressure. The test is often referred to as the open-ended burst test but the term pressure test is used in this context since specimen failure was not generally sought. The hydraulic fluid is retained within the specimen by pistons in its ends; these pistons are assumed to provide a frictionless seal (Fig. 5.18). Radial stress (numerically equal to the pressure) and the effects of the finite value of wall thickness contribute to small errors in the stresses and strains calculated using simple theory; some of these errors have already been discussed in Section 5.4.3.

Average values of stress are easily calculated knowing specimen dimensions and hydraulic pressure, and strains are measured using electrical resistance strain gauges.

In practice the pistons are a sliding fit in the ends of the specimens and the seal is provided by means of O-rings. Under conditions of zero hydraulic pressure the forces required to overcome friction between piston and specimen are small (a few tens of Newtons) but when the system is pressurised the friction forces are likely to be higher as the O-ring is pressed against the inside surface of the specimen with a contact pressure of the same order of magnitude as the hydraulic pressure. However, if the pistons and rings are well-lubricated then the coefficient of friction is likely to be low (less than 0.1). Since the area of contact of the O-ring with the specimen is likely to be (at worst) only around 10% of the piston area, it seems reasonable to assume that any end-load applied to the specimen will only be in the order of 1% of the force opposed by the piston.

5.7.2 *Manufacture of specimens*

The specimens were manufactured, as in previous cases, using the 5-axis filament winding machine and the same programs as previously for the ply angles down to ±30°. Although earlier attempts had clearly shown the manufacture of ±15° specimens to be impractical with the available equipment, a successful attempt was made to manufacture ±20° specimens although the winding quality was noticeably more uneven than for the higher values of winding angle and successive fibres needed to be more closely spaced to avoid gaps between fibres. The winding details are summarised in Table 5.10. The end regions of the specimens were heavily reinforced with circumferential fibres to prevent excessive change in diameter of the tube with consequent piston leakage. Diameter change under pressure was thus limited to around 0.03mm, a figure easily accommodated by the O-ring seals.

The same fibre and resin were used as for the earlier specimens but the process parameters were changed slightly since the wound material was judged to be excessively "dry" in appearance: the doctor blade setting was opened up from 0.2mm to 0.32mm, causing the composite to be slightly more resin-rich than that produced on previous occasions.

Four strain gauges of type FLA-30-11 were bonded to each specimen (two circumferential, two axial). Two strain gauges on each specimen (one in each direction) were bonded using freshly-purchased Loctite 330/738[121]; the others were bonded using a two-part epoxy strain gauge adhesive (TML EA2[120]) necessitating clamping the gauges onto the specimens (using G-clamps and wooden saddles with closed-cell sponge as a clamping medium) during the curing of the adhesive. The use of the two types of adhesive provided a verification that the suspected shearing of the Loctite adhesive was of no practical significance for fresh adhesive, while saving considerable time compared with using the EA2 adhesive for all the gauges.

Because of the potentially hostile environment of hydraulic fluid, all gauges were protected with a coating of TML N2 neoprene rubber[120]. Fig. 5.19 shows a typical set of strain gauges bonded to the specimen and protected with this coating.

5.7.3 *Apparatus*

The experiment was carried within the laboratories of the Applied Mechanics Division of the Department of Mechanical Engineering, UMIST, Manchester, where a rig exists for open-ended pressure testing to be carried out. A photograph of a typical specimen in the rig is shown in Fig. 5.20. The pistons with O-rings were manufactured to a general design recommended by UMIST. The rig provided axial restraint for the pistons. The hydraulic pressure was supplied by means of a manually-operated pump and was measured with a pressure transducer which was calibrated immediately before the experiment using a dead-weight calibration rig. The experimental readings of pressure and strain

were recorded automatically on a Schlumberger Orion 3530 datalogging system; output was obtained in the form of hard copy.

5.7.4 *Procedure*

Because of the size of the specimens and the need to transport them to Manchester it was not feasible to store them in a desiccator or an oven as had been possible with the earlier specimens. Each specimen was assembled with both pistons and filled with Shell Tellus hydraulic oil (grade 37). The assembly was placed in the loading rig with the lower piston supported on a flat platen and the upper piston centrally loaded by means of a steel ball placed in a countersunk hole. The hydraulic supply and transducer were connected to the specimen and the datalogger leads soldered onto the gauge terminal pads. The datalogger was supplied with the calibration constant of the pressure transducer and the gauge factor of the gauges (2.12 in all cases) and was programmed to record readings of strain and pressure whenever the pressure changed by a certain increment (typically 5 or 10 psi depending upon the specimen). The pressure was applied slowly by manual pumping until the desired level of strain (typically 2000 με) and was then released by means of a bleed valve. All but one of the specimens were subjected to at least two tests; the test on one specimen ended in failure of the gauges on the specimen due to errors in operating the rig.

The thicknesses of the specimens were measured using a dial caliper. This has one approximately spherical anvil and one roller anvil, making the measurement of peak thickness very simple; a second spherical anvil was improvised so that trough thicknesses could also be measured. The resin-rich nature of the specimens meant that none (except to some extent the ±20° specimens) had any sharp fluctuations in thickness, enabling a two-ball measurement system to be justified for estimating the trough thicknesses. Errors inherent in the dial caliper were estimated at ±0.02mm, an insignificant figure compared with the variation in material thickness of typically 0.15 mm. Burnoff tests[114] were carried out upon the specimens to determine the fibre content of the composite.

5.7.5 *Results*

The observations of pressure and strain were entered manually into a spreadsheet on a personal computer from the datalogger printout and the pressures were converted from Imperial units (psi) to bar. The results were then transferred to the ICL VME mainframe computer where they were processed using FORTRAN programs described in Appendix C (Section C.5). The strain-pressure relationship was calculated using two alternative rules: the first was a linear regression of the points corresponding to increasing load in the first test on each specimen (concentrating on the approximately linear region of the strain-pressure curve if significant non-linearities occurred); the second was a linear regression on the results for the whole of a subsequent loading cycle.

The results of the calculations of Young's modulus are presented in Tables 5.11 and 5.12 and included in Figs. 5.14 and 5.21; the calculations of Poisson's ratio are presented in Table 5.13 and included in Fig. 5.15. These results should be interpreted in the light of the following discussion.

5.7.6 *Discussion of open-ended pressure test results*

The results from the open-ended pressure tests are in good general agreement with other comparable results including those from reference 106 and Sections 5.3, 5.4 and 5.5. Where the results of the open-ended pressure tests (for the repeated loading cycle) overlap with the split disc results, it is found that agreement is generally close at least for the ply angles up to ±45° (Fig. 5.14). The values from the pressure test are a few percent greater and this is largely explained by the fact that the circumferential strain at the outer surfaces of the tubes is 5% lower than at the inner surface and hence 2.5% lower than the average circumferential strain. Calculations based upon strains accurately measured at the outside will therefore overestimate E_θ by 2.5%. Surprise was expressed in Section 5.5 at the high values of circumferential Young's modulus measured using the split-disc method, especially those relating to ply angles of 0° and ±15°. While the results from the pressure tests do not offer an explanation of these results they do suggest that experimental error was not the cause. The reason for the discrepancies in the

earlier estimates of Young's moduli for laminates with high values of ply angle (>45°) became apparent to the author during the processing of the results of the open-ended pressure tests. It was noticed that although the results obtained for the specimens wound at ±60° and ±75° (ply angles of ±30° and ±15° respectively) were repeatable within a few percent between successive tests, very significant changes were found between the results of successive tests on the remaining specimens (especially those with winding angles of ±30° and ±20°). Examination of the strain-pressure graphs for these specimens revealed that even fairly moderate values of strain such as 2000 με (which are insufficient to cause departures from linearity for laminates with smaller values of ply angle) cause not only nonlinearity but a permanent change in elastic properties of laminates with large ply angles. This change in properties is observed on the strain-pressure graphs as a large hysteresis loop. Within these, the points corresponding to loading lie close to a line with significantly different gradient from those corresponding to unloading. Repeated cycling of the load will result in an asymptotic set of elastic properties being approached but these will correspond to a much more compliant material than existed before loading took place. Thus the properties measured by the pinched ring and split disc tests were probably realistic estimates of the properties of a material following repeated flexural and tensile loading but were quite inaccurate estimates of the properties of the material under its first monotonically-increasing loading cycle. The non-linearity of the material behaviour under such an increasing load is vividly illustrated (as a conventional plot of stress vs. strain) in Fig. 5.22. Strain levels in the pinched rings reach peaks of around ±4000 με at the loads and ±900 με at each side, so material damage will occur locally in the regions of the loads leading to some degree of hinging. It is suggested that inherent weaknesses in the material (discussed in Section 5.3.4) may be partly responsible for the ease with which material damage occurs. The mechanism of this damage has not been investigated but it is likely to consist of matrix micro-cracking or degradation of the fibre/matrix bond. It may be concluded that the cycling of the load in the proving ring, split disc and axial compression tests prior to the measurement of the material properties was misguided even though it did result in improved linearity and reduced hysteresis in the results.

The next section discusses an attempt to use the properties of the angle-ply laminates to obtain estimates of the properties of the unidirectional composite material. It is noteworthy that unidirectional properties fitted to the results obtained from the first test on each of the open-ended pressure specimens are the only ones which have realistic values as well as yielding predicted values of laminate properties which are a close fit to the experimental values.

5.8 Fitting of theoretical equations to experimental data

5.8.1 *Theory*

It has been shown in Section 5.3 that if a laminated proving ring has many layers and is therefore assumed to have homogeneous specially orthotropic properties, the circumferential Young's modulus E_θ may be calculated from the stiffness and dimensions of the ring. E_θ may also be calculated from the off-axis compliance matrix of the unidirectional composite. Equations (3.4)(a) and (b) are normally used to calculate the off-axis properties of a composite from an assumed (or previously-estimated) set of on-axis material properties, but on this occasion an attempt has been made to calculate these properties from the behaviour of the angle-ply laminated rings. It was considered that inadequacies in the assumptions underlying equations (3.4), and in particular the use of unidirectional test data as the basis of laminate calculations, might be a significant source of error when these equations are invoked during a finite element analysis. To overcome this problem it was decided to obtain the values of the material properties which are known to give the correct values of in-plane Young's modulus for the laminate, even if the values obtained do not precisely agree with those measured in uniaxial tests.

To achieve this, it was noted that the circumferential Young's modulus of the filament-wound rings may be expressed as a non-linear function $\mathscr{F}$ of the four on-axis compliances and the ply angle to the circumferential direction ϕ:

$$(E_\theta)_i = \frac{\bar{S}_{66}}{\bar{S}_{11}\bar{S}_{66} - \bar{S}_{16}^2} = \mathscr{E}(S_{11}, S_{12}, S_{22}, S_{66}, \phi_i) \quad (5.15)$$

Thus for every individual ring i, a function f_i may be defined which (if the value of E_θ agrees precisely with the theoretical value) will be equal to zero:

$$f_i(S_{11}, S_{12}, S_{22}, S_{66}) = \mathscr{E}(S_{11}, S_{12}, S_{22}, S_{66}, \phi_i) - (E_\theta)_i \quad (5.16)$$

Where E_θ is measured experimentally, it will not be precisely equal to the function $\mathscr{E}$ (because of experimental error and inadequacies in the theory) and hence the function f_i, known as the residual, will take a small but finite value.

Experimental data may be made available which will give the measured values of E_θ for a large number of rings having a variety of winding angles. There may therefore be stated a large number of simultaneous nonlinear equations in four unknowns (the compliances S_{ij}), and the algorithm for finding the optimal solution is to choose the combination of S_{ij} such that the sum of squares of the residuals is minimised:

$$\text{Minimise } F(S_{11}, S_{12}, S_{22}, S_{66}) = \sum_{i=1}^{m} [f_i(S_{11}, S_{12}, S_{22}, S_{66})]^2 \quad \text{where } m \geq n \quad (5.17)$$

This is achieved using the subroutine E04GEF in the NAG FORTRAN library[122]; this is an implementation of a modified Gauss-Newton algorithm for finding an unconstrained minimum of a sum of squares of m nonlinear functions in n variables where $m \geq n$.

In the example under consideration, it was found that the system of simultaneous equations was ill-conditioned with respect to the variable S_{12}, i.e. small errors or discrepancies in the supplied data will lead to drastic variations in the "optimised" value of S_{12}. This problem was overcome by making use of the fact that $S_{12} = -\nu_{12} S_{11}$ and choosing a value for ν_{12} from existing data (such as tensile tests).

It was found the actual value of ν_{12} chosen made no significant difference to the optimised values of the three remaining independent variables.

Although the method described was derived independently by the author, a recent paper by Al-Salehi et al[123] describes methods for fitting linear and non-linear material models to the behaviour of laminates. This paper includes a review of the (very limited) literature relevant to their technique but there is no duplication of the method described above.

5.8.2 *Results*

The normalised values of Young's modulus obtained from the pinched ring, split disc/axial compression and open-ended pressure test were all used (separately) as the input data for fitting of unidirectional properties. The results of the fitting are tabulated in Table 5.1 for comparison with the "nominal" properties assumed for the sensitivity analysis. The fitted properties were used in turn to predict the theoretical relationships between ply angle and laminate Young's modulus for each set of data (using equation (5.9)(a)) and these curves are superimposed on Figs. 5.10, 5.14 and 5.21. Similarly, a theoretical relationship for Poisson's ratio is superimposed upon Fig. 5.15. The results relating to a number of pinched ring specimens were omitted from the input data to the fitting procedure. In some cases this was because the results were found to lie well away from the overall trend and caused problems in the convergence of the fitting procedure. In other cases the rings were inaccurately manufactured and hence unrepresentative.

5.8.3 *Discussion of results obtained from fitting procedure*

The fitting procedure appears to perform its task effectively and to produce useful results. The only major problem encountered was the ill-conditioning with respect to S_{12} and this was overcome by applying a constraint to this value. With this problem solved, it was found that a curve could be fitted to most sets of data without difficulty. Some editing of outlying data was sometimes necessary to achieve satisfactory convergence to realistic results.

Some differences are observed between the properties fitted to the different sets of data. It will be observed that the values of longitudinal Young's modulus E_1 calculated during the optimisation vary with a range of about 20%. The flexural (pinched ring) tests yield results for E_1 which are lower than those from the tests based upon tensile stress (the split disc and pressure tests). This would appear to be because the compressive longitudinal Young's modulus of the composite in question is known to be considerably less than the tensile modulus[106]. The apparent value of E_1 measured in flexure will lie approximately midway between these values. The values of E_1 fitted to the split disc and pressure test data agree closely with each other but are rather higher than expected. The problem of high measured values of E_1 has already been discussed in Sections 5.6 and 5.7.6 and no further explanation is apparent.

It may be observed from Fig. 5.21 that the theoretical curve fitted to the points from the open-ended pressure specimens subjected to monotonically-increasing pressure fits passes through all the relevant clusters of points. This contrasts with the curves fitted to the other sets of data (Figs. 5.10 and 5.14) where the best-fit curves do not follow so closely the data to which they have been fitted. Despite the high value of E_1 obtained from the pressure tests, this suggests that if the material is tested in a manner which allows its behaviour to remain linear, satisfactory prediction of laminate behaviour can be obtained from the orthotropic material model.

The theoretical curve of Poisson's ratio fitted to the split disc and axial compression test data may be seen to agree closely with all the available measured values except in two cases (Fig. 5.15). Of particular interest is that the data for ν_{21} directly measured from the axial compression tests lies well away from the curve; this is because the measured values of ν_{12} and ν_{21} (averages 0.1952 and 0.1105) are in quite a different ratio from the measured values of E_1 and E_2 (averages 54849 MNm^{-2} and 15136 MNm^{-2} respectively). By contrast, the orthotropic material model defined in equation (3.1) assumes these ratios to be equal. These specimens appeared to behave in a much more linear manner than

most of the angle-ply specimens and would be expected to exhibit good agreement with theory. Disagreement between the theoretical curve and the measured data is also observed for a ply angle of ±30°. No explanation can be found for these discrepancies except that the orthotropic material model is unreliable for the material under test.

The values of transverse Young's modulus E_2 fitted to the different sets of data varied from around 2582.9 MNm^{-2} (pinched ring) to around 15398 MNm^{-2} (open-ended pressure test). The reason for this is that the pinched ring tests included repeated loading causing some degree of material damage whereas the values fitted to the open-ended pressure test results are based upon the initial loading cycle before any change in material properties has occurred.

5.9 Conclusions

Two loadcases have been developed as tests of material properties by means of enhancements to the experimental and analytical techniques involved. Analysis has shown that (for a well-behaved material) the errors inherent in the methods are limited to a few percent. Experimental results obtained, however, show a considerable degree of scatter and non-linearity. There is some disagreement between the results obtained using the different methods and some clear inconsistencies with the orthotropic material model. It may be concluded that filament-wound glass-reinforced polyester resin obeys the overall trends predicted by classical theory. However there is sufficient disagreement within the results to suggest that for future projects involving theoretical modelling a more well-behaved (linear elastic) material should be chosen for the experimental aspects of the work. It is suggested that epoxy resins (for example) should be examined to find a matrix material which satisfies both the need for linear elastic behaviour and for ease of use in filament winding.

Of particular interest to the industrialist is the need for adequate and consistent product quality. The ease with which material damage occurs, and the appearance of the specimens, suggests that specimen quality was barely acceptable despite

considerable effort to avoid problems. Work currently being planned to improve the relevant areas of manufacturing quality is therefore likely to be of considerable benefit.

Table 5.1: Unidirectional orthotropic properties: nominal values, values calculated using Halpin-Tsai equations and values fitted to experimental data

Property and units	Nominal values used for sensitivity analyses	Theoretical values from Halpin-Tsai equations for 78% fibre by mass		Estimated from Weatherby[106] (for 73-75% fibre by mass)	Unidirectional properties fitted to results for angle-ply laminates (normalised to 78% fibre by mass)		
		E_2 using ξ = 2	E_2 using ξ = 0.2		Pinched ring tests	Split disc & axial compression tests	Open-ended pressure tests
E_1 (MNm^{-2})	50000	46891.1	46891.1	28500-49000	44592.8	54105.5	55265.2
E_2 (MNm^{-2})	10000	15945.2	9512.8	8000-12000	2582.9	11219.9	15398.6
G_{12} (MNm^{-2})	5000‡	4679.3	4679.3	5000	5137.8	2740.3	4135.7
ν_{12}	0.3	0.28011	0.28011	0.32	0.3 (assumed)	0.1952†	0.1952†

† The value of 0.1952 was obtained from the directly-measured values of strain for the hoop-wound split disc specimens, the raw values being normalised to 78% and averaged. It was then assumed during the fitting of the unidirectional properties to the laminate data.

‡ This value was also used for $G_{\theta z}$ for the error analysis in Fig. 5.2 and Table 5.2.

Table 5.2: Comparison of terms in equation (5.6) for orthotropic pinched ring

Ply angle (±degrees)	Effect on transverse diametral deflection δ_h (mm) for load W=1N					Total deflection of homo-geneous ring δ_h (mm)
	$\frac{WR^3}{FR}\left(\frac{2}{\pi}-\frac{1}{2}\right)$		$\frac{WR}{2AE_\theta}\left(1-\frac{8}{\pi}\right)$ (effect of axial compression)	$\frac{2WI_{eff}}{\pi A^2 E_\theta R}$ (effect of curvature on flexural rigidity)	$\frac{1.2WR}{2G_{\theta z}A}$ (shear deformation)	
	FR=$E_\theta I_{eff}$ (homogeneous)	FR from Eq.(5.10) (CLT)				
0	0.00932	0.00932	-0.00001	0.174×10^{-8}	0.000082	0.009392
10	0.009881	0.00982	-0.00001	0.186×10^{-8}	0.000082	0.009891
20	0.011759	0.011594	-0.00001	0.235×10^{-8}	0.000082	0.011662
30	0.01578	0.015541	-0.00002	0.346×10^{-8}	0.000082	0.015604
40	0.023138	0.022894	-0.00003	0.523×10^{-8}	0.000082	0.022947
50	0.032968	0.032811	-0.00004	0.697×10^{-8}	0.000082	0.032853
60	0.041104	0.041046	-0.00005	0.803×10^{-8}	0.000082	0.04108
70	0.045281	0.045268	-0.00005	0.848×10^{-8}	0.000082	0.045299
80	0.046715	0.046713	-0.00005	0.861×10^{-8}	0.000082	0.046743
90	0.047003	0.047003	-0.00005	0.864×10^{-8}	0.000082	0.047032

Table 5.3: Details of winding patterns and mandrels for pinched ring/roller-assisted split disc specimens

Nominal winding angle (and specimen numbers) (±deg)		Mandrel type All cases: Ø112mm without film Ø112.1mm with film	Part program name	Nominal diameter of mesh (mm)	Progr'n factor	Winding angle (degrees) (before applying progression factor)	Bandwidth (mm)	Band pattern No.	Total number of cycles	Cycles per cover (nom'l)
30		Dome-ended	DCYL112M.PRG	114.8	0.9918	±30.14	4.5	2	282	70
45		Dome-ended	DCYL112F.PRG	114.8	1.0188	±45.135	4.5	1	228	57
60	spec'ns 4 & 5	Split	SPLTCYL5.PRG	114.5	1.0292	±59.57	4.5	1	160	40
	spec'n 7	Dome-ended	DCYL112Q.PRG	114.8	0.9768	±60.66	4.5	1	160	40
75		Split	SPLTCYL7.PRG	114.5	1.0268	±75.19	4.5	1	80	20
90		Split	SPLITCYL.HOP	n/a		90 nom'l	5.0			

Table 5.4: Fibre and matrix properties assumed for Halpin-Tsai calculations (including normalisation)

Component of composite material	Fibre		Matrix	
Name of component material	E-glass		Scott Bader Crystic 272 polyester resin	
Material properties	Value	Source of value	Value	Source of value
Young's modulus (MNm^{-2})	73000	Silenka data sheet	3500	Scott Bader data sheet
Poisson's ratio	0.22	Vetrotex data sheet	0.38	Average for polyester resin from Banks[124]
Specific gravity (no units) ≈ density ($g\ cm^{-3}$)	2.56	Fibreglass Ltd data sheet	1.2	Scott Bader data sheet

Table 5.5: Observations and results from tests on pinched rings

Nominal winding angle (±deg)	Specimen number	Ring number	Width (mm)	Average thickness (mm)	Mid-surf. dia. (mm)	True winding angle (±deg)	Ply angle to circumf'l direction (±deg)	% Fibre (by mass)	Defl. per unit load (mm/N)	Raw Young's modulus (MNm^{-2})	Young's modulus (MNm^{-2}) normalised to 78% fibre (by mass) with 95% conf. limits		
											Best fit	Lower limit	Upper limit
Hoop	5	1	31.5	2.48	114.58	89.204	0.796	77.46	0.01448	43870.4	44353.3	44170.3	44537.8
	5	3	31.45	2.442	114.542	89.204	0.796	77.46	0.01496	44500.7	44990.5	44810.8	45141.4
	5	4	31.15	2.426	114.526	89.204	0.796	77.46	0.01507	45472.4	45972.9	45820.9	46125.9
	5	5	31.36	2.453	114.553	89.204	0.796	77.46	0.01492	44162.9	44649	44499.9	44829.3
	6	2	30.8	2.521	114.621	89.204	0.796	76.58	0.01433	43216	44479.4	44324.7	44666.4
	6	7	29.75	2.528	114.628	89.205	0.795	76.58	0.01473	43184.5	44447	43998.8	44935
	7	1	31.15	2.421	114.521	89.204	0.796	77.91	0.01482	46520.1	46605	46448.3	46762.8
	7	2	31.3	2.427	114.527	89.204	0.796	77.91	0.01468	46399.2	46483.9	46326.1	46642.7
	7	3	31.1	2.422	114.522	89.204	0.796	77.91	0.0151	45676	45759.4	45578.2	45972.5
	7	4	31.3	2.44	114.54	89.204	0.796	77.91	0.01505	44554.9	44636.2	44458.9	44785
	7	5	31.07	2.406	114.506	89.204	0.796	77.91	0.01558	45181.8	45264.3	45061.8	45497.9
	7	6	30.35	2.378	114.478	89.203	0.797	77.91	0.0155	48124.2	48212	47995.2	48430.7
	7	7	30.55	2.432	114.532	89.204	0.796	77.91	0.01518	45703	45786.4	45576.2	45998.5
	13	1	30.235	2.524	114.624	89.205	0.795	76.08	0.0148	42482.6	44171.4	43845.6	44471.9
	13	2	30.335	2.549	114.649	89.205	0.795	76.08	0.01458	41757	43417	43209.6	43596.4
	13	5	29.97	2.497	114.597	89.204	0.796	76.08	0.01542	42454.8	44142.5	43355.3	44959
	13	6	30.44	2.564	114.664	89.205	0.795	76.08	0.01473	40486.3	42095.8	41925	42239.2
	13	7	29.55	2.551	114.651	89.205	0.795	76.08	0.01536	40603.7	42217.9	41999.1	42438.9
	13	8	30.275	2.54	114.64	89.205	0.795	76.08	0.01541	39999.1	41589.2	41401.1	41806.3
	14	1	28.65	2.476	114.576	89.204	0.796	76.91	0.01625	43212.9	44179	43935.7	44397.6
	14	2	29.75	2.452	114.552	89.204	0.796	76.91	0.01565	44450.2	45444	45299.2	45618.9
	14	4	30.3	2.487	114.587	89.204	0.796	76.91	0.01533	42735.5	43690.9	43492.4	43920.1
	14	7	30.3	2.517	114.617	89.204	0.796	76.91	0.01523	41530.6	42459.1	42182.1	42711.5
	14	8	30.27	2.495	114.595	89.204	0.796	76.91	0.01484	43776.6	44755.3	44575.1	44967.3
75	1	2	30.94	2.741	114.841	75.601	14.399	77.65	0.01183	40054.2	40354.7	40185	40560.5
	1	3	31.28	2.732	114.832	75.6	14.4	77.65	0.01259	37576.3	37858.3	37324.7	38407.3
	1	4	31.02	2.713	114.813	75.598	14.402	77.65	0.01229	39622	39919.3	39597.1	40246.7
	1	5	31.23	2.751	114.851	75.602	14.398	77.65	0.01202	38634.1	38924	38698.6	39152
	2	1	30.24	2.781	114.881	75.606	14.394	79.04	0.01228	37868.5	37035.2	36825.2	37278
	2	2	30.2	2.686	114.786	75.595	14.405	79.04	0.01269	40607.5	39713.8	39526.9	39902.5
	2	3	30.42	2.681	114.781	75.594	14.406	79.04	0.0126	40815.9	39917.6	39665.8	40204.7

Table 5.5 (cont)

Nominal winding angle (±deg)	Specimen number	Ring number	Width (mm)	Average thickness (mm)	Mid-surf. dia. (mm)	True winding angle (±deg)	Ply angle to circumf'l direction (±deg)	% Fibre (by mass)	Defl. per unit load (mm/N)	Raw Young's modulus (MNm^{-2})	Young's modulus (MNm^{-2}) normalised to 78% fibre (by mass) with 95% conf. limits		
											Best fit	Lower limit	Upper limit
75	2	4	30.15	2.685	114.785	75.595	14.405	79.04	0.01249	41372.8	40462.3	40300.9	40657.6
	2	5	30.31	2.639	114.739	75.589	14.411	79.04	0.01286	42031.5	41106.4	40915.5	41299.1
60	4	2	30.98	2.876	114.976	60.387	29.613	78.77	0.01232	31476.9	30826.9	30383	31309.7
	4	3	30.92	2.691	114.791	60.348	29.652	78.77	0.01757	26758.6	26205.6	25593.8	26831.8
	4	4	29.18	2.687	114.787	60.347	29.653	78.77	0.01922	26215.4	25673.6	25214.5	26149.9
	4	5	29.17	2.723	114.823	60.354	29.646	78.77	0.01918	25297.6	24774.9	24268.8	25289.1
	5	2	31.14	2.852	114.952	60.382	29.618	77.95	0.01458	27086.2	27122.6	26737.5	27499.8
	5	3	31.1	2.692	114.792	60.348	29.652	77.95	0.01806	25836.7	25871.5	25310.8	26457.5
	5	4	31.01	2.713	114.813	60.352	29.648	77.95	0.01767	25908.9	25943.8	25341.5	26575.4
	5	5	31.18	2.756	114.856	60.362	29.638	77.95	0.01569	27722.8	27760.1	27188.2	28374.9
	7	3	30.34	2.779	114.879	60.099	29.901	76.45	0.01837	23819.1	24823.3	24542.7	25124.1
	7	4	30.18	2.724	114.824	60.087	29.913	76.45	0.01849	25207.4	26270.3	25906.1	26645.1
	7	5	30.27	2.753	114.853	60.094	29.906	76.45	0.01893	23806.5	24810.2	24499.6	25128.8
	7	6	30.29	2.761	114.861	60.095	29.905	76.45	0.01936	23068.1	24040.7	23661.7	24419
	7	7	30.35	2.767	114.867	60.097	29.903	76.45	0.01931	22933.5	23900.4	23415.3	24405.9
	7	8	30.33	2.761	114.861	60.095	29.905	76.45	0.01963	22717	23674.8	23341.8	24017.3
	7	9	30.37	2.771	114.871	60.097	29.903	76.45	0.01907	23109.1	24083.4	23600.7	24599.3
	7	10	30.15	2.79	114.89	60.101	29.899	76.45	0.01964	22184.8	23120	22681.2	23564
45	2	2	30.42	2.883	114.983	45.714	44.286	76.08	0.02418	16283.6	17340.9	17010.2	17684.6
	2	3	30.175	2.82	114.92	45.699	44.301	76.08	0.02601	16270.1	17326.6	16828.5	17855.3
	2	4	30.4	2.791	114.891	45.691	44.309	76.08	0.03033	14238.8	15163.5	14717.1	15637.8
	2	5	30.3	2.806	114.906	45.695	44.305	76.08	0.02906	14695.7	15650	15185	16138.7
	2	6	30.33	2.842	114.942	45.704	44.296	76.08	0.02873	14321.5	15251.5	14843.4	15682.8
	2	7	30.23	2.812	114.912	45.696	44.304	76.08	0.03027	14062.4	14975.6	14524.5	15450.2
	2	8	30.425	2.851	114.951	45.706	44.294	76.08	0.02774	14645.7	15596.7	15202	16006.4
	2	9	30.26	2.847	114.947	45.705	44.295	76.08	0.02828	14517.5	15460.2	15019.4	15921.8
	3	2	30.32	2.894	114.994	45.717	44.283	75.61	0.02572	15204.7	16433.5	15943.8	16954.2
	3	4	30.385	2.759	114.859	45.683	44.317	75.61	0.02973	15016.3	16230.2	15656.2	16853.8
	3	5	30.36	2.763	114.863	45.684	44.316	75.61	0.02992	14874.7	16077.2	15562.1	16627.3
	3	7	30.31	2.774	114.874	45.687	44.313	75.61	0.02932	15039.3	16255	15776.1	16763.9
	3	8	30.32	2.766	114.866	45.685	44.315	75.61	0.02833	15686.2	16954.3	16460.4	17472.3

Table 5.5 (cont)

Nominal winding angle (±deg)	Specimen number	Ring number	Width (mm)	Average thickness (mm)	Mid-surf. dia. (mm)	True winding angle (±deg)	Ply angle to circumf'l direction (±deg)	% Fibre (by mass)	Defl. per unit load (mm/N)	Raw Young's modulus (MNm^{-2})	Young's modulus (MNm^{-2}) normalised to 78% fibre (by mass) with 95% conf. limits		
											Best fit	Lower limit	Upper limit
45	3	9	30.23	2.807	114.907	45.695	44.305	75.61	0.02883	14839.2	16038.7	15558.4	16555.5
	3	10	30.325	2.885	114.985	45.715	44.285	75.61	0.02655	14856.6	16057.3	15616.2	16517.7
	3	11	30.29	2.946	115.046	45.73	44.27	75.61	0.02227	16718.4	18069.3	17900.5	18249.6
30	1	2	30.34	2.784	114.884	29.954	60.046	77.31	0.1242	3714.5	3805.3	3444.2	4250.9
	1	3	30.22	2.764	114.864	29.949	60.051	77.31	0.11923	3967.8	4064.7	3596.6	4672.9
	1	5	30.325	2.802	114.902	29.958	60.042	77.31	0.13137	3449	3533.3	3132.4	4051.7
	1	6	30.38	2.796	114.896	29.956	60.044	77.31	0.10239	4443.9	4552.5	4065.3	5172.3
	1	7	30.34	2.79	114.89	29.955	60.045	77.31	0.10113	4533.7	4644.5	4183.6	5219.4
	1	8	30.29	2.777	114.877	29.952	60.048	77.31	0.09879	4712.5	4827.6	4434.4	5297.3
	1	10	30.235	2.792	114.892	29.955	60.045	77.31	0.09039	5081.1	5205.2	4815.8	5663.9
	1	11	30.33	2.769	114.869	29.95	60.05	77.31	0.08035	5833.9	5976.4	5585.1	6426
	1	12	28.4	2.79	114.89	29.955	60.045	77.31	0.06004	8202.7	8403.1	7956.5	8904.4
	2	1	28.51	2.752	114.852	29.947	60.053	77.26	0.06057	8424.4	8645.1	8241.1	9090.9
	2	2	30.33	2.747	114.847	29.946	60.054	77.26	0.06618	7247.9	7437.8	7069.2	7848
	2	3	30.27	2.746	114.846	29.945	60.055	77.26	0.07137	6742.4	6919	6500.1	7394.6
	2	5	30.29	2.757	114.857	29.948	60.052	77.26	0.07517	6323.6	6489.3	6089.9	6944.8
	2	6	30.345	2.747	114.847	29.946	60.054	77.26	0.06878	6970.1	7152.7	6727.2	7634.4
	2	7	30.4	2.774	114.874	29.951	60.049	77.26	0.06864	6776.7	6954.2	6601.3	7348.2
	2	8	30.33	2.776	114.876	29.952	60.048	77.26	0.07186	6475.9	6645.6	6289.4	7045.6
	2	10	30.19	2.755	114.855	29.947	60.053	77.26	0.08008	5969.8	6126.2	5715.1	6601
	2	11	30.32	2.768	114.868	29.95	60.05	77.26	0.07234	6489	6659	6287	7078.8

Table 5.6: Observations and results from tests on rings subjected to roller-assisted split disc test

Nominal winding angle (±deg)	Specimen number	Ring number	Width (mm)	Average thickness (mm)	Mid-surf. dia. (mm)	True winding angle (±deg)	Ply angle to circumf'l direction (±deg)	% Fibre (by mass)	Strain per unit load ($\mu\varepsilon kN^{-1}$)	Raw Young's modulus (MNm^{-2})	Young's modulus (MNm^{-2}) normalised to 78% fibre (by mass) with 95% conf. limits		
											Best fit	Lower limit	Upper limit
Hoop	13	5	29.97	2.497	114.597	89.204	0.796	76.08	120.291	55543.1	57751.1	56750	58788.2
									132.022	50607.9	52619.8	51609.8	53669.9
	13	6	30.44	2.564	114.664	89.205	0.795	76.08	121.404	52768.6	54866.4	54055	55702.4
									132.399	48386.1	50309.6	49875.2	50751.8
	13	7	29.55	2.551	114.651	89.205	0.795	76.08	127.313	52098.9	54170	53697.8	54650.6
									138.103	48028.5	49937.8	49328.9	50562
	14	4	30.3	2.487	114.587	89.204	0.796	76.91	121.177	54755.9	55980.1	55436.6	56534.3
									123.377	53779.4	54981.7	53988.4	56015
	14	7	30.3	2.517	114.617	89.204	0.796	76.91	118.648	55256.6	56491.9	55421.5	57604.5
									109.189	60043.3	61385.7	60533.1	62262.6
75	1	3	31.28	2.732	114.832	75.6	14.4	77.65	136.682	42806.7	43127.9	43014.5	43241.9
									131.478	44501	44834.9	44716.2	44954.3
	1	4	31.02	2.713	114.813	75.598	14.402	77.65	133.563	44482.7	44816.5	44723.6	44909.8
									131.986	45014.3	45352.1	45171.3	45534.3
	2	3	30.42	2.681	114.781	75.594	14.406	79.04	134.376	45624	44619.9	44513.6	44726.7
									140.307	43695.4	42733.7	42670.3	42797.3
60	4	4	29.18	2.687	114.787	60.347	29.653	78.77	230.081	27716.4	27143.6	26063	28317.7
									231.088	27595.6	27025.3	25875.8	28281.8
	5	3	31.1	2.692	114.792	60.348	29.652	77.95	214.94	27785.4	27822.8	26937.4	28768.4
									213.779	27936.4	27974	27019.6	28998.3
	7	6	30.29	2.761	114.861	60.095	29.905	76.45	253.282	23604.7	24599.9	23666.1	25610.5
									284.087	21045.2	21932.5	20690	23333.7
45	2	6	30.33	2.842	114.942	45.704	44.296	76.08	725.108	7999.6	8519.1	7353.5	10123.9
									699.636	8290.9	8829.3	7650.5	10437.4
	3	5	30.36	2.763	114.863	45.684	44.316	75.61	611.75	9743.5	10531.2	9480.6	11843.5
									632.945	9417.2	10178.5	9187.7	11408.7
	3	7	30.31	2.774	114.874	45.687	44.313	75.61	632.424	9403.1	10163.2	9040.9	11603.7
									524.541	11337	12253.5	11097.3	13678.5
30	1	6	30.38	2.796	114.896	29.956	60.044	77.31	2157.649	2728.1	2794.8	2524.5	3129.8
									2264.361	2599.6	2663.1	2402.7	2986.7

Table 5.6 (cont.)

Nominal winding angle (±deg)	Specimen number	Ring number	Width (mm)	Average thickness (mm)	Mid-surf. dia. (mm)	True winding angle (±deg)	Ply angle to circumf'l direction (±deg)	% Fibre (by mass)	Strain per unit load ($\mu\varepsilon kN^{-1}$)	Raw Young's modulus (MNm^{-2})	Young's modulus (MNm^{-2}) normalised to 78% fibre (by mass) with 95% conf. limits		
											Best fit	Lower limit	Upper limit
30	1	7	30.34	2.79	114.89	29.955	60.045	77.31	1926.664	3065.8	3140.7	2811.7	3556.9
									2233.839	2644.2	2708.8	2430.1	3059.9
	2	3	30.27	2.746	114.846	29.945	60.055	77.26	1149.619	5232.4	5369.5	5021.9	5768.9
									1516.8	3965.8	4069.7	3790.2	4393.8
	2	6	30.345	2.747	114.847	29.946	60.054	77.26	923.157	6497.5	6667.7	6194	7220
									2697.598	2223.6	2281.9	2014.6	2630.7

Table 5.7: Calculation of Poisson's ratio for rings subjected to roller-assisted split disc test and tubes subjected to axial compression

Specimen description and section	Ply angle to load (± deg.)	Longitudinal strain ε_1 per unit load ($\mu\varepsilon$ kN^{-1})		Transverse strain ε_2 per unit load ($\mu\varepsilon$ kN^{-1})		Poisson's ratio ν_{12} of laminated composite	
		Measured	Average	Measured	Average	Raw	Norm'd
±30° no. 1 ring 6	60.044	2157.649 2264.361	2211.01	-566.833 -1150.548	-858.69	0.388	0.387
±30° no. 1 ring 7	60.045	1926.664 2233.839	2080.25	-721.534 -1105.069	-913.30	0.439	0.437
±30° no. 2 ring 3	60.055	1149.619 1516.800	1333.21	-607.616 -489.442	-548.53	0.411	0.409
±30° no. 2 ring 6	60.054	923.167 2697.598	1810.38	-472.050 -703.587	-587.82	0.325	0.324
±45° no. 2 ring 6	44.296	725.108 699.636	712.37	-486.123 -533.223	-509.67	0.716	0.704
±45° no. 3 ring 5	44.316	611.750 632.945	622.35	-389.312 -370.512	-379.91	0.610	0.597
±45° no. 3 ring 7	44.313	632.424 524.541	578.48	-474.181 -289.991	-382.09	0.661	0.647
±60° no. 4 ring 4	29.653	230.081 231.088	230.58	-137.724 -136.617	-137.17	0.595	0.602
±60° no. 5 ring 3	29.652	214.940 213.779	214.36	-106.093 -128.613	-117.35	0.547	0.548
±60° no. 7 ring 6	29.905	253.282 284.087	268.68	-176.452 -182.416	-179.43	0.668	0.655
±75° no. 1 ring 3	14.400	136.682 131.478	134.08	-45.600 -44.207	-44.90	0.335	0.334
±75° no. 1 ring 4	14.402	133.563 131.986	132.77	-41.779 -44.336	-43.06	0.324	0.323
±75° no. 2 ring 3	14.406	134.376 140.307	137.34	-44.297 -45.877	-45.09	0.328	0.333
Hoop spec. no.13 ring 5	0.796	120.291 132.022	126.16	-26.191 -20.195	-23.19	0.184	0.181
Hoop spec. no.13 ring 6	0.795	121.404 132.340	126.87	-27.808 -26.905	-27.36	0.216	0.213
Hoop spec. no.13 ring 7	0.795	127.313 138.103	132.71	-26.603 -21.987	-24.30	0.183	0.180
Hoop spec. no.14 ring 4	0.796	121.177 123.377	122.28	-22.465 -24.579	-23.52	0.192	0.190
Hoop spec. no. 14 ring 7	0.796	118.648 109.189	113.92	-28.513 -20.244	-24.38	0.214	0.212
Hoop tube no. 1 sect. 2	89.204	-73.831 -75.708	-74.77	9.210 9.321	9.27	0.124	0.124
Hoop tube no. 2 sect. 1	89.203	-81.595 -75.117	-78.36	8.365 6.965	7.67	0.098	0.097

Table 5.8: Details of winding patterns and mandrels for compression specimens

Nominal winding angle (±deg)	Mandrel type All cases: Ø112mm without film Ø112.1mm with film	Part program name	Nominal diameter of mesh (mm)	Progr'n factor	Winding angle (degrees) (before applying progression factor)	Bandwidth (mm) (before applying progression factor)	Band pattern	Total number of cycles	Cycles per cover (nominal)
60	Dome-ended	DCYL112Q.PRG	114.5	0.9768	±60.66	4.5	1	160	40
75	Dome-ended	DCYL75A.PRG	114.5	1.0033	±75.11	4.5	1	80	20
90	Split	SPLITCYL.HOP	n/a		90.0 nom'l	5.0			

Table 5.9: Observations and results from tests on tubes subjected to axial compression

Nominal winding angle (±deg)	Tube specimen number	Tube section number	Width (mm)	Average thickness (mm)	Mid-surf. dia (mm)	True winding angle = ply angle to meridional direction (±deg)	% Fibre (by mass)	Strain per unit load ($\mu\varepsilon kN^{-1}$)	Raw Young's modulus (MNm^{-2})	Young's modulus (MNm^{-2}) normalised to 78% fibre (by mass) with 95% conf. limits		
										Best fit	Lower limit	Upper limit
Hoop	1	1	109.65	2.425	114.525	89.204	77.91	72.439	15822.2	15870.1	15791.2	15949.7
								74.13	15461.3	15508.1	15399.9	15617.7
	1	2	109.62	2.452	114.552	89.204	77.91	73.831	15349.2	15395.7	15307.9	15484.4
								75.708	14968.7	15014	14884.9	15145.5
	2	1	109.83	2.369	114.469	89.203	78.97	81.595	14385.9	13913.2	13700.6	14132.5
								75.117	15626.3	15112.9	14988.6	15239.3
75	1	1	110.05	2.577	114.677	75.142	79.35	139.832	7702.9	7344	7030.5	7686.6
								131.008	8221.7	7838.6	7506	8202.2
	1	2	109.55	2.606	114.706	75.145	79.35	121.093	8793.7	8384	8049.6	8747.3
								122.303	8706.7	8301	7959.8	8672.9
	1	3	109.96	2.615	114.715	75.146	79.35	119.955	8845.8	8433.6	8067.4	8834.7
								118.118	8983.5	8564.9	8204	8959
	1	4	109.865	2.586	114.686	75.143	79.35	114.614	9364.3	8928	8612.3	9267.7
								114.31	9389.2	8951.7	8666.1	9256.7
60	1	1	110.04	2.682	114.782	60.078	77.84	82.185	12581.3	12652.7	12256.9	13074.9
								94.066	10992.2	11054.6	10649.4	11491.9
	1	2	109.76	2.67	114.77	60.076	77.84	89.927	11551	11616.6	11248.4	12009.7
								89.699	11580.3	11646	11293.3	12021.5
	1	3	109.975	2.687	114.787	60.079	77.84	90.158	11446.8	11511.8	11197.1	11844.8
								92.284	11183.1	11246.6	10949.8	11559.8

Table 5.10: Details of winding patterns and mandrels for open-ended pressure specimens

Nominal winding angle (±deg)	Mandrel type All cases: Ø112mm (no film used)	Part program name	Nominal diameter of mesh (mm)	Progr'n factor	Winding angle (degrees) (before applying progression factor)	Bandwidth (mm) (before applying progression factor)	Band pattern	Total number of cycles	Cycles per cover (nominal)
20	Dome-ended	DCYL20.PRG	114.8	1.0099	±20.51	3.5	3	400	100
30	Dome-ended	DCYL112M.PRG	114.8	0.9918	±30.14	4.5	2	282	70
45	Dome-ended	DCYL112F.PRG	114.8	1.0188	±45.135	4.5	1	228	57
60	Dome-ended	DCYL112Q.PRG	114.8	0.9768	±60.66	4.5	1	160	40
75	Dome-ended	DCYL75A.PRG	114.8	1.0033	±75.11	4.5	1	80	20

Table 5.11: Observations and results from pressure tubes for initial (monotonically increasing) loading

Pressure tube specimen number	Nominal winding angle (±deg)	Average thickness (mm)	Mid-surface diameter (mm)	True winding angle (±deg)	Ply angle to cicumf'l direction (±deg)	% Fibre (by mass)	Strain per unit pressure ($\mu\varepsilon$ bar^{-1})	Raw Young's modulus (MNm^{-2})	Young's modulus (MNm^{-2}) normalised to 78% fibre (by mass) with 95% conf.limits		
									Best fit	Lower limit	Upper limit
8	20	3.713	115.713	20.846	69.154	74.94	135.26	11150.5	12317.3	11650.8	13061.5
							136.481	11050.7	12207	11647.5	12823
10	20	4.072	116.072	20.905	69.095	70.31	122.361	11239.2	14126.1	13953.8	14303.2
							121.368	11331.2	14241.7	14076.7	14410.6
1	30	2.948	114.948	29.967	60.033	72.23	154.963	12258.4	14717.9	13578.1	16066.3
6	30	2.851	114.851	29.947	60.053	74.68	172.644	11377.3	12702.2	12097.3	13370.6
							169.337	11599.5	12950.3	12411.3	13538.1
2	45	2.919	114.919	45.698	44.302	74.17	205.688	9327.1	10535.1	9747.6	11461.1
							185.273	10354.8	11695.9	10908.4	12606
7	45	2.911	114.911	45.696	44.304	74.31	140.963	13647.1	15350	14859	15874.9
							142.226	13525.9	15213.7	14720.2	15741.5
3	60	2.788	114.788	60.079	29.921	76.1	77.352	25967.1	27311.4	27042.8	27585.2
							78.76	25502.9	26823.1	26519.4	27134.2
9	60	3.032	115.032	60.132	29.868	72.13	71.618	25789.1	29982.5	29724	30258.1
							72.888	25339.8	29460.2	29197.4	29727.3
4	75	2.942	114.942	75.174	14.826	72.14	44.798	42490	48149.3	48091.3	48207.5
							45.935	41438.3	46957.6	46800.6	47116.5
5	75	2.938	114.938	75.186	14.814	71.68	45.434	41952.3	48007.2	47958.6	48055.9
							45.963	41469.4	47454.6	47349.6	47561.3

Table 5.12: Observations and results from pressure tubes for repeated loading cycle

Pressure tube specimen number	Nominal winding angle (±deg)	Average thickness (mm)	Mid-surface diameter (mm)	True winding angle (±deg)	Ply angle to cicumf'l direction (±deg)	% Fibre (by mass)	Strain per unit pressure ($\mu\varepsilon$ bar^{-1})	Raw Young's modulus (MNm^{-2})	Young's modulus (MNm^{-2}) normalised to 78% fibre (by mass) with 95% conf.limits		
									Best fit	Lower limit	Upper limit
8	20	3.713	115.713	20.846	69.154	74.94	314.806	4790.9	5292.2	4049.5	7635.6
							282.578	5337.3	5895.8	4498.4	8552.9
10	20	4.072	116.072	20.905	69.095	70.31	130.335	10551.6	13261.9	12878.3	13669.2
							126.359	10883.6	13679.1	13363	14010.8
6	30	2.851	114.851	29.947	60.053	74.68	315.522	6225.3	6950.2	6406.7	7594.5
							288.502	6808.4	7601.2	7062.1	8229.5
2	45	2.919	114.919	45.698	44.302	74.17	172.007	11153.4	12597.9	11788.1	13527.3
							157.724	12163.4	13738.8	13028.7	14530.8
7	45	2.911	114.911	45.696	44.304	74.31	140.435	13698.4	15407.7	14739.9	16139.1
							142.015	13546	15236.3	14600.4	15930.3
3	60	2.788	114.788	60.079	29.921	76.1	73.078	27485.8	28908.7	28570.5	29255
							74.141	27091.7	28494.2	28125.8	28872.4
9	60	3.032	115.032	60.132	29.868	72.13	69.284	26657.9	30992.6	30708	31282.9
							70.015	26379.6	30669	30330.3	31014.9
4	75	2.942	114.942	75.174	14.826	72.14	44.804	42484.3	48142.9	48073.2	48211.8
							46.152	41243.4	46736.7	46610.5	46864.6
5	75	2.938	114.938	75.174	14.826	71.68	45.121	42243.3	48340.8	48296.8	48385.8
							45.663	41741.9	47767	47717.8	47817.2

Table 5.13: Calculation of Poisson's ratio for open-ended pressure tube specimens

Pressure tube specimen number	Nominal winding angle (±deg)	Ply angle to circumf'l direction (±deg)	Circumferential strain ε_θ per unit pressure ($\mu\varepsilon$ bar^{-1})		Meridional strain εx per unit pressure ($\mu\varepsilon$ bar^{-1})		Poisson's ratio $\nu\theta x$ of laminated composite	
			Measured	Average	Measured	Average	Raw	Normalised
8	20	69.154	135.260	135.871	-21.793	-21.995	0.162	0.161
			136.481		-22.196			
10	20	69.095	122.361	121.865	-20.123	-20.205	0.166	0.162
			121.368		-20.286			
1	30	60.033	154.963	154.963	-41.311	-41.886	0.270	0.263
					-42.461			
6	30	60.053	172.644	170.991	-49.532	-48.252	0.282	0.278
			169.337		-46.971			
2	45	44.302	205.688	195.481	-129.868	-124.348	0.636	0.616
			185.273		-118.827			
7	45	44.304	140.963	141.595	-88.423	-89.201	0.630	0.611
			142.226		-89.979			
3	60	29.921	77.352	78.056	-55.703	-55.287	0.708	0.691
			78.76		-54.87			
9	60	29.868	71.618	72.253	-47.983	-49.505	0.685	0.644
			72.888		-51.026			
4	75	14.826	44.798	45.367	-19.179	-18.822	0.415	0.391
			45.935		-18.465			
5	75	14.826	45.434	45.699	-17.434	-18.310	0.401	0.376
			45.963		-19.186			

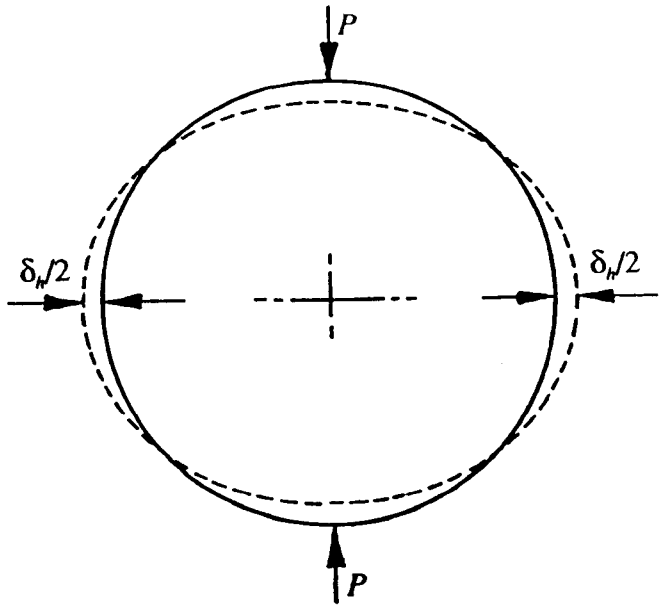

Fig. 5.1: Ring subjected to vertical pinching load P undergoing change δ_h in transverse (horizontal) diameter

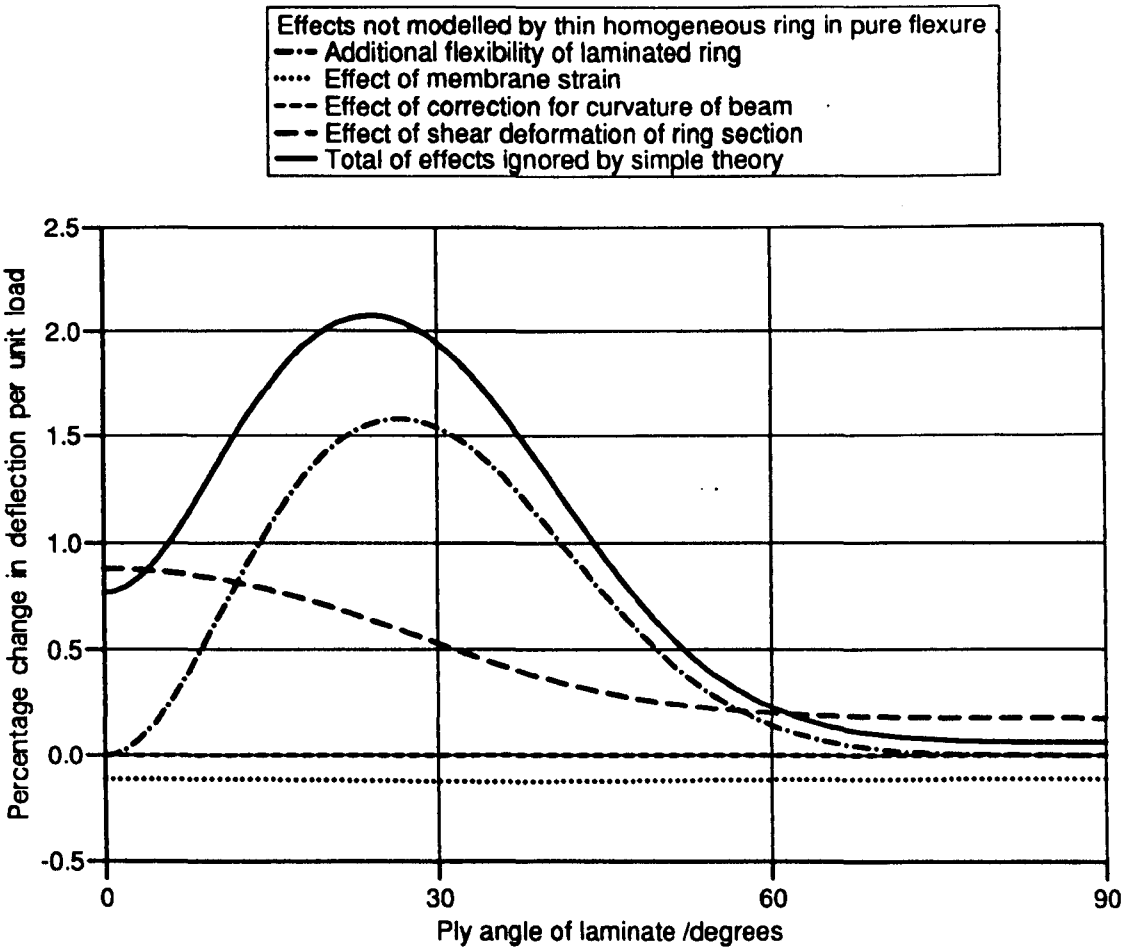

Fig. 5.2: Effects of simplifications made in modelling of laminated orthotropic pinched ring

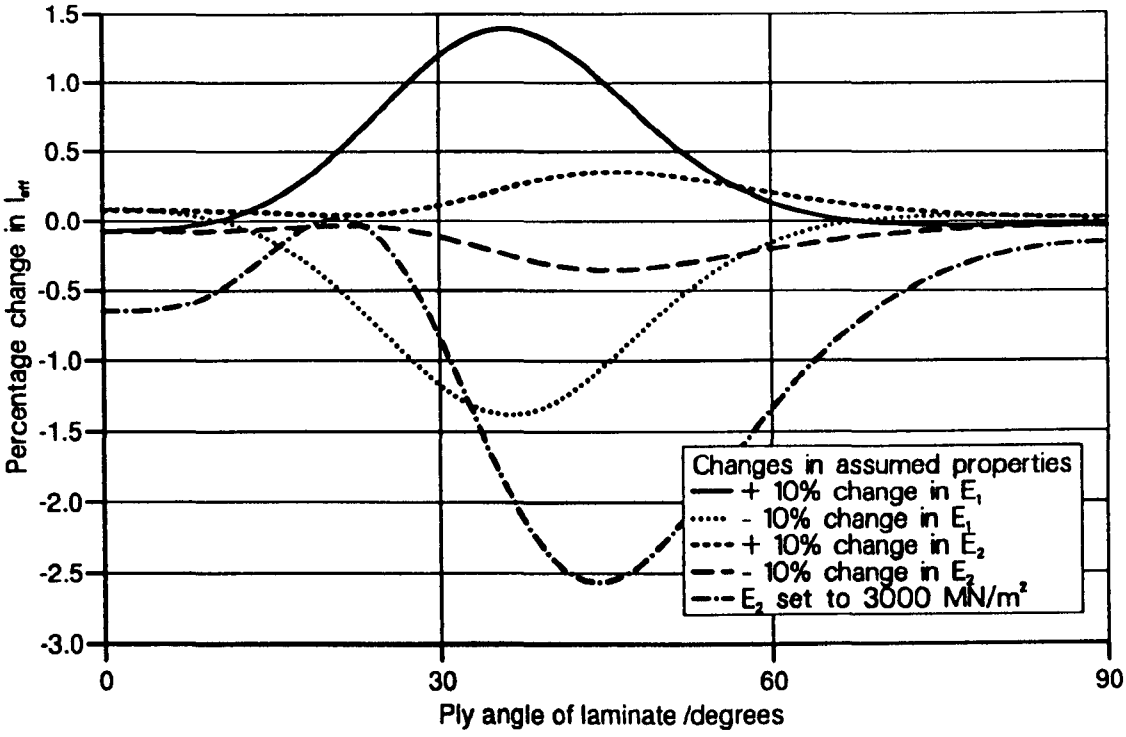

Fig. 5.3: Sensitivity analysis: Changes in effective second moment of area I_{eff} of ring specimen caused by changes in assumed values of unidirectional material properties E_1 and E_2. Assumed properties appear in Table 5.1.

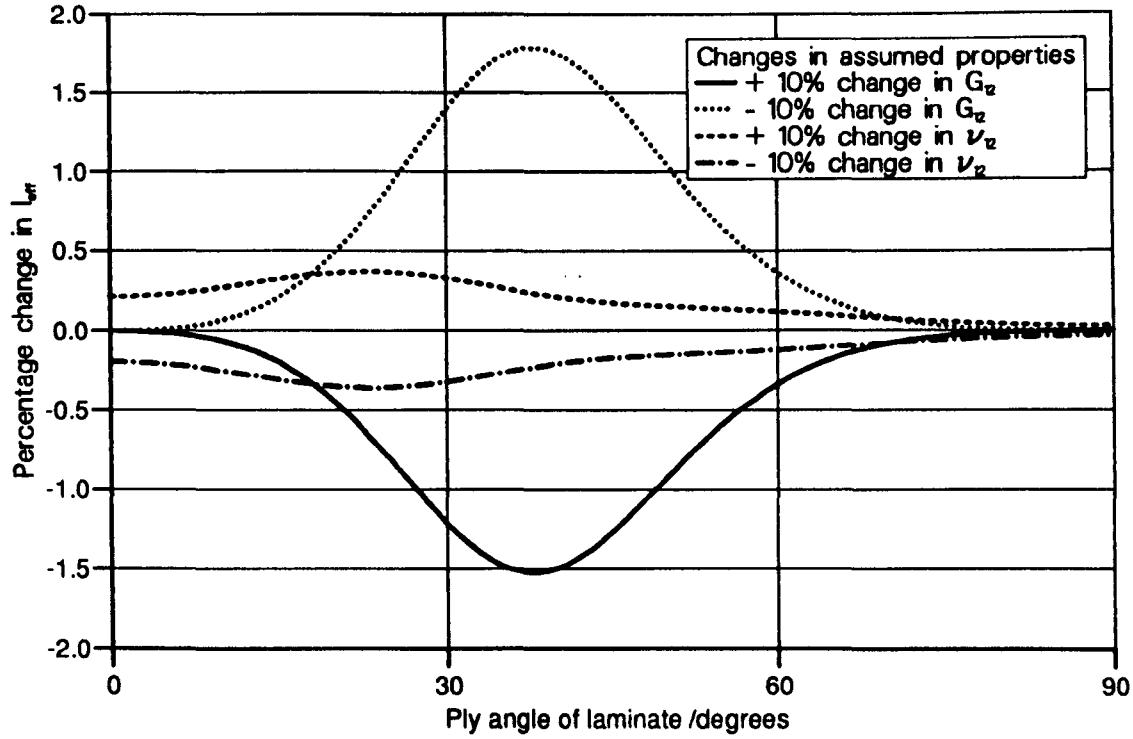

Fig. 5.4: Sensitivity analysis: Changes in effective second moment of area I_{eff} of ring specimen caused by changes in assumed values of unidirectional material properties G_{12} and ν_{12}

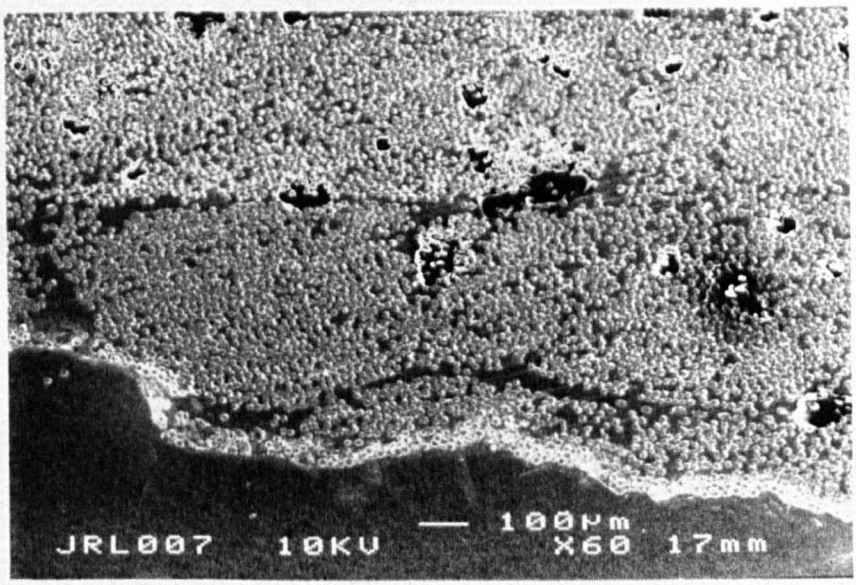

Fig. 5.5: Scanning electron micrograph: cross-section through typical filament-wound ring specimen showing voidage. Micrograph courtesy of J. Lowe.

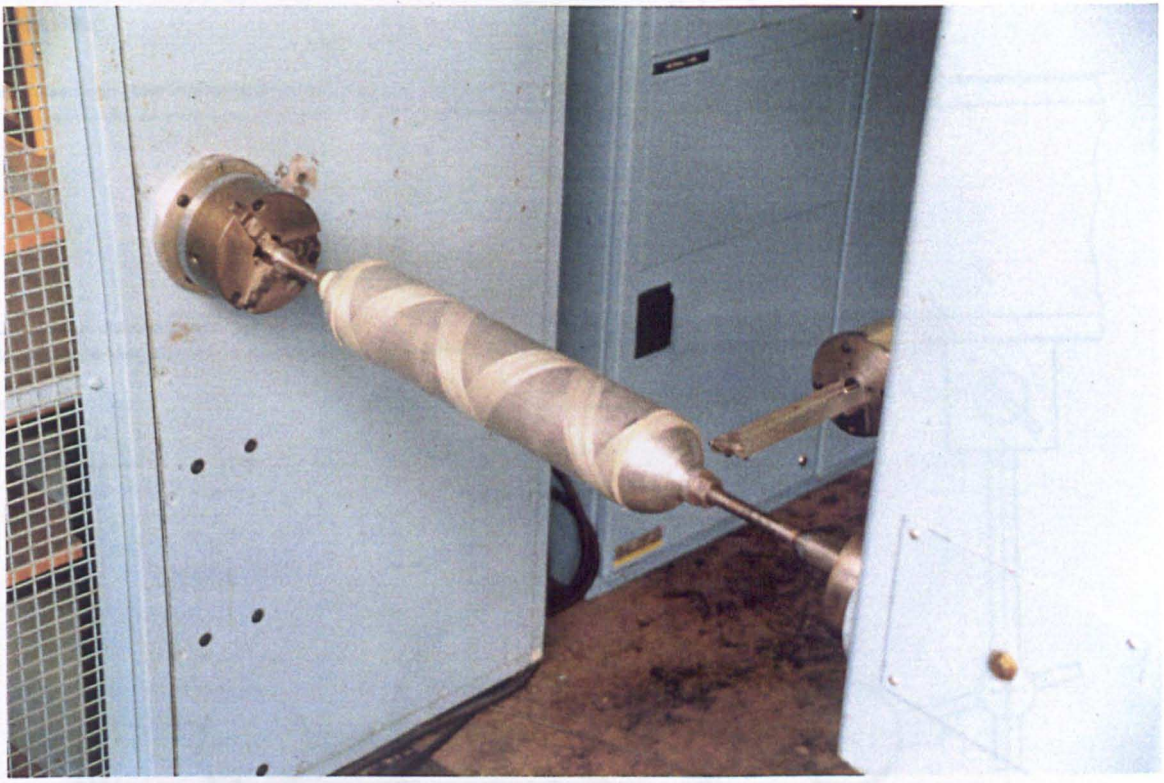

Fig. 5.6: Filament winding of typical specimen with ±60° winding angle

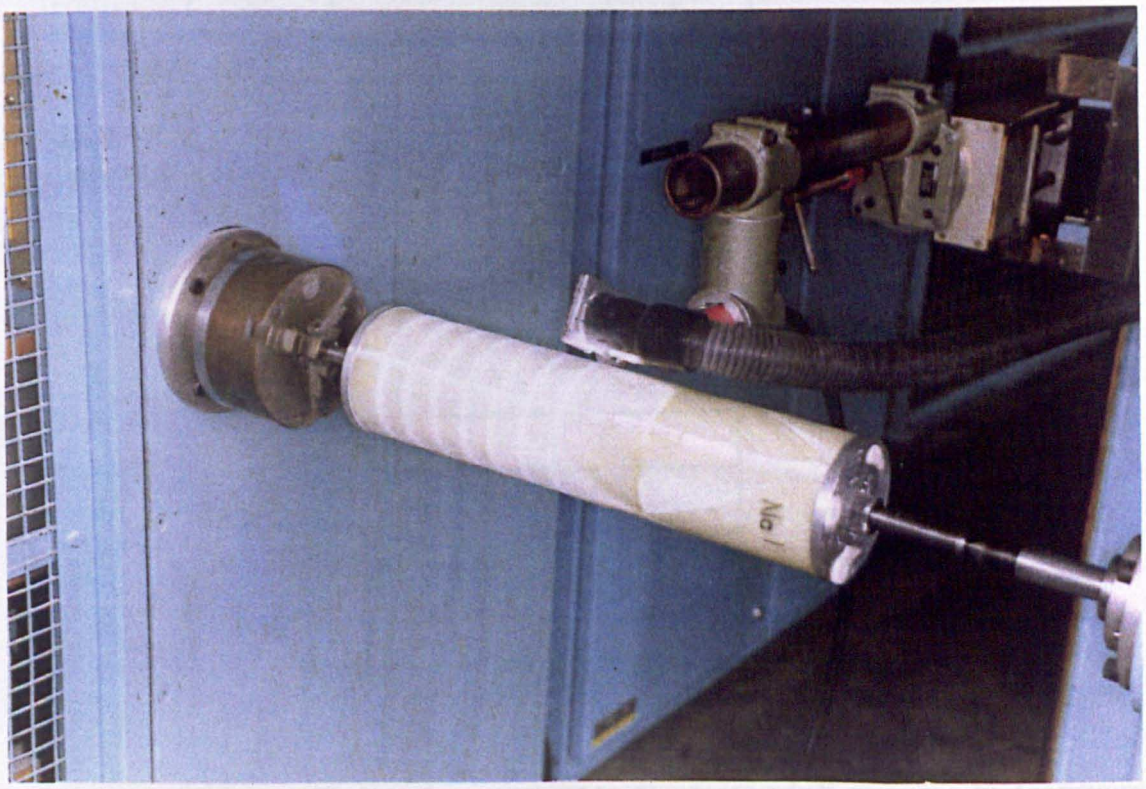

Fig. 5.7: Slicing of typical specimen (±30° winding angle) into rings using a diamond saw driven by an air turbine

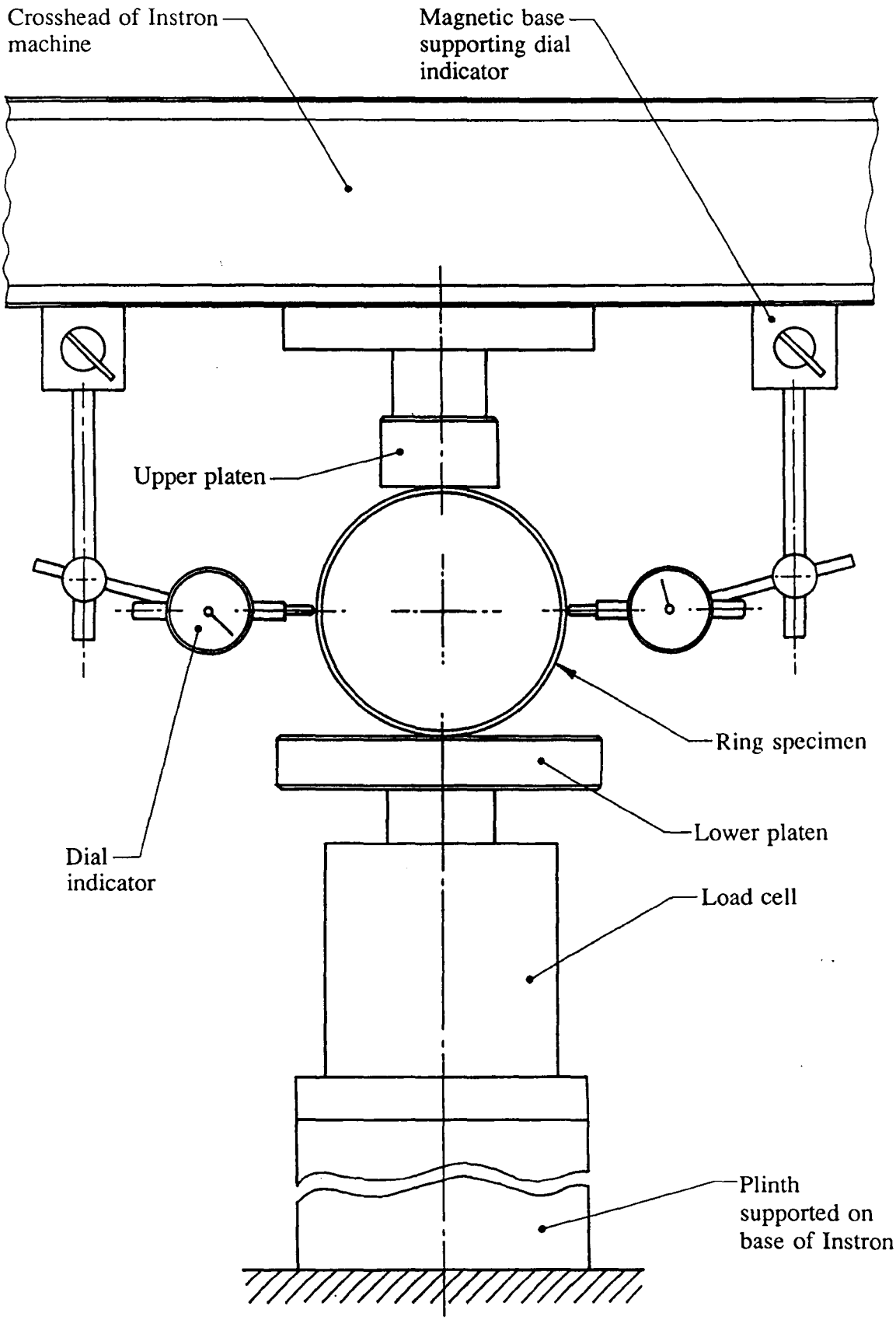

Fig. 5.8: Diagram illustrating apparatus for measuring changes in transverse diameter of ring under pinching load

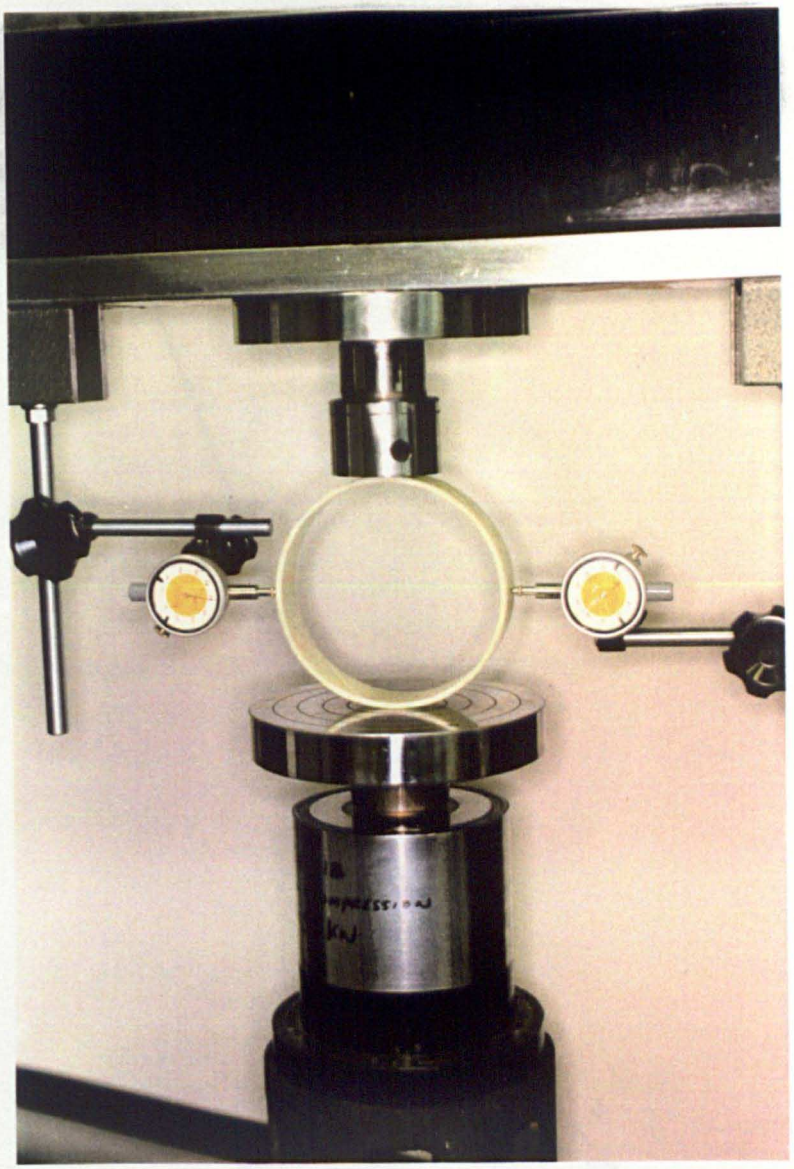

Fig. 5.9: Photograph illustrating apparatus for measuring changes in transverse diameter of ring under pinching load

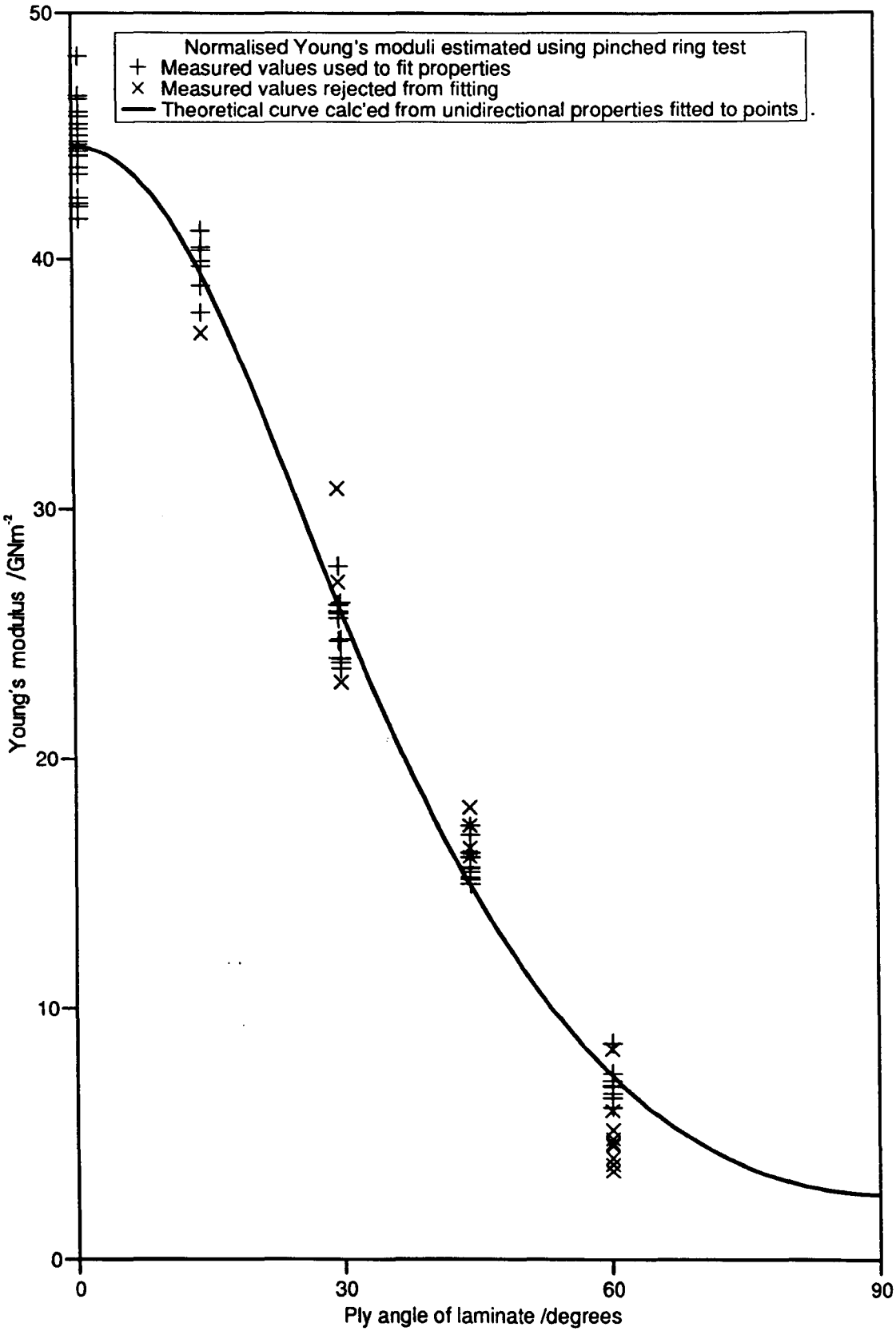

Fig. 5.10: Young's Moduli (normalised to 78% fibre by mass, estimated from pinched ring tests) vs. ply angle of specimens with respect to direction of bending stress

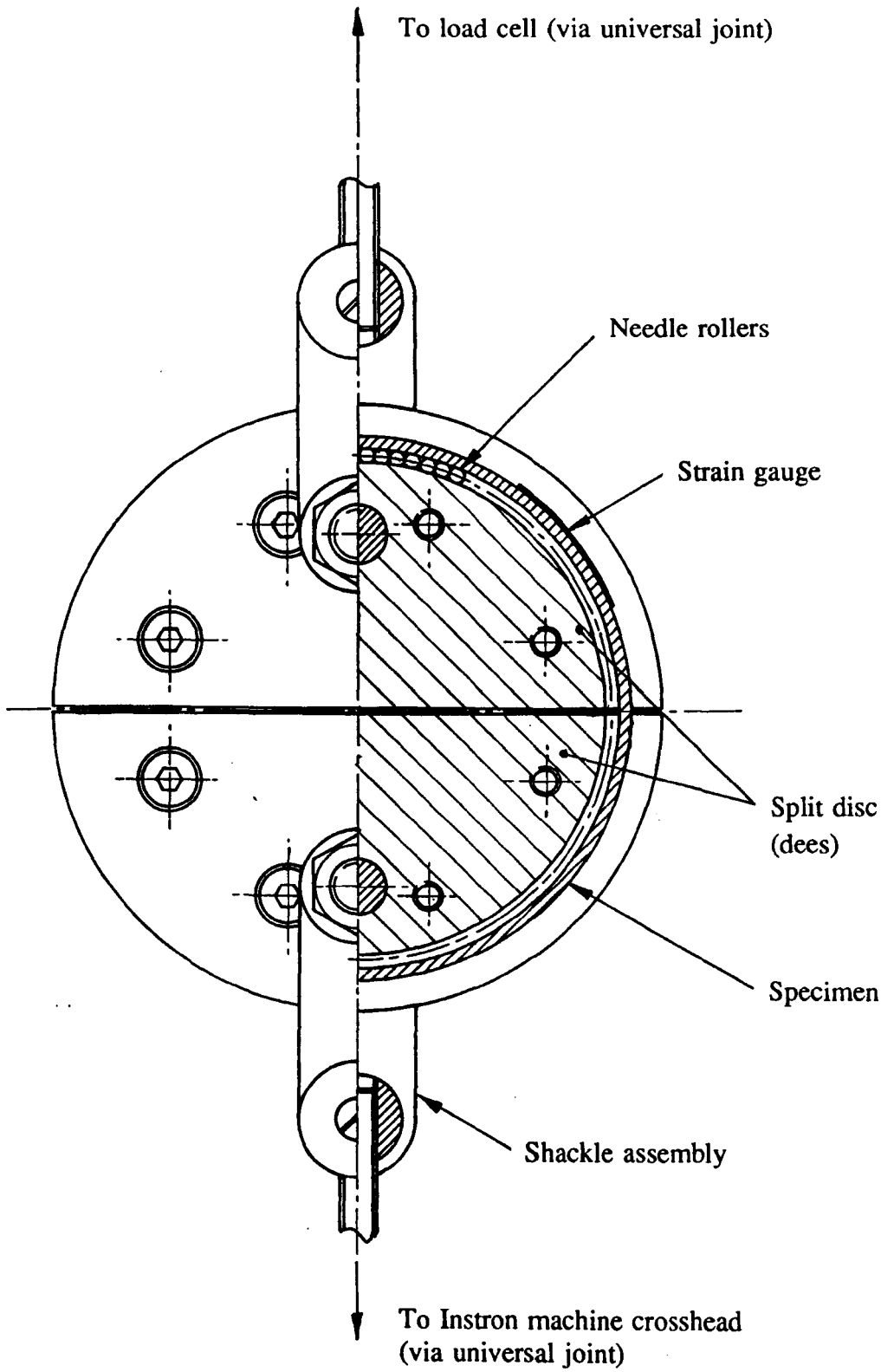

Fig. 5.11: Part-sectioned view of roller-assisted split disc apparatus

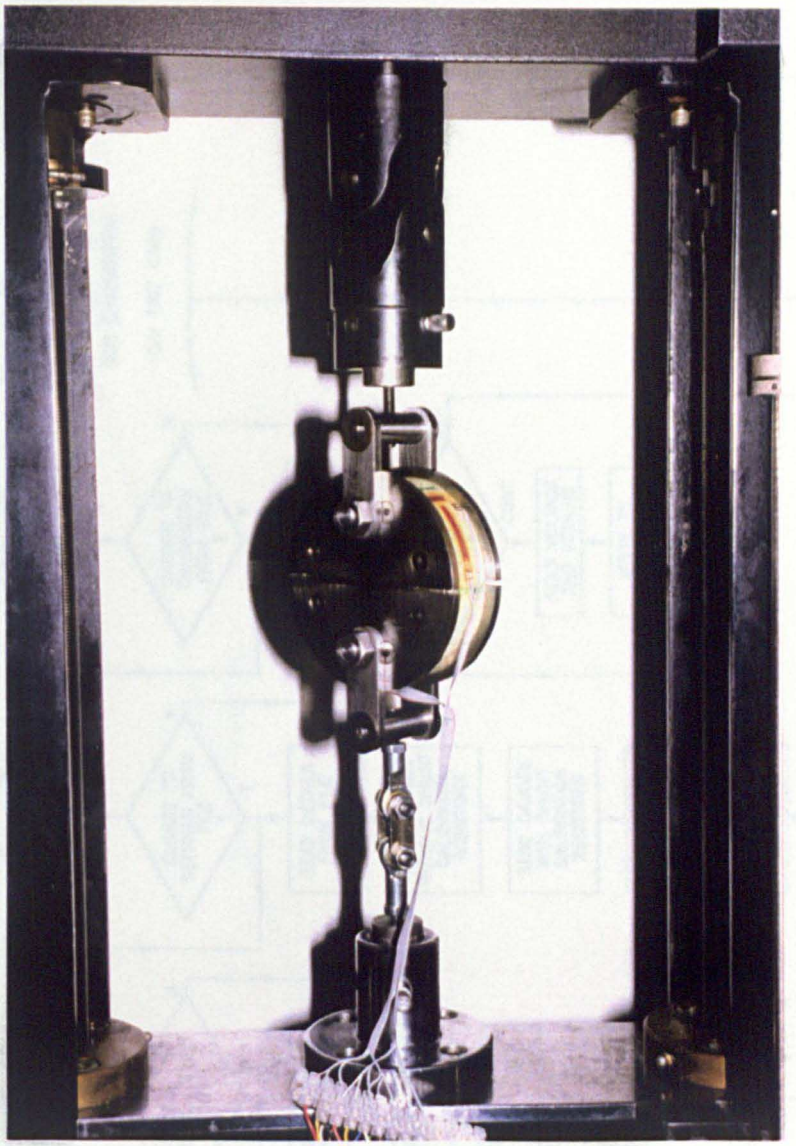

Fig. 5.12: Photograph of roller-assisted split disc apparatus

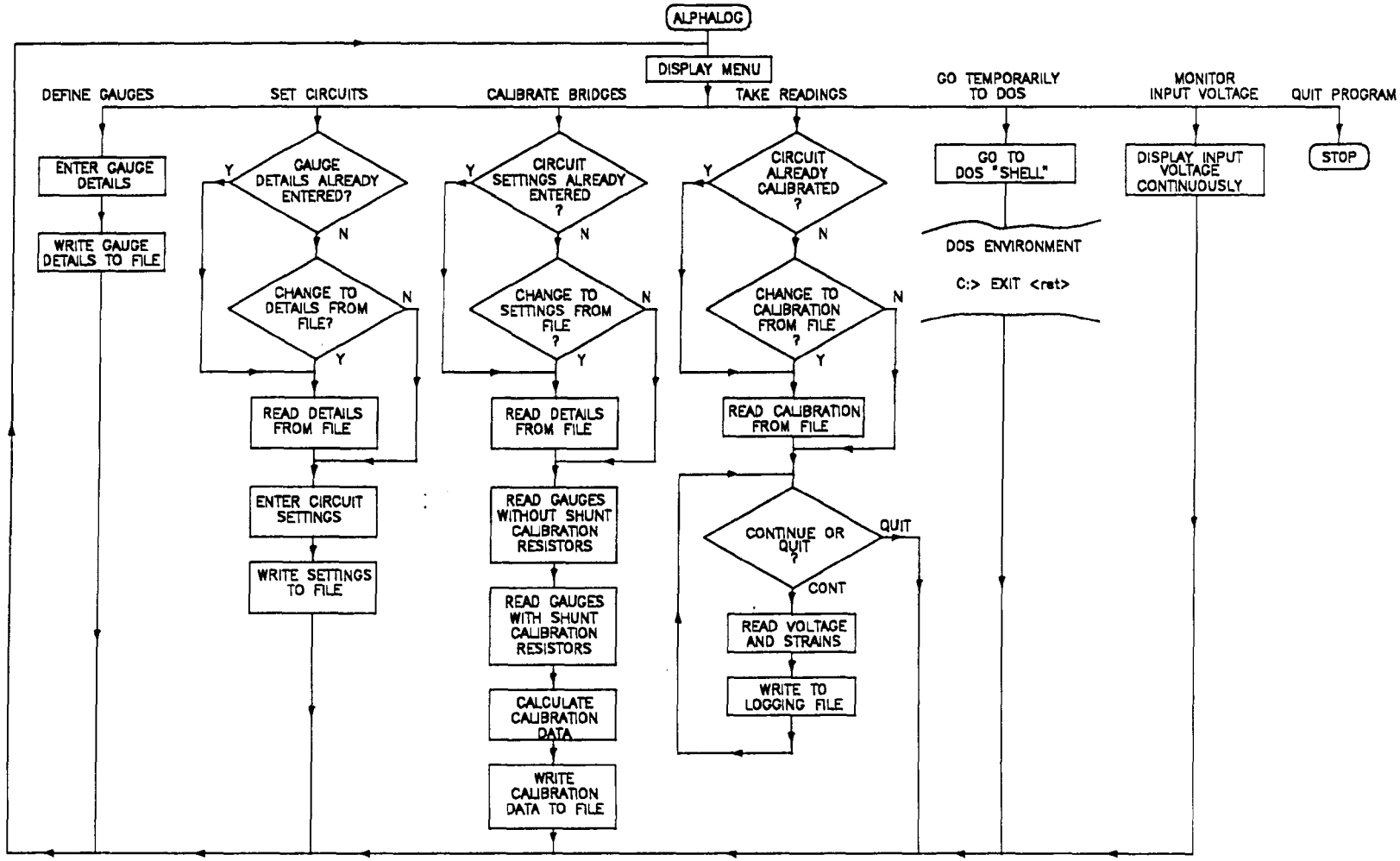

Fig. 5.13: Flow chart of ALPHALOG datalogging control and data management program for IBM-PC-controlled Amplicon/CIL data acquisition hardware

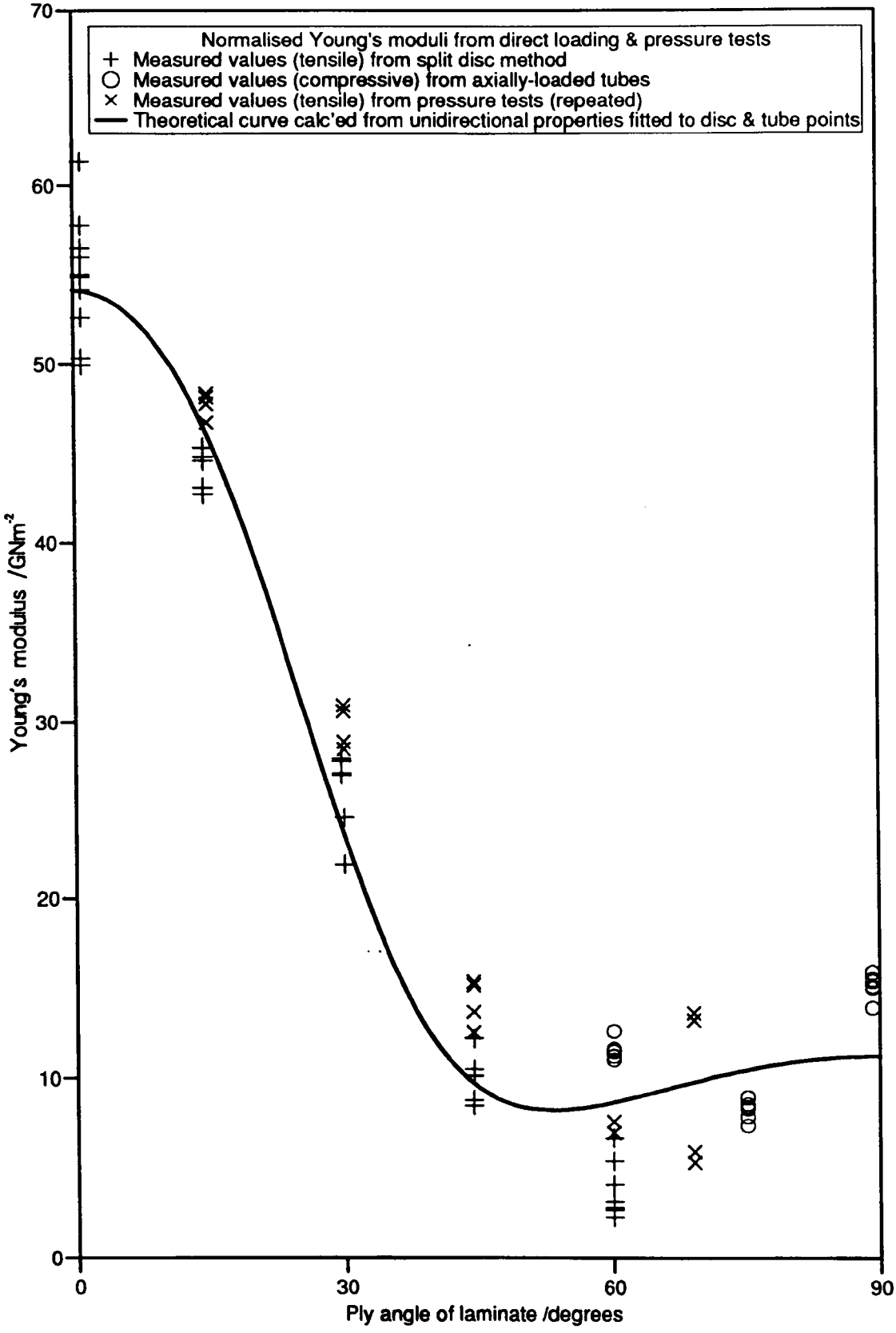

Fig. 5.14: Young's Moduli (normalised to 78% fibre by mass, estimated from split disc and axial compression tests) vs. ply angle of specimens with respect to direction of applied stress. Pressure test results are shown for comparison.

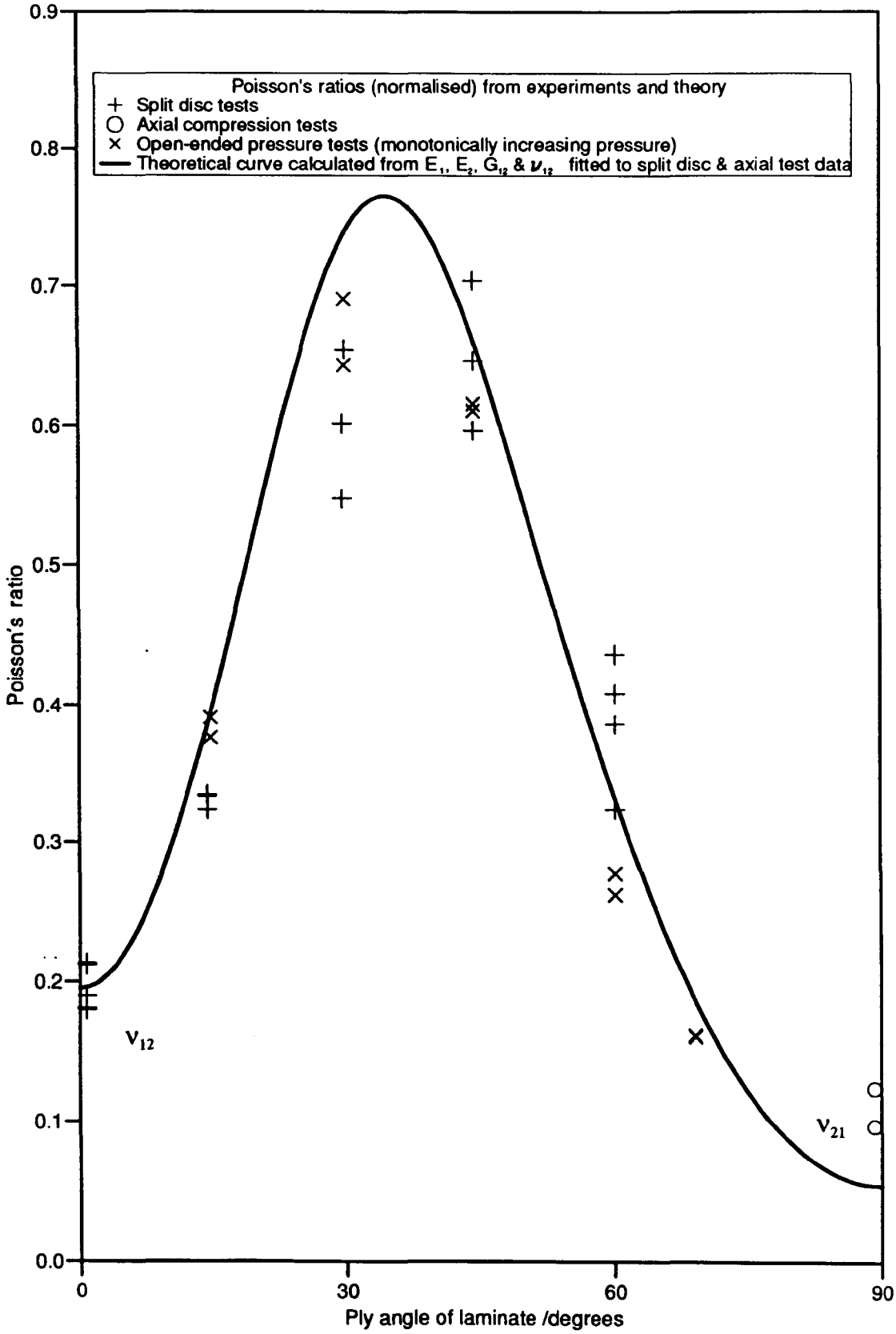

Fig. 5.15: Poisson's ratio (normalised to 78% fibre by mass, estimated from experimental data) vs. ply angle of specimens with respect to direction of applied stress

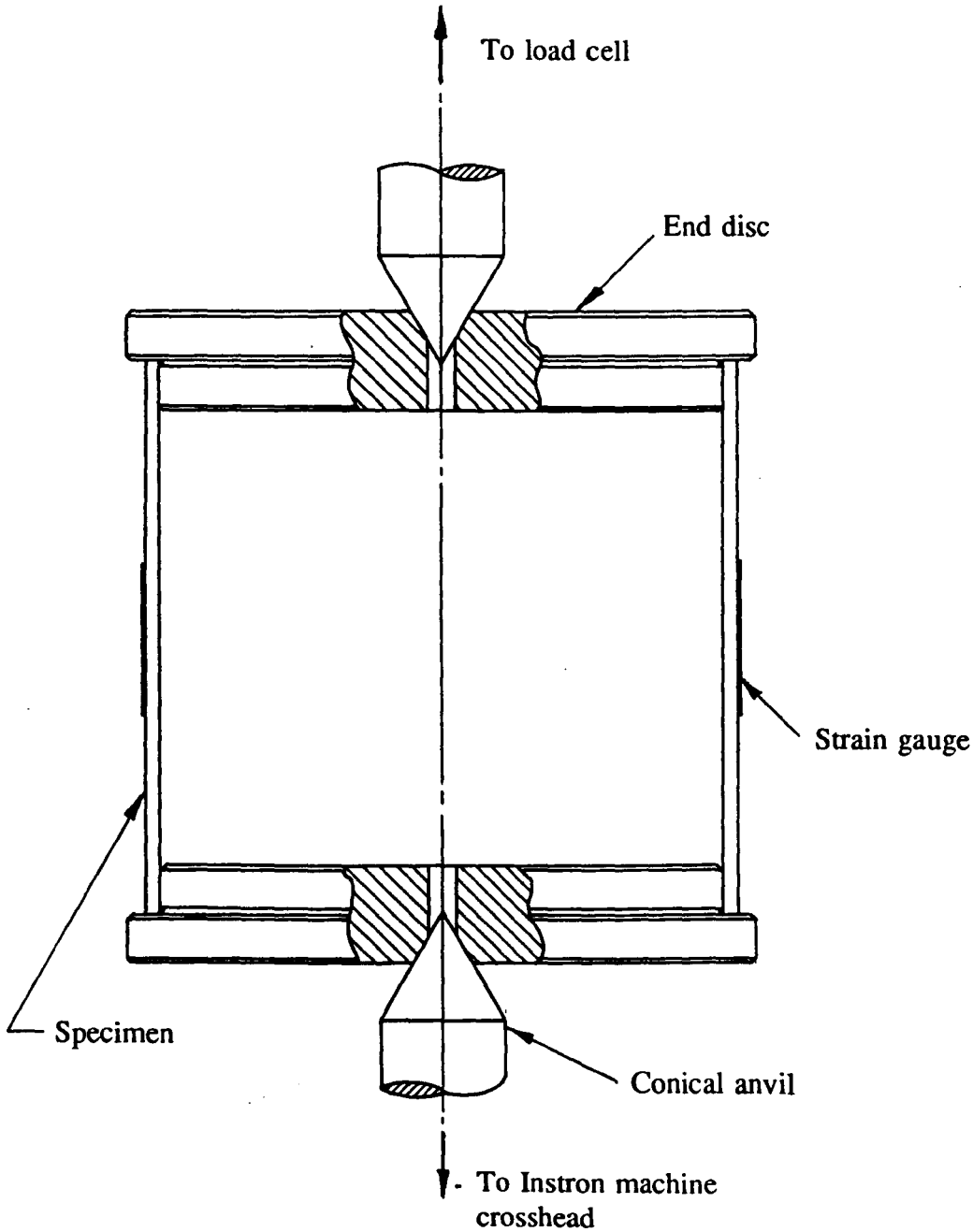

Fig. 5.16: Section through axial compression apparatus

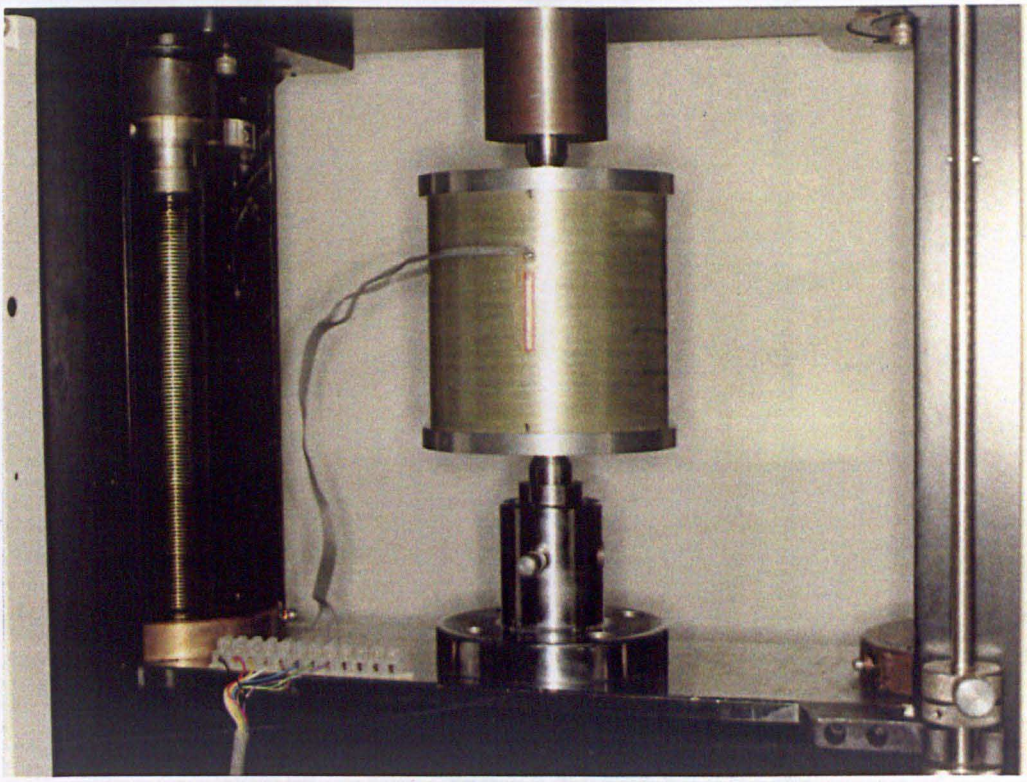

Fig. 5.17: Photograph of axial compression apparatus

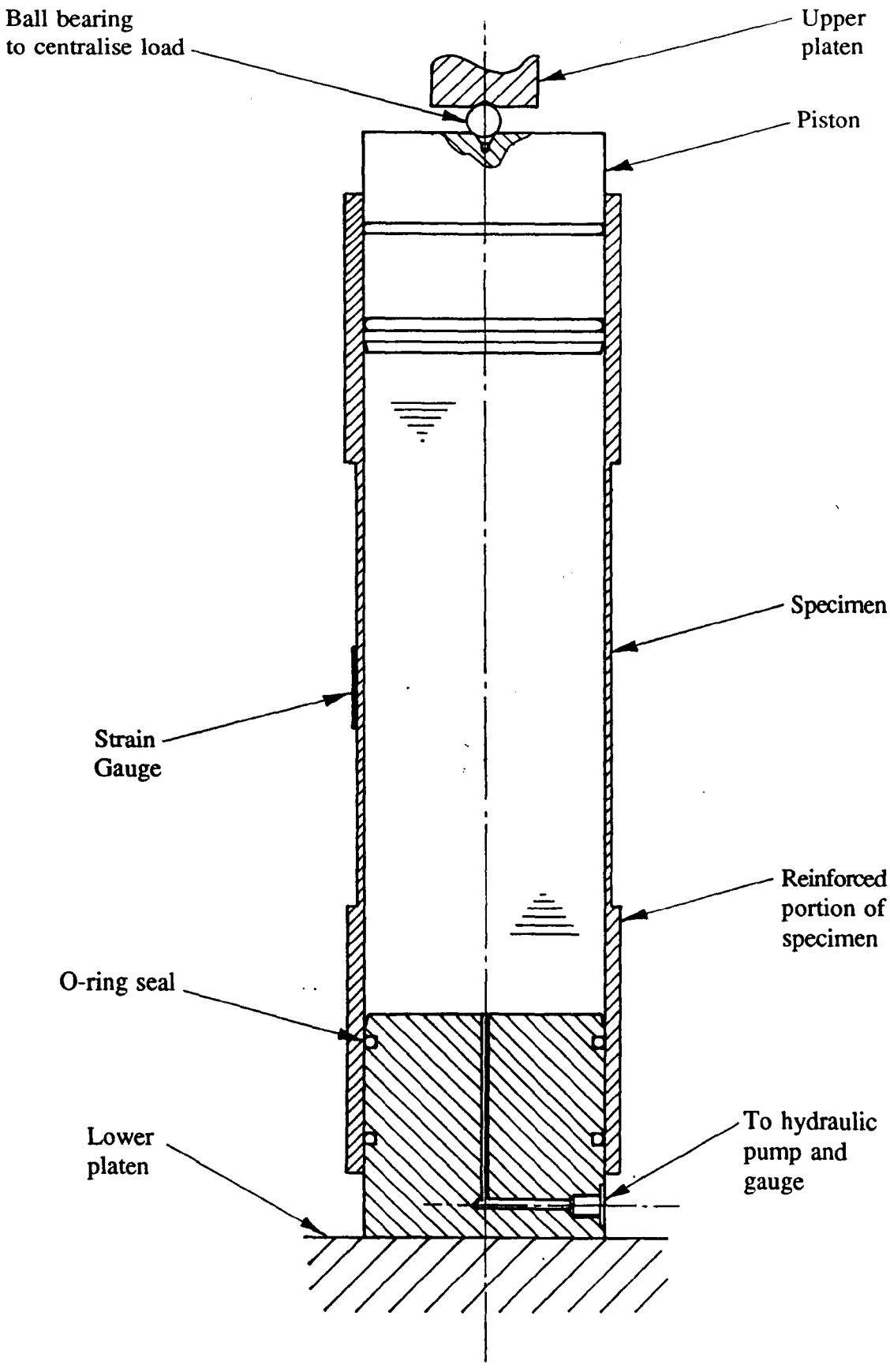

Fig. 5.18: Open-ended pressure test specimen showing end pistons

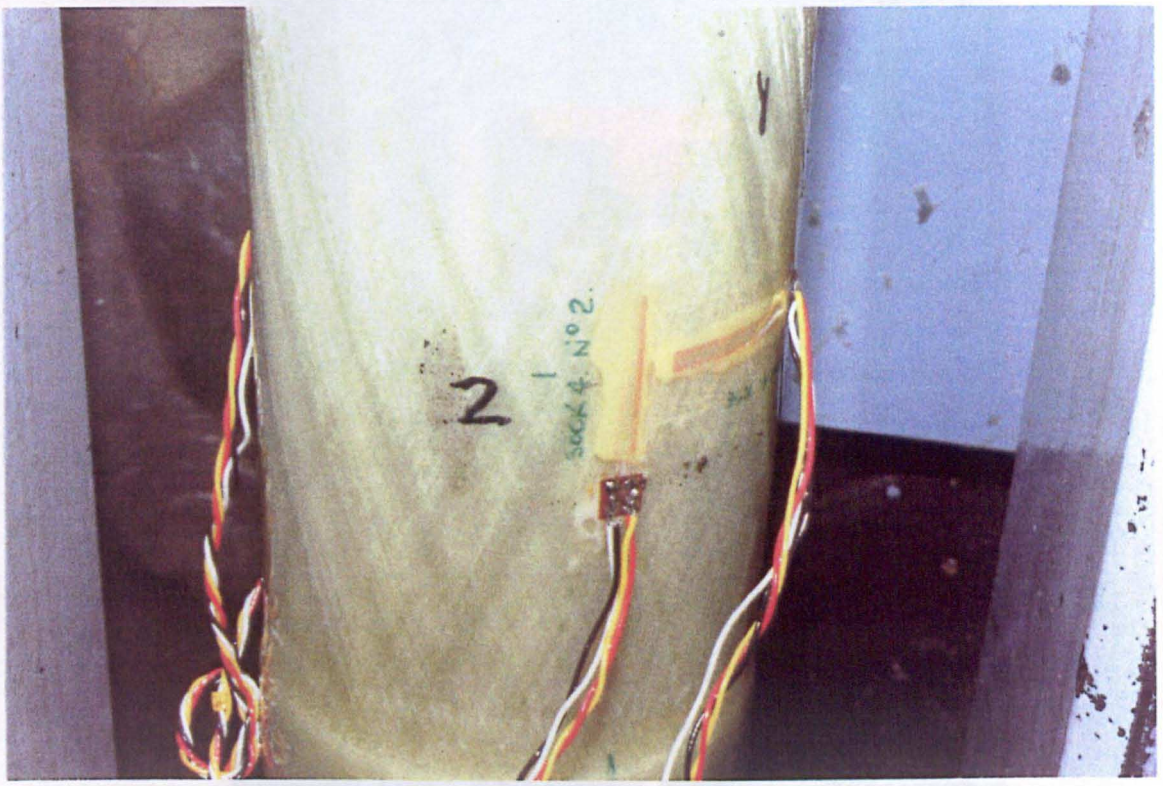

Fig. 5.19: Strain gauges on open-ended pressure specimen, showing protective rubber coating

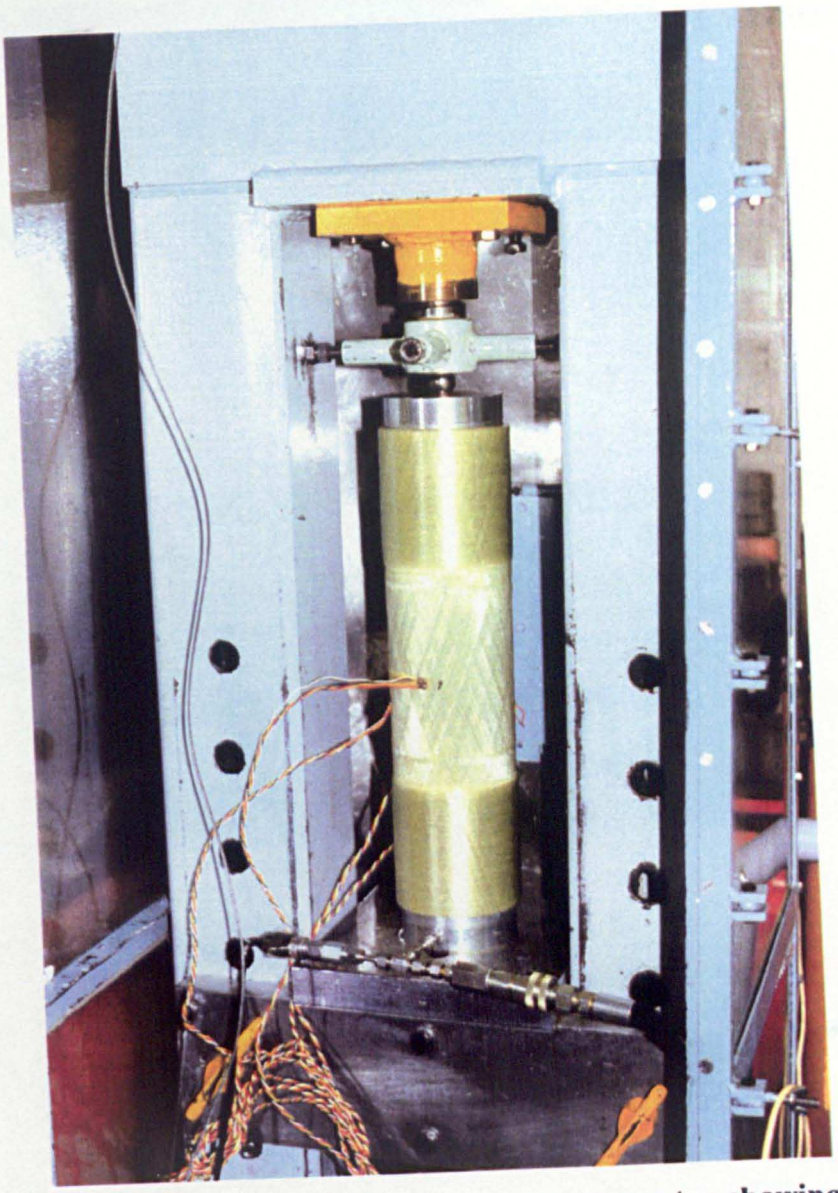

Fig. 5.20: Photograph of open-ended pressure test apparatus showing specimen in place

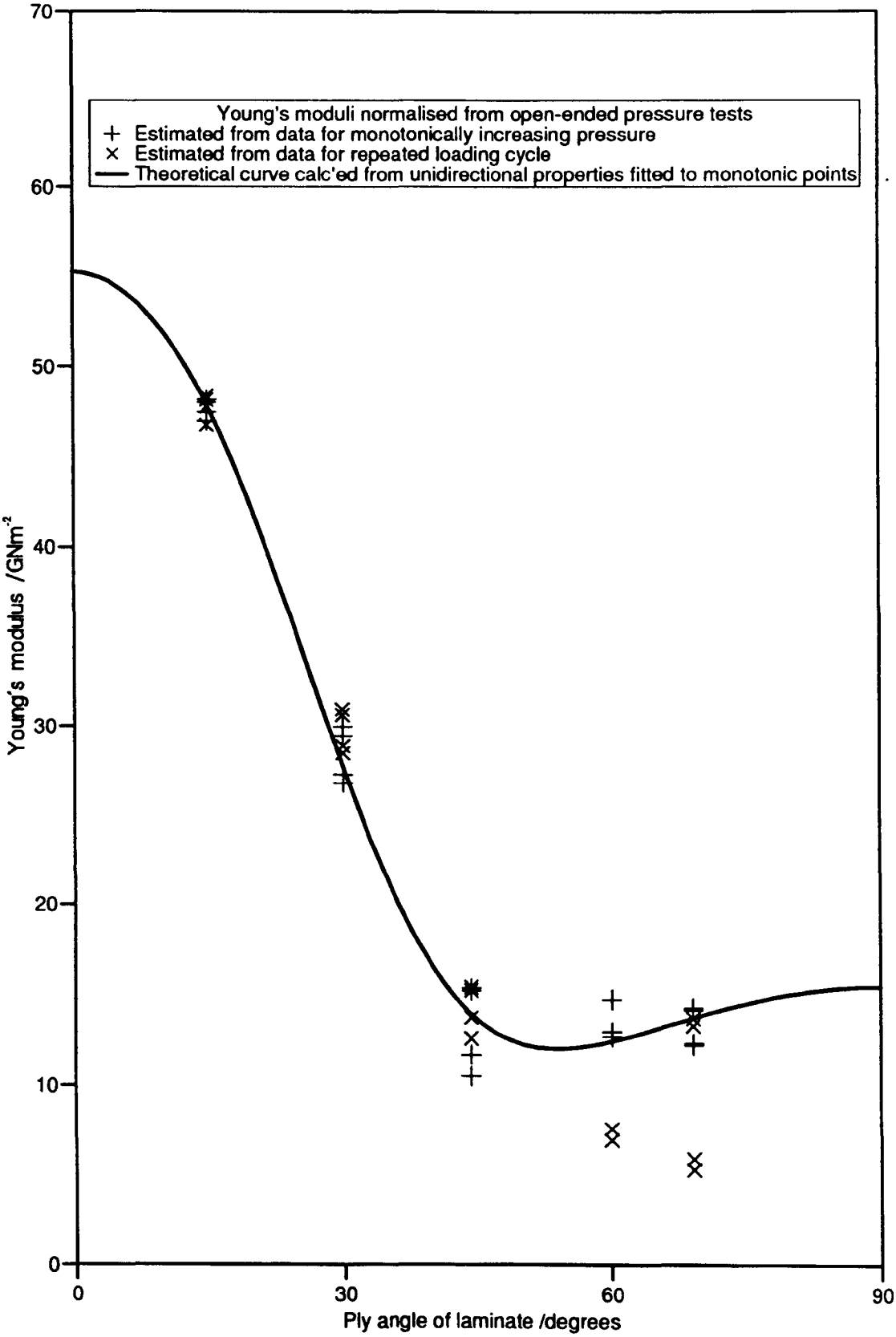

Fig. 5.21: Young's moduli (normalised to 78% fibre by mass, estimated from open-ended pressure tests) vs. ply angle of specimens with respect to circumferential stress direction

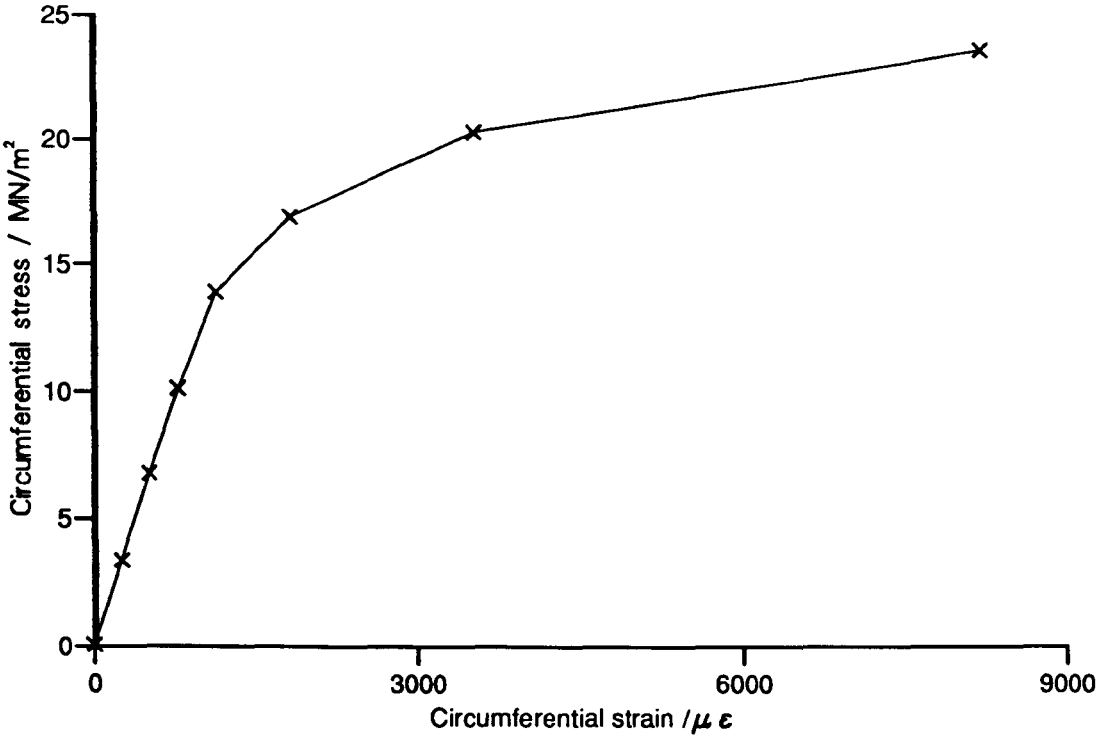

Fig. 5.22: Graph of stress vs. strain for laminate with ply angle of ±60° to direction of loading (Open-ended pressure tube specimen 1 with winding angle ±30°)

CHAPTER 6: DESCRIPTION OF FILFEM: THE CADFIL/FINITE ELEMENT LINK

6.1 Introduction

It has already been established that a serious obstacle to finite element analysis of filament-wound structures is the large numerical task involved in the preparation of the data defining an accurate finite element model, the exact structure of a component being heavily dependent upon the manufacturing process. This chapter describes work performed to investigate and develop methods for automating this data preparation task. They make use of the existing data generated within the CAD/CAM systems for generating the CNC part-program data for the winding process. The algorithms, geometry and numerical methods have been derived and selected as required and have been encoded as two separate model generation systems. FILFEM I automatically generates models of nominally axisymmetric components designed and manufactured using CADFIL I. FILFEM II (written to a basic level of completion with a view to considerable further development) achieves the same objective for non-axisymmetric components created using CADFIL II but requires a very different approach.

6.2 Existing links between filament winding CAD/CAM and FE systems

The CADFIL systems for filament winding have already been outlined together with a mention of other systems with broadly similar objectives and capabilities. It is clear that the link between filament winding CAD/CAM software and commercial FE codes has already been considered by other workers although little has been presented in the way of achieved results. Menges and Effing[14] proposed a link between CADFIBER and ABAQUS but have presented no implementation of this suggestion. DiVita et al[125] presented the mathematical theory required for a CAD/CAM system for non-axisymmetric filament winding. Their ARIANNA program[19] used this theory but was not named in this reference. They also presented the results of a finite element analysis of a simple (hypothetical) non-axisymmetric filament-wound component.

However, no indication was given that the mesh-generation was automatically linked to the ARIANNA program. The lamination sequence was simplified and assumed to be symmetrical.

Only one clear example of the establishment of a link between filament winding CAD/CAM software and an FE code has been found. This link was described by Wells and Eckold[16,18], who presented two different examples of how an axisymmetric filament-wound structure could be modelled using PAFEC with wall thickness and material stiffness values predicted from the data within the CADMAC system. It would appear that the models assumed the material to be homogeneous and that no account was taken of true laminate structure. It is understood[126] that some limited work was performed to extend this link to cope with non-axisymmetric components; however, nothing to this effect has been published.

Existing applications of finite element analysis to filament-wound structures have been explored in Chapter 4, together with existing element formulations especially applicable to these structures. This thesis does not describe either a new application of finite element analysis or the development of new element formulations. However, in forming a link between finite element analysis and CAD/CAM for filament winding, especially with respect to non-axisymmetric components, this work appears to be covering territory which is largely unexplored or unpublished.

6.3 FILFEM I: link between CADFIL I and FE systems

The aim of this work was set early in the project and may be summarised as being to identify, derive, develop and encode methods of automatically creating finite element models of filament-wound structures formed on axisymmetric mandrels. In practice this requires the design of a computer program capable of processing the appropriate data files from the CADFIL I system with the purpose of creating an FE model of the structure in the form of a PAFEC or ABAQUS input data file. In addition to the aim of establishing a useful engineering tool in the form of a model-generation system, it

was intended to gain experience of the usefulness of the available FE systems in the stress or strain analysis of complex laminated structures.

6.3.1 *Background: the problems of alternating lamination sequence and the turnaround region*

It is necessary to elaborate upon the detailed structure of axisymmetric components outlined in Chapter 1. An axisymmetric mandrel is wound with fibre by moving the payout eye in a repeated end-to-end movement as the mandrel rotates. This lays fibres with alternating positive and negative winding angles. These are normally laid side-by-side in a neatly repeating manner but this results in the component being divided into regions of alternating lamination sequence. It is not a practical manufacturing proposition to avoid this pattern by reversing the winding direction during the payout eye return strokes, although this could be achieved for test purposes with the aid of special end fixtures. This alternating structure presents the stress analyst with a dilemma. The true structure can be modelled involving considerable data preparation effort. Alternatively, the structure can be simplified by ignoring the alternation and possibly simplified still further using homogeneous orthotropic axisymmetric elements. All the published analyses found by the author use simplified models, mainly using the last approach. For many-layered laminates this will be a valid simplification. However, for laminates with few layers (for example 2, 4 or 6) the coupling effects describes in Chapter 3 become significant and this could affect the validity of a simplified analysis. It was considered therefore that if a three-dimensional analysis of a structure is to be undertaken (if, for instance, complex non-axisymmetric loads are applied), the correct lamination sequence should be modelled if at all possible. An algorithm for modelling this effect has been developed enabling FILFEM I to achieve this objective.

Another practical problem facing the stress analyst is the simulation of end regions of the component where the fibre reverses its helix angle. Close to the ends the fibre builds up in thickness as the winding angle becomes steep and approaches 90°. At the extreme ends of the component the fibres follow a

circumferential path and they will be laid on top of each other as far as the inevitable slippage will allow. The result is a thick buildup of fibre resembling a piece of rope wrapped around the end of the mandrel (Figs 6.1(a) and (b)). The geometry and dimensions of this region are difficult to predict theoretically. The calculations of thickness (based upon tow area, winding angle and component radius) give excellent results elsewhere but an infinite value at turnaround. Since the turnaround region is often cut off the finished component or is lightly stressed, no attempt has been made to pursue the accurate modelling of this region of filament-wound components.

6.3.2 *Inputs and outputs of FILFEM I*

The FILFEM I system will be first described in terms of its inputs and outputs, before describing its operation in greater detail in Section 6.3.3. The input data it requires are as follows:

(a) The mandrel geometry file. This is the definition of the mandrel surface based upon that used within CADFIL I, but with additional information defining cone angles at the mandrel ends and where cusps occur.

(b) The fibre path file. This defines the locus of points defining the fibre path generated within CADFIL. These points are defined in terms of their Cartesian coordinates.

(c) Material property data. This set of data includes fibre and matrix densities as well as elastic properties. The composite properties can be specified if required.

(d) Miscellaneous data. This information relates primarily to the processing of the fibre path to produce the CNC part-program, and includes the number of windings to give complete mandrel coverage, the number of covers, the progression factor and the fibre fraction of the composite (by mass).

Future development of FILFEM I would benefit from the establishment of a more satisfactory interface with CADFIL I so that the miscellaneous items in (d) above can be transferred automatically rather than manually.

The output from FILFEM I is a PAFEC or ABAQUS input file. Its contents are as follows.

(a) The component geometry is defined in terms of node coordinates and element topology. The component may be modelled using either an axisymmetric mesh (suitable for many-layered vessels) or as a mesh of triangular or quadrilateral curved shell elements. The latter can represent the continuously-varying lamination sequence over the structure but require greater memory and processing time to analyse.

(b) The material fibre direction, lamination sequences and thicknesses are obtained by numerical analysis of the input data and incorporated in the model definition. The equivalent homogeneous material properties of the laminated structure are also calculated if an axisymmetric model is being generated.

Boundary conditions such as loads and restraints, together with program control information defining the type of analysis, are edited manually into the FE input file since these items of data cannot be inferred from the component structure.

6.3.3 *Description and operation of FILFEM I*

In addition to the logic required, most of the theory utilised in FILFEM I is that of numerical analysis and three-dimensional geometry. A complete description of the operation of the program, including all methods of operation of all the subroutines, is given in a report by the author[127]. Duplication of these details would be inappropriate here and instead a step-by-step description of the main features of program operation is presented. The letters denoting each stage can be cross-referenced to the flow chart in Fig. 6.2.

A The program is initialised. This includes the initialisation of the numerous arrays and the naming of the various input and output files.

B The mandrel definition is read from the mandrel geometry file as a series of *x-r* co-ordinates, and a cubic spline curve[128] (or a series of such curves) is fitted through these to represent each smoothly-curved region of the mandrel profile. This spline curve is used later in the program to ensure accurate placement of the nodes defining the FE model.

C The fibre path is read and processed. CADFIL bases its winding program generation on the simulation of the winding of a single piece of fibre over a three-dimensional surface model of the axisymmetric structure. The Cartesian co-ordinates of points along this fibre path are read into FILFEM and converted into *x-r*-θ polar co-ordinates.

D Fibre closure is performed. It will be appreciated that the fibre path projected over the surface model in CADFIL I will not normally form a closed loop (Fig. 6.3). In Section 2.4.1 and Fig. 2.4 it was described how the CADFIL post-processing software compensates for this by multiplying the mandrel rotation by a progression factor close to unity so that successive payout eye paths will lay a repeating pattern of adjacent fibres. A slightly different fibre closure process occurs in FILFEM I. The turning points of the fibre path with respect to axial and/or radial position are found. This is achieved by finding the turning points of quadratic curves fitted (using a least-squares technique) to the five points in the region of each turnaround. The θ-co-ordinates of the points on the fibre are then scaled by a progression factor so that the new positions of the turnarounds subtend exactly 180° or an exact fraction thereof. This results in a path which can be repeated to form a closed loop. This process is illustrated in Fig. 6.4; for ease of illustration the diagram shows the adjustment for closure of a complete cycle of the fibre rather than the adjustment of half

a cycle between turnarounds. The identification of this repeating pattern is necessary if the alternating lamination sequence is to be modelled.

It should be noted that this method of predicting the boundaries between the regions of alternating lamination sequence is a good approximation rather than an exact prediction. Strictly speaking, the regions of alternating lamination sequence should be defined by the edges of the first and last winding of fibre. These edges are coincident if complete coverage of the mandrel has been achieved. This boundary does not form an exactly closed loop but includes a deliberate mismatch equal to the width of the fibre roving (the bandwidth) so that successive fibres are laid side-by-side (Fig. 2.4(a) and (b)). In practice, this mismatch is hidden in the turnaround region and is not detectable by eye. The placing of the boundaries in the model will therefore be subject to a slight error averaging half the bandwidth. This distance is small in many applications (typically 2mm) and is comparable with practical limitations upon the accuracy of fibre placement. In the author's opinion this simplification to the true structure will have no practical significance.

The exact operation of the program now changes depending upon whether the component is to be modelled with a three-dimensional mesh (using thin shell elements) or with an axisymmetric mesh (using axisymmetric isoparametric elements). For three-dimensional meshes the sequence is designated **E-I.**

E The following method was developed for simulating the pattern formed by the areas of alternating lamination sequence. The co-ordinates of the points on the fibre path are adjusted to lie on the mandrel surface defined by the cubic spline function, and any serious discrepancies are noted. The fibre path is divided into regions each subtending a known fraction of full circle around the mandrel. This angle is actually π/m where m is the band pattern number defined in section 2.4.1. Fig. 6.5 illustrates this process. The points on the fibre dividing these regions are found by fitting a quadratic

parametric equation to the fibre path and finding the intersection of this curve with the appropriate meridian. Enough information is now defined to divide the component into regions of uniform lamination sequence (Fig. 6.6). The boundaries between the regions on the component are represented by boundaries between regions of elements on the model. In practice, further subdivision of the fibre takes place to create refinement of the mesh within these regions of constant lamination sequence, and typical meshes illustrating this are described in Chapter 7 (Figs. 7.17 and 7.18).

F In order to reduce the effects of any interpolation error, the points obtained in **E** are fitted to the mandrel surface defined in terms of the cubic spline curve. Any movement of the points is carried out normal to the mandrel surface. The procedure to perform this was developed by the author and involves using the Newton-Raphson method to solve a quintic equation in axial position x. The coefficients of the quintic are formed from the x-r co-ordinates of the point to be fitted, and from the coefficients defining the relevant region of the cubic spline curve.

G A first approximation to the winding angle at each point of interest along the fibre is obtained by differentiating a quadratic fitted to the x-θ co-ordinates of points on the fibre. This winding angle is then used (in conjunction with the cross-sectional area of the wet tow of fibres) to calculate the thickness of the wound fibre.

H At this stage there exists within the computer memory a set of points which are (in effect) the projections of the node positions on to the mandrel surface. There also exists at each point a value of thickness and fibre direction. It is a straightforward task to obtain from this information the co-ordinates of a set of nodes placed at mid-surface, and to connect these nodes with elements. Less straightforward is the incorporation of an algorithm which aligns the appropriate element boundaries as closely as possible with the boundaries between the regions of uniform lamination

sequence. This includes the use of triangular shell elements as "fill-in" elements along the helical borders between the regions. The use of thin shell elements becomes inappropriate as the turnaround regions of the composite are approached (the triangular elements would be geometrically distorted and all elements would be excessively thick) and meshing is therefore suspended when the winding angle exceeds 75° to the meridian. An attempt was made to use three-dimensional wedge elements to simulate the turnaround region but this was not pursued because of difficulties in predicting the shape of the turnaround.

I The element definitions include reference to material property definitions and these include a ply-by-ply listing of the fibre orientations and ply thicknesses. These take full account of the alternating stacking sequences on the specimen. The algorithm to predict the alternation of the stacking sequence within the different regions actually occurs twice in the PAFEC model generation subroutine in order to create a material property definition which accurately matches the material definition list. The ABAQUS model generation subroutine closely follows the methods used for the PAFEC subroutine but the data is created in a sequence appropriate to the different layout of the ABAQUS input file.

If the generation of an axisymmetric finite element model was chosen, a simpler mesh generation sequence was adopted. This is designated in Fig. 6.2 by the letters **J-M**.

J A first approximation to the ply angle and laminate thickness are calculated at each point defining the original fibre path.

K There is now no need to create elements whose boundaries coincide with those of regions on the specimen surface. Instead the rule has been used that the mesh will have a constant node spacing at the inner surface. This is achieved using a technique developed by the author which interpolates

the position of each new node quadratically by performing a line integral of distance along the fitted parabola. Any interpolation error is then eliminated by fitting this point to the mandrel surface defined by the cubic spline function; this process also involves the calculation of the normal to the mandrel at each node.

L The thickness and winding angle at each node are interpolated linearly from the values calculated in J. The value of thickness at each (inner surface) node is used to create the remaining nodes (at the mid-surface and outer surface) required to define the axisymmetric quadrilateral elements.

M The material properties of the material are assumed to be orthotropic but homogeneous; no attempt is made to model the laminate on a layer-by-layer basis. Accordingly, a set of equivalent homogeneous properties is calculated based upon formulae of similar form to equations (5.9)(a-d). All this information is written to the FE input data file.

The modelling of a very simple structure (a pinched cylinder) using both the three-dimensional and the axisymmetric (Fourier element) models will be described in Chapter 7.

6.3.4 *Programming aspects of FILFEM I*

The FILFEMI system was written to demonstrate the automatic modelling process and as a useful engineering tool, rather than as a programming exercise. However, efforts have been made to ensure that good computing practice has been followed where possible by the use of well-structured code and ample commenting. Unnecessary writing of code was avoided by the incorporation of cubic spline facilities modified from programs by Conte and De Boor[128] and existing curve-fitting subroutines written by Crescent Consultants Limited[8]. A few individual lines of code from CADFIL I were also incorporated into the program. The program, like most of the FORTRAN programs used for this thesis, was developed on the University's ICL VME mainframe computer system. It is

intended that a final version of the program could be implemented upon a personal computer. It is suggested that this development could be undertaken at the same time as the development of an improved interface with CADFIL I.

6.4 Development of a strategy for automatic modelling of non-axisymmetric filament-wound structures: the FILFEM II system

6.4.1 *Background and scope of work*

The aims of the thesis include the achievement of a link between both of the CADFIL systems and the available FE codes. It was apparent in the planning of the project that the creation of a system to link CADFIL II to the FE systems would not be a trivial exercise. This is because of the complexity of non-axisymmetric filament-wound structures and hence the need to make appropriate assumptions in simplifying the structure and to test these assumptions experimentally. It is quite possible that these difficulties lie behind the lack of published material on the automatic modelling of non-axisymmetric filament-wound structures.

The objective was therefore set of establishing a strategy or methodology forming the basis of a link between CADFIL II and an FE system (e.g. PAFEC). This work consisted of the identification and/or derivation of the appropriate mathematical techniques and logic to analyse the data available from CADFIL II and to create the FE models. This strategy has been established and has been encoded as the FILFEM II program. This program is in running order and its basic operation has been tested. The strategy and program form the foundation of a substantial programme of possible future work; this includes the testing of typical meshes against experimental data, refinement of some of the simplifying assumptions incorporated in the strategy, and development of the software to provide a useful design tool.

6.4.2 *Problems inherent in modelling non-axisymmetric filament-wound structures*

To illustrate this study and to provide suitable test data, a relatively simple filament-wound structure was chosen for manufacture and analysis. The chosen geometry, a 90° elbow-shaped circular-section pipe, was one which had not previously been manufactured at the University of Nottingham and despite its simplicity it illustrates some of the main difficulties both in manufacture and modelling. A full account of its manufacture is given in Chapter 8.

One of the main problems in modelling components of this type is the very complex laminate structure. In components wound using CADFIL II, fibre paths run parallel over the mandrel surface forming a wide ribbon of fibres (Fig. 6.7). This ribbon is likely in many structures to cross over itself, overlap and interweave several times giving a laminate structure which cannot be predicted by simple rules. An added complication is that several different families of fibres are used to provide complete and even coverage of the mandrel as far as possible. Two families of fibres are normally wound simultaneously as the payout eye moves back and forth along the mandrel. The resulting pattern is sufficiently complex that it is quite impracticable to match the element boundaries to the boundaries between regions of differing lamination sequence, and also difficult to predict the exact lamination sequence.

6.4.3 *Simplifications assumed in modelling non-axisymmetric filament-wound structures*

In order to provide a starting point in solving an apparently intractable problem, the following simplifications were adopted.

(a) Pairs of fibre families wound simultaneously will form a woven or under-and-over pattern of the kind described in Section 6.3.1, giving an alternating lamination sequence in some regions. For simplicity in modelling an arbitrary fixed lamination sequence is assumed for each pair of fibre families. When a series of such pairs of fibre families is wound, the result will be a many-layered laminate. The positions within the laminate of the

set of plies relating to each pair of fibre families will be specified correctly in the model. However, the sequence of plies within this set is modelled arbitrarily and will not necessarily be correct. This simplification will therefore alter slightly (typically by a distance equal to one ply thickness) the positions of the relevant plies with respect to the laminate's mid-surface. Classical laminate theory (equation (3.5)) suggests that this change in the values of z will slightly affect the coupling and bending behaviour represented by B_{ij} and D_{ij} and will not affect the in-plane behaviour (A_{ij}) at all.

(b) The following simplification was suggested by A.P. Priestley of Crescent Consultants Limited. Where a family of fibres only overlaps part of an element, these fibres are assumed to be averaged or spread more thinly over the whole of the element. This simplification has no basis in theory and will inevitably affect the accuracy of the finite element model. However, it does provide a route through a shortcoming common to both PAFEC and ABAQUS, since neither of these packages can model ply thickness variations within an element.

6.4.4 *Programs comprising FILFEM II: overview, inputs and outputs*

The model-generation strategy which forms the basis of FILFEM II is implemented as a suite of three programs. The method of operation of the model-generation process is summarised in Sections 6.4.4.1-6.4.4.3 in terms of the operation of each program. Complete details of the operation of the system are given in a report by the author[129].

6.4.4.1. *Purpose and operation of MESHGEN program*

This program creates the node and topology data forming the basis of the finite element model. The nodes are defined in terms of their projections on to the mandrel surface, i.e. no account is taken of the thickness of the composite material at this stage of the modelling process. The input to this program is a data file (Appendix G) defining the dimensions of the

component. The component shape is then built up node by node from its geometrical features; these are defined parametrically within the code of the MESHGEN program. The output is a mesh definition file containing the node co-ordinates and normals, the topology of the elements and the element attachment data for each node. An abridged example of such a file is presented in Appendix H.

At present, the MESHGEN program is component-specific, a specialised program being required for each generic component such as the elbow-shaped duct created by this version of the program. This component consists of two straight cylindrical shanks joined by a toroidal sector. The centreline of the duct is defined as two lines joined by an arc, and at intervals along the centreline a series of circles of nodes is defined (Fig. 6.8) in terms of node number and co-ordinates and written to the file. The node numbers are then used to define elements in terms of element topology, the ABAQUS topology convention being used (Fig. 6.9).

The concepts, operation and FORTRAN programming of MESHGEN are very straightforward and this description is included for completeness. The program includes a small amount of code imported from a data conversion program written by Crescent Consultants Limited. A flowchart of MESHGEN is given in Fig. 6.10.

It is envisaged that any computer-literate engineer should have no difficulty in customising MESHGEN to cope with many alternative component geometries. Some components such as the filament-wound tee piece require a less straightforward mesh-generation algorithm than the elbow and some further work will be required here in the future. It is possible, for instance, that mandrel geometry could be imported from commercially-available surface modelling software. A straightforward option would be to use an existing general-purpose mesh generation system such as FEMGEN[130] in lieu of MESHGEN to create the node and topology data required within

FILFEM II. It would be a simple data conversion and sorting exercise to rearrange this information into a format compatible with FILFEM II.

6.4.4.2. *Purpose and operation of MODELGEN program*

This program forms the core of FILFEM II. It implements the logic and geometry required to define the laminate structure within the FE model using the data from the filament winding process.

The main inputs to MODELGEN are:

a) the mesh definition file created by MESHGEN

b) the list of fibre families required to wind the component, together with other data including the number of times the winding pattern is repeated and data relating to the composite material itself

and c) CADFIL II data files containing the loci of points defining the families of fibre paths.

The output from MODELGEN is a file which contains:

a) the ply angles, thicknesses and number of layers within each element

b) the node co-ordinates defined at the mid-surface of the laminate

c) the surface normal vectors at each node, carried over from the mesh definition file

and d) the element topology, carried over from the mesh definition file.

An abbreviated version of a file produced by MODELGEN is given in Appendix I. It may be seen that although the file contains all the information required to construct an FE model, it is created in a neutral format, i.e. one which is not specific to any particular FE package. The conversion of the data to the format required by a given FE package is described in Section 6.4.4.3.

The model generation strategy operates by identifying which fibres pass over each element. This is achieved by erecting a box of planes to enclose

the element and using vector geometry to identify which fibres penetrate this box. It will be appreciated that fibres generally exist as families (Fig. 6.7) and each family of parallel fibres may pass more than once over a given element. A fairly involved search algorithm was therefore developed to categorise the various fibres crossing an element into the various separate plies within the laminate sequence. When determining the fibre direction for each ply, it is also necessary to choose the most representative region of fibre within each fibre family when it enters a given element. The logic for achieving the model generation is presented in simplified form in Fig. 6.11; the logic and geometry are described in full in reference 129.

Care has been taken to use good programming practice in encoding the MODELGEN program since it is intended as a foundation for further development work. Unnecessary code-writing was avoided by the use of existing vector arithmetic subroutines written by Crescent Consultants Limited. The only significant programming-related problem encountered was that the searching of the very large amount of fibre path data required the use of large arrays. For this reason, the computer's random access memory (RAM) capacity was only just large enough to cope. Retrieving the fibre path data from disc as required rather than storing it continuously in RAM would alleviate this problem but would make program execution slow.

The correct execution of MODELGEN has been tested using the fibre path data used in the manufacture of the elbow described in Chapter 8. Suggestions for more rigorous testing of the FILFEM II system are given in Section 6.6.2.

6.4.4.3. *Purpose and operation of FEDATGEN program*

FE packages require data input in a format which is specific to each package, and it is the purpose of FEDATGEN to convert the neutral-format

output of MODELGEN to the format required for FE data input. The version of FEDATGEN developed to date is compatible only with PAFEC but it would be simple to develop equivalent programs to provide data input for other FE codes such as ABAQUS.

The program is very straightforward in its operation, its function being purely that of data conversion and formatting. One characteristic of the PAFEC input data format is that ply orientations are specified in terms of the rotations of the global axis system. FEDATGEN includes a subroutine which obtains these angles from the direction cosine vectors of the principal material directions. Each ply of the laminate must be specified explicitly in the definition of the laminate, so if the lamination sequence forms a repeating pattern the sequence is written to the FE data file the appropriate number of times. A flowchart of FEDATGEN is shown in Fig. 6.12, and a typical mesh generated using FILFEM II is plotted in Fig. 6.13.

6.5 Discussion

Work has been carried out to link both of the CADFIL systems to typical finite element codes. Some detailed algorithms have been developed to achieve this, and these form the basis of the FILFEM model generation systems. Although the aims of FILFEM I and FILFEM II are superficially similar, their methods of operation are very different. FILFEM I accurately models the alternating lamination sequence of the nominally-axisymmetric filament-wound component. Only a minimal amount of information is available to define this structure since only a single fibre path is explicitly defined by CADFIL I. The details of the structure are therefore re-created by the logic of the FILFEM I program. By contrast, CADFIL II defines each fibre path separately and a very large amount of data is searched to extract the required information before sorting this information into a useful form. It is believed that most of the algorithms required to achieve these tasks form original work since little evidence can be found to suggest that similar objectives have been achieved elsewhere. The only aspect of the FILFEM systems which appears to overlap

significantly with earlier work is in the generation of meshes using axisymmetric shells because the CADMAC[16,18] system developed at Harwell included this facility.

6.6 **Recommendations for further work**

The FILFEM systems are intended to be used eventually as practical design tools, and this thesis describes the original work of establishing the theoretical basis of these tools. A certain amount of refinement, development and testing of these tools will be required if they are to be used in a working environment.

6.6.1 *Further work suggested for FILFEM I*

(a) Both the thin shell and axisymmetric models can be generated at present only for a single fibre pattern. Practical components, especially pressure vessels, usually include several winding patterns. This is to ensure complete coverage and to provide a structure with fibre angles appropriately chosen for supporting the required loads. It will require a certain amount of development work to extend FILFEM I to take account of multiple patterns. Such an extension should be straightforward for axisymmetric models but for the thin shell models it is difficult to imagine how the accurate representation of the lamination sequences could be extended to cover the complexities of a multi-pattern vessel.

(b) No satisfactory account is taken of the fibre build-up at the turnaround regions of the vessel, and wall thickness calculations near these regions show signs of inaccuracy. Some development work is required, probably to find empirical methods which give realistic practical predictions of component shape.

(c) Practical experience needs to be gained of FILFEM I in use. Some experience has already been gained and this is described in detail in Chapter 7. Further work on specimens with more complex geometries and

on real components would be of benefit in developing a practical design tool.

(d) The software has been written piecemeal and although a maintainable modular format has been adopted, a certain amount of rationalisation and software engineering would be beneficial. The user interface is currently somewhat basic and would benefit from development. Work is also required on both CADFIL I and FILFEM I to improve the interface between these packages or even to integrate them into a single system.

6.6.2 *Further work suggested for FILFEM II*

(a) This system currently exists largely as a testbed for the non-axisymmetric model-generation strategy which has been developed. Considerable further development would be beneficial to increase its versatility both in terms of the kind of components that can be modelled and in terms of its ability to function with FE systems other than PAFEC. Links with existing commercially-available surface modelling software and general-purpose mesh generation systems should be considered for development.

(b) A more rigorous search algorithm should be developed to simulate the sequence of laying each fibre and hence to provide a more accurate prediction of lamination sequence. Such a search would be in addition to the family-by-family search currently used for detecting the presence of fibres. The aim in developing FILFEM II and its underlying strategy was to lay the foundations for further work rather than to attempt a complete solution to the non-axisymmetric model-generation problem, and this area of development is typical of the kind of tasks that could form a continuation project.

(c) Because of the simplifications made to structures when automatically modelling them using FILFEM II, it is essential that experimental experience is gained to evaluate the usefulness of these automatically-

generated models. The assumptions and simplifications made in generating the models can then be refined in the light of the results obtained. Chapter 8 describes the manufacture of a filament-wound elbow and this work would form the foundation for an experimental programme to evaluate models such as the one illustrated in Fig. 6.13. It appears likely that the amount of work involved in such an investigation would be substantial. Such a programme of work would be able to make use of existing equipment for the in-plane and out-of-plane bending of tubular components and the elbow was designed to be compatible with this apparatus.

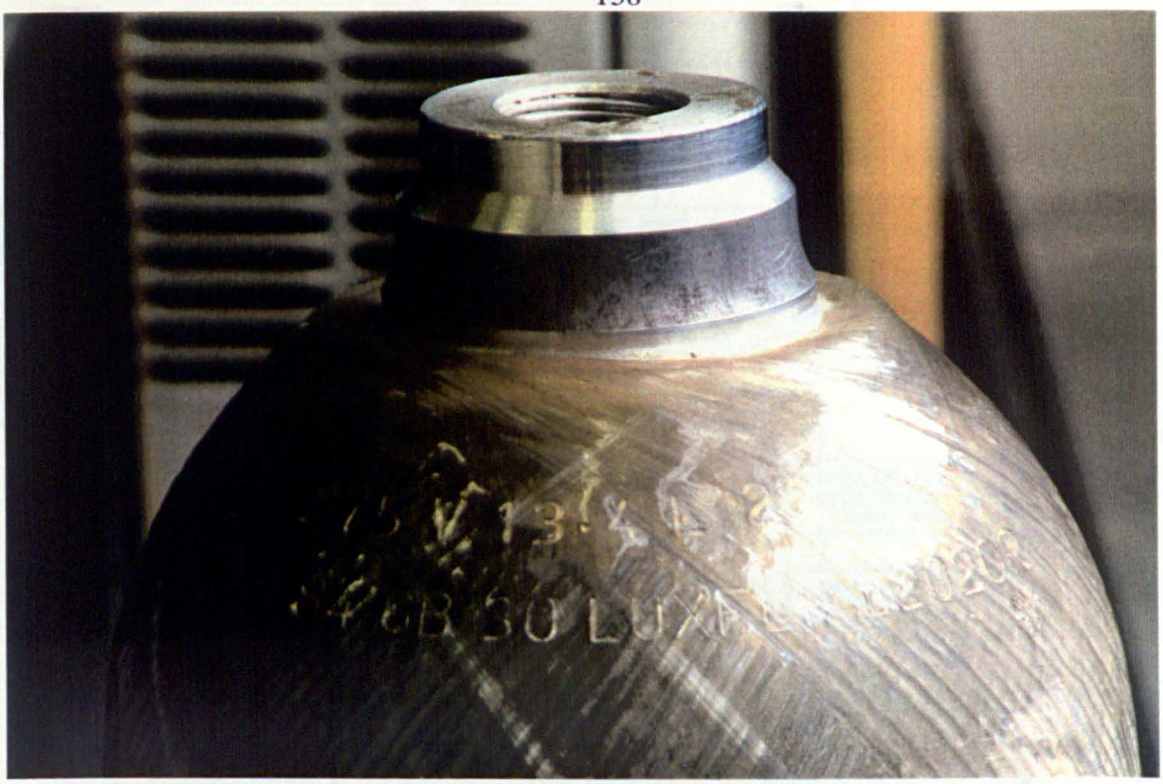

(a)

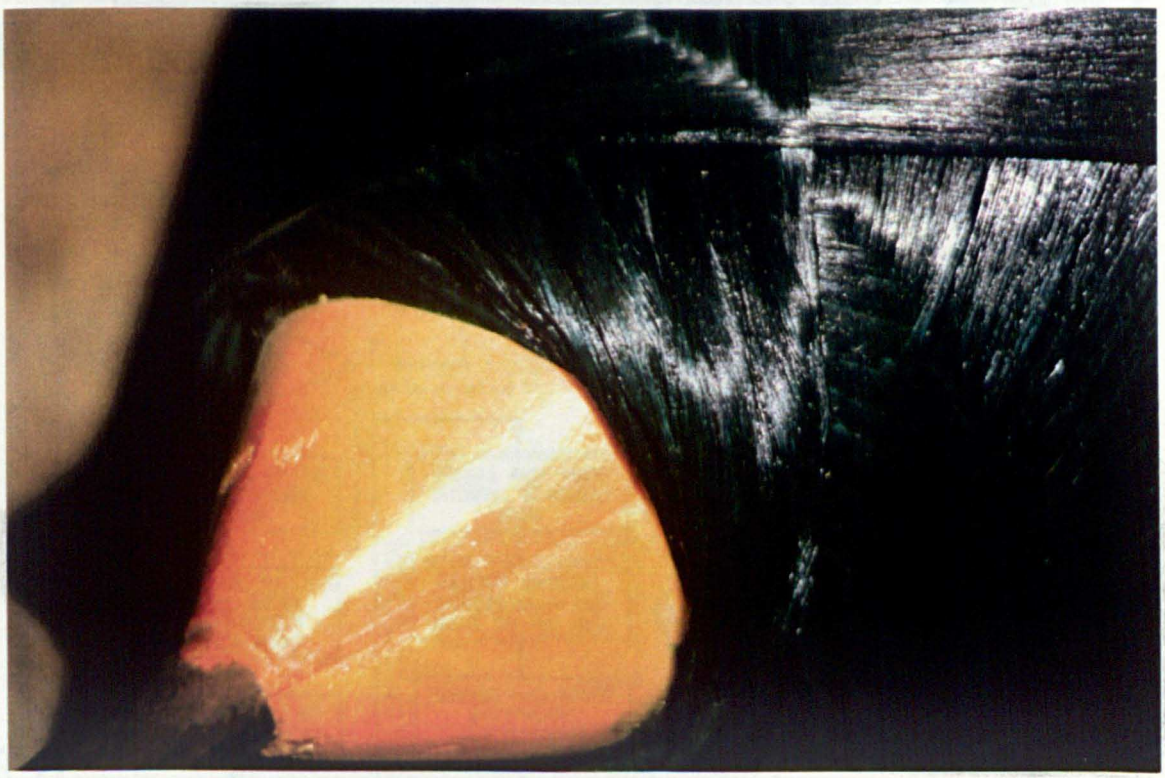

(b)

Fig. 6.1: Turnaround regions on two typical filament-wound components showing rope-like buildup of material where fibres run circumferentially

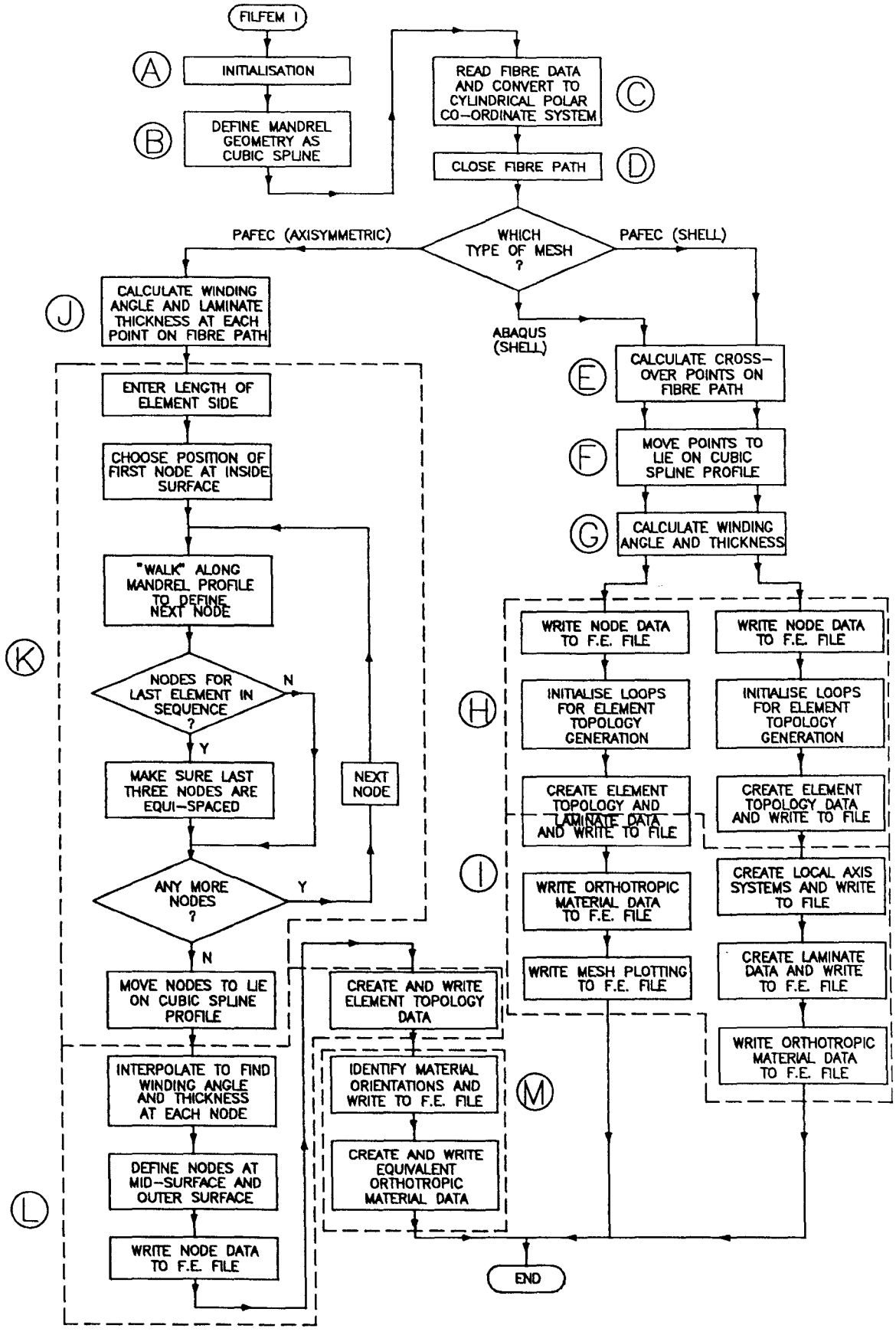

Fig. 6.2: Flowchart of program FILFEM I

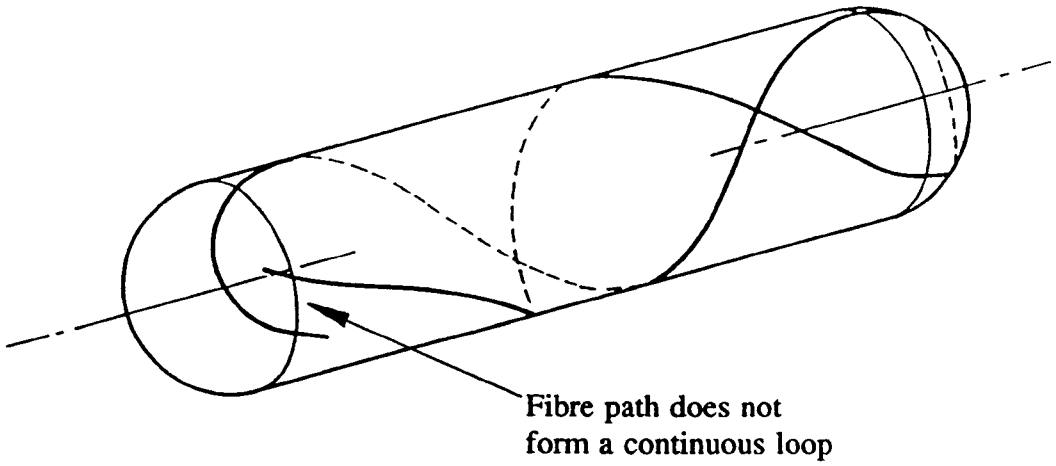

Fig. 6.3: Fibre path forming an open loop around a typical mandrel (dome-ended cylinder)

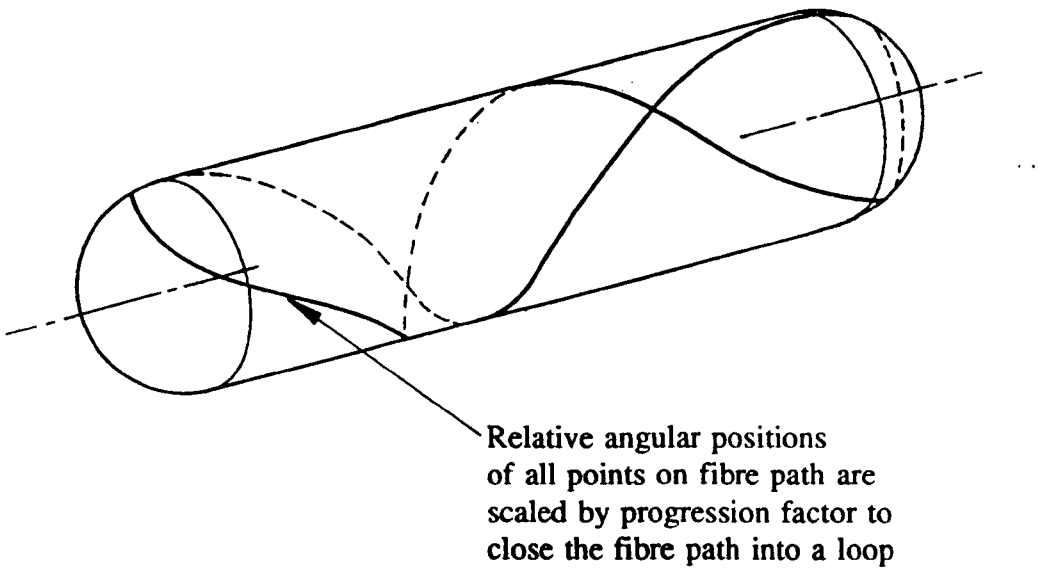

Fig. 6.4: Fibre path modified by application of a "progression factor" to form a closed loop

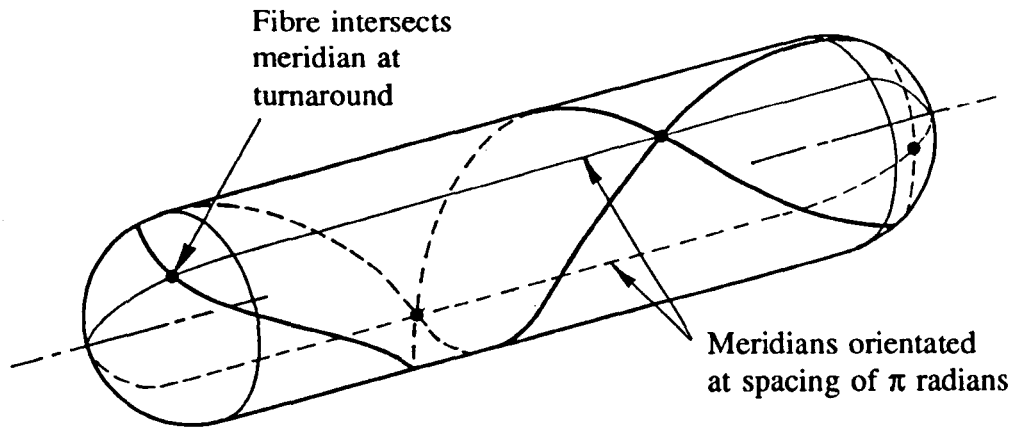

Fig. 6.5: Intersection of fibre with appropriate meridians predicts positions of turnaround and crossover points (Band pattern = m = 1, hence spacing of meridians = $\pi/m = \pi$ radians)

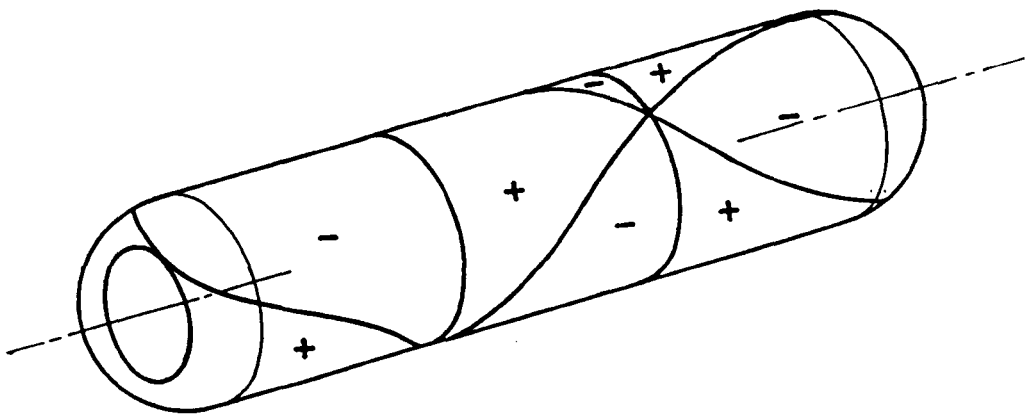

Fig. 6.6: Alternating lamination sequence built up using crossover points predicted in Fig. 6.5

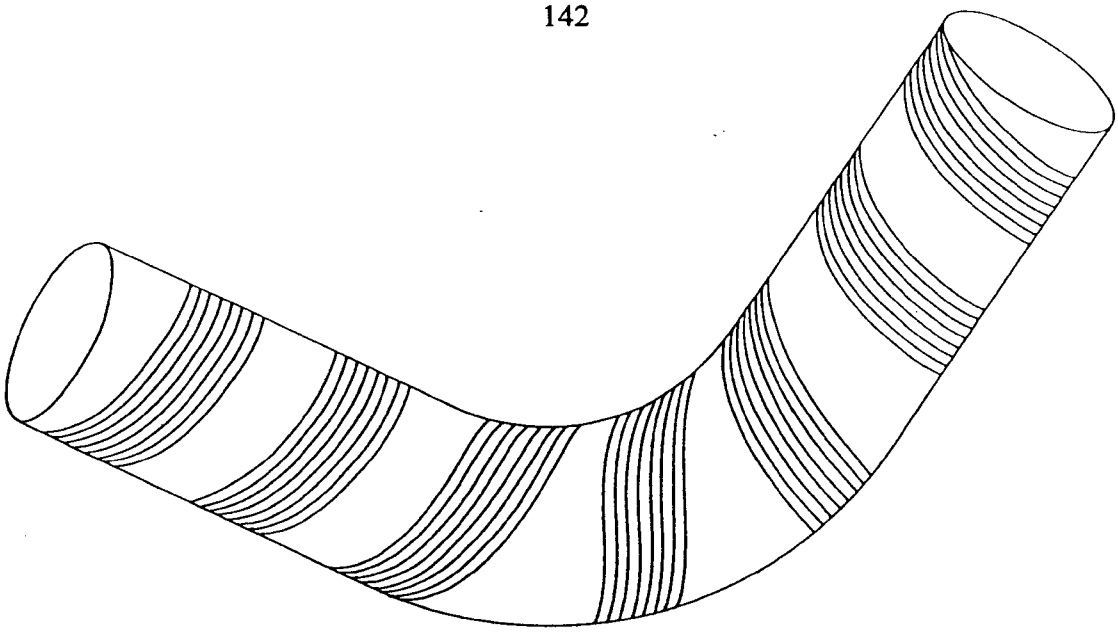

Fig. 6.7: A "family" of fibres over the surface of an elbow-shaped mandrel (simplified from plot of CADFIL II simulation)

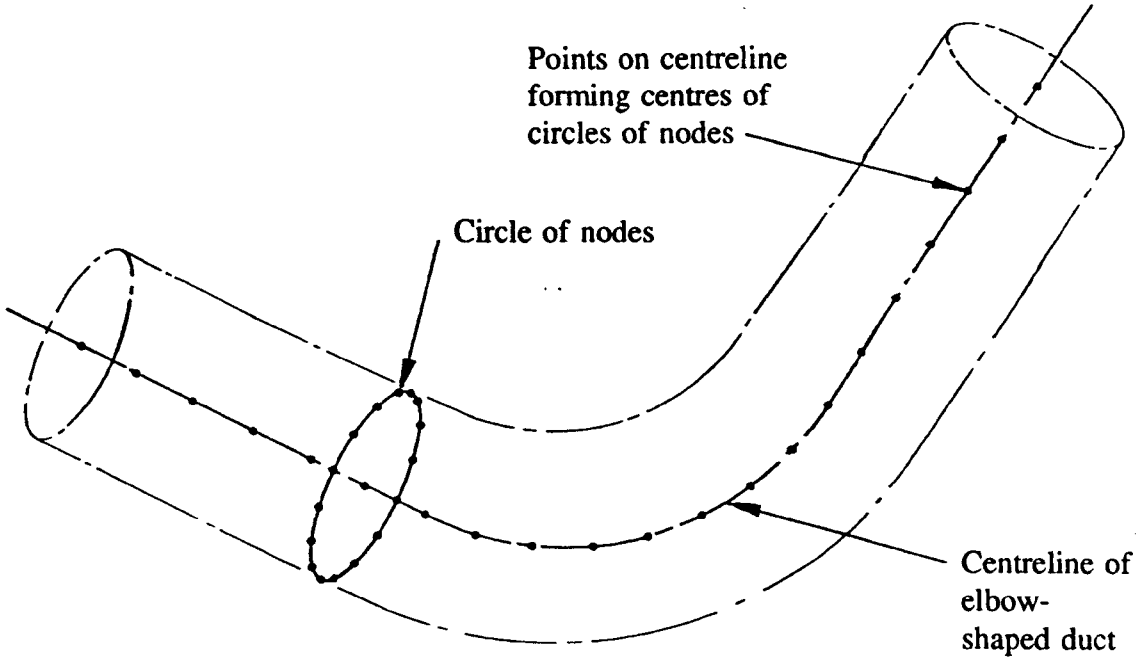

Fig. 6.8: Generation of nodes forming elbow-shaped duct using program MESHGEN

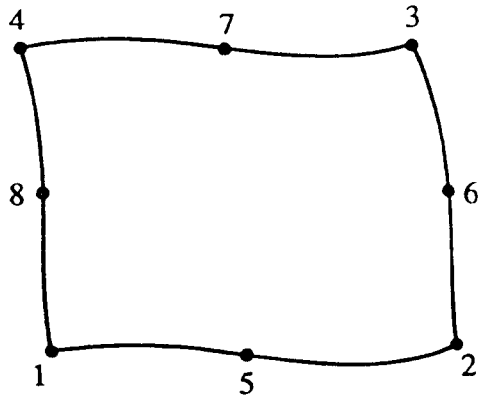

Fig. 6.9: Element topology convention used within ABAQUS and adopted for FILFEM II neutral file

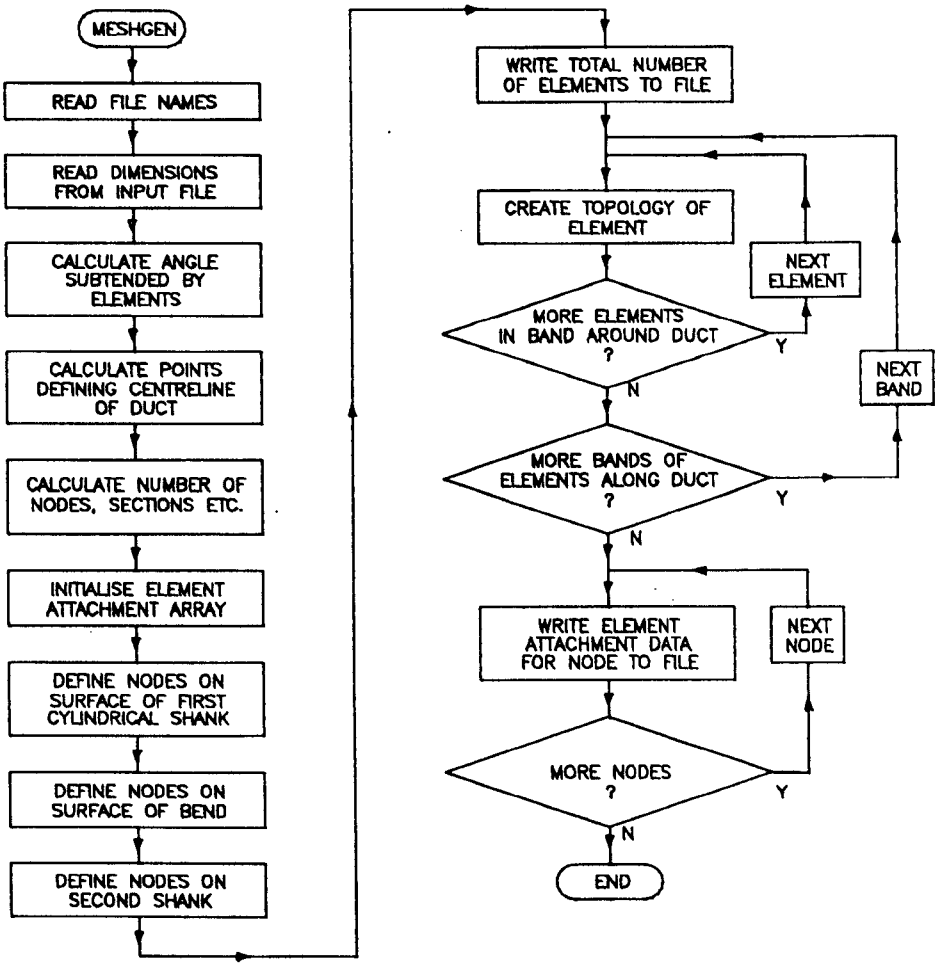

Fig. 6.10: Flowchart of program MESHGEN

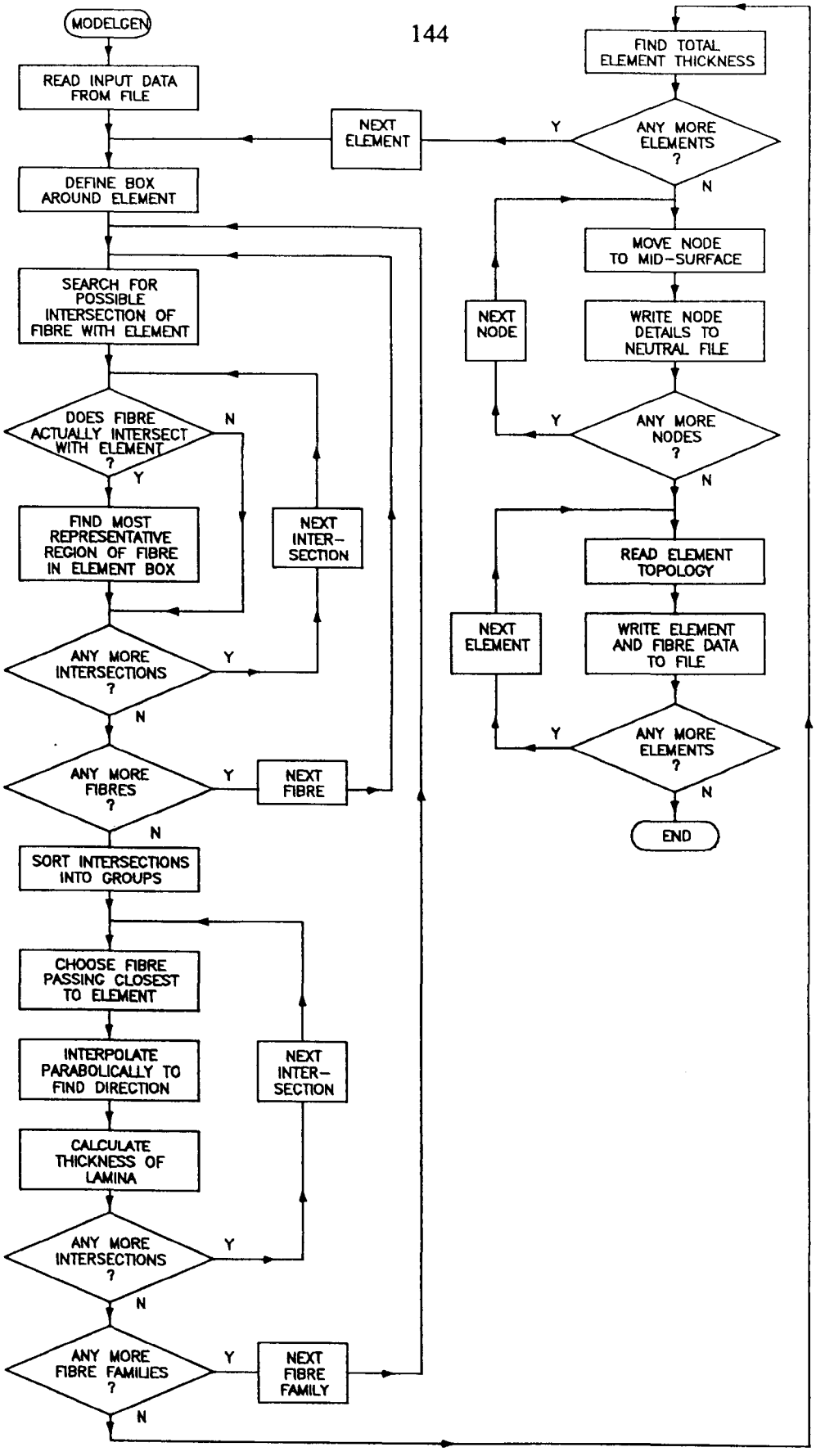

Fig. 6.11: Simplified flowchart of program MODELGEN

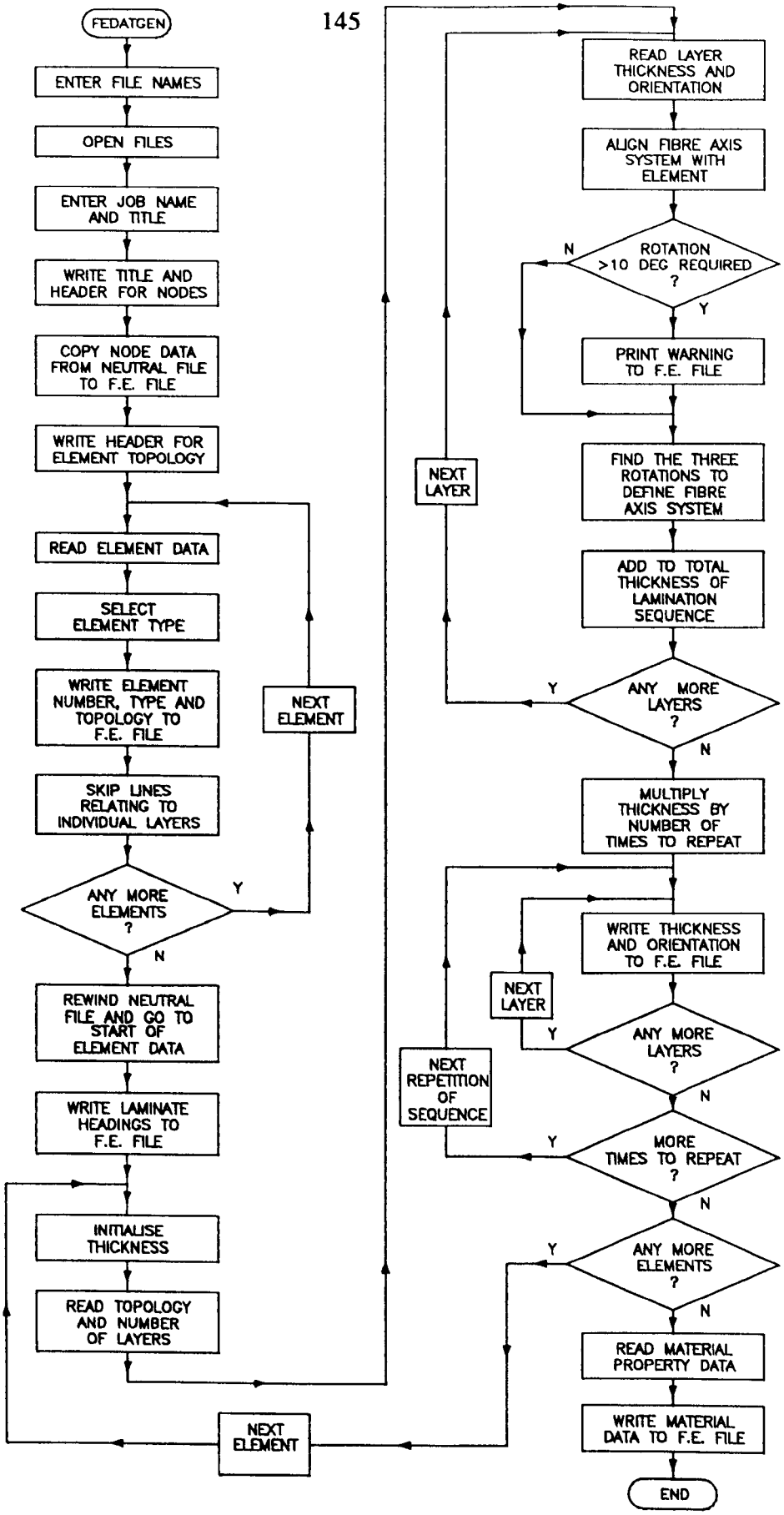

Fig. 6.12: Flowchart of program FEDATGEN

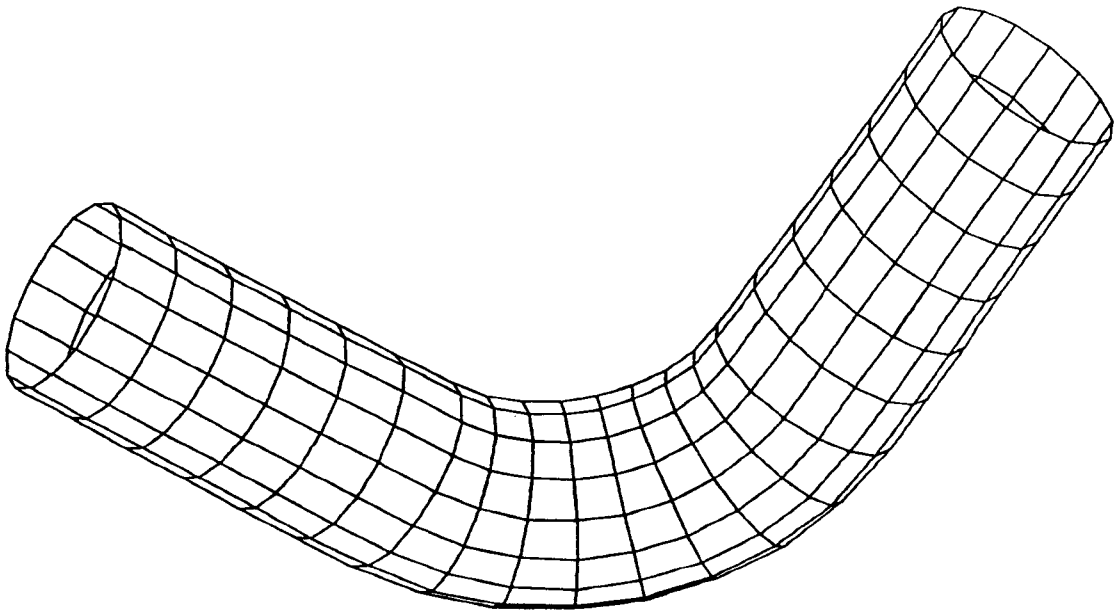

Fig. 6.13: Typical mesh created using the FILFEM II model generation program suite

CHAPTER 7: THEORETICAL, COMPUTATIONAL AND EXPERIMENTAL MODELLING OF A PINCHED ORTHOTROPIC CYLINDER

7.1 Introduction

In earlier chapters the scene has been set for the linking of the CAD/CAM filament winding process to existing finite element codes, with the aim of performing structural analysis of filament-wound components with a minimum of data preparation effort. The FILFEM software for achieving this link was described in Chapter 6, and it is the aim of this chapter to outline some practical experience gained in the use of this software. Manufacture and testing of a simple filament-wound cylindrical specimen has been undertaken, along with modelling of the test with the aid of FILFEM I. The objective is not to present a verification of the formulations of the elements used but rather to show that meshes generated using FILFEM I can be used to obtain realistic results when applied to a practical situation, namely the pinched cylinder problem. Various finite element models have been used and compared with experimental results, and a simple analytical model has also been developed to provide a further comparison. This chapter includes a description of the background to the analytical model, manufacture of the specimen using the CADFIL I software, the experimental testing of the specimen, and the use of a variety of finite element models generated using FILFEM I to model the situation.

7.2 Choice of specimen and load case

It was decided to tackle a component where the geometry could be defined as precisely as possible and to load it in a manner where the boundary conditions could be applied simply and reliably. The pinched cylinder problem was chosen since it provides a combined stress system, primarily bending and tension/compression. This is a reasonably challenging modelling task making use of a loadcase which is experimentally straightforward. In addition it is a problem for which a simple but

realistic analytical solution exists which can be extended to model the orthotropic and laminated situation.

7.3 Theory of the pinched cylinder problem

The pinched cylinder problem is well-known as an exercise in shell theory, and has been used by a variety of workers (e.g. Ashwell and Sabir[131]) as a benchmark for the testing of shell finite elements. It involves the determination of change in diameter of a cylindrical tube of finite length when subjected to a concentrated pinching load across a diameter (Fig. 7.1). Various alternative boundary conditions at the cylinder ends may be assumed.

Existing solutions all rely upon the modelling of the pinching load using a Fourier series. It is simple to show[140] that a pinching load P across a cylinder may be represented as a Fourier series of sinusoidally-varying loads acting on a band of infinitesimal width around the circumference of the cylinder (Fig. 7.2):

$$q(\theta) = q_0 + \sum_{n=1}^{\infty} q_n \cos\theta n \qquad (7.1)$$

where $q(\theta)$ is the load per unit of circumferential length at angular position θ, $q_0 = P/\pi$, $q_n = 0$ (n odd), $q_n = 2P/\pi$ (n even and positive). A graphical representation of this synthesis of a pinching load is given in Fig. 7.3.

The simplest solution to the problem of a pinched cylinder with free ends is quoted by Timoshenko and Woinowski-Krieger[132]. It uses Rayleigh's energy method and assumes that the deformations of the cylinder are purely inextensional (i.e. there are no membrane strains). For a cylinder pinched at its mid-length this solution yields results identical to those for a wide pinched ring (equation(5.2)); edge effects and any local dimpling of the shell under the load are ignored. This solution is useful only where circumferential bending is the only significant mode of deformation. Ashwell and Sabir[131] calculate a benchmark solution for a short, very thin cylinder based upon the solution in reference 132 corrected for edge effects using theory due to

Ashwell[133,134] extending the analysis by Lamb[109]. For longer cylinders, membrane strains become significant and more sophisticated solutions are required. One such solution, due to Ting and Yuan[135], is based upon shell theory, namely the complete Donnell shell equation[136] for the radial displacement w of a cylindrical shell (radius a, thickness t) under distributed load q:

$$\nabla^8 w + \frac{12(1-\nu^2)}{a^2 t^2}\frac{\partial^4 w}{\partial x^4} + \frac{2}{a^8}\frac{\partial^6 w}{\partial \theta^6} + \frac{1}{a^8}\frac{\partial^4 w}{\partial \theta^4} - \frac{12(1-\nu^2)}{Et^3}\nabla^4 q = 0 \qquad (7.2)$$

where x and θ are the axial and circumferential co-ordinates on the shell surface. This equation is solved by specifying q to be a Fourier series of sinusoidally-varying radial loads acting around the circumference of the cylinder. This solution does not readily lend itself to extension to the orthotropic case, at any rate not by extending the original derivation. This derivation is based upon identifying a rigorous solution of the complete Donnell equation then neglecting terms found to be insignificant. For an infinitely long cylinder pinched with load P between points (0,0) and (0,π), Ting and Yuan's solution may be presented in the following form:

$$w_\infty(|x|,\theta) = \frac{P}{Et}\sum_{n=2,4}^{n\ll c}\left(\frac{2c}{\pi}\right)\left(\frac{c}{n}\right)^2\frac{1}{(1-n^{-2})^{3/2}}\{\cos(\lambda_n|x|)+\sin(\lambda_n|x|)\}e^{-\lambda_n|x|}\cos n\theta$$

$$\text{where: } c = \sqrt[4]{3(1-\nu^2)}\left(\frac{a}{t}\right)^{1/2} \quad \text{and} \quad \lambda_n = \frac{n(n^2-1)^{1/2}}{2ac} \qquad (7.3)$$

Strictly speaking, the series is only accurate for $n \ll c$ because the assumption that $(n/c) \ll 1$ was made in truncating various expansions encountered in the derivation of equation (7.3). If one ignores localised edge effects of the kind discussed in Section 5.3.1, deflections may be calculated for a finite-length cylinder of with ends at $x=L_1$ and $x=-L_2$ by the superposition of additional terms, with constants $H_{1\text{-}4n}$ chosen to satisfy the boundary conditions at the cylinder ends (for instance, $\partial^2 w/\partial x^2 = \partial^3 w/\partial x^3 = 0$ for free ends):

$$w(x,\theta) = w_\infty(x,\theta) + \sum_{n=2,4}^{n\ll c}\Big\{\big[H_{1n}\cos[\lambda_n(L_1-x)] + H_{2n}\cos[\lambda_n(L_1-x)]\big]e^{-\lambda(L_1-x)}\cos n\theta + \big[H_{3n}\cos[\lambda_n(L_2+x)] + H_{4n}\sin[\lambda_n(L_2+x)]\big]e^{-\lambda(L_2+x)}\cos n\theta\Big\} \qquad (7.4)$$

In presenting an alternative solution to the pinched cylinder problem, Calladine[137] reverts to the use of Rayleigh's method. In this instance the contributions to strain energy due to axial membrane strain and circumferential bending are considered. The published version of Calladine's theory assumes that circumferential and shear membrane strain are constrained to zero. Once again a Fourier series of loads is assumed, and for each Fourier harmonic an expression for the total potential energy is found. It is observed that for each harmonic this expression is analogous to the corresponding expression for a beam on an elastic foundation, the analogy being expressed as the equivalence of the following quantities:

Quantity (referred to beam on elastic foundation problem)	Symbol		Equivalent quantity for pinched cylinder problem
	Used in this chapter	Used by Hetenyi[52]	
Deflection	w	y	$w_n \cos n\theta$
Beam flexural rigidity	B	EI	$B_n = \dfrac{\pi E t a^3}{(1-\nu^2)n^4}$
Foundation modulus (force per unit length per unit deflection)	k	k	$k_n = \dfrac{\pi E t^3 (n^2-1)^2}{12(1-\nu^2)a^3}$
Concentrated load on beam	F	P	$F_n \cos n\theta = 2P \cos n\theta$ for even $n \geq 2$
Decay parameter (derived from k and B)	λ	λ	$\lambda_n = \sqrt[4]{\dfrac{k_n}{4B_n}} = \sqrt[4]{\dfrac{t^2 n^4 (n^2-1)^2}{48a^6}}$

It is now a simple matter to construct an analogous beam-on-elastic-foundation problem and to select the appropriate solution from Hetenyi's catalogue of results[52]. For each Fourier component of the load, Q_n, B_n, k_n and λ_n may be evaluated and inserted into the chosen solution and the Fourier component of the deformations evaluated. For instance, the deformation of a cylinder of infinite length may be expressed as:

$$w_{\infty}(x,\theta) = \sum_{n=2,4}^{m<(a/t)^{1/2}} \frac{F_n \lambda_n}{2k_n}\left[\cos(\lambda_n |x|) + \sin(\lambda_n |x|)\right] e^{-\lambda_n |x|} \cos n\theta \qquad (7.5)$$

The terms of the series start to become inaccurate for $n \approx (a/t)^{1/2}$ when the strain energy used in meridional bending becomes significant. In the author's experience, the difference between the deflections predicted by the theories of Calladine and Ting and Yuan is typically in the order of one percent.

The assumption that circumferential membrane strain is constrained to zero appears intuitively to be an unrealistic one and is responsible for the $1/(1-\nu^2)$ factor in the formula for B_n. Calladine states that a more complex derivation shows that the analogue can be improved by the elimination of this term. λ_n may now be re-calculated and inserted into equation (7.5). The author has observed that if this is achieved, the result is almost precisely equivalent to Ting and Yuan's theory summarised in Equation (7.3), the only discrepancy being a slight difference in the rule for the validity of the high-order terms. Similarly, the corresponding modifications to Calladine's results for finite-length pinched cylinders can be re-arranged into the form of Ting and Yuan's general solution, equation (7.4). Surprisingly, Calladine makes no reference to Ting and Yuan's solution.

The theory and derivation presented by Calladine are especially useful because they are easily extended to cover the orthotropic case; the main steps of achieving this extension are presented in Section J.2 of Appendix J and the following expressions are obtained:

$$B_n = \frac{\pi E_x t a^3}{(1-\nu_{x\theta}\nu_{\theta x})n^4}, \quad k_n = \frac{\pi E_\theta t^3 (n^2-1)^2}{12(1-\nu_{x\theta}\nu_{\theta x})a^3} \text{ and } \lambda_n = \sqrt[4]{\frac{E_\theta t^2 (n^2-1)^2 n^4}{48 E_x a^6}} \qquad (7.6)\ (a\text{-}c)$$

It would be of interest to investigate whether the adaptation of Calladine's theory to that of Ting and Yuan could be extended to consider the homogenous orthotropic case, for instance by the elimination of the $1/(1-\nu_{x\theta}\nu_{\theta x})$ factor in the expression for B_n, and additional work would be required here to check the validity of such an approach.

It may be observed that the expressions for B_n and k_n in Calladine's original theory include the factors $Et/(1-\nu^2)$ and $Et^3/12(1-\nu^2)$, with equivalent orthotropic quantities appearing in equations (7.6)(a-c). It is tempting to extend the theory to cover the behaviour of laminates by making appropriate substitutions for these shell section stiffnesses using classical lamination theory. Some suggestions are outlined in Section J.4 of Appendix J, along with results in Section J.7 which show good agreement with an appropriate FE solution. However, such intuitive modifications should be regarded as useful engineering approximations rather than rigorous engineering mechanics.

Although analytical solutions of this kind are apparently only useful for a cylinder with uniform properties along its length, it is possible to extend the orthotropic Calladine solution to analyse a cylinder with varying properties (Fig. 7.4(a)). This is achieved by discretising the cylinder into a series of short rigidly-linked (contiguous) homogeneous cylinders each with uniform properties (Fig. 7.4(b)). This system is modelled (using Calladine's analogy) as a contiguous series of elastically mounted beams each with different flexural rigidity and foundation modulus (Fig. 7.4(c)). It is then a matter of linear algebra to enforce equilibrium and compatibility between the beams[138] and hence to find the behaviour of the whole system under the appropriate load case. The matrix displacement method[139] was used to achieve this solution, which was then applied to the pinched cylinder problem. The theory underlying this solution, and a description of the computer program used to implement it, are presented in sections J.3 and J.5 respectively of Appendix J. Results obtained from this model are included in Fig. 7.23 and will be discussed in Section 7.9. This approach is similar to that adopted by Highton and Soden[54] to the problem of axisymmetric loading of non-uniform filament-wound tubes (Section 3.4.2) but the application of this approach and its implementation are different.

7.4 Selection of specimen dimensions and structure

The inside diameter of the cylinder was originally chosen as 76.2 mm (3") to be compatible with some existing loading equipment, although no advantage was

eventually taken of this compatibility. The length was chosen to be several times the diameter of the tube (approximately 6 times) to minimise the influence of edge effects upon the accuracy of the analytical solution. The winding pattern (4 layers, band pattern number of 1) was chosen to provide a laminate structure with significant coupling between bending and tension, enabling some degree of evaluation to be made of the effects of accurate and simplified modelling of the lamination sequence whilst retaining reasonable robustness of the specimen.

The winding pattern was developed using CADFIL I; to facilitate removal of the specimen the turnaround of the fibre was achieved on the cylindrical portion of the mandrel using frictional steering. The fibre path (as originally generated, before processing to give complete coverage) is shown in Fig. 7.5. The winding angle was arbitrarily chosen to be approximately ±45° halfway along the specimen, gradually increasing in value as the turnaround regions were approached. The value of winding angle at the points where the turnaround regions were cut off was approximately ±65°. The distribution of winding angle along the specimen is given in Fig. 7.6; this data was calculated within FILFEM I from the CADFIL I fibre path data.

The specimen was manufactured by filament-winding directly onto an aluminium mandrel. The same materials were used as were described in Chapter 5 (Scott Bader Crystic 272 polyester resin with catalyst powder B[112], Silenka 2400 TEX E-glass rovings[111]). Several coats of aqueous release agent (Würtz PAT-607/PCM[113]) were used to avoid adhesion of the resin to the mandrel. The completed specimen was cured in an oven and was removed from the mandrel by sliding axially. The turnaround regions were cut off manually using a diamond-edged circular saw; the exact positions of the sawcuts were chosen to maximise the length of the cylinder without encroaching upon the distorted winding pattern of the turnaround regions. The dimensions of the cylinder are shown in Fig. 7.7; this also specifies the locations of the points at which the change in diameter is measured.

7.5 Apparatus

The equipment used was an Instron 1195 universal testing machine with load measurement being achieved using the Instron's 50kN load cell on the lowest (1kN FSD) range. Sensitivity and calibration have already been discussed in Section 5.3.5. The usual arrangement of jaws or grips was replaced with a pair of cylindrical anvils of approximate diameter 25mm. A diagram showing the method of loading is given in Fig. 7.8, and a general view of the apparatus is shown in Fig. 7.9. Fig. 7.10 shows the specimen in position in the Instron machine.

7.6 Dimensional measurement techniques

Earlier attempts to perform a pinched cylinder exercise with similar filament-wound tubes had made use of a 75-100mm micrometer to measure the change in diameter of the tube at various marked points on the specimen. The advantages of this method are as follows.

a) It is simple and cheap; the only capital equipment required was an existing micrometer, in comparison with automated measurement techniques using (for example) linear variable differential transformers (LVDTs).
b) It is potentially very accurate: there are none of the calibration problems associated with remote-sensing devices such as LVDTs.

However, the following drawbacks were experienced.

a) The method is tedious, each test taking several hours. The main problem associated with this characteristic was that viscoelastic creep and relaxation of the specimen became significant within the set of readings relating to any particular value of load.
b) It proved difficult to obtain consistent micrometer readings across a filament-wound GRP tube because of surface irregularities.

Drawback (a) was alleviated by the deliberate use of overshoot in the loading cycle (see below). Drawback (b) was overcome by attaching small mild steel cups to the

surface of the specimen at the points of interest; these acted as locations in which the anvils of an improvised ball micrometer could rest, giving a repeatable position for the micrometer. The positions of the cups are specified in Fig. 7.7 and were chosen to coincide with crossover points on the winding pattern. This enabled accurate comparison to take place between positions on the specimen and on the FE model. Rapid-setting epoxy adhesive was used to bond the cups to the specimen. Fig. 7.11 shows the finished specimen and Fig. 7.12 illustrates one of the micrometer cups.

Although the FILFEM system automatically calculates the thickness of the structure at every node, it was considered important to measure the actual thicknesses of the specimen in case serious errors persisted in the results and required investigation. Accordingly, a simple thickness measurement rig was manufactured; this consisted of a dial test indicator and a cantilevered anvil and is illustrated in Fig. 7.13. It was estimated that errors due to the flexibility of the cantilever bar were typically 0.01-0.02mm and that the total error due to this source and to misalignment of the anvils was typically 0.05 mm. This was judged to be insignificant in view of the thickness variations of the specimen due to the irregular nature of the filament-wound surface. The thickness of the cylinder was measured at 25mm intervals along four meridians on the cylinder. These thickness measurements are plotted against axial position in Fig. 7.14, along with the thicknesses calculated within the FILFEM program. It may be seen that despite the considerable scatter in the individual measurements of thickness there is good agreement between the mean readings and the calculated thicknesses except at the ends where the measured thicknesses are a few percent greater than those calculated. One possible source of this error is the finite width of the flattened rovings since this invalidates the thickness calculation method at steep winding angles. Another possible source of this error is fibre slippage as the friction-controlled fibre path approaches the turnaround.

7.7 Experimental procedure

The equipment was switched on and allowed to warm up for several hours before calibration. The specimen was placed in the machine so that point contact took place

between the specimen and the anvils at the desired position. In preliminary experiments it was decided to place rubber pads between the anvils and the specimen to avoid damage at the contact points, but it was discovered in practice that the viscoelasticity of the rubber led to load relaxation during the tests. It was also found using experiments with FE models that significant errors could be introduced if the pads were to spread the load over too large a contact area. As an extreme example, differences in deflection ranging between 7% and 30% were found for a pinching load spread over an approximately square area subtending an angle of 45° on a simple isotropic cylinder when compared with corresponding results for a point-loaded model. Accordingly, for the final experiments the rubber pads were omitted leading to very small contact areas only a few millimetres across. It was found necessary to place a layer of masking tape over the anvils to increase the friction between the contacting surfaces and hence to discourage the specimen from slipping at low levels of load.

Before taking readings, the specimen was subjected to several load cycles up to a maximum of 300N and back to zero in an attempt to reduce hysteresis effects during the actual test of deflections vs. load, although for reasons outlined in Chapter 5 this procedure was probably misguided. The specimen was then loaded up to 50N and hence in increments of 25N up to a maximum of 300N and back to 50N and zero. At each load increment the diameter across each pair of micrometer cups was measured using a ball-anvil micrometer. The readings at 25N were omitted as the cylinder tended to slip at low values of load. Two sets of readings were taken using this method. The first (Test 1) involved straightforward incremental loading and unloading according to the above procedure with only slight overshoot when setting each load value. The second (Test 2) involved significant and deliberate overshoot (of typically 10N per reading) in a successful attempt to reduce the effects of viscoelasticity and hysteresis upon the nominally elastic load-deflection characteristics. The readings of load and deflection for the two tests are given in Tables 7.1 and 7.2, and the results of a linear regression on the observations are given in Tables 7.3 and 7.4. Typical graphs of diametral deflection vs. load are presented in Figs. 7.15 and 7.16. A program very similar to CORREL (described in Section C.2.2 of Appendix C) was used for carrying out the linear regression analysis.

On completion of the tests it was observed that there was visible delamination damage to the specimen covering an irregular patch approximately 10mm in diameter in the region where each roller had made contact. This patch did not necessarily correspond to the actual area of contact. No other damage was visible.

When no further tests were required, the cylinder was sliced for fibre mass fraction measurements. Three such measurements were made using a burnoff procedure based upon BS2782: Part 10: Method 1002[114]. The values obtained were 75.86%, 74.35%, 76.11%, which average to 75.44%.

It may be seen from Figs. 7.15 and 7.16 that there is some scatter and hysteresis, although it would appear to be reasonable to fit a straight line through the experimental points in each case. The two different procedures for load application gave results with differing degrees of hysteresis and non-linearity but with no significant differences in the gradients calculated by the linear regression. It is results from the second test which will be compared with the theoretical and finite element results.

7.8 Finite element models

The models of the cylinder dimensions and laminate structure were all based upon data files generated within FILFEM I. In all cases however, modifications were made by editing the data in order to remove unwanted parts of the structure, to refine the mesh locally around the loading and restraining points, to select alternative element formulations, to set the values of material properties and to add boundary conditions and program control commands. In all cases but one, the material properties used were those fitted to the flexural (pinched ring) results in Chapter 5, normalised to a fibre content of 75.44%. These properties are presented in Table 7.5 and were used because they represented material behaviour in the experimental situation most closely matching the system being modelled. The bending strains in the pinched cylinder situation are comparable with those in the pinched rings, being typically 1150 με at

the positions (0, $\pm\pi/2$) rising to a large (theoretically infinite) value at the loading and restraining points.

7.8.1 *ABAQUS thin shell models*

These are based upon two meshes, with 24 and 32 elements respectively around the circumference of the cylinder. Two meshes were used to confirm that the meshes under consideration were adequately refined. In both cases, the ends of the mesh were modified (by deletion of unwanted elements and redefinition of the end nodes) to coincide with the true positions of the cylinder ends after removal of the turnaround sections. In all cases, curved thin shell elements S4R5 (quadrilateral) and STRI35 (triangular) elements are used. The undeformed shapes of the meshes are illustrated in Figs. 7.17 and 7.18. The element edges are represented as straight lines due to the limitations of the graphical output facilities.

The boundary conditions were added manually and were as follows. Restraint against translation in all three directions was provided at the support point for the cylinder; vertical movement only was permitted at the loading point. The cylinder was restrained against rigid body rotation (about the line of action of the load) by applying a restraint against transverse movement to a point at one end of the cylinder. The boundary conditions are included in Fig. 7.18.

No attempt was made to utilise the symmetry of the mesh. This was because although the pattern of element boundaries is symmetrical about the plane z=0, the element properties are antisymmetric about this plane and hence there is no overall symmetry of structural behaviour about this plane; attempts to impose such symmetry would lead to spurious restraints upon the coupling effects present in this laminated structure. The apparent rotational symmetry of the mesh structure about a diameter perpendicular to the line of action of the load is only approximate and is dependent upon the winding pattern used in manufacture.

Two variations were made upon the model with 32 elements around the cylinder. One of these models was edited to represent a uniform lamination sequence rather than an alternating one. The other model includes the alternating lamination sequence but uses the material properties calculated using the Halpin-Tsai equations (equations (5.1) (a-d)) for the appropriate fibre content (Table 7.5). These properties were used as an alternative to the best-fit properties used elsewhere.

The models were run without difficulty. A typical plot of the deformed shape of the mesh is shown in Fig 7.19. The deflection results from all models were processed to give changes in vertical and horizontal diameter at node positions along the cylinder. The results are compared with the experimental results (test 2) in Fig. 7.20.

7.8.2 *PAFEC thin shell and thick shell models*

The mesh structure and boundary conditions are equivalent to those represented in the ABAQUS model with 32 elements around the cylinder. As with the ABAQUS models, the PAFEC data files were automatically generated then edited manually. Three models were used, each using a different set of element formulations within the PAFEC element library. The elements used were the Ahmad thick-shell elements 46215 (quadrilateral) and 46115 (triangular) and the equivalent semi-Loof thin shell elements 43215 and 43115, with the 43215 elements used in both their full (9-point) integration and reduced (4-point) integration formulations. In all cases the material properties used were those fitted to experimental flexural data.

The models were run without major difficulties, although some warnings were flagged for all three models. Some of these related to elements in the regions of mesh refinement where there is just sufficient distortion of element shape to merit a warning. More seriously it was noted for all three models that ill-conditioning (difficulty in achieving a numerically stable solution) was suspected in the region of the restraint against rigid-body rotation. A typical cause of ill-conditioning is

a major variation in the stiffness of different parts of a structure although such variations are not obvious to the writer in this instance. An attempt was made to alleviate the problem using alternative restraints against rigid-body rotation but this only caused more warnings of this type to be flagged. While some degree of caution should be exercised in examination of the results in these circumstances, no spurious or unexpected deflections were observed in the relevant region and it is the writer's belief that no significant problem exists. The deflections from these models are compared with the experimental results (Test 2) in Fig. 7.21.

7.8.3 *PAFEC axisymmetric Fourier model*

It has already been described in Section 7.3 how a Fourier series of sinusoidally-varying radial loads can be used to construct a pinching load on a cylinder, and this technique may be used in conjunction with the axisymmetric Fourier elements available within PAFEC. If these are used, it is necessary to simplify the laminate structure by representing it as an equivalent homogeneous orthotropic material with properties defined by equations (5.9)(a-d). In making this simplification it is necessary to assume that the laminate has many layers and hence that the coupling effects present in the laminate become negligible. An antisymmetric laminate with four layers is a poor candidate for this simplification; however, the problem has been modelled in this way as a demonstration of the application of FILFEM I to axisymmetric meshes and as a comparison with the analytical solution to the pinched cylinder problem for which the same assumptions may be made.

Once again the finite element model is based upon a file generated by FILFEM I; in this case the equivalent orthotropic properties of the laminate are automatically calculated within FILFEM I based upon the supplied unidirectional material properties (in this case, the values fitted to experimental flexural data). The level of mesh refinement was chosen to preserve a reasonable aspect ratio to the elements, and no convergence checks on mesh refinement have been performed. The maximum aspect ratio (ratio of element edge lengths) was

approximately 2.8:1 for this mesh; the ideal ratio is 1:1 but warnings are not given below a ratio of 5:1. The file defining the FE model was edited to remove unwanted parts of the structure and to add boundary conditions. The mesh used for the analysis of the problem is shown in Fig. 7.22. The plot is misleading as it would appear that the cylinder is stepped rather than of having the smooth profile shown in Fig. 7.14; this is due to the limited resolution of the graphical output facilities.

The loading on these elements is defined as the total load per circumference for n=0 and $q_n\pi$ for n=2...∞ where q_n is defined in equation (7.1); therefore the values of load specified in the FE data file are $2P$ for n = 0, 2, 4...∞[140,141]. A restraint against axial movement was provided at the point of application of the load. The finite element model was run separately for each harmonic in the Fourier series. The vertical displacements w_v are obtained by summing the terms in the series; the horizontal displacements w_h are obtained by adding and subtracting alternate terms:

$$\begin{aligned} w_v &= w_0 + w_2 + w_4 + w_6 \ldots \\ \text{and} \quad w_h &= w_0 - w_2 + w_4 - w_6 \ldots \end{aligned} \tag{7.7}$$

These radial displacements are multiplied by 2 to give change in diametral measurements, and are compared with experimental results in Fig. 7.23. Also presented in Fig. 7.23 are equivalent results obtained by the orthotropic extension to Calladine's pinched cylinder solution described in Appendix J (sections J.2 and J.3).

7.9 Discussion

It may be seen that, with the exception of the results obtained from the axisymmetric mesh, all the finite element models based upon the material properties fitted to experimental flexural data agree within a few per percent with the experimental results for the pinched cylinder. It will be observed that they also agree closely with each other. In particular, it may be noted that the refinement of the ABAQUS mesh from

24 elements to 32 elements around the cylinder alters the results typically by 2%; this suggests that the results have converged to an acceptable degree. It is also noted that accurate representation of lamination sequence alters the results by even less (typically 1%) compared with an otherwise identical mesh which assumes the lamination sequence to be uniform. The PAFEC thick shell elements and the semi-Loof elements with full integration agree within about 2% with each other but are typically 5-12% over-stiff compared with the experimental results; the reduced-integration semi-Loof elements give results almost identical to the ABAQUS thin shell elements, are around 3% more flexible than the same elements with full integration, and are within 3-6% of the experimental results.

It should be noted that the accuracy of material properties used in any structural analysis are crucial to the validity of its comparison with experimental data. Considerable difficulties were encountered in obtaining consistent material property data and these problems were discussed in Chapter 5. FE analyses carried out using properties obtained by alternative means will give results with differing levels of agreement with experimental data. For example, if the material properties predicted from the Halpin-Tsai equations are used, the disagreement between FE results and experimental results increases to around 15% using the ABAQUS thin shell elements.

It is predictable that the axisymmetric Fourier elements will lead to inaccurate results for this particular problem because of the simplifications made when modelling the four-layered laminate as a homogeneous material; the predicted deflections are smaller than those measured experimentally by typically 10%. However, the results from these elements are in close agreement (differences of between 2% and 4%) with those from the analytical solution. Agreement between these two solutions is to be expected since they both assume that the same simplification is made to the laminate structure.

It should be noted that the thickness and winding angle data for the analytical solution was prepared using a version of FILFEM I modified to write these data to a file. The analytical solution does not, therefore, provide independent verification that these values have been correctly processed within FILFEM I. However, close agreement

was observed between the predicted and measured wall thicknesses of the specimen except near fibre turnaround. This in turn suggests that the winding angles used in predicting wall thickness are also correctly predicted.

7.10 Conclusions

An analytical solution has been obtained to the problem of a pinched filament wound cylinder, and various suggestions have been made for refinement to this solution. The FILFEM I mesh generator has been successfully used to model this situation, and a number of different models created with it have all yielded results which agree reasonably well between themselves and with experimental data. The results from two of the thin shell element models (ABAQUS thin shell, PAFEC semi-Loof with reduced integration) agree closely with each other and are closest to the experimental results. Simplification of the model to ignore the variations in lamination sequence over the component made no significant difference to the results obtained from this analysis. The results from the axisymmetric finite element mesh agree closely with another set of results which they are most likely to be comparable, namely the results of the analytical solution to the problem of the pinched cylinder with equivalent homogenous orthotropic material properties.

It may be concluded that FILFEM I provides an effective method of generating the vast majority of the data required to model nominally-axisymmetric filament-wound structures using a variety of different types of mesh, although a moderate amount of manual effort is required in adapting the data to model the actual component and load case under consideration. Some improvements may need to be made in the calculation of wall thickness in the region of the fibre turnaround.

Table 7.1: Diametral measurements of filament wound cylinder under pinching load: test 1

Load (N)	Measurement point number: table gives micrometer reading (mm) for each value of pinching load												
	1	2	3	4	5	6	7	8	9	10	11	12	13
0.000	101.455	101.155	101.345	101.200	100.820	100.895	100.235	100.495	100.530	100.725	100.835	99.505	101.145
50.000	101.385	101.255	101.220	101.340	100.575	101.085	100.499	100.240	100.755	100.565	101.010	99.470	101.255
75.000	101.350	101.275	?101.420	101.420	100.450	101.200	100.635	100.095	100.895	100.480	101.100	99.415	101.250
100.000	101.310	101.295	101.040	101.500	100.310	101.295	100.735	99.965	101.000	100.380	101.180	99.380	101.335
125.000	101.240	101.350	100.945	101.580	100.170	101.450	100.865	99.830	101.130	100.300	101.255	99.350	101.345
150.000	101.220	101.400	100.875	101.635	100.010	101.580	101.000	99.680	101.230	100.200	101.310	99.290	101.370
175.000	101.150	101.430	100.790	101.740	99.885	101.685	101.140	99.535	101.385	100.125	101.450	99.235	101.435
200.000	101.125	101.480	100.700	101.840	99.750	101.860	101.280	99.400	101.510	100.045	101.510	99.200	101.480
225.000	101.090	101.520	100.615	101.915	99.600	101.975	101.420	99.250	101.630	99.940	101.625	99.150	101.520
250.000	101.035	101.565	100.500	102.010	99.440	102.105	101.535	99.105	101.775	99.835	101.735	99.100	101.535
275.000	100.995	101.610	100.410	102.105	99.270	102.190	101.725	98.925	101.925	99.750	101.830	99.040	101.625
300.000	100.950	101.635	100.320	102.195	99.105	102.285	101.900	98.750	102.085	99.650	101.910	99.000	101.655
275.000	100.985	101.605	100.360	102.140	99.215	102.280	101.775	98.875	101.980	99.710	101.840	99.040	101.610
250.000	101.025	101.570	100.440	102.065	99.330	102.190	101.660	99.000	101.855	99.790	101.750	99.070	101.580
225.000	101.070	?101.645	100.540	101.985	99.440	102.075	101.550	99.115	101.720	99.870	101.680	99.110	101.540
200.000	101.105	101.515	100.615	101.910	99.600	101.944	101.415	99.240	101.620	99.955	101.610	99.145	101.495
175.000	101.130	101.465	100.690	101.835	99.725	101.830	101.290	99.380	101.500	100.035	101.535	99.185	101.470
150.000	101.180	101.440	100.755	101.760	99.840	101.705	101.155	99.520	101.385	100.125	101.440	99.240	101.435
125.000	101.220	101.400	100.845	101.665	99.980	101.580	101.010	99.665	101.250	100.200	101.340	99.285	101.390
100.000	101.265	101.355	100.930	101.590	100.100	101.470	100.920	99.780	101.150	100.285	101.293	99.315	101.350
75.000	101.295	101.300	101.015	101.530	100.265	101.340	100.765	99.925	101.000	100.355	101.195	99.355	101.300
50.000	101.340	101.270	101.070	101.435	100.380	101.220	100.640	100.040	100.910	100.445	101.110	99.395	101.250
0.000	?101.210	101.185	101.245	101.235	100.620	100.950	100.350	100.325	100.590	100.615	100.915	99.460	101.175

? indicates measurements where a recording error may have occurred; these points are omitted from the linear regression

Table 7.2: Diametral measurements of filament wound cylinder under pinching load: test 2

Load (N)	Measurement point number: table gives micrometer reading (mm) for each value of pinching load												
	1	2	3	4	5	6	7	8	9	10	11	12	13
0	101.400	101.210	101.235	101.270	100.610	100.950	100.355	100.295	100.625	100.605	100.944	99.475	101.160
50	101.360	101.270	101.100	101.410	100.425	101.170	100.575	100.110	100.845	100.480	101.085	99.420	101.245
75	101.310	101.295	101.035	101.495	100.295	101.300	100.710	99.980	100.965	100.400	101.160	99.370	101.295
100	101.265	101.340	100.980	101.560	100.185	101.415	100.845	99.860	101.075	100.330	101.235	99.355	101.300
125	101.230	101.370	100.905	101.640	100.050	101.500	100.935	99.730	101.185	100.260	101.295	99.300	101.345
150	101.180	101.425	100.820	101.705	99.930	101.640	101.090	99.595	101.315	100.150	101.395	99.260	101.395
175	101.140	101.455	100.740	101.800	99.800	101.770	101.215	99.460	101.425	100.090	101.485	99.225	101.455
200	101.100	101.495	100.660	101.890	99.640	101.895	101.350	99.340	?101.560	100.010	101.555	99.160	101.500
225	101.065	101.530	100.570	101.970	99.500	102.020	101.495	99.180	101.695	99.900	101.655	99.120	101.525
250	101.030	101.575	100.465	102.060	99.345	102.160	101.645	99.035	101.810	99.820	101.720	99.085	101.545
275	100.975	101.625	100.370	102.145	99.180	102.285	101.795	98.885	101.975	99.725	101.815	99.045	101.610
300	100.935	101.650	100.290	102.230	99.060	102.435	101.935	98.695	102.110	99.635	101.915	99.000	101.640
275	100.975	101.630	100.360	102.170	99.160	102.320	101.805	98.850	101.995	99.715	101.865	99.040	101.620
250	?101.005	101.595	100.455	102.090	99.300	102.205	101.695	98.970	101.855	99.795	101.755	99.070	101.595
225	101.050	101.550	100.515	102.015	99.425	102.090	101.525	99.075	101.770	99.870	101.695	99.115	101.540
200	101.085	101.515	100.600	101.940	99.550	101.970	101.435	99.235	101.640	99.950	101.605	99.140	101.520
175	101.120	101.460	100.680	101.850	99.690	101.860	101.285	99.350	101.515	100.035	101.525	99.180	101.475
150	101.140	101.420	100.730	101.750	99.825	101.735	101.175	99.490	101.400	100.105	101.455	99.225	101.420
125	101.205	101.395	100.840	101.690	99.965	101.610	101.035	99.640	101.270	100.185	101.350	99.275	101.365
100	101.240	101.350	100.935	101.595	100.095	101.475	100.900	99.790	101.145	100.290	101.265	99.320	101.340
75	101.290	101.295	101.010	101.520	100.230	101.355	100.775	99.920	101.010	100.375	101.200	99.350	101.300
50	101.330	101.270	101.090	101.445	100.365	101.230	100.650	100.050	100.880	100.445	101.090	99.390	101.265
2.4	101.415	101.185	101.245	101.255	100.590	100.925	100.340	100.260	100.600	100.585	100.920	99.460	101.155

? indicates measurements where a recording error may have occurred; these points are omitted from the linear regression

Table 7.3: Linear regression data for cylinder pinching test 1

	Measurement point number												
	1	2	3	4	5	6	7	8	9	10	11	12	13
Gradient (mmN^{-1})	-0.00167	0.00157	-0.00328	0.00326	-0.00543	0.00482	0.00527	-0.0055	0.00500	-0.00342	0.00344	-0.00168	0.00162
y-intercept (mm)	101.447	101.176	101.303	101.220	100.746	100.917	100.295	100.421	100.568	100.675	100.880	99.508	101.165
95% confidence limits on gradient													
Upper (mmN^{-1})	-0.00157	0.00166	-0.00302	0.00347	-0.00500	0.00514	0.00562	-0.00510	0.00529	-0.00319	0.00367	-0.00153	0.00172
Lower (mmN^{-1})	-0.00176	0.00147	-0.00354	0.00304	-0.00586	0.00449	0.00492	-0.00590	0.00470	-0.00365	0.00321	-0.00182	0.00152
Correlation coefficient	-0.993	0.992	-0.986	0.990	-0.985	0.989	0.989	-0.987	0.992	-0.989	0.989	-0.982	0.991

Table 7.4: Linear regression data for cylinder pinching test 2

	Measurement point number												
	1	2	3	4	5	6	7	8	9	10	11	12	13
Gradient (mmN^{-1})	-0.00160	0.00157	-0.00320	0.00326	-0.00529	0.00495	0.00528	-0.00532	0.00497	-0.00325	0.00330	-0.00161	0.00164
y-intercept (mm)	101.414	101.188	101.261	101.258	100.652	100.945	100.340	100.335	100.610	100.622	100.925	99.482	101.165
95% confidence limits on gradient													
Upper (mmN^{-1})	-0.00153	0.00162	-0.00307	0.00336	-0.00507	0.00513	0.00545	-0.00509	0.00514	-0.00313	0.00341	-0.00153	0.00172
Lower (mmN^{-1})	-0.00167	0.00152	-0.00334	0.00315	-0.00550	0.00477	0.00510	-0.00555	0.00480	-0.00337	0.00318	-0.00168	0.00156
Correlation coefficient	-0.996	0.998	-0.996	0.997	-0.996	0.997	0.997	-0.995	0.997	-0.997	0.997	-0.995	0.994

Table 7.5: Material properties used for model definition

Property	Calculated from Halpin-Tsai equations for 75.44% fibre by mass	Properties from flexural (proving ring) data normalised to 75.44% fibre
E_1 (MNm^{-2})	44514.54	42331.92
E_2 (MNm^{-2})	8770.27 (using ξ=0.2)	2381.27
G_{12} (MNm^{-2})	4271.25	4689.74†
ν_{12}	0.2856	0.30482

† This value was also used as the value of through-thickness shear modulus for the PAFEC thick shell and axisymmetric models

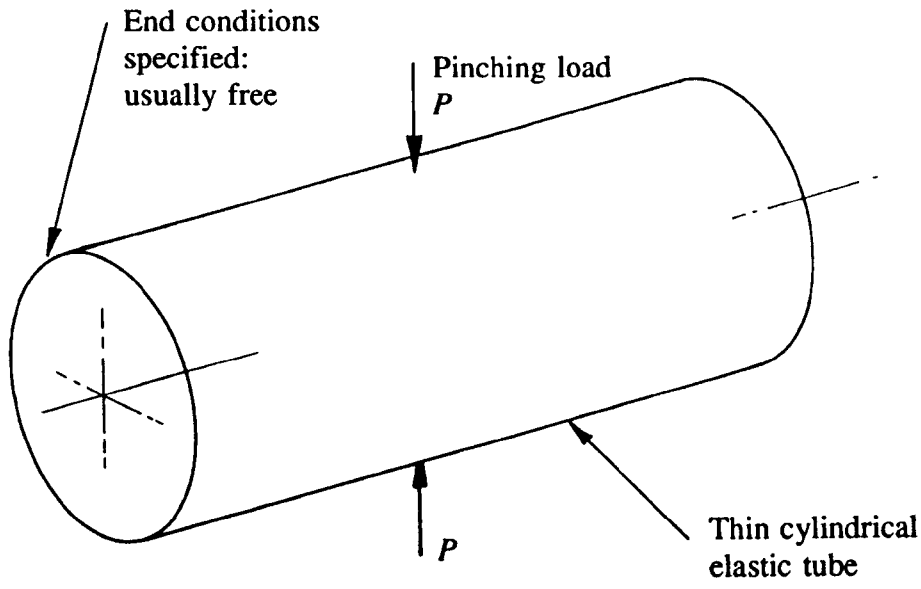

Fig. 7.1: The pinched cylinder problem

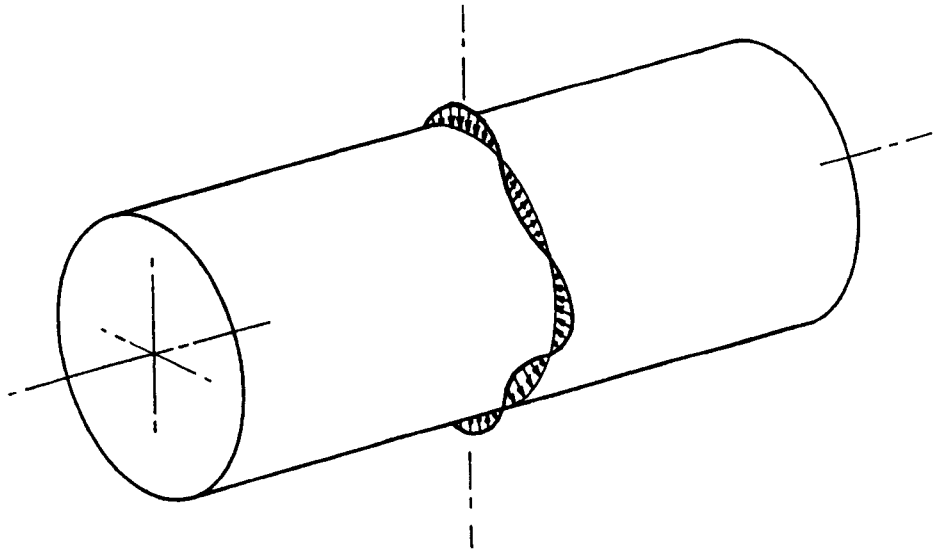

Fig. 7.2: A sinusoidally-varying radial load around the circumference of a cylinder (after Calladine[137])

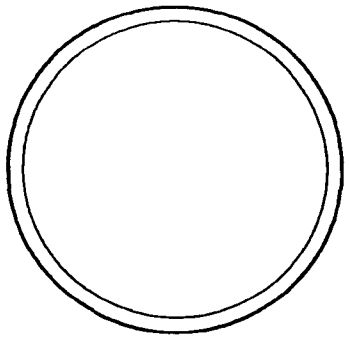

(a) $q_0 = P/2\pi$

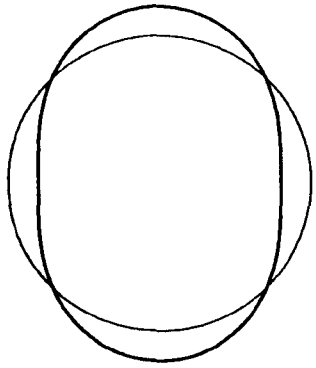

(b) $q_2 \cos 2\theta = (P/\pi) \cos 2\theta$

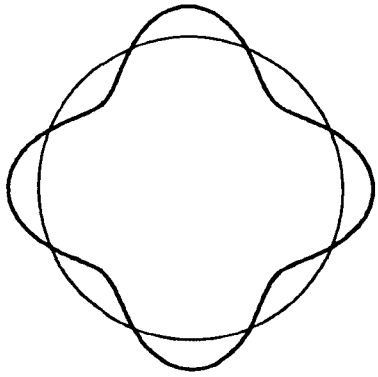

(c) $q_4 \cos 4\theta = (P/\pi) \cos 4\theta$

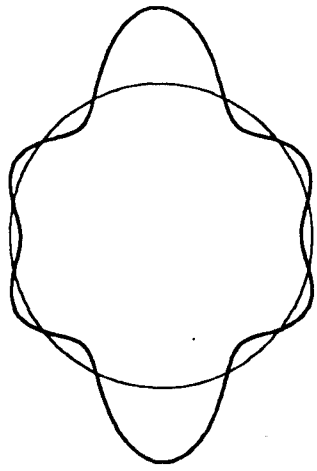

(d) Fourier series summed to n=6

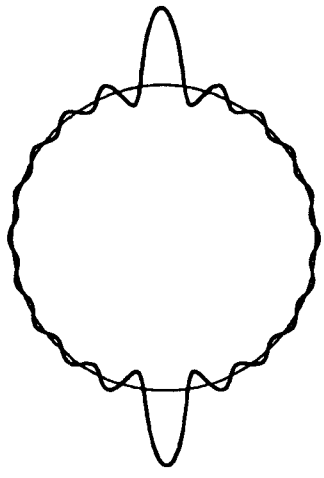

(e) Fourier series summed to n=20

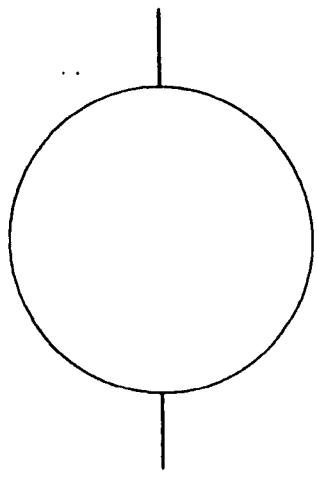

(f) Infinite summation (point loads)

Fig. 7.3: Synthesis of pinching load using a Fourier series of sinusoidally-varying radial loads (N.B. (d)-(f) are not drawn to scale)

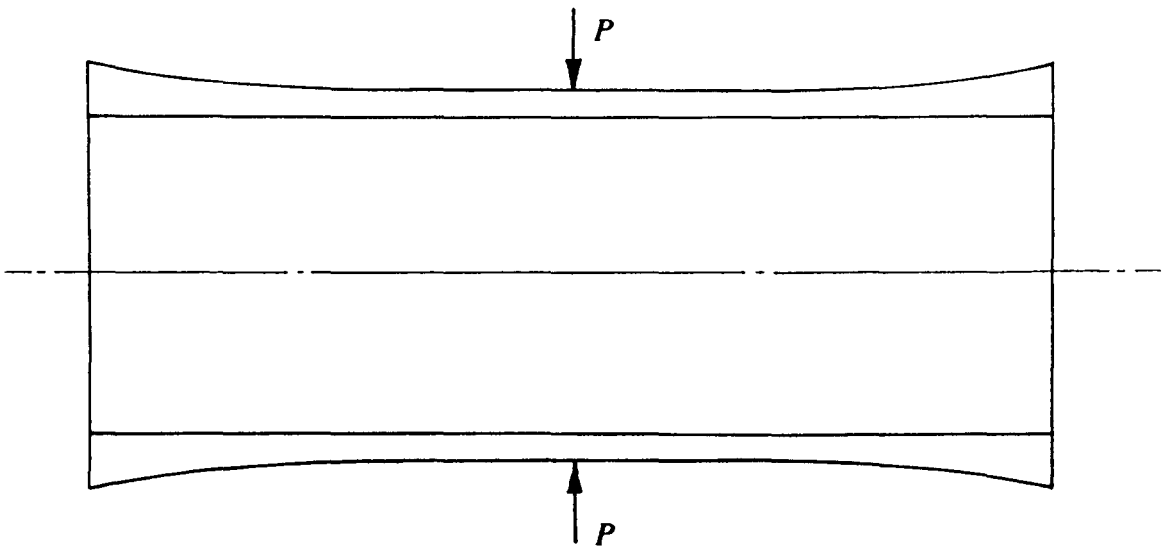

(a) Cylindrical tube with continuously-varying thickness and properties, subjected to a pinching load

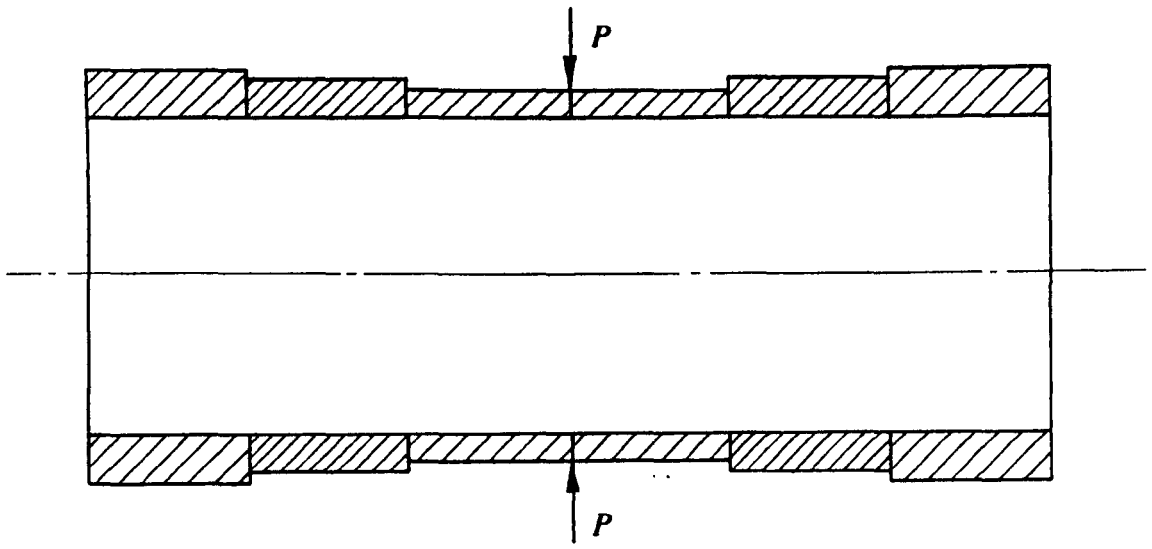

(b) Cylinder in (a) discretised into a series of uniform cylindrical tubes with different thicknesses and properties

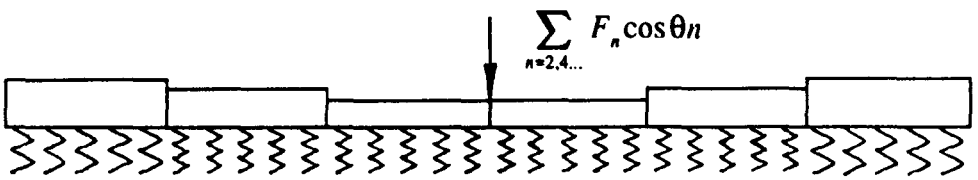

(c) Series of contiguous beams-on-elastic-foundations, analogous to (b)

Fig. 7.4: Modelling of pinched cylindrical shell with continuously-varying thickness and properties, using Calladine's beam-on-elastic-foundation analogy

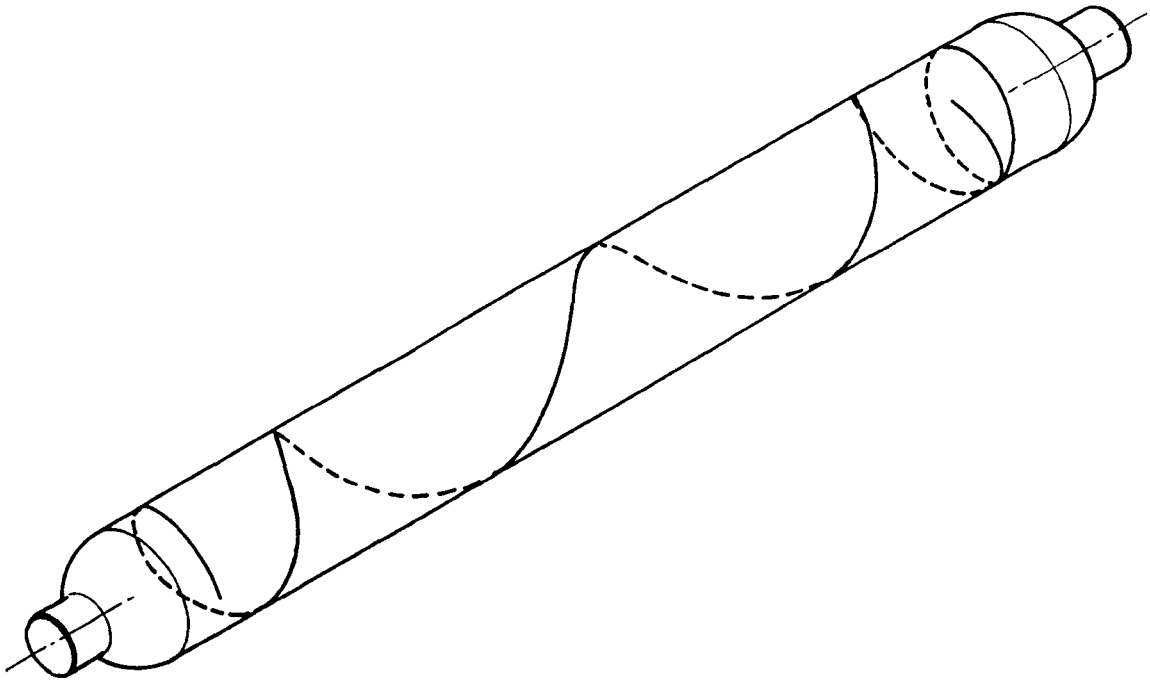

Fig. 7.5: Fibre path used for winding cylindrical specimen on dome-ended mandrel. Illustration shows fibre path as generated within CADFIL I, prior to processing of path to give complete coverage of mandrel.

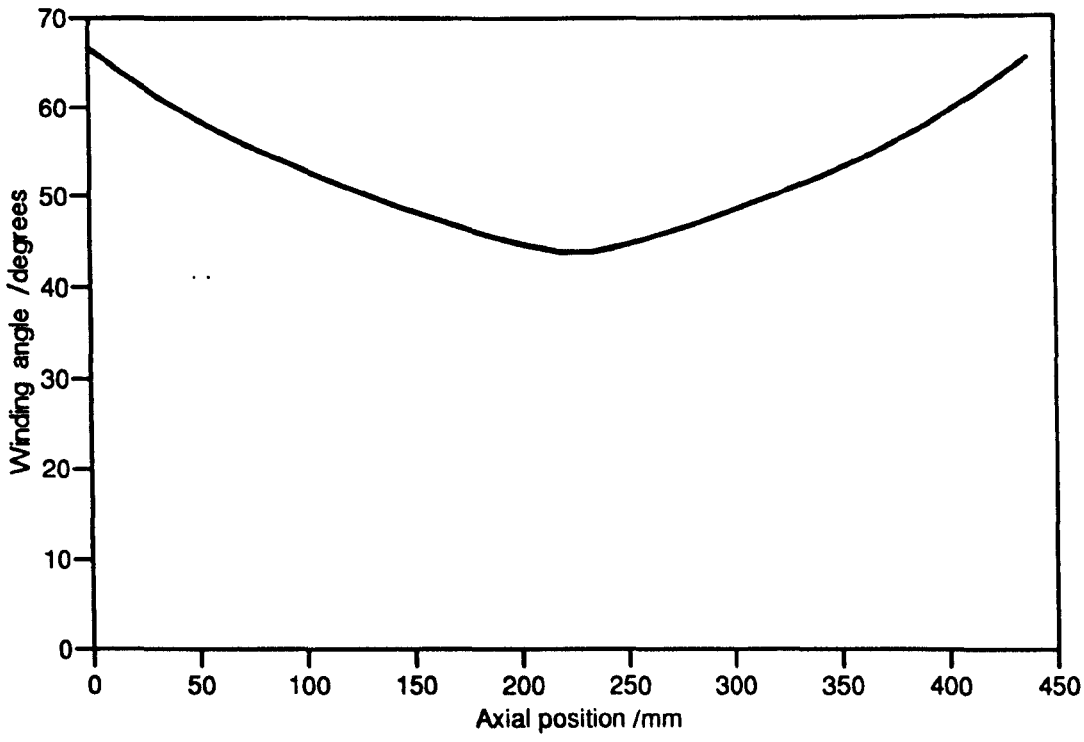

Fig. 7.6: Distribution of winding angle along length of cylinder (predicted from CADFIL I data using FILFEM I).

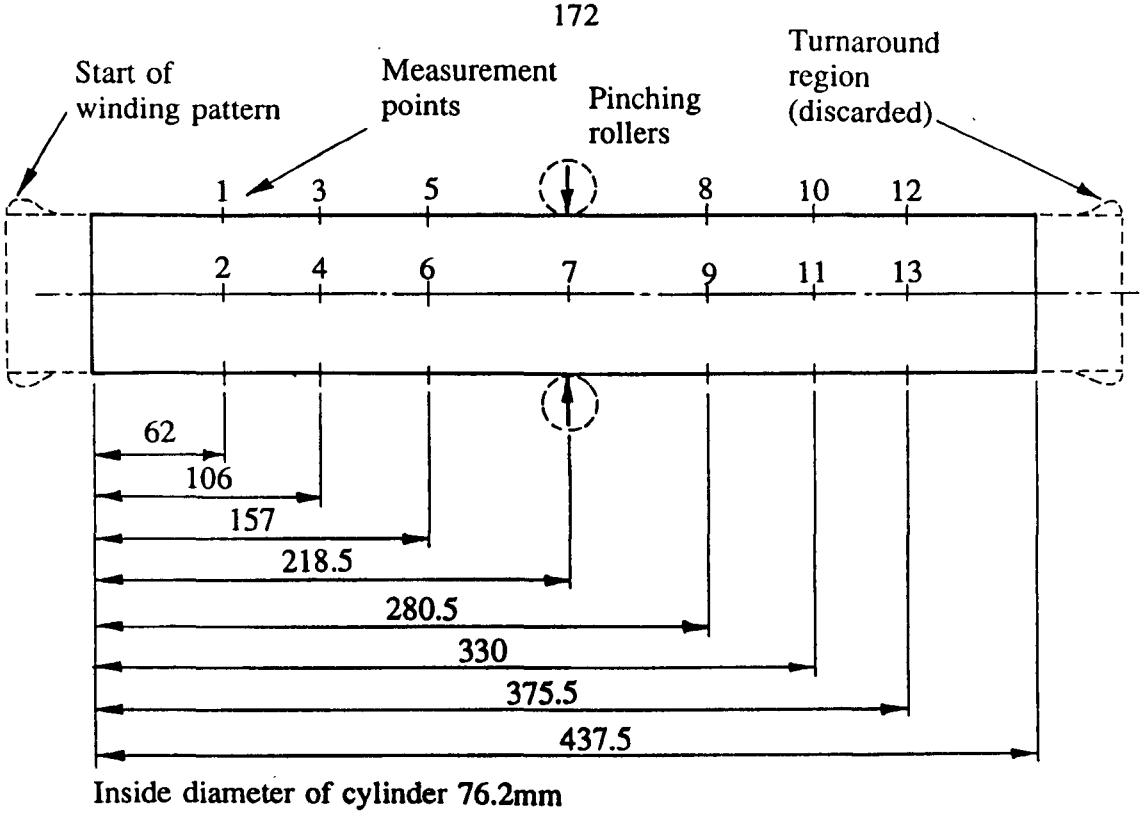

Fig. 7.7: Dimensions of cylinder and locations of measurement points

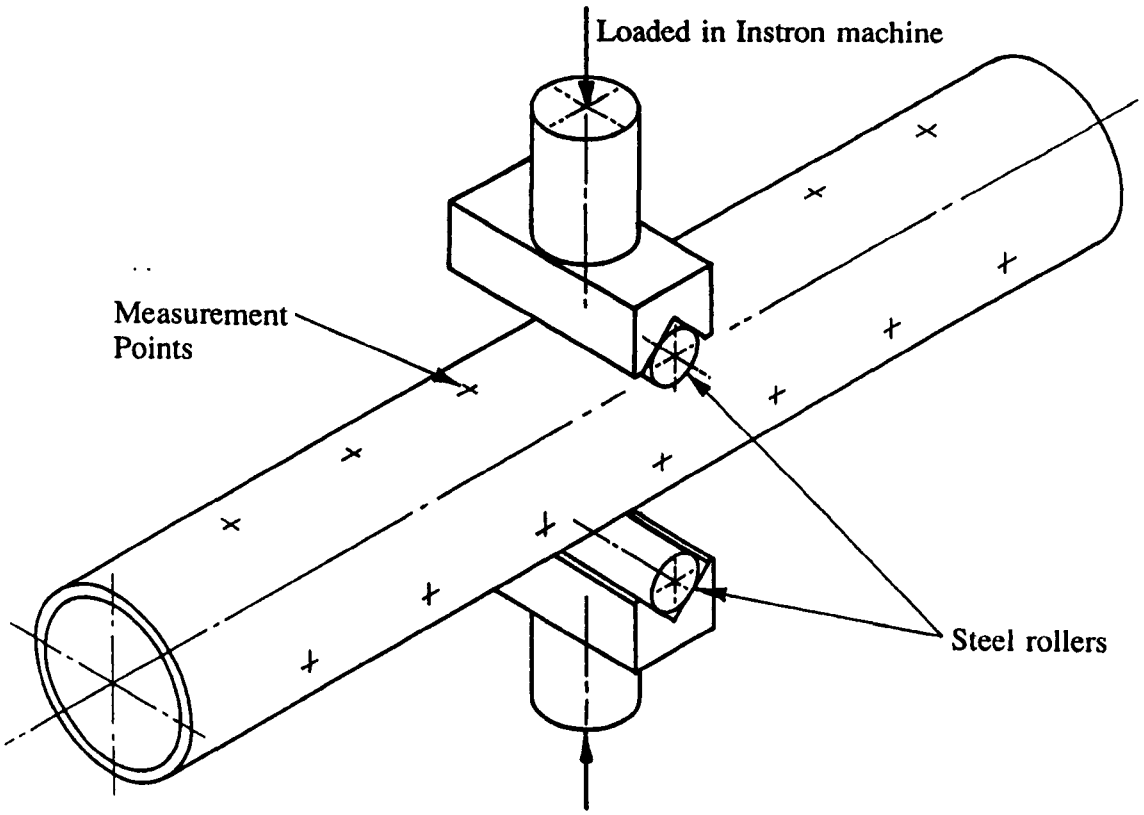

Fig. 7.8: Method of pinching cylinder, showing roller-shaped anvils

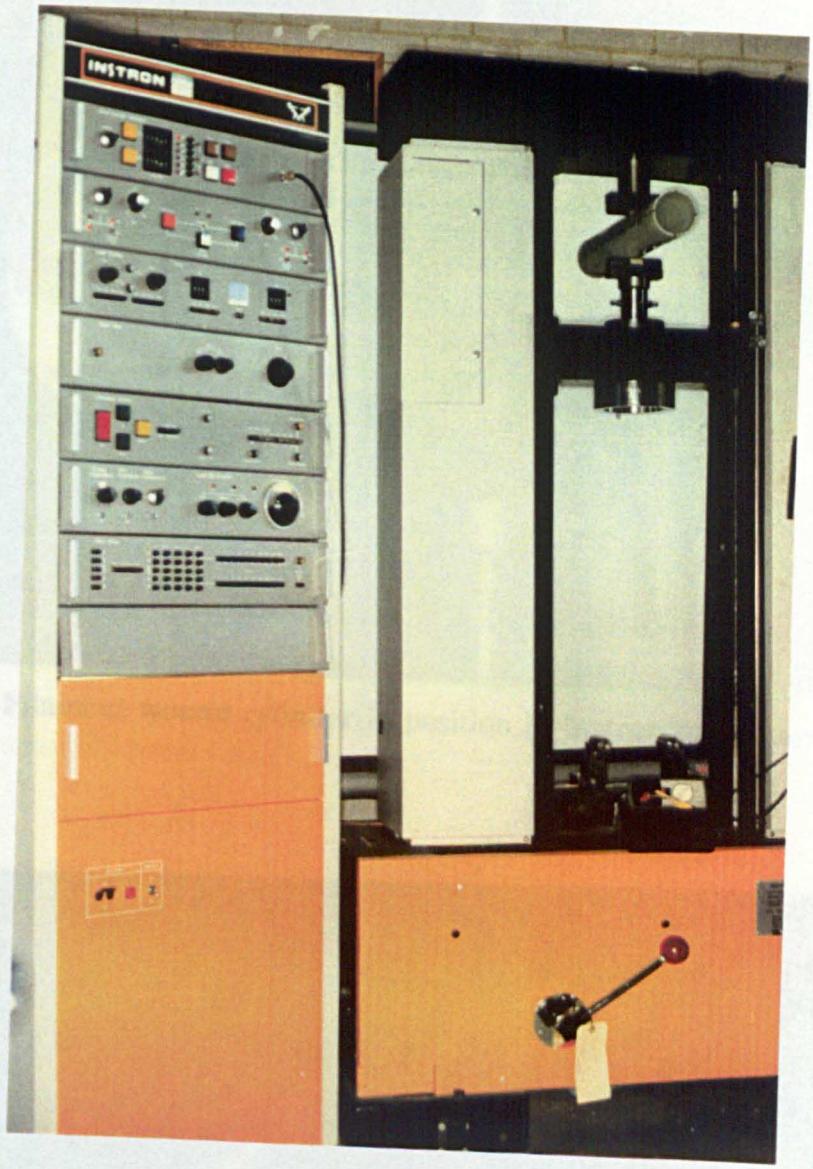

Fig. 7.9: Instron universal testing machine showing cylinder in position.

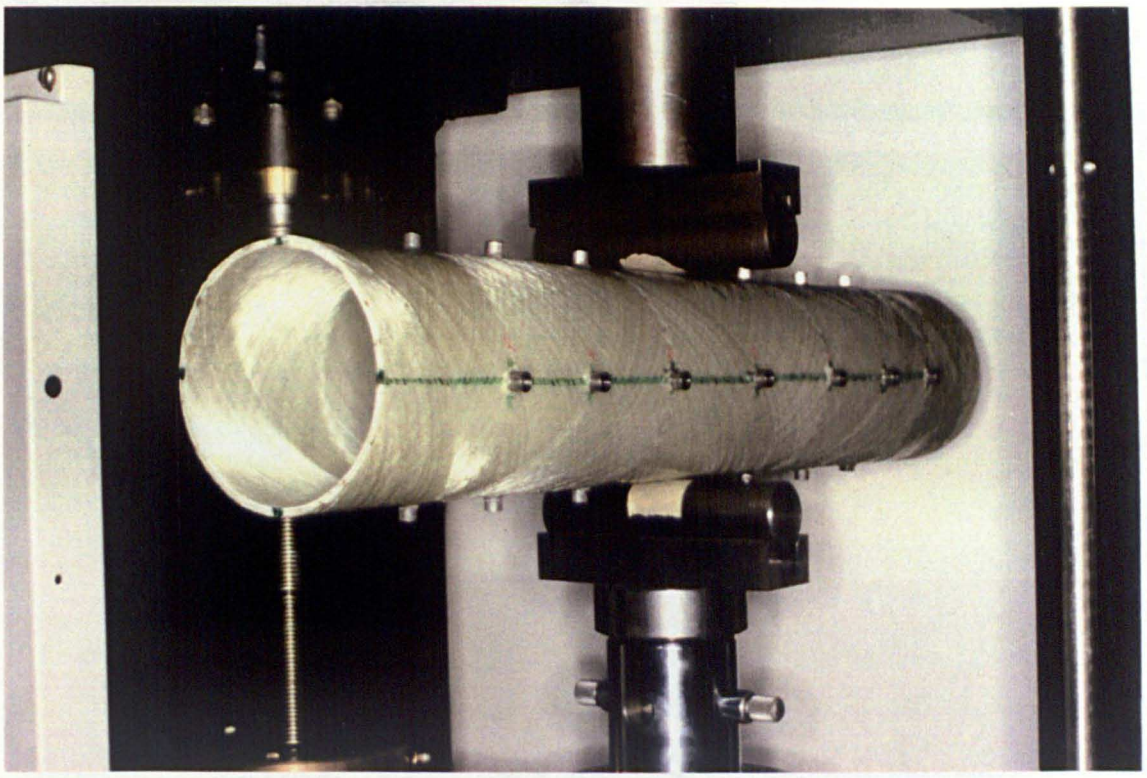

Fig. 7.10: Filament wound cylinder in position in Instron machine.

Fig. 7.11: Finished filament-wound cylinder with micrometer cups attached

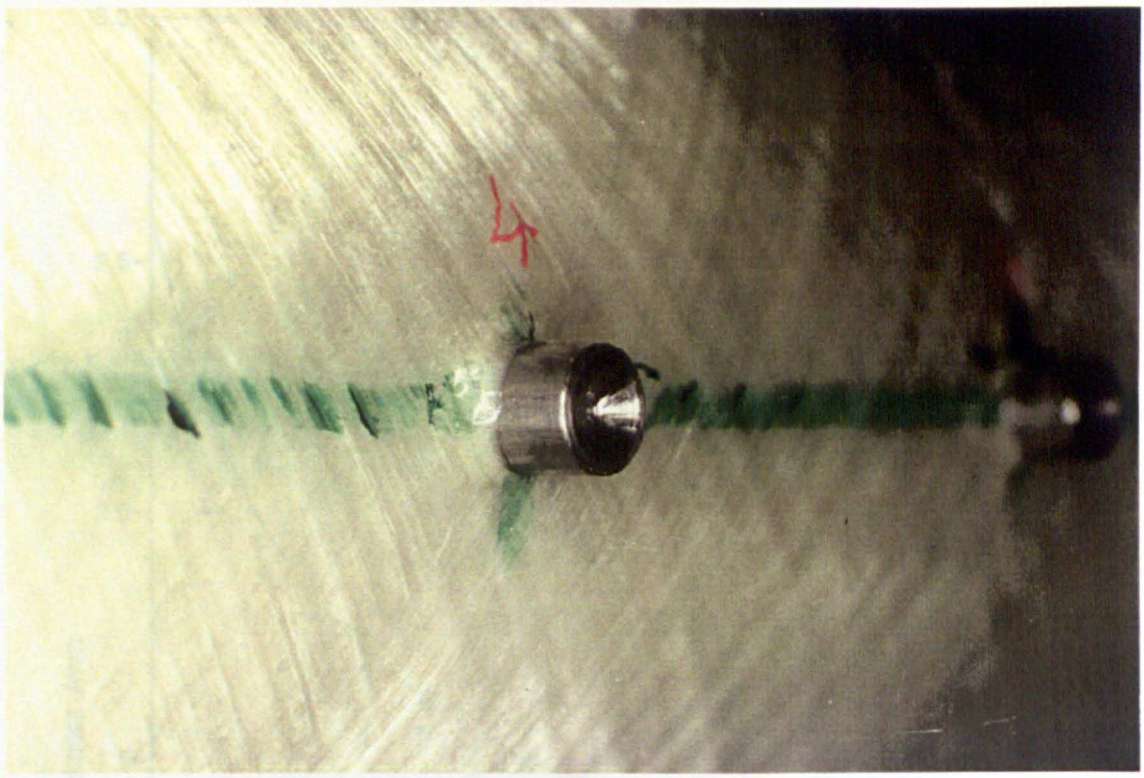

Fig. 7.12: Detail of locating cup for ball-anvil micrometer, attached at each measurement point

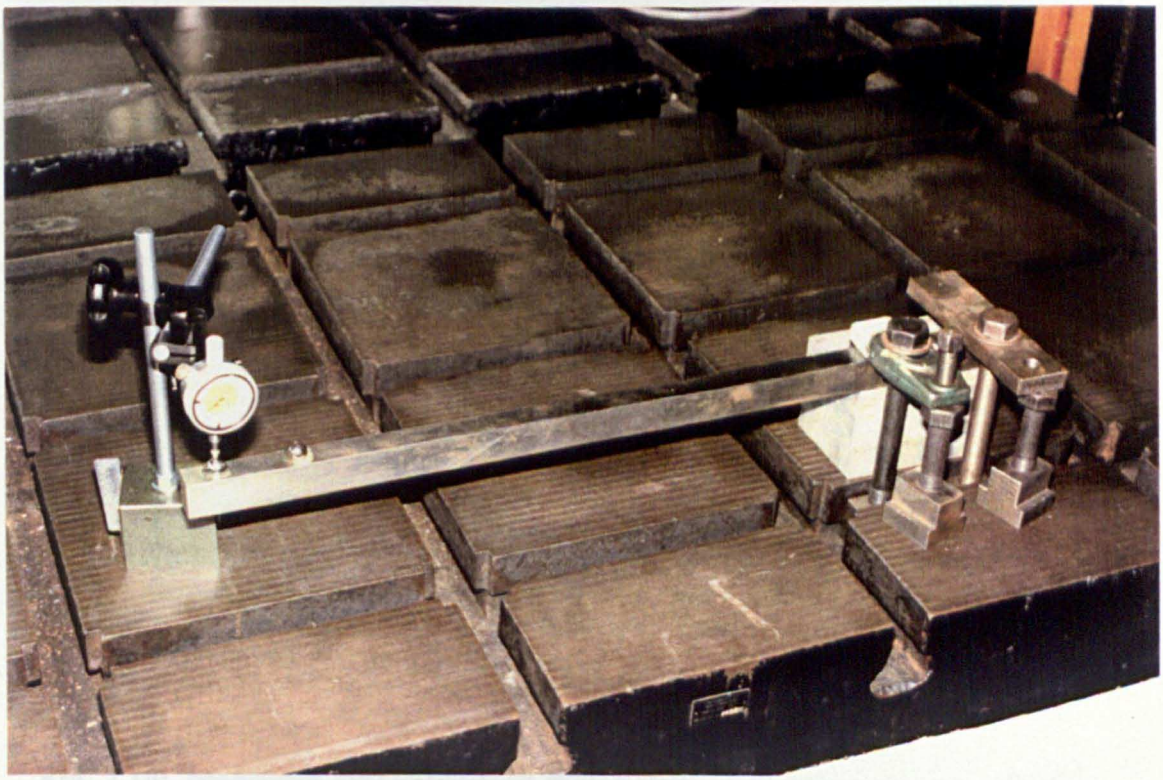

Fig. 7.13: Apparatus for measuring wall thickness of filament wound cylinder

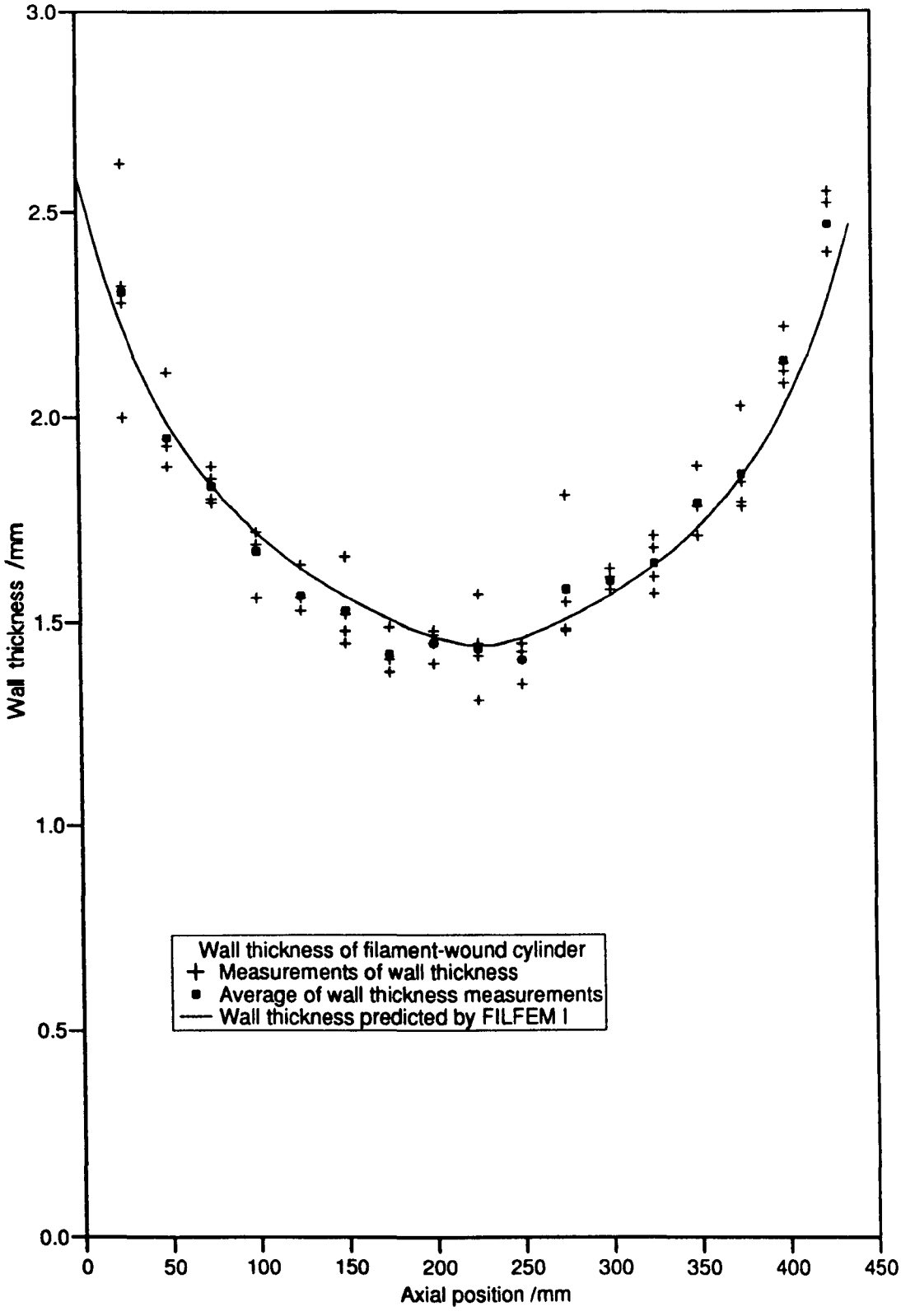

Fig. 7.14: Measured and calculated thicknesses of filament wound cylinder

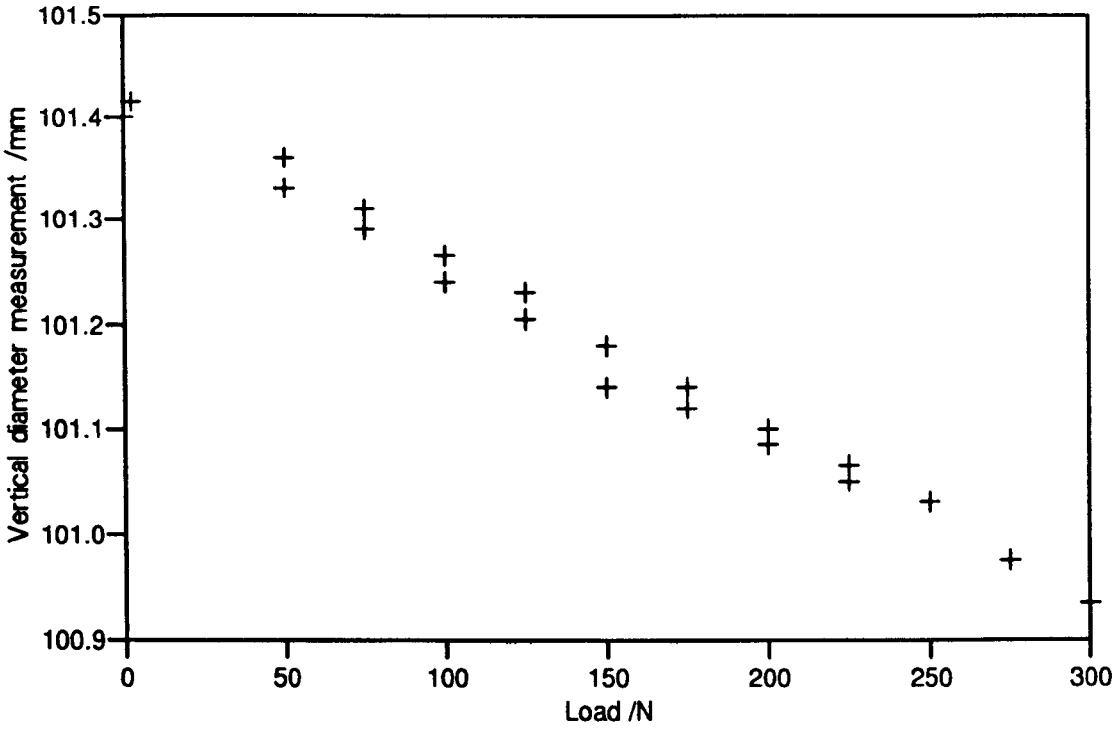

Fig. 7.15: Variation of vertical diameter measurement with load for measurement point 1 (N.B. Measured vertical diameter includes dimensions of measurement cups and micrometer ball anvils).

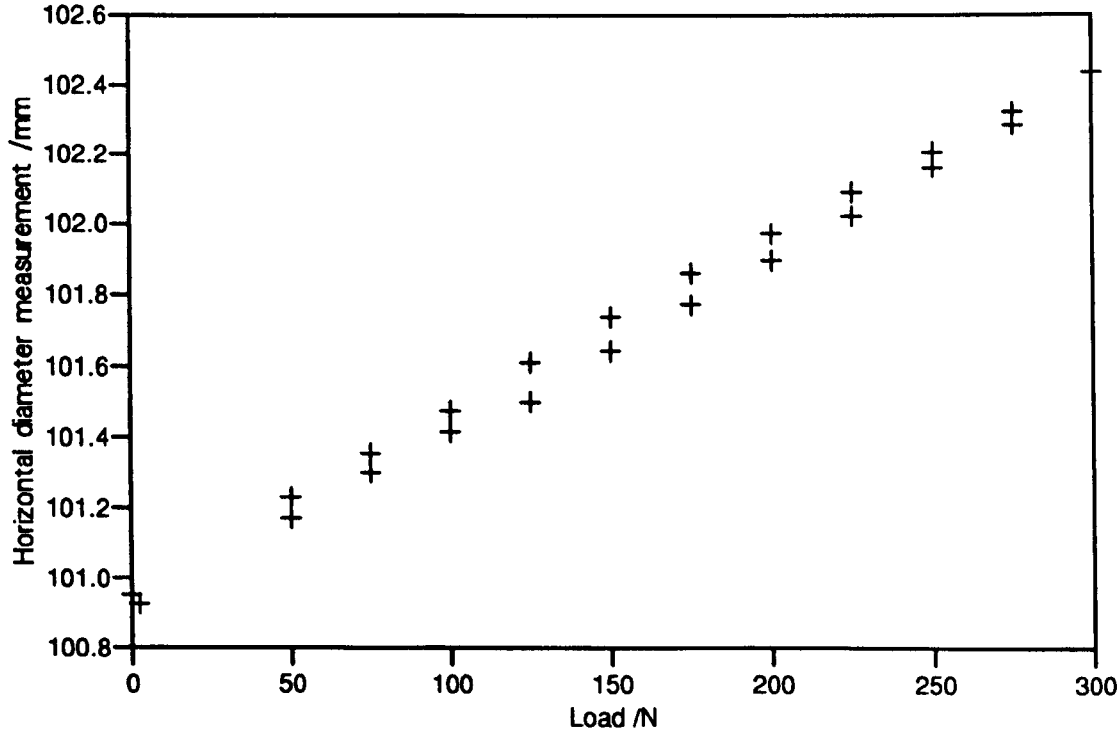

Fig. 7.16: Variation of horizontal diameter measurement with load for measurement point 6

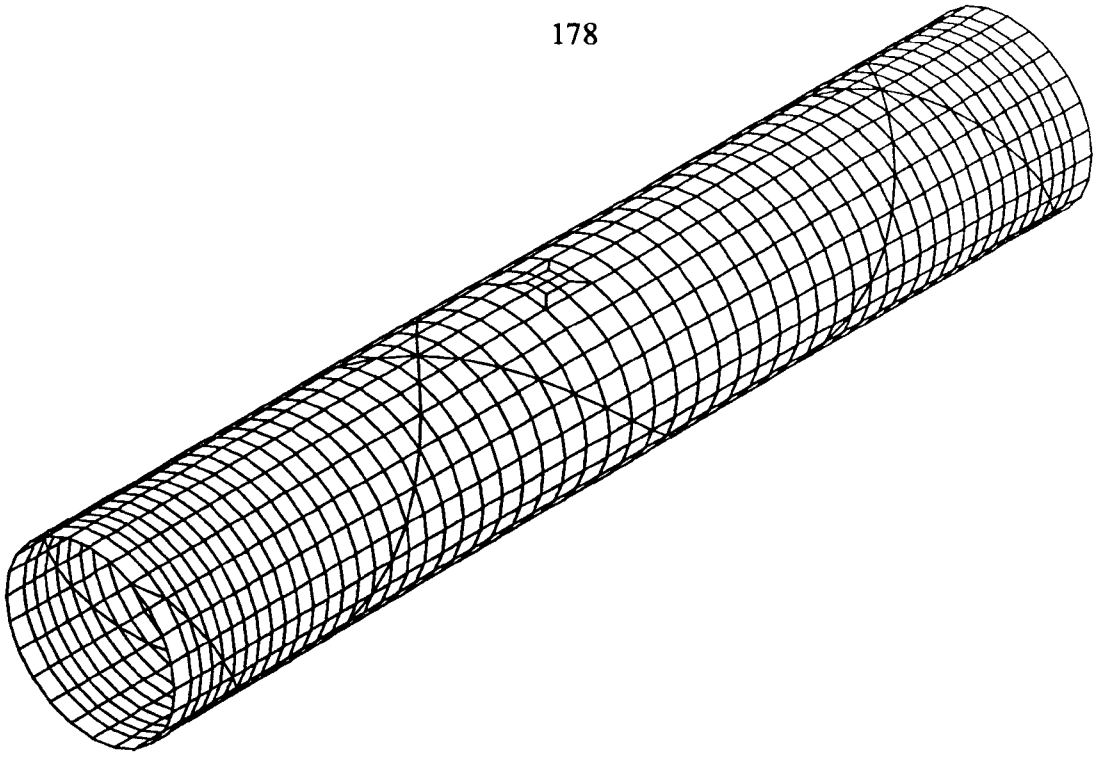

Fig. 7.17: ABAQUS mesh with 24 elements around circumference of cylinder

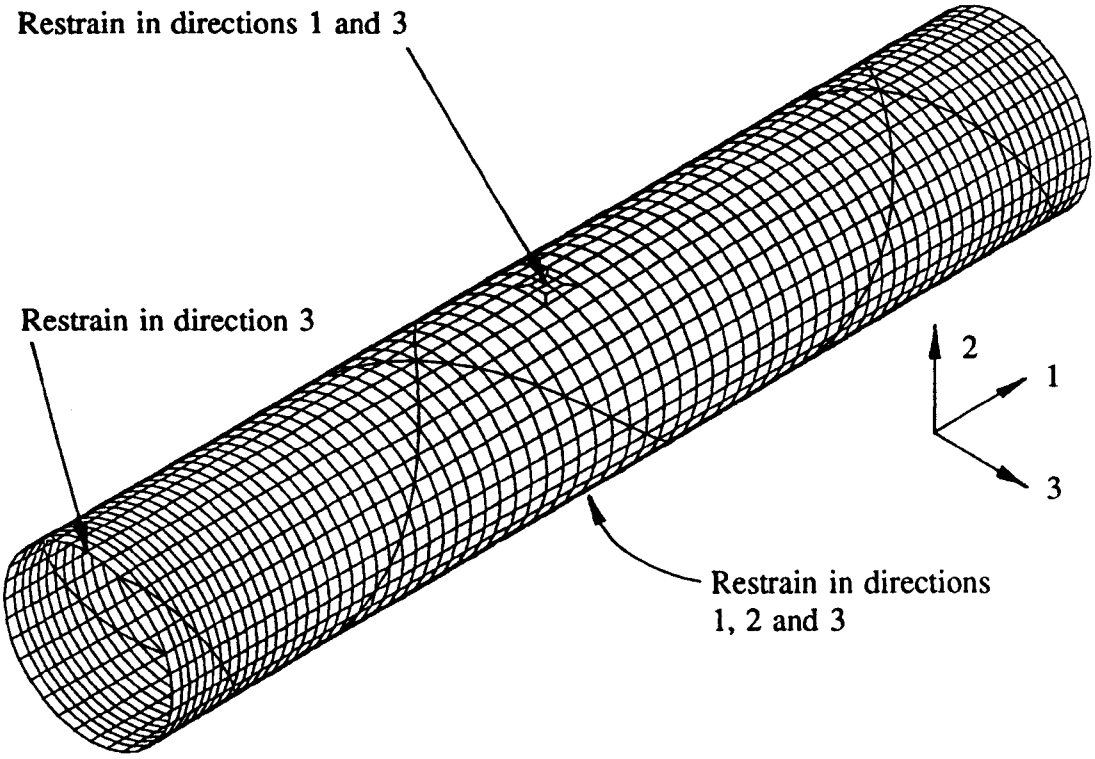

Fig. 7.18: ABAQUS mesh with 32 elements around circumference of cylinder, showing boundary conditions.

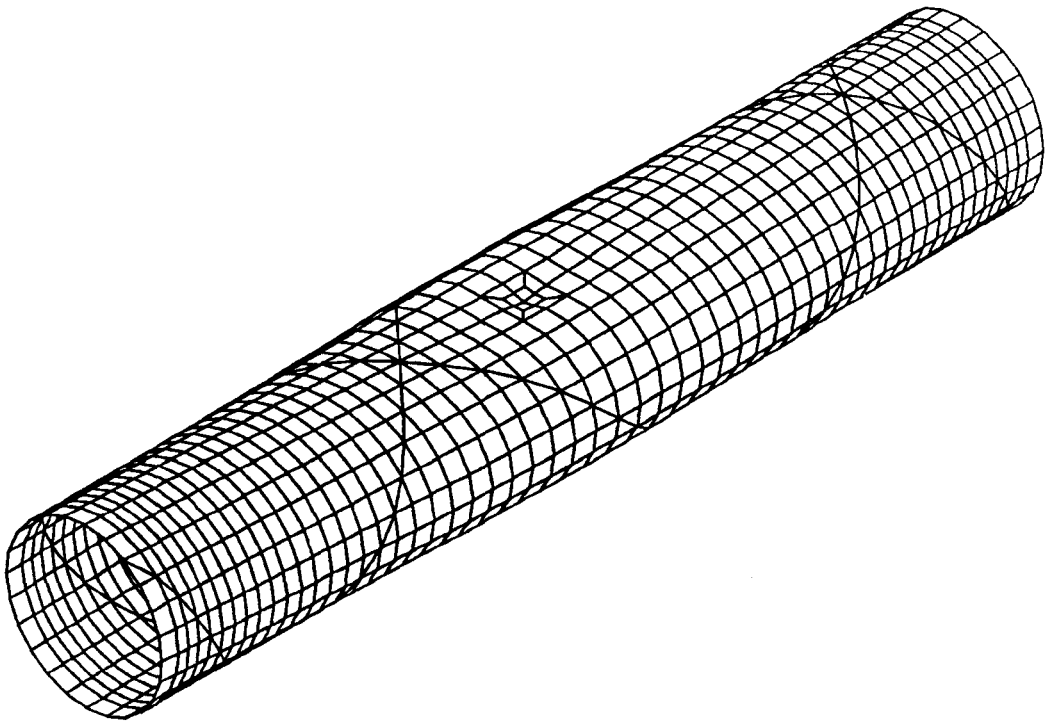

Fig. 7.19: Displaced shape of a typical mesh (ABAQUS mesh with 24 elements around circumference of cylinder)

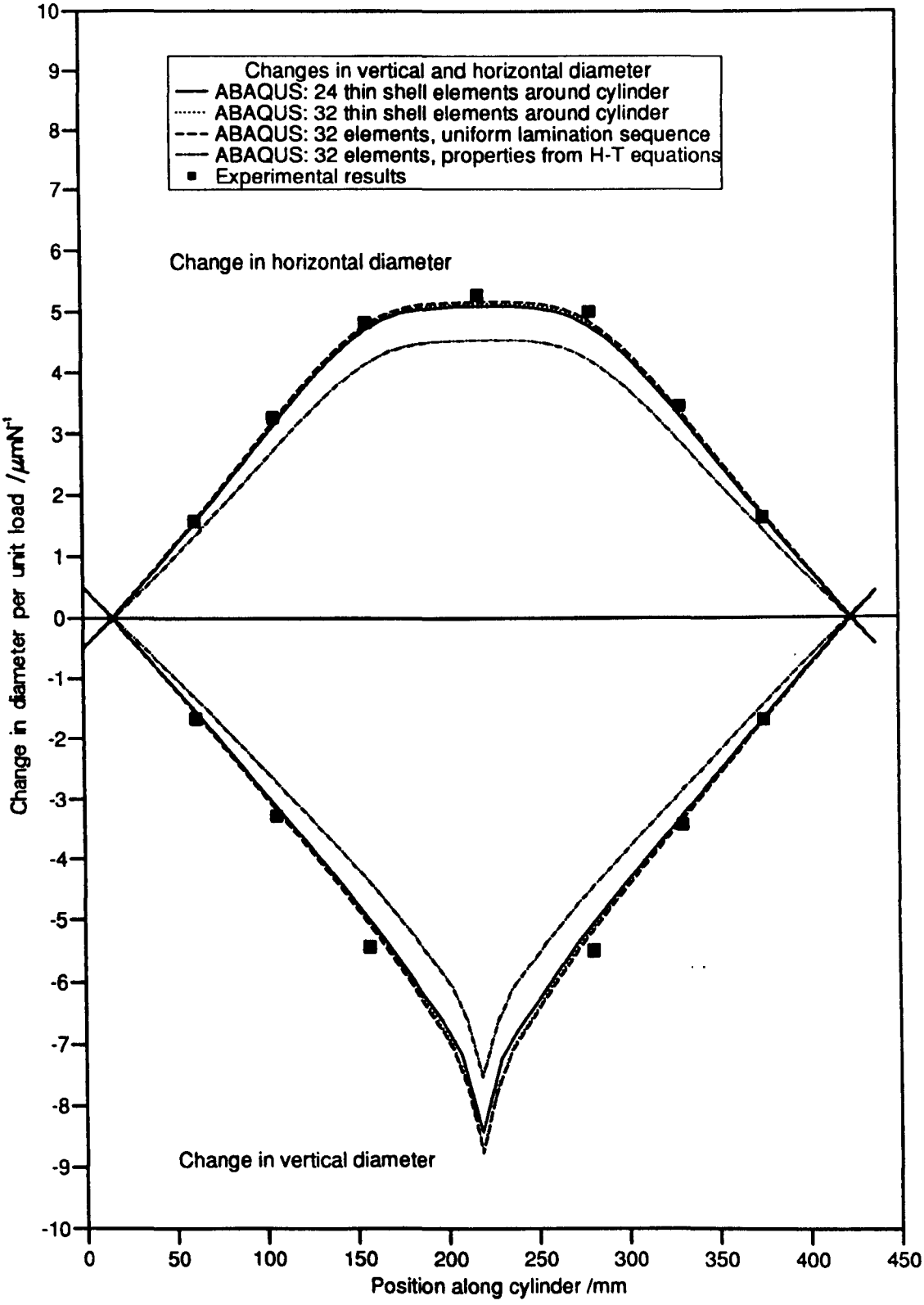

Fig. 7.20: Comparison of deflections predicted by ABAQUS thin shell models with experimental results

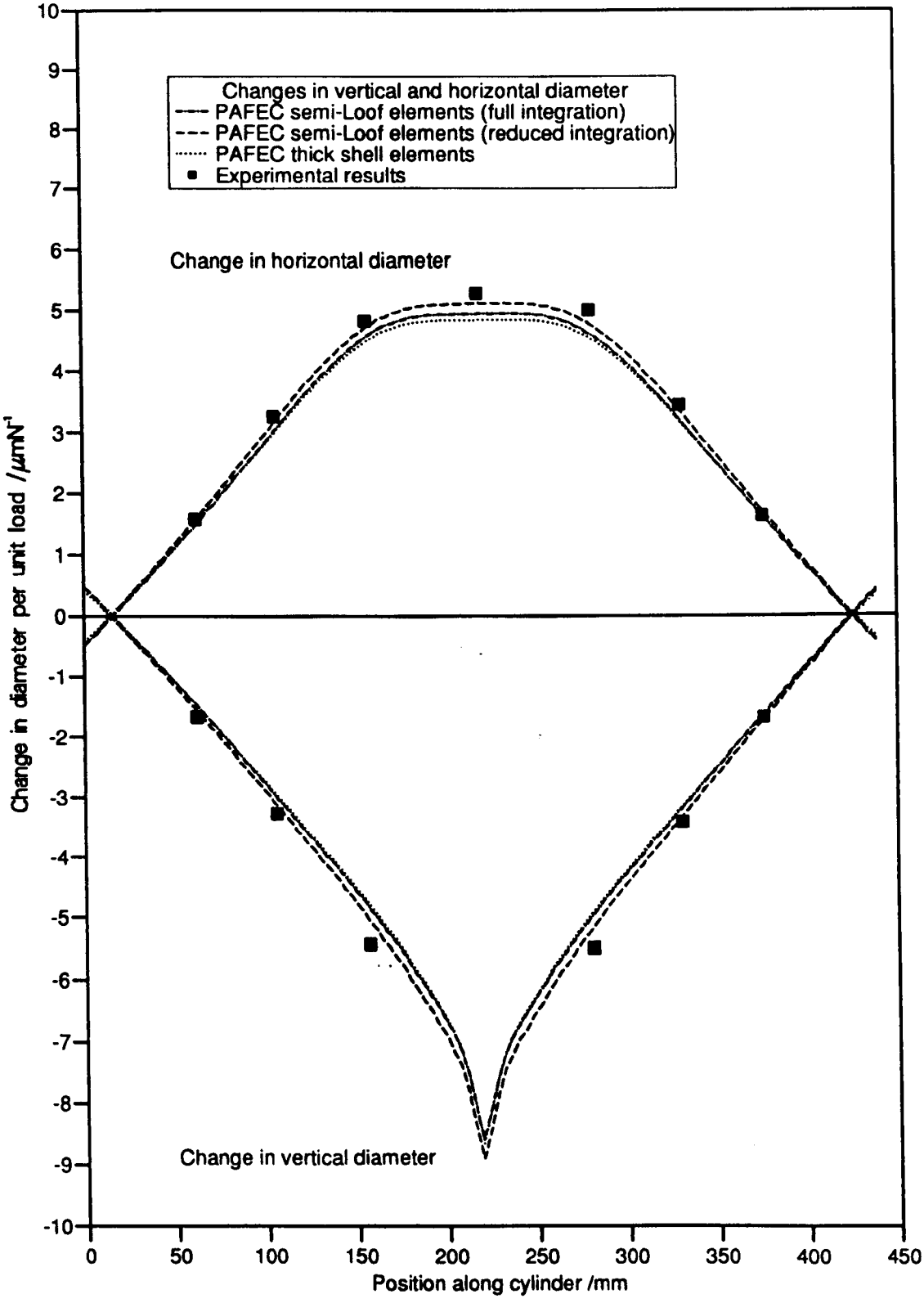

Fig. 7.21: Comparison of deflections predicted by PAFEC shell models with experimental results

(a) Complete axisymmetric model (represented as a half-section through cylinder)

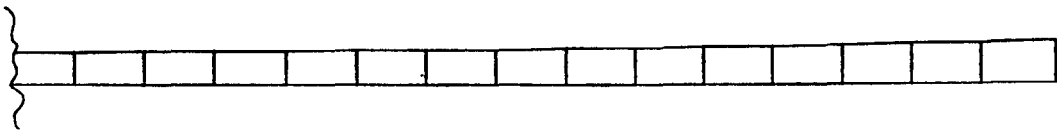

(b) Detail of R.H. end of axisymmetric model

Fig. 7.22: PAFEC mesh of axisymmetric Fourier quadrilateral elements

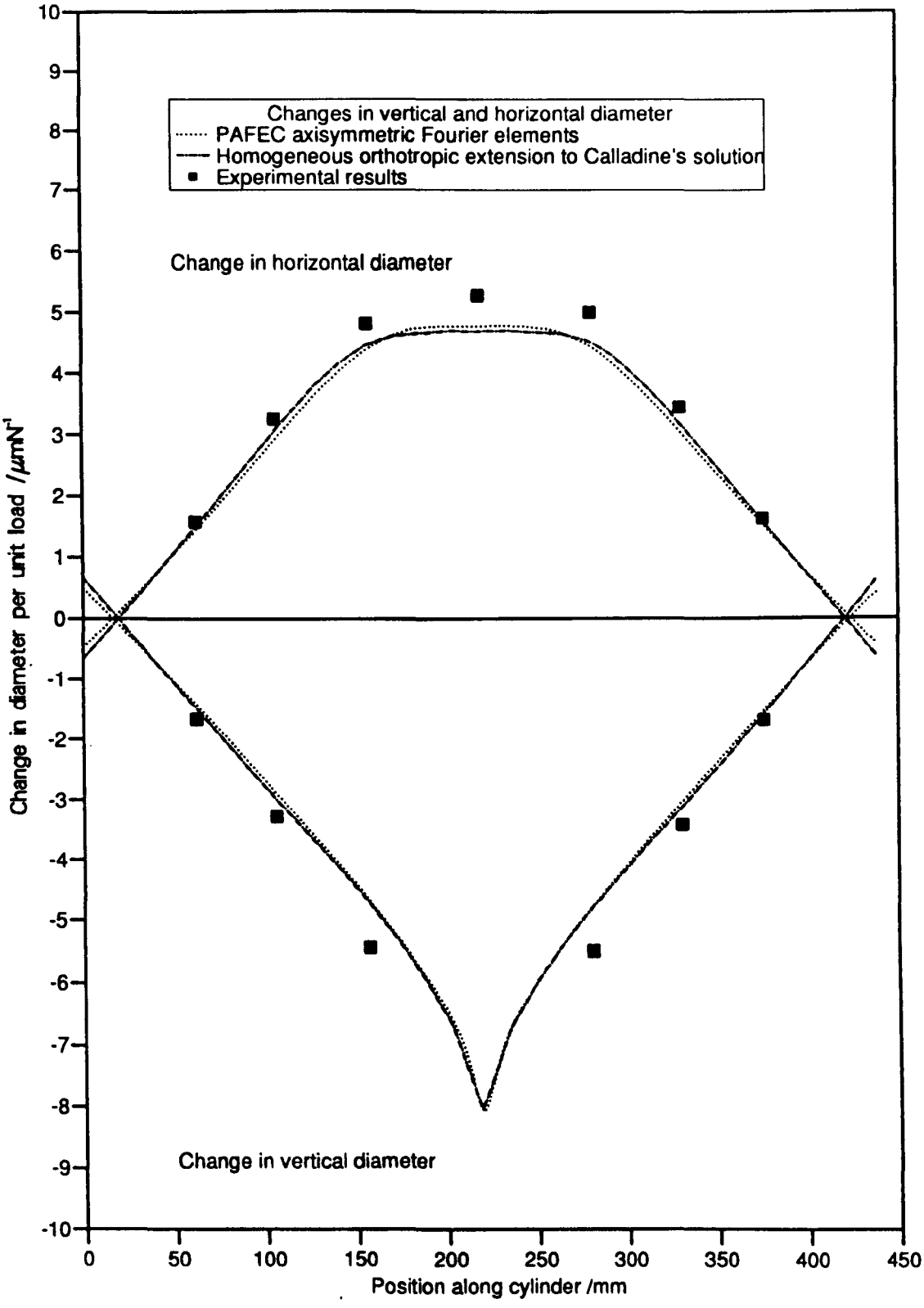

Fig. 7.23: Comparison of deflections predicted by PAFEC axisymmetric model with analytical solution and experimental results.

CHAPTER 8: COMPUTER AIDED FILAMENT WINDING OF AN ELBOW-SHAPED PIPE

8.1 Introduction

This chapter describes the various stages in the design and manufacture of a non-axisymmetric component. It is included because the data generated was used as the test data for FILFEM II (described in Chapter 6). The work also forms a necessary foundation for further work if the project is to be continued to include experimental verification of meshes generated using FILFEM II.

In the work described in this chapter, use is made of the existing CADFIL II system for the computer-aided filament winding of non-axisymmetric components. An overview of this system was given in Chapter 2 (Section 2.4). This is the first time that CADFIL II has been used for winding an elbow-shaped component and limitations were found in the existing software. Although no work was carried out by the author on the fibre path generation aspects of CADFIL II, it was necessary to develop modified methods for processing the fibre paths in order to obtain feasible winding programs for the CNC winding machine.

The complete process of manufacturing the elbow (including full details of the software modifications and technical procedures) is described in a report[142] and is too extensive to describe fully in this thesis. This chapter, however, contains an overview of the process, and begins by examining the various objectives of manufacturing the elbow. The manufacturing process is then described in three main stages. The first of these is the theoretical stage of design and winding data. The second stage is the manufacture of the mandrel and a description of tooling required. The final stage is the winding and curing of the elbow itself. Practical problems encountered in the manufacture of the elbow are then discussed, and the chapter concludes by reviewing the work which has been achieved.

8.2 Background and objectives

It will be recalled from Chapter 6 that a strategy or procedure has been developed for the automatic generation of finite element models of components manufactured with the aid of CADFIL II, and that this strategy has been encoded for trial purposes as a suite of programs named FILFEM II. Because of the simplifications made in modelling the very complex structure of the components, it will clearly be necessary to perform an experimental assessment of the usefulness of the automatically-generated finite element models. It will probably be necessary to undertake further development work upon the strategy underlying FILFEM II in the light of the experimental results obtained. Time constraints have meant that such a programme of development work will need to form the basis of a subsequent project. It was however necessary to define a typical component suitable for modelling using FILFEM II. Design and manufacture of this component were carried out with the aim of using similar components for experimental testing at a later date.

The design and manufacture of the component had two further objectives besides providing a set of test data for FILFEM II and a test component for its experimental validation. One of these objectives was for the author to gain experience of the non-axisymmetric filament winding process, with particular reference to the generation of fibre paths within CADFIL II and of the techniques involved in converting these paths to CNC part-programs. The other objective was to establish the software to facilitate the manufacture of elbow-shaped components not previously attempted using the CADFIL II system.

8.3 Design, fibre path generation and CNC program generation

8.3.1 *Choice of dimensions for filament-wound elbow*

The dimensions of the elbow were chosen initially to provide some compatibility with existing experimental apparatus for the testing of tubular joints. This resulted in the choice of a bore of 3" (76.2mm); the shank length was chosen so as to give some degree of isolation from end effects according to St Venant's

principle. For this reason shank length was made approximately equal to twice the tube diameter, the assumption being made that end effects would become small at a distance of approximately one diameter away from the ends. The tube centreline radius was chosen arbitrarily to give approximately the same proportions as the existing filament-wound tee pieces (i.e. the inner radius of the torus is made approximately equal to the bore). The exact dimensions were chosen so that the toroidal section of the elbow pattern could be manufactured from 12" diameter aluminium stock. Fig. 8.1 shows the dimensions of the mandrel.

8.3.2 *Generation of fibre paths and CNC programs*

The stages in the computer-aided filament winding of non-axisymmetric components using CADFIL II has already been described in Section 2.3.2, and the following description should be read in conjunction with that section.

(a) Mandrel surface definition. For the purpose of generating the fibre paths the mandrel surface was defined as a data file of node co-ordinates, from which CADFIL II creates a surface model of rectangular elements. This data file was created using a program very similar to MESHGEN described in Section 6.4.4.1.

(b) Fibre path generation. The existing CADFIL II software, running on an Apollo workstation, was used to create the paths of the fibres on the surface of the mandrel. The aim was to build up a sequence of fibre path families (such as that illustrated in Fig. 6.7) which give as far as possible an even and complete coverage of the mandrel. To avoid unnecessary fibre generation effort, fibres were replicated by taking account of mandrel symmetry (refer to next paragraph) to provide complete coverage.

(c) Fibre path replication and linking. Each family of fibre paths was used to produce three more families by reflecting in the planes shown in Fig. 8.2. In order to provide a continues fibre path, fibres wound in the same

direction around the mandrel were joined at the ends by a path such as that shown in Fig. 8.3, made up of helical extensions to the fibre path joined by a circular arc. Similar paths are used to secure the fibre before winding begins and after it finishes. An existing end-linking program was modified by the author to achieve this. In practice the circular fibre tightens around the shaft which protrudes from the end of the mandrel, but the end linking path illustrated is a satisfactory assumption for the purpose of generating the payout eye path. Slippage is avoided at the ends of the mandrel by the use of pinned end-caps (Fig. 8.4) which locate the fibre as it is laid.

(d) Payout eye path generation. The payout eye path is created by extending a tangent to the fibre path from the mandrel surface and finding its intersection with a control surface which is defined to be clear of the mandrel. Existing control surface models were found to be inadequate and the software was modified to provide a control surface consisting of a series of intersecting conical and cylindrical ducts (Fig. 8.5). Modification was also made to the rules governing the co-ordinate transformations applied to the payout eye position. These are related to the orientation of the mandrel to the winding machine at any instant during the winding, and hence define the position of the payout eye in terms of an absolute (stationary) co-ordinate system. The rule chosen was that the mandrel and payout eye maintained the fibre within a plane of constant slope relative to the Y-axis. This strategy was found necessary to prevent the payout eye from fouling the mandrel or the end shafts during winding.

As an illustration, Fig. 8.6 shows a single winding of fibre consisting of two fibre paths linked as shown in Fig. 8.3. Fig. 8.7 shows the payout eye path required to wind this pattern, plotted relative to a stationary mandrel. Fig. 8.8 shows the absolute movement of the payout eye.

(e) CNC part-program generation. An existing post-processing program was used, with only minor modifications, to translate the absolute payout eye and mandrel positions into machine control instructions.

8.4 Manufacture of washable mandrel and associated tooling

8.4.1 *The need for a removable mandrel, and selection from available methods*

It will be readily appreciated that an elbow-shaped filament-wound component cannot be slid off its mandrel in the same way as a cylinder. Therefore it was necessary to create a mandrel which could not only be located accurately and positively in the winding machine but could also be removed from inside the elbow, possibly by destroying it in situ. Rosato and Grove[1] describe some of the options available for removable mandrels, as does Edwards[5] who presents a review of the limited amount of literature available on the subject. Wilson[4] describes some recent incremental developments in mandrel technology. One of the options considered for this application was a multi-part metal mandrel which could be dismantled from within the elbow, although this would have been very complex to design and use. Another option was to make the mandrel from low melting point alloy, but this would have been very heavy unless some means were found to make it hollow. The melting temperature of the metal would be chosen to be above the cure temperature of the resin otherwise it would melt out during the cure cycle. Eventually the concept of a washable or soluble mandrel was chosen since this technology had already been used in the Department for the manufacture of axisymmetric components. Ludur Wash-Away plaster[143] was chosen as being a close substitute for the Paraplast washable plaster used previously.

8.4.2 *Manufacture of pattern*

Before a washable mandrel could be made it was necessary to manufacture a mould and this in turn required the existence of an accurate pattern. This was manufactured from a number of aluminium components. The curved (toroidal) region of the elbow was assembled from two quadrants of a semi-toroidal ring

machined from round stock on a profiling lathe. These were bonded back-to-back using epoxy adhesive and the assembly was machined to give orthogonal end faces. The shanks of the elbow were made from aluminium tube and attached to the toroidal section using end discs with spigots. The whole pattern was assembled using epoxy adhesive with some screw reinforcement. As well as being used in mould manufacture, the pattern acted as a robust dummy mandrel for dry (resin-free) trial winding during fibre path development. End shafts protruding from the shanks provided a means of location of the mandrel in the machine.

8.4.3 *Manufacture of mould for plaster mandrel*

Some experimentation was involved in the evolution of the mould. The first mould followed existing practice by using soft plasticised vinyl rubber cast around the mandrel within a split wooden box. However, the plaster castings produced exhibited severe dimensional instability and distortion which was attributed to the compliant nature of the mould material.

A rigid two-part mould was manufactured from slate-filled epoxy resin and this gave promising results despite the occurrence of a crack during mould manufacture. Finally, a four-part mould (Fig. 8.9) was professionally manufactured from GRP and this gave satisfactory results. Some room for improvement exists in the mould filling arrangement which is at present via a single filler hole.

8.4.4 *Manufacture of steel-reinforced plaster mandrel*

The casting of the mandrel is essentially a simple process, during which a steel reinforcement structure is incorporated into the mandrel. This structure is necessary because the mandrel assembly is subjected to significant loads during winding and curing due to fibre tension, self weight and inertia. Unlike mandrels for axisymmetric components and many non-axisymmetric components such as tee-pieces and gently curved cranked arms, the elbow mandrel cannot be cast around a single straight shaft. The straight shanks of the elbow are joined by a

curved region and it was the author's opinion that it would be unwise to rely upon the strength of this region if it were made entirely from plaster. It was therefore decided to include in the plaster casting a dismountable elbow-shaped steel assembly. This consisted of two end shafts (co-axial with the cylindrical shanks of the elbow) linked by a mitre-shaped steel block into which the shafts screwed. The result was a steel structure which provided a strong framework for the mandrel yet was easily dismantled by unscrewing the shafts before washing out the plaster. The steel reinforcement, along with other tooling used in the manufacture of the elbow, is illustrated in Fig. 8.10.

The mould was greased with petroleum jelly and assembled around the steel reinforcement (Fig. 8.11). The mould was then filled with the slurry of mixed plaster which was compacted within the mould with the aid of a vibrating table. The plaster was allowed to set in the mould which was then progressively dismantled, allowing the plaster to dry out in a warm oven at 45°C. Flash was removed from the plaster casting and the surface sealed using Araldite mould release agents QZ11 (wax) and QZ19 (polyvinyl alcohol)[144].

8.4.5 *Additional tooling*

Before loading into the winding machine, a number of other items of tooling were used or fitted. Pinned end turnaround caps (intended to catch the fibres to prevent slippage during turnaround) were assembled onto the end shafts at this stage. The mandrel was held via its end shafts in the winding machine using 45° cranked arms and these were assembled with the aid of a wooden jig (Fig. 8.12) so that the axis of rotation of the mandrel was correctly located.

An additional item of tooling was used during loading of the mandrel into the machine and during curing. This was a brace which clamped around the end shaft of the elbow, converting it into a rigid A-frame structure to reduce further the effects of shock and cyclic loading during handling and curing. The brace is illustrated in Fig. 8.10 along with the other tooling already described.

8.5 Winding, curing and mandrel removal

8.5.1 *The winding process*

The elbow assembly was loaded into the machine and positioned relative to the machine datums using a steel rule and a spirit level. The brace was removed and winding of the various fibre patterns proceeded in the appropriate sequence. The fibre was cut and the winding sequence re-started whenever the direction of rotation of the mandrel changed between successive fibre patterns. A circular ceramic payout eye was used in preference to the roller-shaped eye used for winding the axisymmetric specimens; although this slightly reduced the flatness of the fibre tow, it eliminated the need for payout eye axis rotation and hence reduced the memory requirements for the winding part-programs. The smaller size of the payout eye also made it possible to approach the mandrel closely without danger of collision. The winding process and materials were otherwise identical to that used for the axisymmetric specimens. Fig. 8.13 shows the winding of an elbow. In the manufacture of a specimen using wet fibre on a white plaster mandrel the fibre is virtually invisible. The photograph therefore shows a black-painted dummy mandrel being wound with dry fibre to give a clear view of the fibre paths.

8.5.2 *Curing and mandrel removal*

On completion of the winding process, the brace was fitted to the elbow assembly. The assembly was then transferred to a curing oven which was fitted with a rotisserie to ensure even curing and to avoid dripping and running of the resin. A counterweighted arm was added to the assembly to minimise imbalance and speed variations.

It was necessary to ensure that the mandrel was thoroughly heated throughout its volume since this caused a chemical change in the plaster (calcining) necessary for satisfactory disintegration during washout. In practice the elbow was cured for 2 hours at 120°C before the turnaround regions were removed by sawing and the end shafts were unscrewed. The elbow was then post-cured at 120°C for 12

hours to calcine the plaster. After cooling, the plaster was removed with the aid of a high-pressure water jet, leaving the mitre block free to be removed. A typical finished elbow is shown in Fig. 8.14. The turnaround fibres were removed from the end caps after digestion of the resin in a suitable agent such as Stironol[145]. The end caps could then be re-used for the manufacture of another elbow.

8.6 Discussion

The software-related challenges of filament winding an elbow were eventually overcome with complete success in that full mandrel coverage could be achieved without collision. Three elbows were wound with apparent success, despite some minor practical difficulties relating to the rotisserie drive. However, a number of problems remain and these will need to be addressed if further use is to be made of the elbow-winding techniques described in this chapter. The most serious relates to the usefulness of the winding pattern from a structural viewpoint. The variety of feasible paths which can be wound upon an elbow is surprisingly limited. A path which appears quite practical (Fig. 8.15(a)) may require payout eye movements which are impractical because of clashes with the mandrel (e.g. Fig. 8.15(b)). Attempts to wind at shallow angles along one of the shanks can lead to nearly-axial paths along the opposite shank (Fig. 8.16) or to paths which will tend to lift from the toroidal region of the mandrel (Fig. 8.17). The fibre paths used for the test elbows were wound at approximately ±75° on the shanks and none of these problems was encountered. However, these patterns did result in a weak spot on the outside of the toroidal region (Fig. 8.18) where the fibres ran almost parallel to each other giving a material which was very weak in the transverse direction. The area where this occurred happened to be the thinnest part of the structure. Two elbows were produced with this set of paths and both of them exhibited lines of opacity in this region. This opacity appears to be due to matrix micro-cracking. It is possible that this cracking was due to thermal movement of the plaster, steel and composite during curing. If an elbow is to be used as a test specimen for verification of the meshes produced using

FILFEM II, it will be essential to investigate these problems and overcome any weaknesses as far as possible.

8.7 Conclusions

It may be concluded that although some refinement to the details of the process are still required, the attempt to manufacture a filament-wound elbow has been largely successful and has produced a number of benefits. The task of manufacturing the elbows has involved the creation of some useful enhancements to the filament winding software which will form an essential foundation for further manufacture of structures of this kind. It has also provided a useful set of fibre path data which was used in the development of FILFEM II. Although no experimental testing of the elbows has taken place, these fibre paths have formed the set of test data which was essential in demonstrating the usefulness of the search algorithms and vector geometry used in FILFEM II. Finally, it has provided the author with a challenging and beneficial learning exercise. This has covered all the aspects of non-axisymmetric filament winding from path generation via fibre path processing to the practical aspects and problems of manufacture.

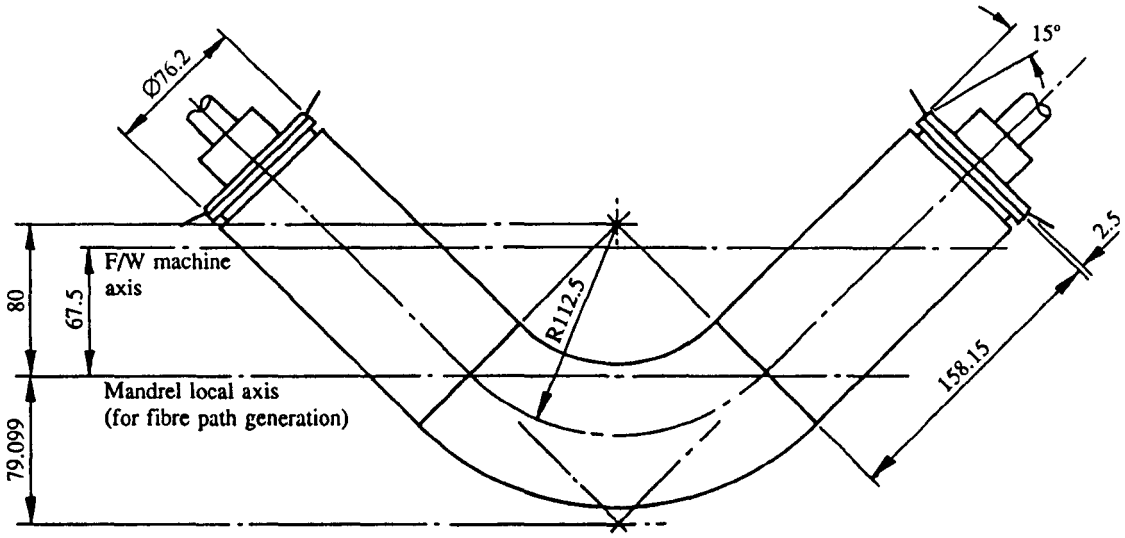

Fig. 8.1: Dimensions of mandrel used for winding elbow

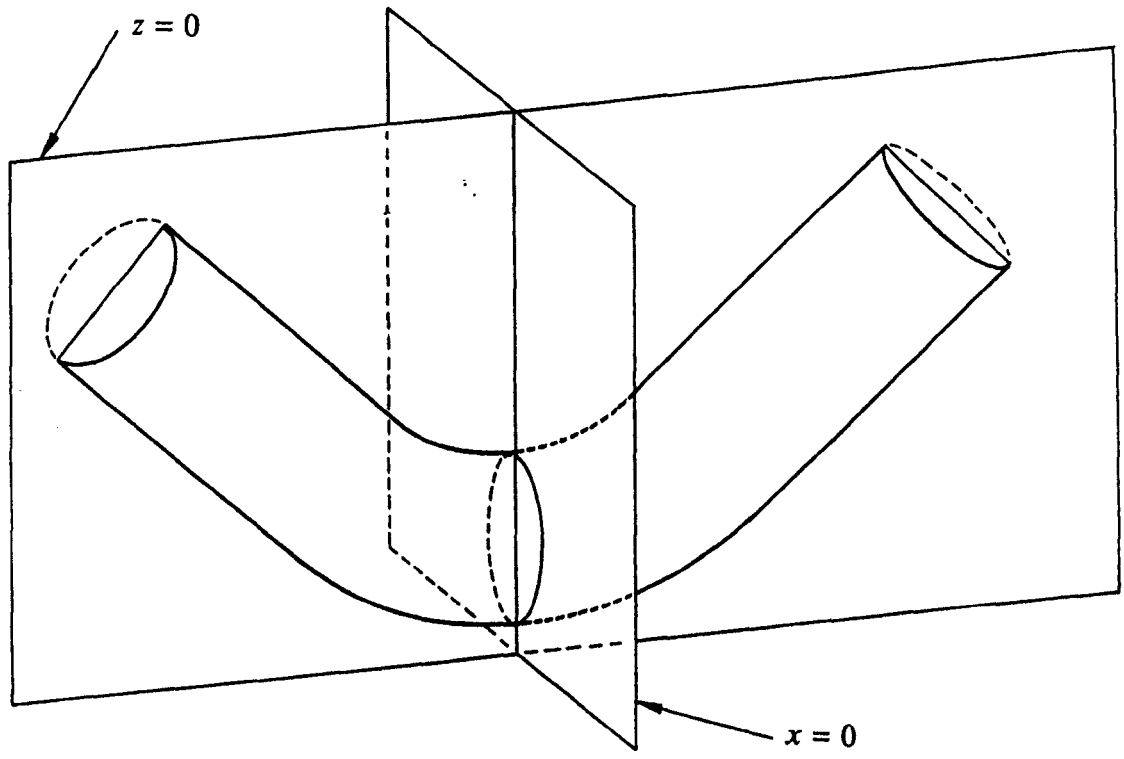

Fig. 8.2: Planes of symmetry used for replication of fibre paths

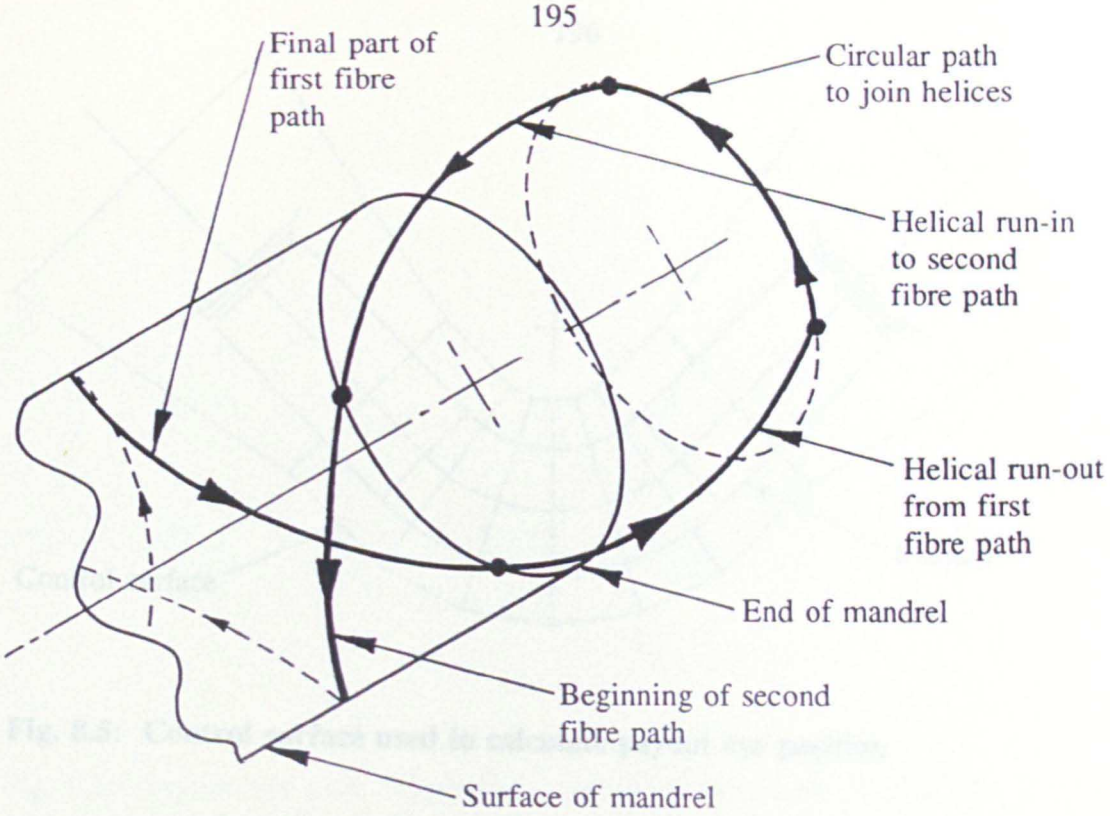

Fig. 8.3: Use of helical and circular paths to join ends of fibre paths

Fig. 8.4: End cap used to prevent fibre slippage at turnaround

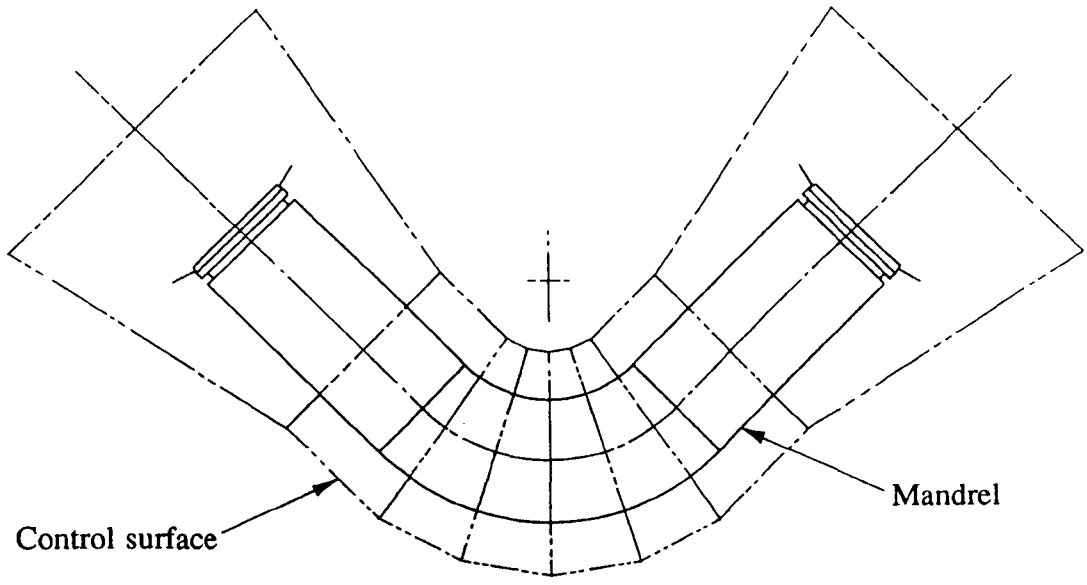

Fig. 8.5: Control surface used to calculate payout eye position

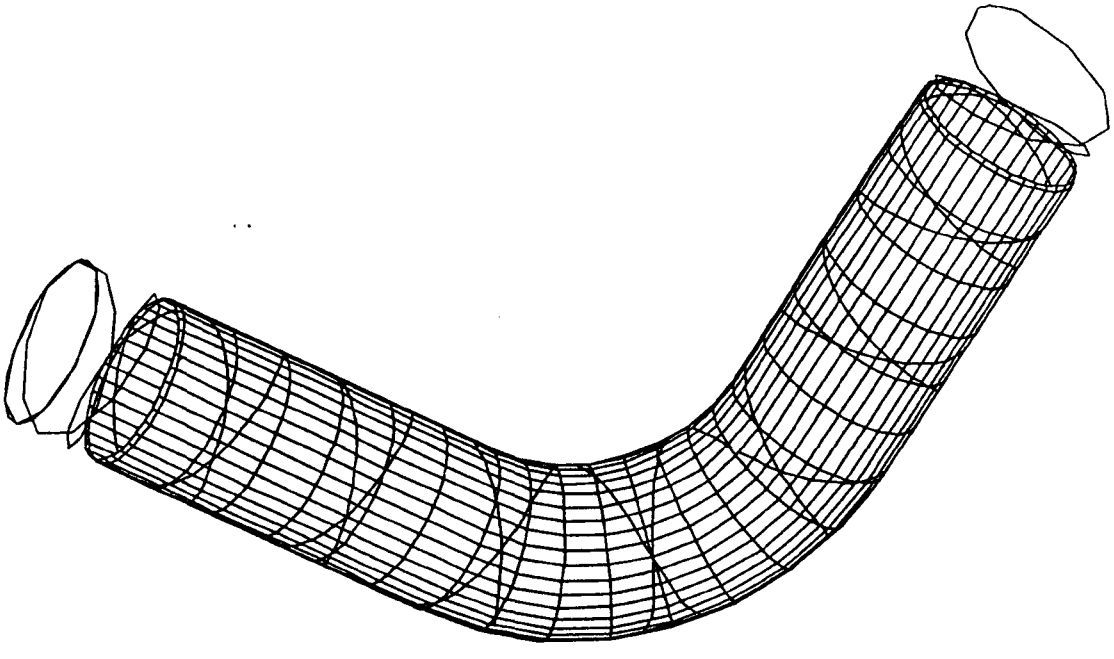

Fig. 8.6: A pair of fibre paths (second fibre path obtained by reflection in x=0) linked using helical and circular end paths to form a single winding of fibre. Also includes circular and helical paths for starting and finishing winding.

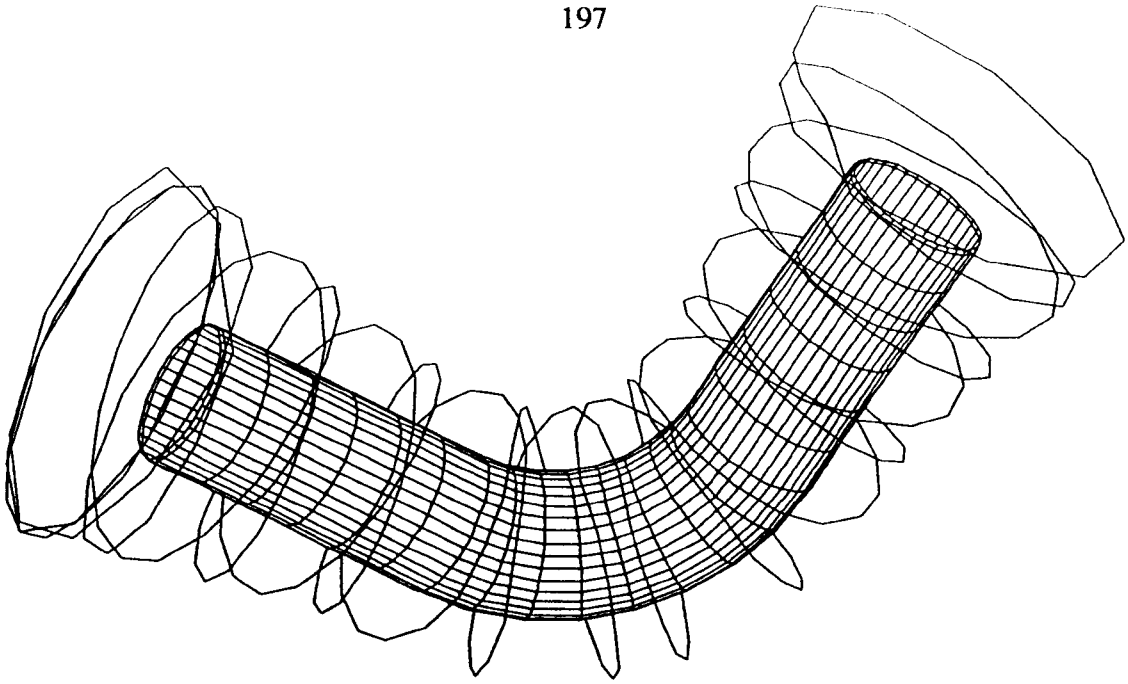

Fig. 8.7: Payout eye path required to wind fibre as shown in Fig. 8.6. Path is shown relative to the mandrel.

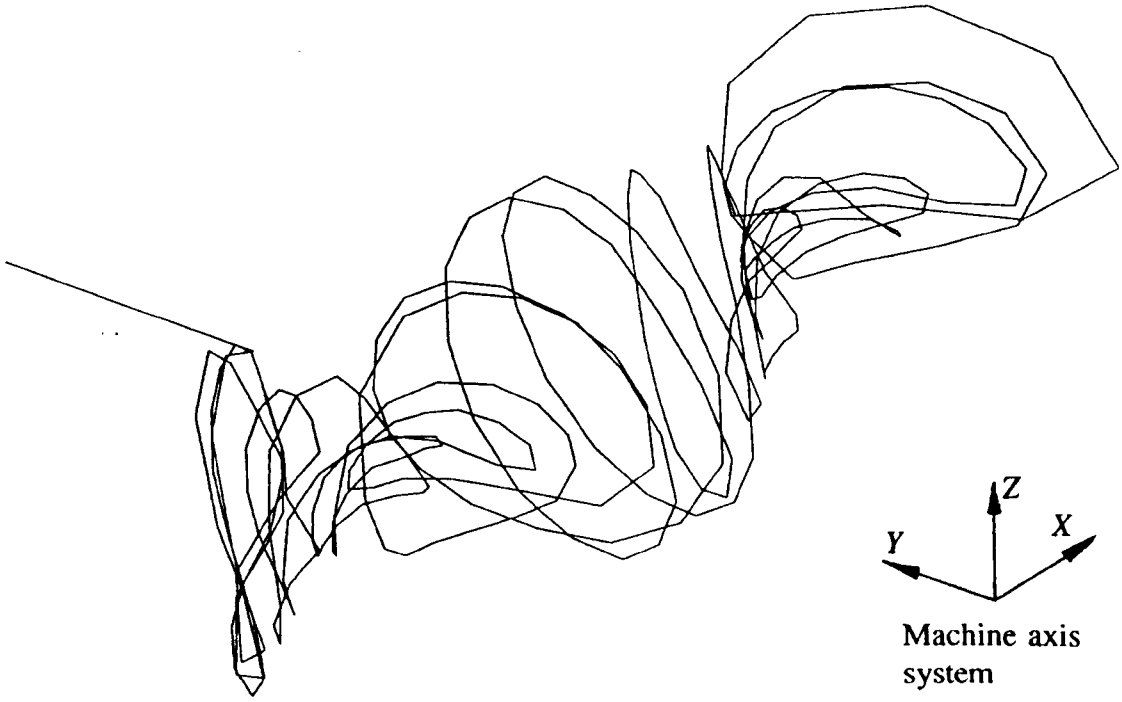

Fig. 8.8: Actual path of payout eye, as seen by a stationary observer. The final movement of the eye takes it clear of the mandrel.

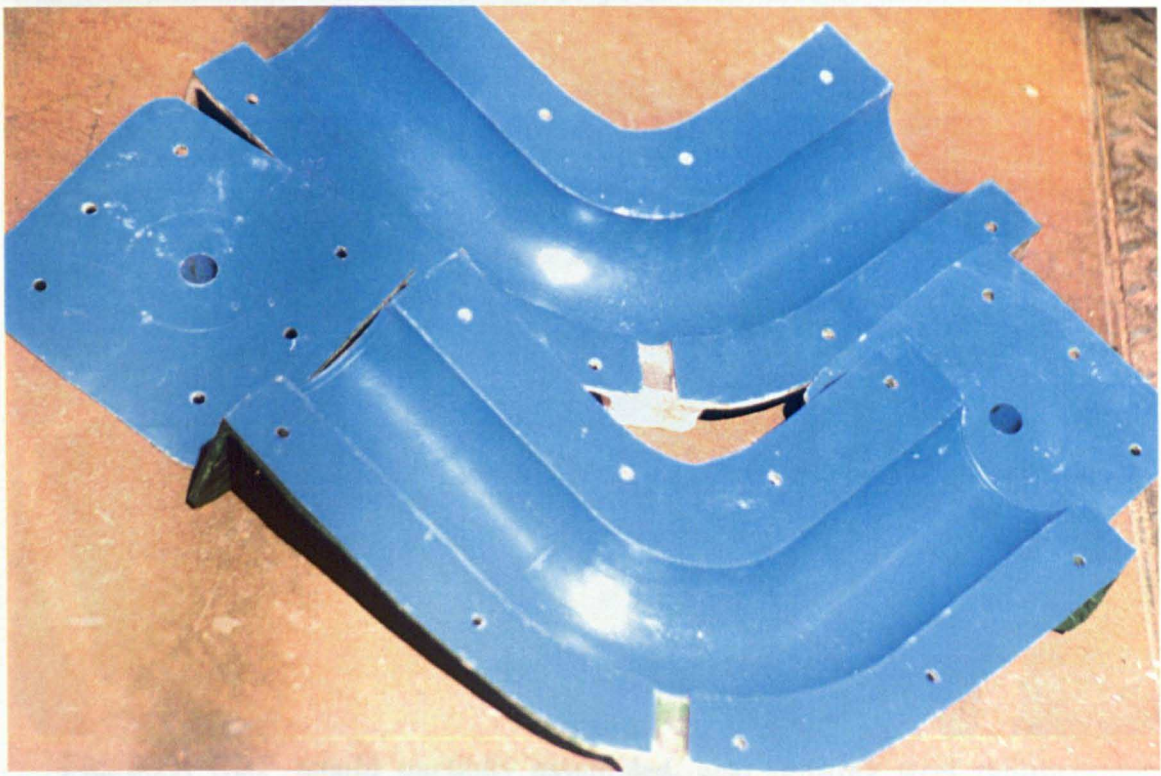

Fig. 8.9: Four-part GRP mould used for casting of plaster mandrels

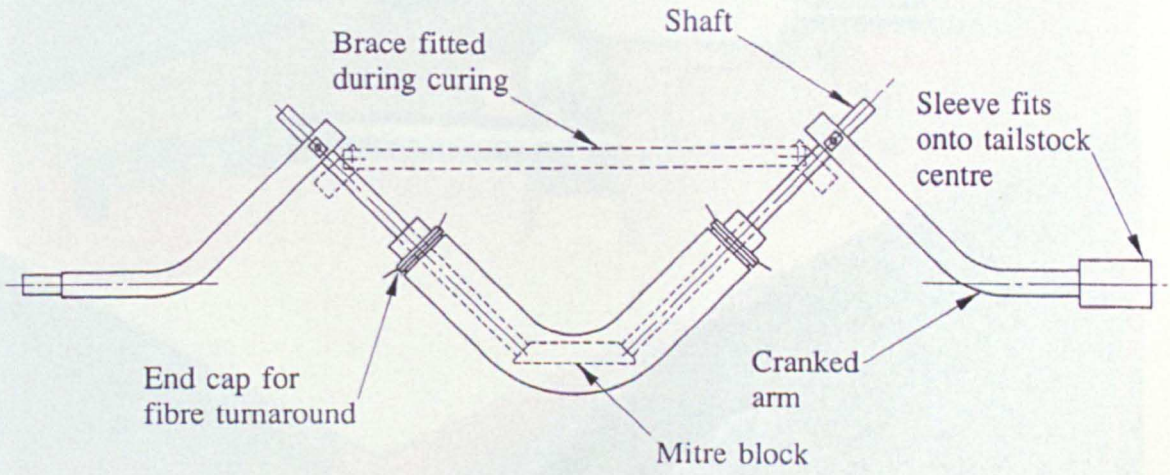

Fig. 8.10: Tooling used for manufacture of filament-wound elbow

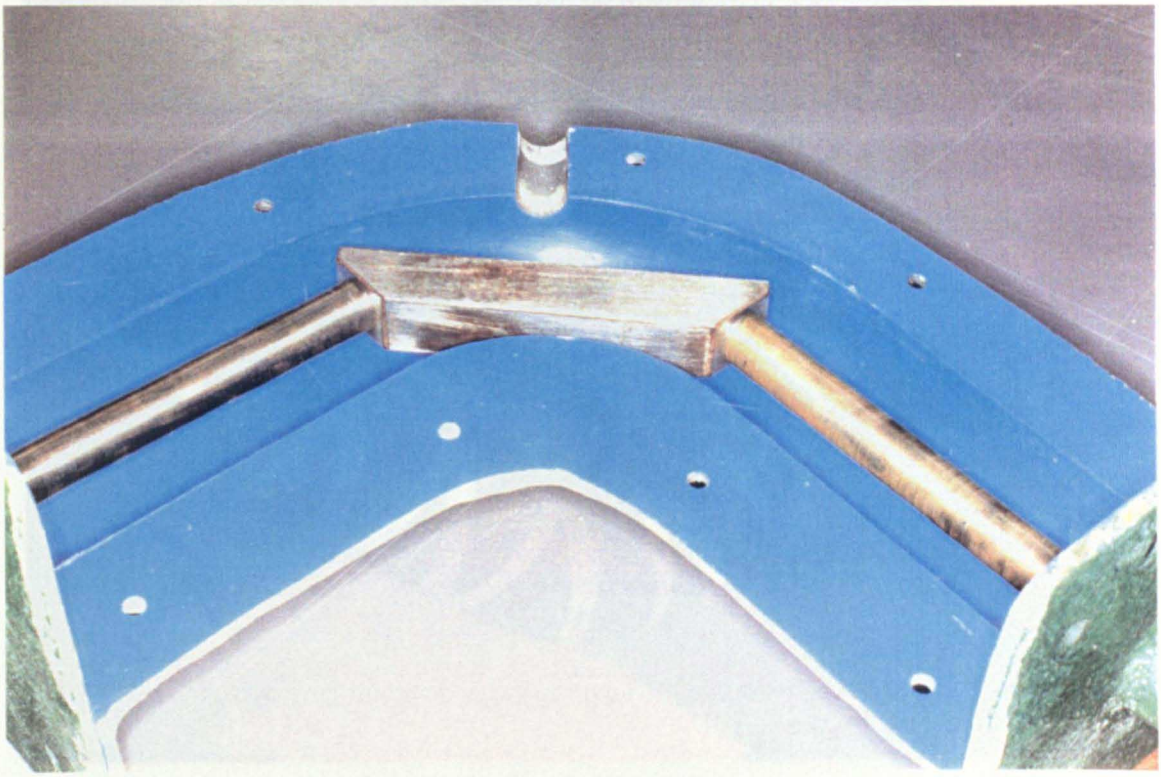

Fig. 8.11: GRP mould partially assembled, also showing steel reinforcements (shafts and mitre block)

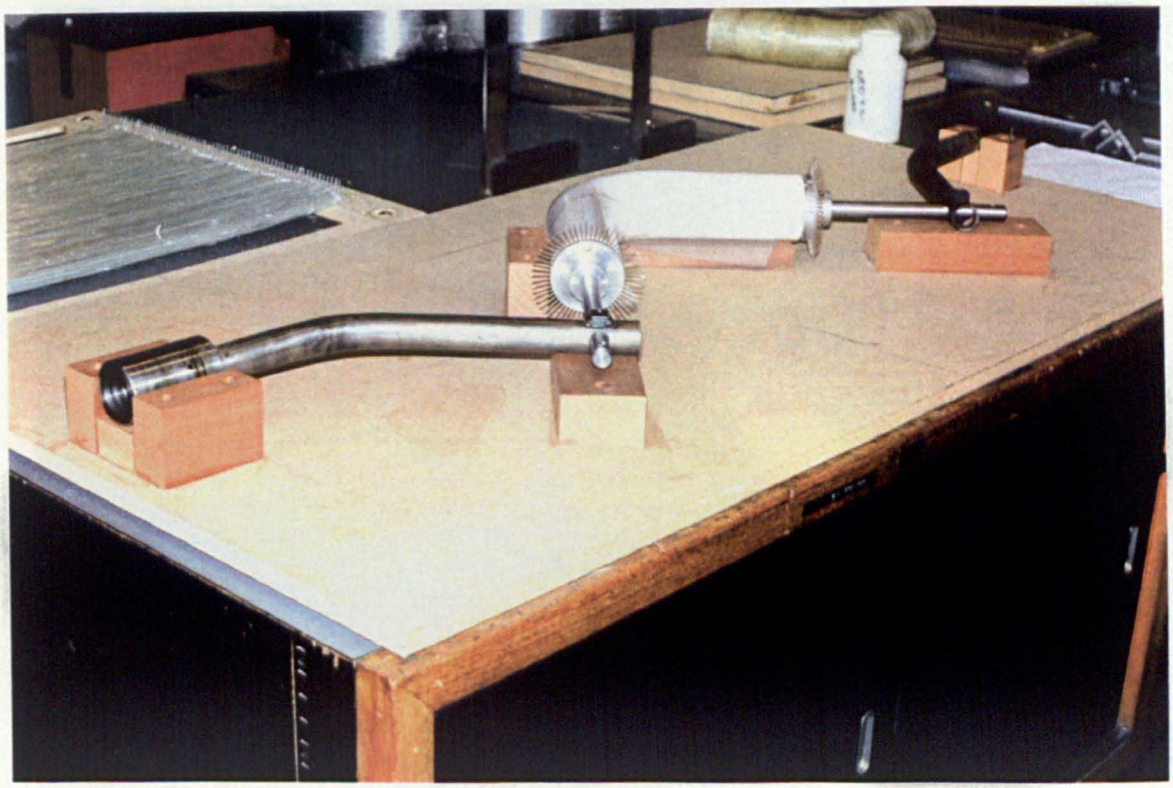

Fig. 8.12: Wooden jig used for assembly of mandrel and tooling

Fig. 8.13: Dry winding of an elbow on a dummy mandrel to demonstrate fibre paths

Fig. 8.14: Typical finished elbow after removal of turnaround regions and washing-out of plaster mandrel

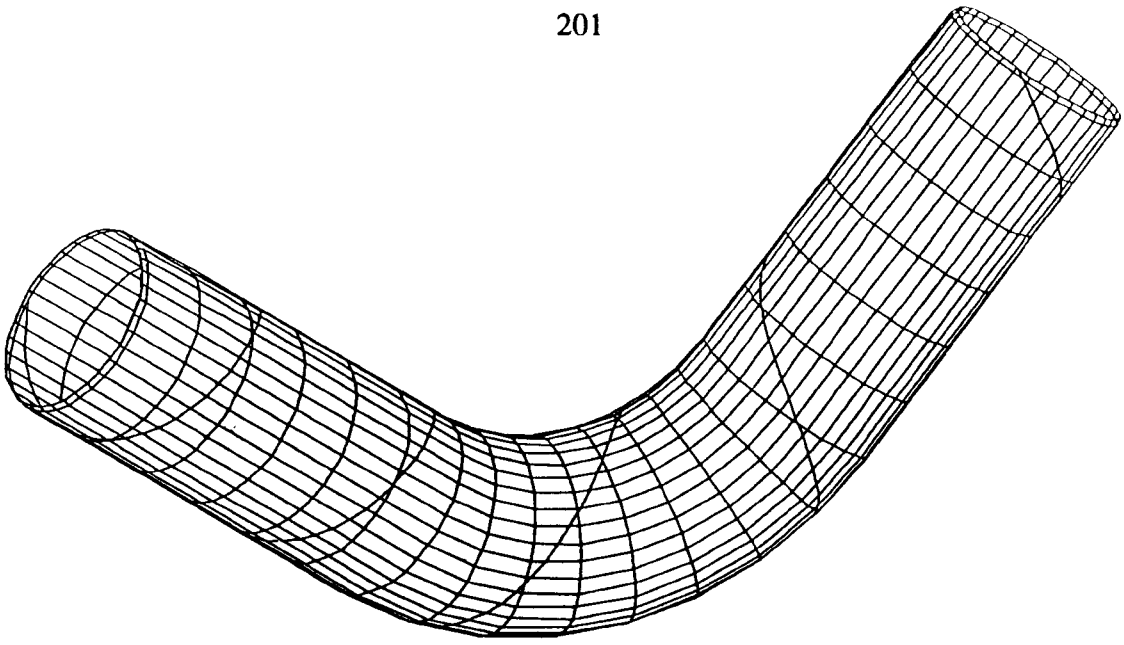

(a) Example of a non-feasible fibre path. The problem is caused by the centremost turn whose tangent projects back into the mandrel without leaving the control surface.

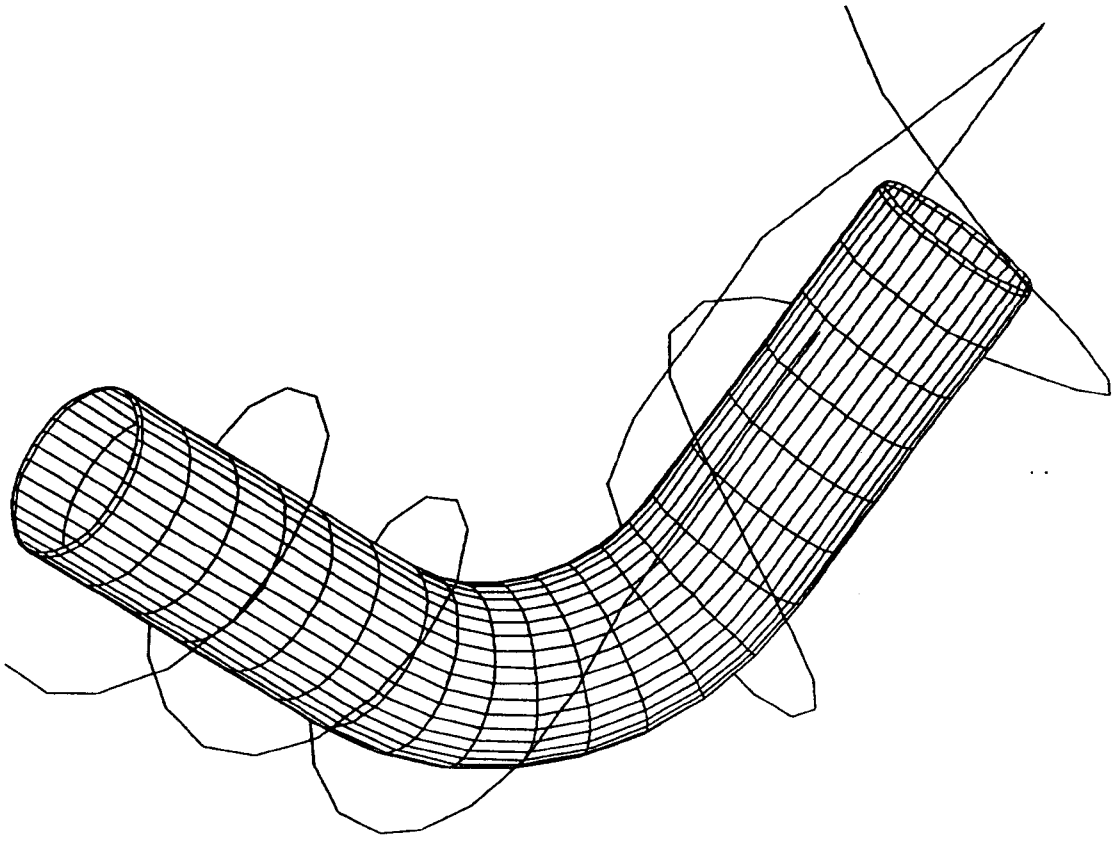

(b) Payout eye path calculated for non-feasible fibre path. Note how the payout eye would have to pass through the mandrel. Other non-feasible paths may require payout eye movements which are less extreme but still impractical.

Fig. 8.15: A non-feasible fibre path and the impractical payout eye path it requires

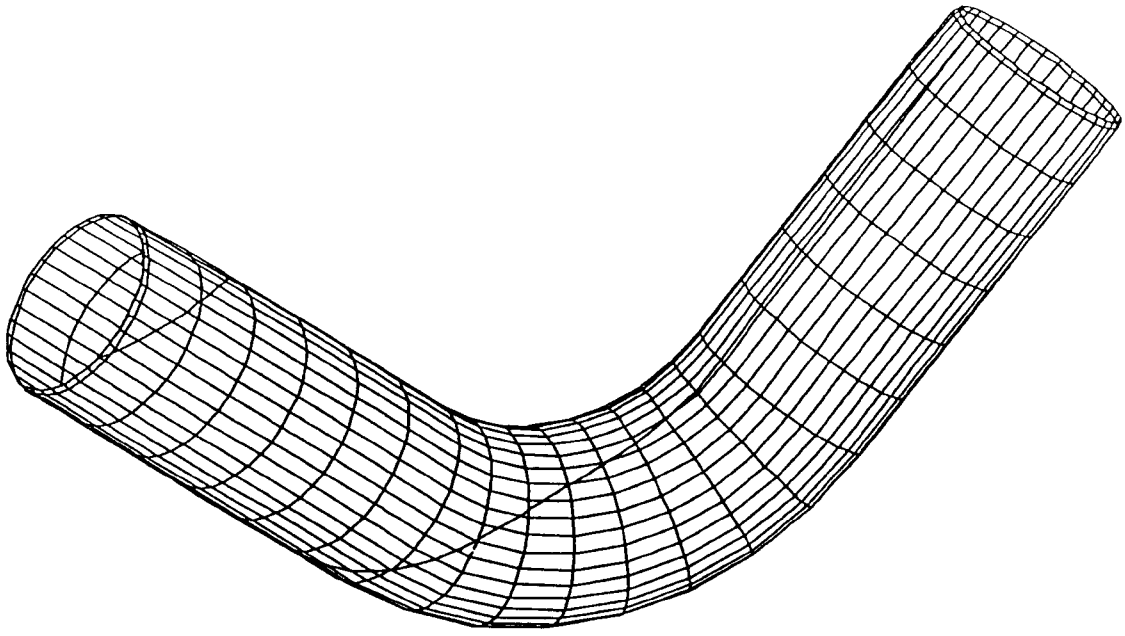

Fig. 8.16: A geodesic fibre path which becomes nearly-axial on one of the shanks of the elbow

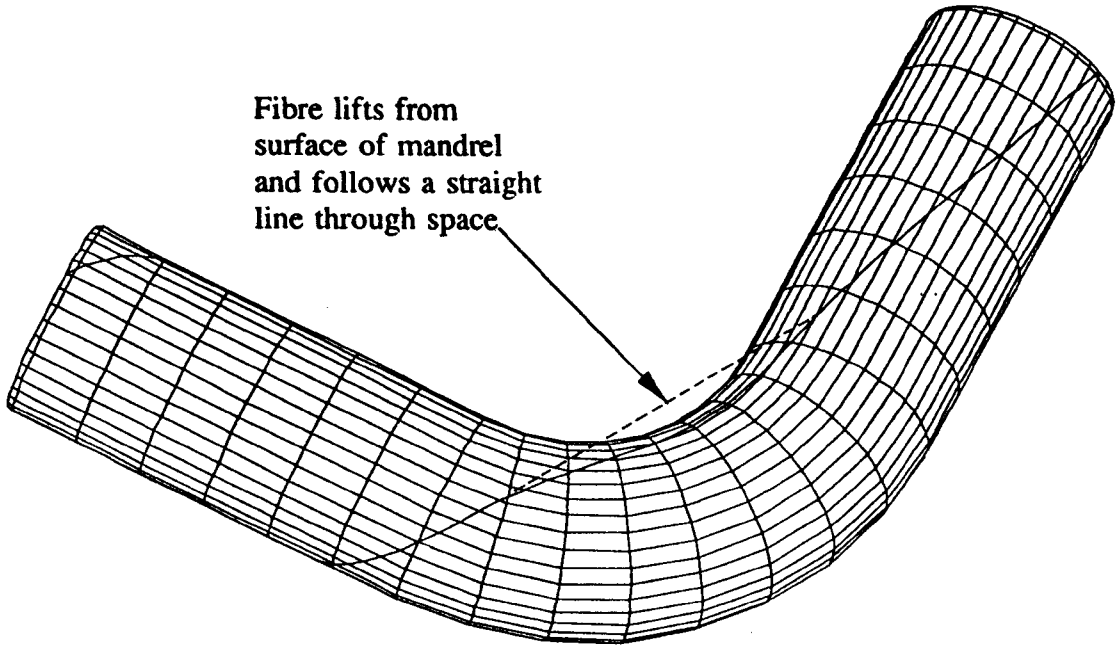

Fig. 8.17: A geodesic fibre path which would lift from the mandrel surface if winding were attempted

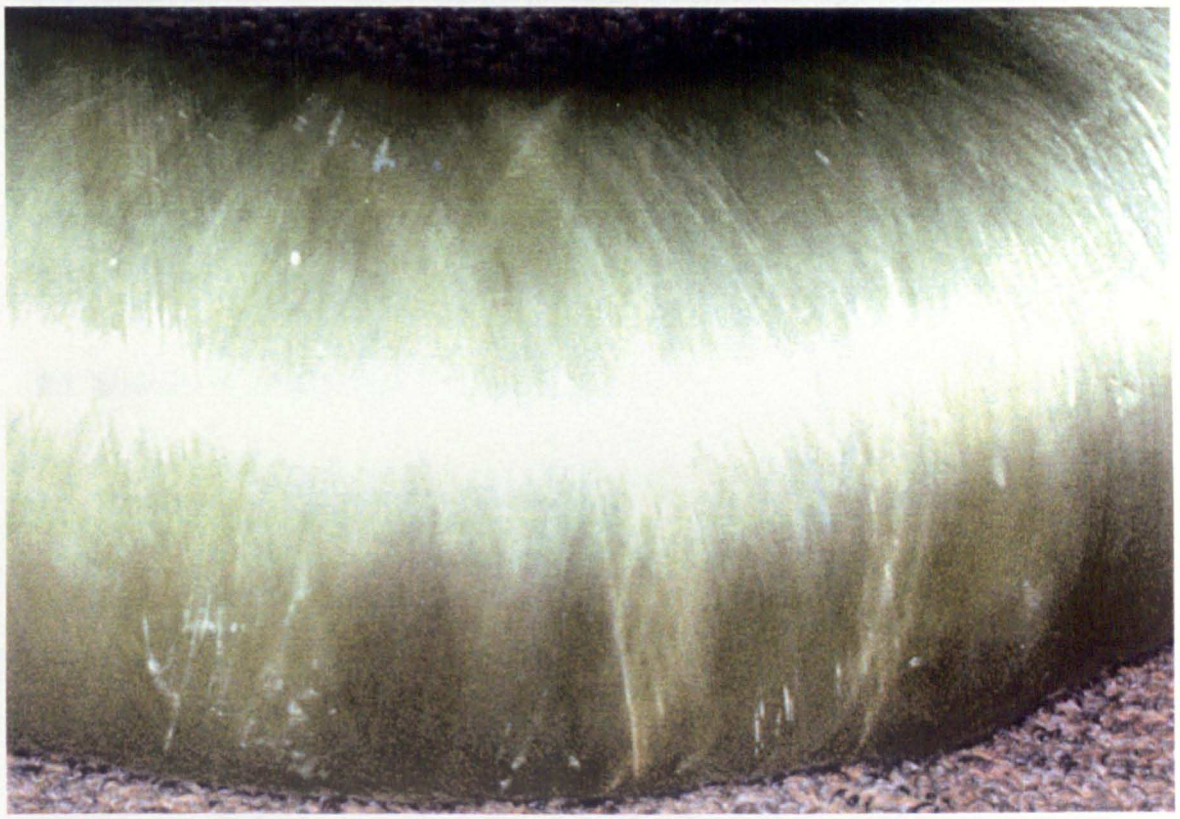

Fig. 8.18: Weak part of filament-wound elbow. The fibres are seen to be almost circumferential leading to a material which is very weak in its transverse direction. Also visible are lines of opacity suggesting poor integrity of the composite material.

CHAPTER 9: DISCUSSION, CONCLUSIONS AND RECOMMENDATIONS FOR FURTHER WORK

9.1 Introduction

This chapter aims to review the work that has been described in this thesis and to compare it with the objectives set at the start of the project. The content of the work and its usefulness will be discussed, and the main conclusions from the work will be listed. Finally, areas for further work will be identified.

9.2 Review of original objectives

The objectives of the project were discussed in general terms in Section 1.1 and were itemised in Section 1.2. The main objectives may be summarised as the creation, implementation and experimental testing of an engineering tool which consists of an interface between two existing areas of technology. These areas are the computer-aided filament winding of composite materials, and the finite element analysis of structures. Both of these areas of technology have reached the level of maturity at which they are being packaged commercially by appropriate producers. Finite element analysis of filament wound composite components is far from being a new process, but a serious obstacle to its routine use especially for complex components is the continuous variation of the laminate structure of a component over its surface. This makes it prohibitively time-consuming to create manually an accurate finite element model of the structure. This obstacle has been largely overcome by the work described in this thesis. This work enables a reasonably accurate finite element model of an axisymmetric filament wound component (or a slightly simplified model of a non-axisymmetric component) to be created with a minimum of manual effort.

An example may be used to illustrate the potential savings in data generation time. The thin shell FE models of the pinched cylinder were defined by files containing typically between 5000 and 15000 lines of data. Conventional model generation

systems are inappropriate to the automation of this task since they cannot generate a description of the laminate structure. This description accounts for a large proportion of the data defining the model. The manual effort which would be required to calculate such a volume of data can easily be imagined. By contrast, it took only a few minutes to generate each data file automatically using FILFEM I. Approximately two hours of extra effort were required to edit the models to include boundary conditions and mesh refinement and to remove the unwanted parts of the structure i.e. the turnaround regions. However, these tasks were still quite small when judged against the complexity of the models. The generation of non-axisymmetric test meshes using FILFEM II was similarly straightforward. The only published evidence that a link of this kind has been achieved by other researchers relates to the simplest of cases, namely the automatic generation of an axisymmetric model of a component wound on an axisymmetric model[16,18]. In this thesis two much more versatile links have been described which can be used to generate axisymmetric and non-axisymmetric models of a variety of filament-wound structures.

The application of the FILFEM I program to the pinched cylinder problem has shown that the accurate modelling of the alternating lamination sequence had no significant effect upon the deflections obtained when these results were compared with a similar model assuming a uniform lamination sequence. Such results suggest that the simplified model is adequate for most engineering purposes. The close prediction of the true structure provided by FILFEM I may therefore not always be necessary. However, extraction of stresses on a ply-by-ply basis can be achieved within the finite element programs and requires data correctly defining the lamination sequence. Accurate modelling of the laminate structure is particularly desirable in a research situation, and previous researchers have been discouraged from achieving this because of the difficulty of the task[76]. FILFEM I eliminates this source of difficulty and makes accurate modelling a much simpler task.

When the project was originally conceived, it had been hoped that it would be possible to take the development of both the axisymmetric (FILFEM I) and non-axisymmetric (FILFEM II) filament winding/finite element link programs to a high

level of completion and testing. In practice, so much time has been spent in identifying and avoiding practical obstacles that this has been achieved only partially. FILFEM I requires further enhancements (itemised in Section 8.3) and experimental verification of the models generated by FILFEM II will require considerable further work.

9.3 Discussion of results and achievement

9.3.1 *The FILFEM programs*

The most tangible and immediately useful work to be produced in this project is the software, primarily the FILFEM programs. However, it should be clearly understood that these programs merely provide the packaging for the original work which is the main subject of this thesis. Before any piece of code could be written it was necessary to gain an understanding of the kinds of structures to be modelled, the data required to define them and the possibilities for extracting these definitions from the data available within the CADFIL systems. It was then necessary to formulate the logical sequence of tasks required to achieve this data conversion and to derive or identify the mathematical or geometrical content of each of these tasks.

The challenges involved in creating FILFEM I and FILFEM II were very different. FILFEM I made particular use of curve-fitting and numerical analysis to predict thicknesses, winding angles and lamination sequences from a series of points on a single fibre path and to construct a finite element mesh to coincide with the naturally-occurring pattern of alternating lamination sequence on the filament-wound component. FILFEM II faced the opposite problem of extracting similar information from an extremely large amount of data where every fibre within a repeating sequence is defined separately. This required the creation of a fairly involved search algorithm to identify the data relevant to each element in turn, and made heavy use of vector arithmetic in the sorting of this data and the extraction of the required numerical values.

In practice, many of the ideas were formulated, coded into the programs, and tested for effectiveness in a step-by-step manner. The language used (FORTRAN77) was entirely adequate for the implementation of the systems and the task of coding the algorithms was very straightforward. It will be appreciated therefore that the main effort required in the creation of the CADFIL/FE links lay not in the task of coding the FILFEM programs but in the analysis of each task to be performed, the formulation of the approach to each task and the detailed breakdown of this approach into individual operations. It should also be noted that every effort was made to avoid unnecessary duplication of work, by making use of existing code for specific tasks wherever possible. In particular, the cubic spline calculations, the curve-fitting and the vector algebra were all carried out using imported code.

9.3.2 *Experimental verification of FE results and investigation of material properties*

It was realised at an early stage that a satisfactory evaluation of typical automatically-generated FE meshes would involve experimental testing of components manufactured using the CADFIL systems. This necessarily involved the characterisation of the properties of the composite material involved. E-glass/polyester had been chosen because of its common use in practical applications, its ease of manufacture, its ready availability and its low cost; in retrospect it was found not to be an ideal material for elastic experimental work. A comprehensive programme of work described in Chapter 5 was aimed at measuring its elastic properties when assembled into an angle-ply laminate. This produced results for laminate behaviour which were in poor agreement with established theory. The reasons for this poor agreement can be summarised as very significant non-linearity and permanent changes in constitutive behaviour due largely to material damage. These matters were discussed more fully in Chapter 5 and were only properly understood towards the end of the project when the investigation of alternative materials was not a realistic option. It is noteworthy that the standard textbooks on the mechanics of composite materials (e.g. reference 25) concentrate on the assumed linear elastic behaviour of

directional composites and make little reference to the practical effects of the non-linear behaviour encountered in real materials. It was for this reason that the linearity of the material was not given sufficient consideration during its selection. The problem of poor prediction of laminate properties was partially overcome by the development of a technique for calculating the unidirectional material properties which gave predicted laminate properties most closely fitting the observed behaviour of the laminated specimens. When this data was used as the basis for modelling the behaviour of the filament-wound pinched cylinder, excellent agreement was obtained between the results from the FE models and the experimental data. However, some caution must be exercised in the interpretation of this good agreement, since the best-fit unidirectional properties included an unrealistically low value of transverse Young's modulus E_2. A more rigorous verification of the results obtained from the automatically-generated meshes would require the specimens to be made from a composite material with constitutive behaviour much closer to the linear elastic orthotropic model.

In performing the material property characterisation experiments, a number of materials tests were used. Two of these, namely the pinched ring and the roller-assisted split disc tests, appear to be original to this work at least as far as the determination of elastic properties of filament-wound composites is concerned. The analysis of the errors in these tests also appears to be new work, as does the fitting of unidirectional properties to the behaviour of laminated specimens. The method of correcting for edge effects in the pinched ring specimens is simple and was derived from first principles by the author; although equivalent results for an isotropic shell already exist[109], no evidence has been found of any edge correction work relating to orthotropic or laminated pinched rings or similar structures.

The practical experience of FILFEM I was based upon the problem of a pinched filament-wound cylinder with varying winding angle and wall thickness, and no analytical solution to this kind of problem could be found in the literature. Calladine's solution to the isotropic pinched cylinder problem (which includes a solution to the orthotropic problem by inference but not explicitly) was extended

in a fairly straightforward manner by the author to cover the practical problem, by making further use of Calladine's analogy with the beam-on-elastic-foundation problem. It would appear that despite its simplicity this work breaks new ground. Since the search for an analytical solution to the pinched cylinder problem formed something of a digression from the main work described in this thesis, the more mathematically involved aspects of this work have not been fully explored.

9.4 Conclusions

9.4.1 The logic and geometry have been identified, and where necessary derived, to provide a link between existing codes for computer-aided filament winding (CADFIL) and finite element analysis (ABAQUS and PAFEC). This link has been achieved both for axisymmetric and non-axisymmetric winding and the two versions of the link have been implemented as items of FORTRAN software named FILFEM I and FILFEM II.

9.4.2 The CADFIL/FE link for axisymmetric filament winding (FILFEM I) has been tested by modelling a filament-wound cylindrical tube under a pinching load. A test mesh of a filament-wound elbow has been generated using FILFEM II. The experience gained in these exercises has demonstrated the effectiveness and time-saving potential of the FILFEM software.

9.4.3 The use of an accurate representation of the variations in laminate structure was found to have little effect upon the thin shell finite element predictions of deflection in the pinched cylinder problem when compared with a model assuming uniform lamination sequence. The difference between these results was approximately 1%. Larger differences (typically 10%) were found between these results and the results obtained by assuming an axisymmetic structure with homogeneous orthotropic properties.

9.4.4 An existing solution to the pinched cylinder problem has been successfully extended to model a pinched filament-wound cylinder with varying winding angle and wall thickness. This model represented the cylinder wall as a homogenous orthotropic material although suggestions for a solution taking account of the laminate structure have also been made. Close agreement has been obtained with finite element results for which similar assumptions are made.

9.4.5 A programme of work has been carried out to characterise the behaviour of filament-wound glass-reinforced polyester resin, and two new tests have been devised to achieve this. These were described in sections 5.2 and 5.3. The behaviour of both unidirectional and laminated material has been investigated.

9.4.6 A technique was developed to determine the unidirectional material properties from the observed laminate behaviour and the results from this fitting exercise were in some disagreement with the values which would have been expected. In particular, the value of transverse Young's modulus (E_2) obtained from flexural tests was 2582.9 MNm^{-2} which is only 25% of typical values obtained from other sources. This discrepancy was eventually ascribed to the severe non-linearity of the material behaviour and in particular to the permanent changes in behaviour of the material when its structure becomes damaged.

9.4.7 When the best-fitted values of unidirectional properties obtained from flexural tests were used in conjunction with the automatically-generated finite element models of the pinched cylinder problem, excellent agreement (within a few percent) was obtained between the predicted and measured deflections.

9.4.8 Existing filament-winding techniques for non-axisymmetric filament winding have been enhanced to include the manufacture of elbow-shaped pipes.

9.5 Recommendations for further work

Although the original aims of the project have largely been satisfied, there inevitably remain a number of items for which work is still outstanding. Many of these have arisen because particular areas of work have proved to be more complex than expected.

9.5.1 It has already been explained that the material used for specimen manufacture was not ideally suited to experimental verification of linear elastic models, and that the problems were understood too late in the project to permit repetition of the experimental work described with a more appropriate material. However, should any further experimental verification work be undertaken, it will be necessary first to choose an appropriate combination of fibre and resin materials. This should be not only acceptably linear and elastic in its constitutive behaviour, but also straightforward to use for filament winding. The elastic properties of epoxy resins have been widely exploited for a variety of experimental stress analysis techniques. It is therefore suggested that this family of materials should be investigated in order to find a formulation suitable for this application. It will then be necessary to characterise its behaviour of the resulting composite using some or all of the methods described in Chapter 5.

9.5.2 A typical model created using FILFEM II will need to be tested against the experimental behaviour of the corresponding structure. While the filament-wound elbow described in Chapter 8 would appear to be a satisfactory structure for this exercise, it is likely that improved fibre paths will need to be generated in order to overcome the weaknesses inherent in the present winding pattern. A considerable amount of apparatus for the testing of tubular joints already exists as a result of other work being undertaken within the Department. The elbow has been designed to be compatible with this apparatus. It would be beneficial therefore if account could be taken of this equipment in designing the experiments.

9.5.3 It is likely that modifications and refinements will need to be made to the logic and geometry underlying FILFEM II in the light of experimental verifications. Although the FILFEM programs themselves are to be regarded primarily as testbeds of the algorithms developed during this project, it is likely that they will be exploited as practical engineering tools and there is room for improvement in the quality of the user interface and the standard of software maintainability. It is also likely that they could be integrated more closely into the relevant parts of the CADFIL software.

9.5.4 There is scope for further work in the derivation of analytical solutions to the pinched orthotropic cylinder problem. In particular, further work is required to investigate whether Ting and Yuan's solution can be extended to cover the orthotropic situation. Any investigation of this would probably benefit from making use of Calladine's approach to the pinched cylinder problem.

9.5.5 Further work is required to produce a satisfactory model of the build-up of fibre in the turnaround regions of components manufactured using CADFIL I. The effects of this inadequacy in FILFEM I were largely avoided in the experimental verification since these regions were sawn off the specimen. The thickness predictions for the end regions were less accurate than the predictions towards the middle of the cylinder. Since the shape of the turnaround region is largely governed by practical considerations such as fibre slippage, it is suggested that experimental work will be required to establish a set of rules for predicting the turnaround shape.

9.5.6 It was observed that all the filament-wound components were milky in appearance rather than clear, and some problems with delamination and lack of fibre bonding were encountered during initial trial winding sessions. It is also apparent from electron micrographs that there is a certain amount of voidage in the composite material. It would appear that wetting-out and penetration of the resin into the fibres is inadequate. Further work is

currently being planned to investigate this general area and hence to improve the integrity of the composite material.

REFERENCES

1. Rosato, D. V. and Grove, C. S., *Filament winding: its development, manufacture, applications and design.* USA: Interscience Publishers, division of John Wiley and Sons, Inc., 1964.

2. Wiltshire, A. J., **Filament winding - a review.** Reinforced Plastics Conference, SPE (Cleveland Section), Technical paper for meeting, Sept. 28-30, 1970, pp 25-26.

3. Munro, M., **Review of manufacturing of fiber composite components by filament winding.** *Polymer Composites*, 1988, Vol. 9(5), 352-359.

4. Wilson, B. A., **Filament winding - past present and future.** *34th International SAMPE Symposium*, 8-11 May, 1989.

5. Edwards, K. L., *Advanced CNC winding of complex FRP shapes.* University of Nottingham PhD thesis, 1985.

6. Elegante, T. L., **Filament Winding**, *Mechanical Engineering*, 1986, Vol. 108(12), 32-36.

7. Young, K. W., *Computer aided design and manufacture for filament wound reinforced plastics.* University of Nottingham PhD thesis, 1986.

8. **CADFIL®** and **CADFIL II®** are registered trade marks of **Crescent Consultants Limited**, Unit 16, Faraday Building, Highfields Science Park, University Boulevard, Nottingham NG7 2QP.

9. Owen, M. J., Middleton, V., Elliman, D. G., Rees, H. D., Young, K. W. and Edwards, K. L., **Developments in filament winding**, in *Advanced Composites: the latest developments*, Proceedings of the Second Conference on Advanced Composites, 18-20 November 1986, pp. 35-43.

10. Shearing, M. R., *Computer aided design, simulation and manufacture of filament wound reinforced plastics.* University of Nottingham PhD thesis, 1988.

11. Middleton, V. and Owen, M. J., **Advanced CNC filament winding.** The Plastics and Rubber Institute (PRI) *3rd International Conference on Automated Composites (ICAC91)*, Netherlands Congress Centre, The Hague, 15-17 October 1991, pp. 23/1-23/7.

12. Sorenti, P., *Robotics applied to filament winding of reinforced plastics.* University of Nottingham PhD thesis, 1988.

13. Brown, L. P., *Design of a filament winding cell.* University of Nottingham PhD thesis, 1988.

14. Menges, G. and Effing, M., **CADFIBER - A software tool for composite engineering.** PRI *2nd International Conference on Automated Composites*, Leeuwenhorst, Netherlands, 26-28 September 1988, pp. 11/1 - 11/21.

15. Kiberg, K. W., Michaeli, W., Menges, G. and Seifert, A., **Process simulation in filament winding - new insights show the way to cost-effective component development.** PRI *2nd International Conference on Automated Composites*, Leeuwenhorst, Netherlands, 26-28 September 1988, pp. 16/1 - 16/15.

16. Eckold, G. C. and Wells, G. M., **Computer aided design and manufacture of advanced composites.** Proceedings of the second *Materials Engineerng Conference*, London, 5-7 November 1985, pp. 39-46.

17. Lloyd-Thomas, D. G., Eckold, G. C. and Wells, G. M., **Asymmetric Filament Winding.** PRI *2nd International Conference on Automated Composites*, Leeuwenhorst, Netherlands, 26-28 September 1988, pp. 12/1 - 12/12.

18. Wells, G. M. and Eckold, G. C., **Computer aided design and manufacture of filament wound composite structures.** PRI *1st Conference on automated composites*, University of Nottingham, 10-12 September 1986, pp. 6/1 - 6/16.

19. DiVita, G., Lucignano, F. and Marchetti, M., **Computer aided design and manufacturing of general shape filament wound composites.** PRI *3rd International Conference on Automated Composites*, Netherlands Congress Centre, The Hague, 15-17 October 1991, pp. 24/1 - 24/5.

20. Vogt, J. C. and Taylor, D. L., **A workstation for off-line filament winding pattern generation.** *34th International SAMPE Symposium*, 8-11 May, 1989.

21. Seereeram, S. and Wen, J. T.-Y., **An all geodesic algorithm for filament winding of a T-shaped form.** *IEEE Transactions on Industrial Electronics*, December 1991, Vol. 38(6), 484-490.

22. *CADFIL users' manual*, version 3.204 (1993), produced by Crescent Consultants Limited[8].

23. *CADFIL II users' manual*, November 1992, produced by Crescent Consultants Limited[8].

24. Haq, S., Middleton, V. and Owen, M. J., **Filament winding controller requirements and B-spline solution.** *CANCOM 93*, Ottowa, Canada, 27-29 September 1993.

25. Jones, R. M., *The Mechanics of Composite Materials*. New York: Hemisphere, 1975.

26. Pagano, N. J., **On the calculation of interlaminar normal stress in composite laminate**. *J. Composite Materials*, 1974, Vol. 8, 65-81.

27. Ambartsumyan, S. A., *Theory of anisotropic plates (strength, stability and vibration)*. USA: Technomic, 1970 (trans. from 1st Russian edition).

28. Kaprellian, P. V., Rogers, T. G. and Spencer, A. J. M., **Theory of laminated elastic plates (I. Isotropic Laminae)**. *Phil. Trans. R. Soc. Lond.*, 1988, A325, 565-594.

29. Pagano, N. J., **Exact solutions for composite laminates in cylindrical bending**. *J. Composite Materials*, 1969, Vol. 3, 398-411.

30. Pipes, R. Byron and Pagano, N. J., **Interlaminar stresses in composite laminates under uniform axial extension**. *J. Composite Materials*, 1970, Vol. 4, 538-548.

31. Spencer, A. J. M., Watson, P. and Rogers, T. G., **Stress analysis of anisotropic laminated circular cylindrical shells**, in Hui, D. and Sun, C. T. (eds.), *Recent developments in composite materials structures*. New York: ASME, 1990, AD 19, AMD 113. Presented at the Winter Annual Meeting of ASME, Dallas, November 1990.

32. Whitney, J. M. and Sun, C.-T., **A refined theory for laminated anisotropic, cylindrical shells**. *J. Appl. Mech.*, 1974, Vol. 41, 471-480.

33. Reddy, J. N., **Exact solutions of moderately thick laminated shells**. *J. Engng Mech.*, 1984, Vol. 110(5), 794-809.

34. Widera, G. E. O. and Logan, D., **Validity of shell theory for layered media**. *Transactions of the 3rd International Conference on Structural Mechanics in Reactor Technology*. Sept 1-5 1975, Vol. 5, part M3/10.

35. Widera, O. E. and Chung, S. W., **Derivation of various non-homogeneous anisotropic shell theories applicable in pressure vessel design**. *Nuclear Engineering and Design*, 1974, Vol. 31, 405-426.

36. Cai, S., **A refined theory for laminated isotropic cylindrical shell**, *Proceedings of International Symposium on Composite Materials and Structures* (eds. T. T. Loo and C. T. Sun), June 10-13 1986, Beijing, China, pp. 154-167.

37. Cai, Si-Wei and Cai, Min, **A refined theory of laminated doubly curved shells**. *Composite Structures 4*, 1987, Vol. 1, 262-274.

38. Gerstle, F. P. Jr., **Analysis of Filament-Reinforced Spherical Pressure Vessels**, in *Composite Materials: Testing and Design (Third Conference) ASTM STP 546*. American Society for Testing and Materials, 1974, pp. 604-631.

39. Whitney, J. J., **Elastic Moduli of Unidirectional Composites with Anisotropic Filaments**. *J. Composite Materials*, 1967, Vol. 1(2), 188-193.

40. Foye, R. L., **Advanced Design Concepts for Advanced Composite Airframes**, *AFML-TR-68-91*, Vol. 1, 190.

41. Love, A. E. H., *A Treatise on the Mathematical Theory of Elasticity*, 4th (1927) ed. Reprinted in USA: Dover, 1944, sections 110 and 114.

42. Kaminski, B. E. and Lantz, R. B., **Strength theories of failure for anisotropic materials**, in *Composite Materials: Testing and Design, ASTM STP 460*, American Society for Testing and Materials, 1969, pp. 160-169.

43. Gerstle, F. P. Jr., **High performance advanced composite spherical pressure vessels**, *ASME Paper no. 74-PVP-42*. New York: American Society of Mechanical Engineers, June 1974.

44. Gerstle, F. P. Jr. and Moss, M., **Thick-walled spherical composite pressure vessels**. *Composites in Pressure Vessels and Piping*, ASME paper PVP-PB-021. New York: American Society of Mechanical Engineers, 1977, pp. 69-87.

45. Guess, T. R., **Spherical Kevlar 49/epoxy vessels with 430-MPa (62-ksi) burst pressures**. *Composites Technology Review*, Spring 1984, Vol. 6(2), 10-18.

46. Lewis, G., **Filament-wound spherical pressure vessles: a state-of-the-art review**. *Journal of Composites Technology and Research*, Summer 1987, Vol. 9(2), 33-39.

47. Martin, P. M. J. W., **Optimal design of filament wound composite pressure vessels**. *Seventh International Conference on Offshore Mechanics and Arctic Engineering*, Houston, Texas. February 7-12, 1988.

48. Schultz, J. C., **"Netting" analysis of filament-wound pressure vessels**, *ASME Publication 63-WA-223*, presented at ASME Winter Annual Meeting, Philadelphis, Penn., November 1963.

49. Moss, M., **Filament-reinforced cylindrical pressure vessels: analysis and numerical evaluation**. Report no. SAND-77-0403, Sandia Laboratories, Albuquerque, New Mexico, USA, March 1977.

50. Hoa, S. V., Ouelette, P. and Sankar, T. S., **Strain analysis in fibre reinforced plastic vessels**, *ASME Paper 83-PVP-43*, American Society of Mechanical Engineers, New York, 1983.

51. Padovec, J., **Stress analysis of shell junctions fabricated by the filament-winding process**. *Filament Winding II*, PI-RPG Conference, London, England, March 15-16, 1972. Published by The Plastics Institute, London.

52. Hetenyi, M., *Beams on elastic foundation*. Ann Arbor, USA: University of Michigan Press, 1946.

53. Timoshenko, S. P. and Woinowski-Krieger, S., *Theory of plates and shells*, 2nd ed. New York: McGraw-Hill, 1959, pp. 566-568.

54. Highton, J. and Soden, P. D. W., **End reinforcement and grips for anisotropic tubes**. *Journal of Strain Analysis*, 1982, Vol. 17(1), 31-43.

55. Gill, S. S., *The stress analysis of pressure vessels and pressure vessel components*. Oxford: Pergamon Press, 1970.

56. Stasa, Frank L., *Applied finite element analysis for engineers*. New York: CBS Publishing Japan Ltd., 1985. pp. 13-15.

57. Davies, A. J., *The finite element method: a first approach*. Oxford: Clarendon Press/Oxford University Press, 1980. pp. 1-5.

58. Zienkiewicz, O. C. and Taylor, R. M., *The Finite Element Method*, 4th ed. UK: McGraw-Hill (UK), 1989.

59. *PAFEC Theory Manual*. Pafec Ltd, Strelley Hall, Nottingham, UK, 1984. pp. 2.31-2.38.

60. NAFEMS (formerly National Agency for Finite Element Methods and Standards), *A finite element primer*. Glasgow: Department of Trade and Industry/National Engineering Laboratory, 1986. pp. 56-65.

61. *ibid.*, pp 61-65.

62. Chen, M. C. and Clewlow, L. N. O., **Computer analysis of filament-reinforced metallic-spheroidal pressure vessels**. *Computers and Structures*, 1977, Vol. 7(1), 93-102.

63. Knight, C. E. Jr., **Analysis of stresses in filament-wound spherical pressure vessels produced by the delta-axisymmetric pattern**. Union Carbide Corp., Nuclear Division Technical Report Y-1972, Aug. 1975.

64. Wilson, E. L., **Structural analysis of axisymmetric solids.** *AIAA Journal*, Dec. 1965, Vol. 3(12), 2269-2274.

65. Wilson, E. L. and Jones, R. M., **Finite element stress analysis of axisymmetric solids.** Aerospace Corporation report TR-0158, Air Force report BSD-T-67-228; Sept. 1967.

66. Knight, C. E., **Analytical failure prediction of spherical composite pressure vessels.** *Journal of Pressure Vessel Technology*, August 1982, Vol. 104, 229-231.

67. Weilbull, W., **Statistical distribution function of wide applicability.** *J. Appl. Mech.*, September 1951, Vol. 18, 293-297.

68. Guess, T. R. and Gerstle, F. P., **Design considerations for spherical, ultra-high pressure, composite vessels.** ASME *Pressure Vessels and Piping Conference*, Denver, Colorado, June 1981.

69. Leavesley, P. J., and Knight, C. E., **An analytical model of strength loss in filament wound pressure vessels.** *Journal of Pressure Vessel Technology*, August 1987, Vol. 109, 352-356.

70. Leavesley, P. J. and Knight, C. E. Jr., **Analytical model of strength loss in filament wound spherical vessels.** ERDA Report No. Y/Sub/-80-7733/201, November 1983.

71. Knoell, A. C., **Structrual design and stress analysis program for advanced composite filament-wound axisymmetric pressure vessels (COMTANK).** Jet Propulsion Lab., Calif., Inst. of Tech., Pasadena, 1 June 1971. Report No. NASA-CR-118669; JPL-T-32-1531.

72. Dong, S. B., **Analysis of laminated shells of revolution.** *J. Eng. Mech. Div.*, ASCE, December 1966, Vol. 92, 135-155.

73. Rizzo, R. R. and Vicario, A. A., **A finite element analysis of laminated anisotropic tubes: Part I - A characterisation of the off-axis tensile specimen.** *J. Composite Materials*, 1970, Vol. 4, 344-359.

74. Hardy, S. J. and Malik, N. H., **Optimum design of laminated structural members.** *Proceedings of the I.Mech.E Conference on Design in Composite Materials*, London, 7-8 March 1989, pp. 49-60.

75. Hardy, S. J. and Malik, N. H., **Optimum Design of Composite-Reinforced Pressure Vessels,** in Hyde, T. H. and Ollerton, E. (eds.), *Applied Stress Analysis*. UK: Elsevier, 1990, pp. 429-438.

76. Li, S., Reid, S. R. and Soden, P. D. W., **Geometrically non-linear analysis of thin filament wound laminated tubes under lateral indentation.** *7th UK ABAQUS User Group Conference*, 17/18 September 1992, University of Cambridge, pp. 259-268.

77. Panda, S. C. and Natarajan, R., **Finite element analysis of laminated shells of revolution.** *Computers and Structures*, 1976, Vol. 6, 61-64.

78. Ahmad, S., Irons, B. M. and Zienkiewicz, O. C., **Curved thick shell and membrane elements with particular reference to axisymmetric problems.** *Proc. 2nd Conf. Matrix Methods in Structural Mechanics*, Wright-Patterson Air Force Base, Ohio, 1968.

79. Pagano, N. J. and Whitney, J. M., **Geometric design of composite cylindrical characterisation specimen.** *J. Composite Materials*, July 1970, Vol. 4, 360-378.

80. Natarajan, R., Hoa, V. and Sankar, T. S., **Stress analysis of filament wound tanks using three-dimensional finite elements.** *Int. J. Num. Meth. Eng.*, 1986, Vol. 23, 623-633.

81. Hoa, S. V., Yu, C. W. and Sankar, T. S., **Analysis of filament wound vessel using finite elements.** *Composite Structures*, 1985, Vol. 3, 1-18.

82. Rogers, C. A., Knight, C. E. Jr. and Dodge, W. G., **Development of high order finite elements to model filament-wound composites,** in Brown, S. J. (ed.), *Proceedings of the 1985 Pressure Vessels and Piping Conference*, PVP - Vol. 98-2. New York: ASME, 1985, pp. 247-255.

83. Rogers, C. A. and Knight, C. E. Jr., **An axisymmetric linear/high-order finite element for filament-wound composite - I. Formulation and Algorithms.** *Computers and Structures*, 1988, Vol. 29, 265-271.

84. Rogers, C. A. and Knight, C. E. Jr., **An axisymmetric linear/high-order finite element for filament-wound composite - II. Evaluation on filament-wound cylinders.** *Computers and Structures*, 1988, Vol. 29, 273-281.

85. Chen, A. T. and Yang, T. Y., **Static and dynamic formulation of a symmetrically laminated beam finite element for a microcomputer.** *J. Composite Materials*, September 1985, Vol. 19, 459-475.

86. Chen, A. T. and Yang, T. Y., **Static, dynamic and buckling formulation of a symmetrically laminated plate finite element for a microcomputer.** *J. Composite Materials*, May 1987, Vol. 21, 441-453.

87. Wanthal, S. P. and Yang, T. Y., **Formulation of Three Simple Triangular Plane Stress Anisotropic Finite Elements for a Microcomputer**. *Journal of Composite Materials*, November 1988, Vol. 22, 1060-1079.

88. Ochoa, O. O. and Reddy, J. N., *Finite element analysis of composite laminates*. Dordrecht, Netherlands: Kluwer, 1992.

89. Griffin, O. H. Jr., **Evaluation of finite-element software packages for stress analysis of laminated composites**. *Composites Technology Review*, 1982, Vol. 4(4), 136-141.

90. Taig, I. C., **Finite element analysis of composite materials**. NAFEMS report R0003, 1992. pp. 12-15, 30.

91. *PAFEC Theory manual*. pp. 2.56-2.65.

92. *ibid.*, pp. 2.38-2.40.

93. Ahmad, S., Irons, B. M. and Zienkiewicz, O. C., **Analysis of thick and thin shell structures by curved finite elements**. *Int. J. Num. Meth. Eng.*, 1970, Vol 2, 419-451.

94. Irons, B. M. and Ahmad, S., *Techniques of finite elements*. Chichester, UK: Ellis Horwood Ltd, 1980. pp. 79-83.

95. Irons, B. M., **The semiloof shell element**, in Ashwell, D. G. and Gallagher, R. H. (eds.), *Finite elements for thin shells and curved membranes*. London: John Wiley and Sons, 1976. pp. 197-222.

96. Irons, B. M. and Ahmad, S., *op. cit.*, pp. 108-116 and 303-314.

97. *PAFEC theory manual*, pp. 2.80-2.84.

98. Rice, E. V. (former PAFEC engineer, now at Crescent Consultants Limited, Nottingham). Private communication.

99. PAFEC Ltd., *Data Preparation Manual Level 7.1*, p. 4.54.

100. *ABAQUS/Standard Users' Manual*, Version 5.2, 1992. Produced by Hibbitt, Karlsson and Sorensen, Inc., 1080 Main Street, Pawtucket, RI02860, USA. Section 3.4.2.

101. *ABAQUS Theory*, Version 5.2, 1992. Hibbitt, Karlsson and Sorensen, Inc. Sections 4.3.1, 4.3.3 and 4.3.6.

102 *Shell elements in ABAQUS* (course notes). Hibbitt, Karlsson and Sorensen, Inc. 1992.

103. Eckold, G. C., **An investigation into the strength and elastic properties of filament wound composites**. Manchester: UMIST, PhD thesis, 1978.

104. Whitney, J. M., **Experimental determination of shear modulus of laminated fiber-reinforced composites**. *Experimental Mechanics*, October 1967, Vol. 7, 447-448.

105. Kavanagh, K. T., **Extension of classical experimental techniques for characterising composite-material behaviour**. *Experimental Mechanics*, January 1972, Vol. 12, 50-57.

106. Weatherby, N. L., **Strength of filament-wound glass reinforced polyester resin**. University of Nottingham PhD thesis, 1987.

107. Reddy, T. Y. and Reid, S. R., **On obtaining material properties from the ring compression test**. *Nucl. Eng., Des.*, 1979, Vol. 52, 257-263.

108. Soden, P. D. W. Private communication relating to unpublished work currently in hand at UMIST.

109. Lamb, H., **On the deformation of an elastic shell**. *Proc. Lond. Math. Soc.*, 1980, Vol. 21, 119-146.

110. Hetenyi, M., *op. cit.*, pp. 30-37.

111. **E-glass** is a standard formulation of glass available in the form of fibre rovings from a variety of manufacturers including Silenka UK Ltd, The Parade, Frimley, Camberley, Surrey, GU16 5HY.

112. **Crystic 272** resin and associated products are manufactured by Scott Bader Company Limited, Wollaston, Wellingborough, Northamptonshire NN9 7RL.

113. **Würtz PAT 607/PCM** release agent is manufactured by E and P Würtz GmbH and Co. KG, Industriegebiet In der Weide 13, 6530, Bingen, Sponsheim, Germany. It is distributed by GRP Materials Supplies Ltd., Eagle Technology Park, Queensway, Rochdale, Lancashire OL11 1TQ.

114. *BS 2782: Part 10: Method 1002: 1977.* British Standard methods of testing plastics. Part 10: Glass reinforced plastics. Method 1002: Determination of loss on ignition. British Standards Institution, 1977.

115. ANSI/ASTM Standard D2290-76, **Standard test method for apparent tensile strength of ring or tubular plastics by split disk method**, in *1978 Annual Book of ASTM Standards*, part 36. USA: American Society for Testing and Materials, 1978.

116. Rosato, D. V. and Grove, C. S. Jr., *op. cit.*, p. 251.

117. Johnson, K. L., *Contact Mechanics*, 1st paperback edition. Cambridge, UK: Cambridge University Press, 1987. p. 131 and Appendix 3.

118. Hetenyi, M., *op. cit.*, pp. 130 and 133.

119. Dally, J. W. and Riley, W. F., *Experimental stress analysis*, 3rd ed. USA: McGraw-Hill, Inc., 1991. p. 244.

120. **TML** strain measurement products are distributed by **Techni Measure**, Alexandra Buildings, 59 Alcester Road, Studley, Warwickshire B80 7NJ.

121. **Loctite** products are distributed by **Loctite UK**, Watchmead, Welwyn Garden City, Hertfordshire AL7 1JB.

122. *The NAG FORTRAN Library Manual Mark 15.* UK: The Numerical Algorithms Group Ltd., NAG Central Office, Mayfield House, 256 Banbury Road, Oxford OX2 2DE.

123. Al-Salehi, F. A. R., Al-Hassani, S. T. S., Al-Bastaki, N. M. and Hinton, M. J., **Extracting dynamic basic ply properties from test data on angle ply laminates. Paper I: Theoretical procedures.** London: HMSO (not published at time of writing).

124. Banks, W. M., **Introduction to composite materials**, (course notes), University of Strathclyde, p. 10.

125. DiVita, G., Marchetti, M., Moroni, P. and Perugini, P., **Designing complex shape filament-wound structures**, *Composites Manufacturing*, Vol. 3, No. 1, 1992, pp. 53-58.

126. Wells, G. M.. Private communication.

127. Jones, I. A., *A further progress report on the development of a system for the finite element analysis of filament wound structures.* University of Nottingham, Department of Mechanical Engineering (internal report), August 1992.

128. Conte, S. D. and De Boor, C., **Elementary numerical analysis: an algorithmic approach**. McGraw-Hill Kogakusha, 2nd ed., 1972, pp. 233-240.

129. Jones, I. A., **Development and trial implementation of a strategy for the automatic finite element modelling of non-axisymmetric filament-wound components.** University of Nottingham, Department of Mechanical Engineering (internal report), June 1993.

130. **FEMGEN** Version 2 is produced by **FEMVIEW Limited**, 1 St Albans Road, Leicestershire LE2 1GF.

131. Ashwell, D. G. and Sabir, A. B., **A new cylindrical shell finite element based on simple independent strain functions.** *Int. J. Mech. Sci.*, 1972, Vol. 14, 171-183.

132. Timoshenko, S. P. and Woinowski-Krieger, S., *op. cit.*, pp. 501-506.

133. Ashwell, D. G., **A characteristic type of instability in the large deflexions of elastic plates** (parts I and II). *Proc. R. Soc.*, 1952, Vol A214, 98-118.

134. Ashwell, D. G., **A characteristic type of instability in the large deflexions of elastic plates** (part III). *Proc. R. Soc.*, 1954, Vol A222, 44-59.

135. Ting, L. and Yuan, S. W., **On radial deflection of a cylinder of finite length with various end conditions.** *Journal of the Aeronautical Sciences*, April 1958, Vol. 25(1), 230-234.

136. Donnell, L. H., **A discussion of thin shell theory,** in *Proceedings of the Fifth International Congress on Applied Mechanics*, Cambridge, Mass., 1938, pp. 66-70.

137. Calladine, C. R., **Thin-walled elastic shells analysed by a Rayleigh method.** *Int. J. Solids Structures*, 1977, Vol. 13, 515-530.

138. Hetenyi, M., *op. cit.*, pp. 97-112.

139. Dawe, D. J., *Matrix and finite element displacement anslysis of structures.* Oxford: Oxford University Press/Clarendon Press, 1984.

140. PAFEC Ltd, *Data Preparation User Manual Level 7.1*, p. 4.25.

141. PAFEC Ltd. FE Support, (John King). Private communication, 27 August 1992.

142. Jones, I. A., **Progress report on manufacture of filament-wound GRP elbow.** University of Nottingham, Department of Mechanical Engineering (internal report), November 1992.

143. **Ludur Wash-Away** is manufactured by **Guilini Chemie GmbH**, Postfach 150480, 6700 Ludwigshafen/Rhein. It is available in the UK from **Denaco (UK) Ltd.**, Gainsborough, Lincs.

144. **Araldite** products are manufactured by **Ciba-Geigy Plastics**, Duxford, Cambridge CB2 4QA.

145. **Stironol** is manufactured by **Argos Electronic Components Ltd**, Stiron House, Electric Avenue, Westclifff-on-Sea, Essex SS20 9NW.

146. Spencer, A. J. M., Parker, D. F., Berry, D. S., England, A. H., Faulkner, T. R., Green, W. A., Holden, J. T., Middleton, D. and Rogers, T. G., *Engineering Mathematics*. Wokingham, Berkshire: Van Nostrand Reinhold Company Ltd., 1977, pp. 382-391.

147. NAFEMS, *op. cit.*, pp. 141-142, 147-150.

148. Hetenyi, *op. cit.*, pp. 50-52.

149. Young, W. C., *Roark's formulas for stress and strain*, 6th ed. USA: McGraw-Hill, 1989, p. 254.

150. Chatfield, C., *Statistics for technology*, 3rd ed. London: Champman and Hall, 1983. pp. 166-199.

151. Chou, Ya-lun, *Statistical analysis*, 2nd ed. USA: Holt, Rinehart and Winston, 1975, pp. 584-600.

152. **SIMPLEPLOT** (version 2-12) is produced by **Bradford University Software Services (B.U.S.S.) Ltd.**, 29 Campus Road, Bradford, West Yorkshire BD7 1HR.

153. **UNIRAS** (version 6.1) is produced by **UNIRAS A/S**, 376 Gladsaxevej, DK-2860, Søborg, Denmark.

APPENDIX A: OVERVIEW OF FINITE ELEMENT THEORY AND FORMULATIONS OF SOME SIMPLE ELEMENTS

A.1 Nomenclature

Because of the highly specialised nature of finite element theory it is considered necessary to include a list of the nomenclature used in this overview. In a few cases the meaning of the symbols differs from that used elsewhere in the thesis for less specialised applications.

A.1.1 *Conventions*

{ }	denotes a column array or column vector of quantities
[ ]	denotes a matrix of numbers or sub-matrices
[0]	denotes a null matrix, typically forming a partition of a larger matrix
'	prime denotes coefficients of the quadrature terms in a Fourier series.

A.1.2 *Symbols*

$\{F\}$	column vector of forces applied to a system
$[K]$	stiffness matrix of a system
$\{u\}$	column vector of displacements of a system
$(u_{xm})_1$	amplitude of mth harmonic of u_x relating to node 1 of element
σ, τ	direct and shear stresses
ε, γ	direct and shear engineering strains
U	strain energy
Π	total potential energy
V	volume
h	thickness of element
x, y, z	global Cartesian co-ordinates
ξ, η	curvilinear co-ordinates used in isoparametric mapping
N_i	shape function relating to the ith node

$[P(\xi,\eta)]$ row matrix of powers of ξ and η forming interpolation polynomial

$[P^*]$ partitioned matrix with sub-matrices $[P(\xi,\eta)]$ forming the leading diagonal

$\{\alpha\}$ column vector of coefficients for interpolation polynomial

$[A]$ matrix relating $\{\alpha\}$ to nodal quantities e.g. displacements $\{u\}$

$[A^*]$ partitioned matrix with sub-matrices $[A]^{-1}$ forming the leading diagonal

$|J|$ the determinant of the Jacobian matrix $[J]$

$[B]$ matrix relating strains to interpolated displacements

$[D]$ material constitutive matrix

E, ν Young's modulus and Poisson's ratio of isotropic material

A.1.3 *Subscripts*

$_e$ relating to element

$_m$ relating to the mth harmonic of a Fourier series

$_{ux}$ etc. relating to displacement u_x etc.

A.2 A brief overview of finite element theory with reference to isoparametric elements

The following account is presented as a statement of the mathematical framework into which the formulations of certain individual elements fit, with particular reference to structural analysis. The theory is covered to varying degrees of depth and complexity in a variety of manuals and texts including reference 58. The following descriptions refer especially to the relevant sections of the PAFEC theory manual[59,91] and the NAFEMS primer[60].

The trivial representation of Hooke's law for a single degree-of-freedom (DOF) system may be extended to multiple DOF systems by the representation of the forces $\{F\}$, deflections $\{u\}$ and stiffnesses $\{K\}$ in matrix form:

$$\begin{Bmatrix} F_1 \\ F_2 \\ \vdots \\ F_n \end{Bmatrix} = \begin{bmatrix} K_{11} & K_{12} & \cdots & K_{1n} \\ K_{21} & K_{22} & \cdots & K_{2n} \\ \vdots & & \ddots & \vdots \\ K_{n1} & K_{n2} & \cdots & K_{nn} \end{bmatrix} \begin{Bmatrix} u_1 \\ u_2 \\ \vdots \\ u_n \end{Bmatrix} \quad \text{or:} \quad \{F\} = [K]\{u\} \qquad (A.1)$$

Where a continuous system or structure is discretised into individual elements, the global stiffness matrix is formed by summing the contributions to the stiffness of the structure of the stiffness matrices for each element.

The stiffness matrix for each element may be obtained by applying the principle of minimum total potential energy. The total potential energy (denoted Π) of an elastic element under external loading may be calculated as:

$$\Pi = U_e - \{u_e\}^T\{F_e\} = \tfrac{1}{2}\{u_e\}^T[K]\{u_e\} - \{u_e\}^T\{F_e\} \qquad (A.2)$$

where U_e is the strain energy of the element. The element displacements $\{u_e\}$ which occur in practice are those which minimise the total potential energy of the system.

$$\frac{\partial \Pi}{\partial \{u_e\}} = \frac{\partial U_e}{\partial \{u_e\}} - \{F_e\} = [K_e]\{u_e\} - \{F_e\} = 0 \qquad (A.3)$$

In order to obtain an expression for strain energy it is necessary to integrate the expression for strain energy per unit volume over the whole volume of the element:

$$U_e = \frac{1}{2}\int_{\text{volume}} [\sigma_x\ \sigma_y\ \tau_{xy}].\begin{Bmatrix}\varepsilon_x\\ \varepsilon_y\\ \gamma_{xy}\end{Bmatrix} dV = \frac{1}{2}\int_{\text{volume}} \{\sigma\}^T\{\varepsilon\}\ dV \qquad (A.4)$$

The evaluation of strain energy is now examined with particular reference to isoparametric elements[59,60], a suitably straightforward example being an isoparametric quadrilateral element. This will be assumed to lie in the x-y plane and to have a thickness h, and to undergo stresses only in the x-y plane (plane stress assumption). In such elements a curvilinear co-ordinate system (ξ,η) is defined such that the corner nodes have the (ξ,η) co-ordinates $(\pm1,\pm1)$. The (x,y) node co-ordinates and the nodal variables are interpolated over the element using polynomials $N_i(\xi,\eta)$ known as shape functions. Isoparametric elements use shape functions for the interpolation of the nodal variables which are identical to those used for the node co-ordinates. Elements which interpolate using a higher order of shape function for the node co-ordinates than for the nodal variables are called superparametric elements. A shape function has the property of having a value of unity at one of the nodes positions in (ξ,η) space, and a value of zero at the other nodes. For example the shape function

$$N_3 = -\frac{1}{4}(1+\xi)(1+\eta)(1-\xi-\eta)$$

takes the value 1 at $(\xi=1,\eta=1)$ and is zero at the other nodes. By summation of eight such shape functions weighted by the x-coordinates of each of the eight nodes an interpolation polynomial may be expressed which gives the x-coordinate at any point (ξ,η):

$$\begin{aligned} x &= \sum_{i=1}^{8} N_i(\xi,\eta)x_i \\ &= \alpha_{x1} + \alpha_{x2}\xi + \alpha_{x3}\eta + \alpha_{x4}\xi\eta + \alpha_{x5}\xi^2 + \alpha_{x6}\eta^2 + \alpha_{x7}\xi^2\eta + \alpha_{x8}\xi\eta^2 \end{aligned}$$

$$\text{or in matrix form:} \quad x = [1 \;\; \xi \;\; \eta \;\; \xi\eta \;\; \xi^2 \;\; \eta^2 \;\; \xi^2\eta \;\; \xi\eta^2] \begin{Bmatrix} \alpha_{x1} \\ \alpha_{x2} \\ \vdots \\ \alpha_{x8} \end{Bmatrix}$$

$$= [\boldsymbol{P}(\xi,\eta)]\{\alpha_x\} \qquad \text{(a)}$$

$$\text{and similarly:} \quad y = [\boldsymbol{P}(\xi,\eta)]\{\alpha_y\} \qquad \text{(b)} \qquad \text{(A.5)}$$

The true shape of the element in the (x,y) domain may be regarded as being mapped onto the square "parent element" with the corner nodes $(\pm1,\pm1)$ in the (ξ,η) domain (Fig. 4.1).

A square matrix $[\boldsymbol{A}]$, which is the assembly of the row matrices $[\boldsymbol{P}(\xi,\eta)]$ for all nodal values of ξ and η, can be defined as follows:

$$\{x_e\} = [\boldsymbol{A}]\{\alpha_x\} \quad \text{and hence} \quad \{\alpha_x\} = [\boldsymbol{A}]^{-1}\{x_e\} \qquad \text{(a)}$$

$$\text{similarly:} \quad \{\alpha_y\} = [\boldsymbol{A}]^{-1}\{y_e\} \qquad \text{(b)} \qquad \text{(A.6)}$$

where $\{x_e\}$ and $\{y_e\}$ are vectors containing the nodal x and y co-ordinates. Similarly if the nodal displacements are defined as column vectors $\{u_{xe}\}$ and $\{u_{ye}\}$ and the constants in the interpolation polynomials are $\{\alpha_{ux}\}$ and $\{\alpha_{uy}\}$ then

$$[\{\alpha_{ux}\},\{\alpha_{uy}\}] = [\boldsymbol{A}]^{-1}[\{u_{xe}\},\{u_{ye}\}] \qquad \text{(A.7)}$$

It is now necessary to obtain an expression for the stresses and strains in the element. The engineering definitions of strain reduce (in the limiting case of small strains) to:

$$\varepsilon_x = \frac{\partial u_x}{\partial x} \quad \text{(a)} \qquad \varepsilon_y = \frac{\partial u_y}{\partial y} \quad \text{(b)} \qquad \gamma_{xy} = \frac{\partial u_x}{\partial y} + \frac{\partial u_y}{\partial x} \quad \text{(c)} \qquad \text{(A.8)}$$

The partial derivatives of u_x and u_y are expressed as partial derivatives of the interpolating polynomials for these displacements, for which the constants $\{\alpha_{ux}\}$ and $\{\alpha_{uy}\}$ are calculated using equation (A.7).

$$\{\varepsilon\} = \begin{Bmatrix}\varepsilon_x\\ \varepsilon_y\\ \gamma_{xy}\end{Bmatrix} = \begin{bmatrix}\dfrac{\partial[\boldsymbol{P}(\xi,\eta)]}{\partial x} & [0]\\ [0] & \dfrac{\partial[\boldsymbol{P}(\xi,\eta)]}{\partial y}\\ \dfrac{\partial[\boldsymbol{P}(\xi,\eta)]}{\partial y} & \dfrac{\partial[\boldsymbol{P}(\xi,\eta)]}{\partial x}\end{bmatrix}\begin{Bmatrix}\{\alpha_{ux}\}\\ \{\alpha_{uy}\}\end{Bmatrix}$$

$$= \begin{bmatrix}\dfrac{\partial[\boldsymbol{P}(\xi,\eta)]}{\partial x} & [0]\\ [0] & \dfrac{\partial[\boldsymbol{P}(\xi,\eta)]}{\partial y}\\ \dfrac{\partial[\boldsymbol{P}(\xi,\eta)]}{\partial y} & \dfrac{\partial[\boldsymbol{P}(\xi,\eta)]}{\partial x}\end{bmatrix}\begin{bmatrix}[\boldsymbol{A}]^{-1} & [0]\\ [0] & [\boldsymbol{A}]^{-1}\end{bmatrix}\begin{Bmatrix}\{\boldsymbol{u}_{xe}\}\\ \{\boldsymbol{u}_{ye}\}\end{Bmatrix} \qquad (A.9)$$

$$= [\boldsymbol{B}][\boldsymbol{A}^*]\{\boldsymbol{u}_e\}$$

The matrix $[\boldsymbol{P}(\xi,\eta)]$ cannot be differentiated directly with respect to x and y; use is made of the chain rule for partial derivatives:

$$\begin{Bmatrix}\dfrac{\partial[\boldsymbol{P}(\xi,\eta)]}{\partial x}\\ \dfrac{\partial[\boldsymbol{P}(\xi,\eta)]}{\partial y}\end{Bmatrix} = [\boldsymbol{J}]^{-1}\begin{Bmatrix}\dfrac{\partial[\boldsymbol{P}(\xi,\eta)]}{\partial \xi}\\ \dfrac{\partial[\boldsymbol{P}(\xi,\eta)]}{\partial \eta}\end{Bmatrix} \qquad (A.10)$$

where: $[\boldsymbol{J}] = \begin{bmatrix}\dfrac{\partial x}{\partial \xi} & \dfrac{\partial y}{\partial \xi}\\ \dfrac{\partial x}{\partial \eta} & \dfrac{\partial y}{\partial \eta}\end{bmatrix}$, known as the Jacobian matrix

It is necessary to define the stresses in terms of the strain:

$$\{\sigma\} = [\boldsymbol{D}]\{\varepsilon\} \qquad (A.11)$$

The material constitutive matrix $[\boldsymbol{D}]$ may take various forms; for the plane stress assumption and for an isotropic material it is given by:

$$[D] = \frac{E}{1-\nu^2}\begin{bmatrix} 1 & \nu & 0 \\ \nu & 1 & 0 \\ 0 & 0 & \frac{1}{2}(1-\nu) \end{bmatrix} \tag{A.12}$$

The integral in equation (A.4) may now be re-stated, substituting for $\{\sigma\}$ and $\{\varepsilon\}$ using the expressions obtained in equations (A.6) - (A.11):

$$U_e = \frac{1}{2}\int_{volume} \{u_e\}^T [A*]^T [B]^T [D][B][A*]\{u_e\}\, dV \tag{A.13}$$

Before the integral in equation (A.13) may be evaluated it is necessary to expand the volume integral $\int dV$ (giving $\iint h\, dx\, dy$) and it is convenient to change the variables from x and y to the curvilinear co-ordinates ξ and η. It will also be noted that the terms h, $\{u_e\}$ and $[A^*]$ are constants which may be taken out of the integration. The strain energy expression now reads:

$$U_e = \frac{1}{2} h \{u_e\}^T [A*]^T \left[\int_{-1}^{1}\int_{-1}^{1} [B]^T [D][B]\,|J|\, d\xi\, d\eta\right][A*]\{u_e\} \tag{A.14}$$

The substitution changes the limits of integration to the convenient values of ± 1 (the nodal co-ordinate values of the parent element). This change requires the introduction of the term $|J|$ which is the determinant of the Jacobian matrix. This may be regarded as a scale factor relating the areas of the element as plotted in the two co-ordinate systems.

Differentiation of equation (A.14) with respect to $\{u_e\}$ and substitution into equation (A.3) may be shown to yield an expression for the element stiffness matrix:

$$[K_e] = h[A*]^T \left[\int_{-1}^{1}\int_{-1}^{1} [B]^T [D][B]\,|[J]|\, d\xi\, d\eta\right][A*] \tag{A.15}$$

Integrals between the limits of ± 1 may easily be evaluated using the numerical technique of Gaussian quadrature[61], which involves the weighted summation of the

kernel of the integral evaluated at "Gauss Points". The number of Gauss points required to integrate a polynomial exactly depends upon the order of the polynomial. It is sometimes advantageous to use a lower order of Gaussian quadrature than the order of interpolation polynomial would suggest ("reduced integration") to avoid the tendency for some elements to give misleadingly "over-stiff" results if integrated exactly.

The element stiffness matrices may be assembled into the global stiffness matrix $[K]$ by the addition of matrix terms relating the nodal variables at individual pairs of nodes, and restraints applied to the appropriate degrees of freedom. The deflections $\{u\}$ under a given set of loads $[F]$ may now be found by solving the set of simultaneous equations $[K]\{u\}=\{F\}$. Normally, the stiffness matrix consists mainly of zeros, i.e. it is sparsely populated; it is also symmetric. Provided that the numbering sequence of the degrees of freedom is appropriately chosen, the non-zero entries all lie close to the leading diagonal of the matrix, which is said to be banded. The simultaneous equations are solved using methods such as Gaussian elimination and Cholesky factorisation[146,147] rather than matrix inversion. Suitable implementations of these methods can take advantage of the symmetric, sparse and banded nature of the stiffness matrix in order to minimise the amount of computation required for the solution. A method known as frontal solution[147] is often used with Gaussian elimination; this combines the assembly of the stiffness matrix with the first stage of the solution. Strains are found by differentiation of the interpolation polynomials for deflection, and hence stresses are found using the constitutive relation (A.11).

A.3 Example of a formulation of an element used in this project: thick shell of revolution element (axisymmetric isoparametric quadrilateral[91])

This element models axisymmetric structures of finite thickness, but has the useful feature of being able to analyse non-axisymmetric loadcases on these structures. For the most straightforward load case (axisymmetric loading), it is adequate to formulate an element which is merely a variation on the isoparametric quadrilateral, the stress-

displacement relationships being modified accordingly. However, for the case where a non-axisymmetric load case is synthesised using a Fourier series of sinusoidally varying loads, a three-dimensional extension of the isoparametric theory is required. Since the axisymmetric loadcase is actually a special case of the more general (non-axisymmetric) situation, only the latter will be described in detail.

Axisymmetric elements with different numbers of nodes are available in PAFEC, but (for ease of comparison with Section A.2) the 8-noded axisymmetric quadrilateral will be described. These elements possess three (translational) degrees of freedom per node; these nodes may be considered to exist on a generator plane which is rotated about the x-axis. For the purposes of this discussion the cylindrical polar co-ordinate system will be given the axis names x, r and θ and the displacements will be termed u_x, u_r and u_θ. Each of these varies with axial, radial and circumferential position and may be represented using a Fourier series:

$$u_x(x,r,\theta) = u_{x0} + \sum_{m=1}^{m=\infty} (u_{xm}(x,r)\cos m\theta + u'_{xm}(x,r)\sin m\theta) \qquad \text{(a)}$$

$$u_r(x,r,\theta) = u_{r0} + \sum_{m=1}^{m=\infty} (u_{rm}(x,r)\cos m\theta + u'_{rm}(x,r)\sin m\theta) \qquad \text{(b)} \qquad \text{(A.16)}$$

$$u_\theta(x,r,\theta) = u_{\theta 0} + \sum_{m=1}^{m=\infty} (u_{\theta m}(x,r)\sin m\theta + u'_{\theta m}(x,r)\cos m\theta) \qquad \text{(c)}$$

Because there is no coupling between different harmonics or phases of each component we are able to consider in isolation the terms which relate to a single harmonic component m. As in the plane stress element discussed earlier, a pair of curvilinear axes ξ and η are defined within the element and the displacement amplitudes u_{xm}, u_{rm} and $u_{\theta m}$ are interpolated from the nodal values of these amplitudes using the concept of shape functions to construct polynomials.

The triaxial strain state in an axisymmetric body may be expressed in terms of the partial derivatives of the displacements u_x, u_r and u_θ with respect to x, r and θ. If the

displacements are expressed using the chosen terms in the Fourier series with amplitudes expressed in terms of the polynomial interpolations between nodal displacements, an equation analogous to equation (A.9) is obtained:

$$\{\varepsilon\} = \begin{Bmatrix} \varepsilon_x \\ \varepsilon_r \\ \varepsilon_\theta \\ \gamma_{r\theta} \\ \gamma_{\theta x} \\ \gamma_{xr} \end{Bmatrix} = \begin{Bmatrix} \dfrac{\partial u_x}{\partial x} \\ \dfrac{\partial u_r}{\partial r} \\ \dfrac{1}{r}\dfrac{\partial u_\theta}{\partial \theta} + \dfrac{u_r}{r} \\ \dfrac{\partial u_\theta}{\partial r} + \dfrac{1}{r}\dfrac{\partial u_r}{\partial \theta} - \dfrac{u_\theta}{r} \\ \dfrac{1}{r}\dfrac{\partial u_x}{\partial \theta} + \dfrac{\partial u_\theta}{\partial x} \\ \dfrac{\partial u_x}{\partial y} + \dfrac{\partial u_r}{\partial x} \end{Bmatrix}$$

$$= \begin{bmatrix} \dfrac{\partial [P(\xi,\eta)]}{\partial x} & [0] & [0] \\ [0] & \dfrac{\partial [P(\xi,\eta)]}{\partial r} & [0] \\ [0] & \dfrac{[P(\xi,\eta)]}{r} & \dfrac{m[P(\xi,\eta)]}{r} \\ [0] & -\dfrac{m[P(\xi,\eta)]}{r} & \dfrac{\partial [P(\xi,\eta)]}{\partial r} - \dfrac{[P(\xi,\eta)]}{r} \\ -\dfrac{m[P(\xi,\eta)]}{r} & [0] & \dfrac{\partial [P(\xi,\eta)]}{\partial x} \\ \dfrac{\partial [P(\xi,\eta)]}{\partial r} & \dfrac{\partial [P(\xi,\eta)]}{\partial x} & [0] \end{bmatrix} \begin{bmatrix} [A]^{-1} & [0] & [0] \\ [0] & [A]^{-1} & [0] \\ [0] & [0] & [A]^{-1} \end{bmatrix} \begin{Bmatrix} (u_{xm})_1 \\ \vdots \\ (u_{xm})_8 \\ (u_{rm})_1 \\ \vdots \\ (u_{rm})_8 \\ (u_{\theta m})_1 \\ \vdots \\ (u_{\theta m})_8 \end{Bmatrix}$$

$$= [B][A^*]\{u_{me}\} \qquad \text{(A.17)}$$

where the column vector $\{u_{me}\}$ is formed from the displacement components u_{xm} at each node in turn, followed by u_{rm} and $u_{\theta m}$. The derivatives of $[P(\xi,\eta)]$ with respect to x and r are obtained using the Jacobian in a similar manner as in equation (A.10). The material stress-strain relation used for isotropic elements is the standard triaxial expression of Hooke's Law:

$$\{\sigma\} = \begin{Bmatrix} \sigma_x \\ \sigma_r \\ \sigma_\theta \\ \tau_{r\theta} \\ \tau_{\theta x} \\ \tau_{xr} \end{Bmatrix}$$

$$= \frac{E(1-\nu)}{(1+\nu)(1-2\nu)} \begin{bmatrix} 1 & \nu/(1-\nu) & \nu/(1-\nu) & 0 & 0 & 0 \\ & 1 & \nu/(1-\nu) & 0 & 0 & 0 \\ & & 1 & 0 & 0 & 0 \\ & & & \dfrac{(1-2\nu)}{2(1-\nu)} & 0 & 0 \\ & & & & \dfrac{(1-2\nu)}{2(1-\nu)} & 0 \\ & \text{symmetric} & & & & \dfrac{(1-2\nu)}{2(1-\nu)} \end{bmatrix} \begin{Bmatrix} \varepsilon_x \\ \varepsilon_r \\ \varepsilon_\theta \\ \varepsilon_{r\theta} \\ \varepsilon_{\theta x} \\ \varepsilon_{xr} \end{Bmatrix}$$

$$= [D]\{\sigma\} \qquad \text{(A.18)}$$

For orthotropic materials it is necessary to apply the appropriate transformations to the orthotropic material constitutive matrix to obtain the $[D]$ matrix for the global x, r, θ system. This is achieved using a fourth-rank tensor transformation; account must be taken of the fact that the constitutive equations and the $[D]$ matrix are expressed in terms of engineering strains rather than mathematical strains.

It is now a simple matter to calculate the stiffness matrix for the element using the same procedure as before:

$$[K_e] = [A*]^T \int_{-1}^{1}\int_{-1}^{1}\int_{-\pi}^{\pi} [B]^T[D][B]\,|[J]|\,d\xi\,d\eta\,[A*] \qquad \text{(A.19)}$$

APPENDIX B: DEFLECTION OF A CIRCULAR RING OF MEDIUM WIDTH UNDER A PINCHING LOAD

B.1 Compensation for edge effects and restraint against anticlastic curvature

B.1.1 *Problem definition*

When a ring is very narrow it may be safely assumed that it will flex circumferentially with no restraint against anticlastic curvature. When the ring is very wide (i.e. when it is a long cylinder) the effects of restraint against anticlastic curvature are virtually constant along the cylinder and the edge effects may be neglected. For a short cylinder or ring of medium width, the edge effects are significant. The aim of this appendix is to calculate the transverse change in diameter of such a ring when subjected to a pinching load.

B.1.2 *Approach to solution*

Visualise restraint against anticlastic curvature as being provided by a meridional stress couple which is uniform along any given meridian. This couple is negated at the edges by an equal and opposite stress couple which decays according to the theory of cylindrical shells presented by Hetenyi[110]. The total stiffness of the shell may be determined by integrating the applied (circumferential) bending moment or stress couple across the width of the ring, which may be assumed to be bent to the same radius of curvature at every point across its width.

The situation may be simplified by assuming that a certain width of ring section adjacent to each edge experiences no restraint against anticlastic curvature, the remainder of the ring experiencing full restraint. It is necessary to determine the width which must be assumed so that the simplified model provides the correct total value of flexural rigidity.

B.1.3 *Analysis*

Co-ordinate system (Fig. B.1): x = axial (meridional) direction

θ = circumferential direction

z = through-thickness direction

Changes of curvature in meridional and circumferential directions are κ_x and κ_θ respectively.

Assume thin ring of radius R and thickness t is made from a homogeneous specially orthotropic material with in-plane properties E_x, E_θ, $\nu_{x\theta}$, $\nu_{\theta x}$ and $G_{x\theta}$ in the usual notation.

For an orthotropic material: $\dfrac{\nu_{x\theta}}{E_x} = \dfrac{\nu_{\theta x}}{E_\theta}$

For plate or shell of thickness t under stress couple M_x:

$\sigma_x = 12M_x z/t^2$ at distance z from the mid-surface, also $\varepsilon_x = z\kappa_x$ etc.

For general case of plane stress:

$$\begin{aligned} \varepsilon_x &= \frac{\sigma_x}{E_x} - \nu_{\theta x}\frac{\sigma_\theta}{E_\theta} \\ &= \frac{\sigma_x}{E_x} - \nu_{x\theta}\frac{\sigma_\theta}{E_x} = z\kappa_x \end{aligned} \qquad \text{(B.1)}$$

Multiplying by $\dfrac{Et^3}{12z}$ and defining $D_x = \dfrac{E_x t^3}{12(1-\nu_{x\theta}\nu_{\theta x})}$:

$$\frac{\sigma_x t^3}{12z} - \nu_{x\theta}\frac{\sigma_\theta t^3}{12z} = M_x - \nu_{x\theta}M_\theta = \frac{E_x t^3}{12}\kappa_x = D_x(1-\nu_{x\theta}\nu_{\theta x})\kappa_x \qquad \text{(B.2)}$$

Similarly: $M_\theta - \nu_{\theta x}M_x = D_\theta(1-\nu_{x\theta}\nu_{\theta x})\kappa_\theta$ where $D_\theta = \dfrac{E_\theta t^3}{12(1-\nu_{x\theta}\nu_{\theta x})}$ (B.3)

Consider restraint against anticlastic curvature κ_x in an infinitely-wide cylindrical shell. This is provided by a transverse stress couple M_x which appears when a circumferential stress couple M_θ is applied:

$$\kappa_x = 0 \quad \therefore \quad M_x = \nu_{x\theta} M_\theta$$

hence from equation (B.3): $M_\theta - \nu_{\theta x}\nu_{x\theta} M_\theta = M_\theta(1 - \nu_{x\theta}\nu_{\theta x})$

$$= D_\theta(1 - \nu_{x\theta}\nu_{\theta x})\kappa_\theta$$

$$\therefore \quad M_\theta = D_\theta \kappa_\theta \qquad \text{(B.4)}$$

$$\text{and} \quad M_x = \nu_{x\theta} D_\theta \kappa_\theta \qquad \text{(B.5)}$$

A cylindrical shell of finite width is now considered. A stress couple in the circumferential direction is applied so that the shell bends with a uniform change of curvature of κ_θ across the whole width. If anticlastic curvature were zero a constant stress couple $D_\theta\kappa_\theta$ would have to be present across the whole width. In practice this may be assumed to be negated at both free edges by an equal and opposite stress couple which is applied at the edges. Making use of the beam-on-elastic-foundation analogy for a cylindrical shell presented by Hetenyi[110] together with his results for a short beam[148], the couple is found to decay away from the edges of the ring (Fig. B.2). The net value of transverse couple M_x is now zero at the edges, increasing towards the mid-width of the ring.

$$\text{Net } M_x = \nu_{x\theta} D_\theta \kappa_\theta \left[1 - \frac{1}{\sinh\lambda w + \sin\lambda w} \left\{ \begin{matrix} \sinh\lambda x \cos\lambda(w-x) + \cosh\lambda x \sin\lambda(w-x) \\ + \sinh\lambda(w-x)\cos\lambda x + \cosh\lambda(w-x)\sin\lambda x) \end{matrix} \right\} \right] \qquad \text{(B.6)}$$

where x is measured from one edge of the ring, and where:

$$\lambda = \sqrt[4]{\frac{E_\theta}{E_x} \frac{3(1 - \nu_{x\theta}\nu_{\theta x})}{R^2 t^2}} \qquad \text{(B.7)}$$

Equation (B.6) is now inserted into (B.3) which is rearranged to give:

$$M_\theta = D_\theta(1-\nu_{x\theta}\nu_{\theta x})\kappa_\theta + \nu_{\theta x}M_x$$

$$= D_\theta(1-\nu_{x\theta}\nu_{\theta x})\kappa_\theta + \nu_{x\theta}\nu_{\theta x}D_\theta\kappa_\theta$$
$$- \frac{\nu_{\theta x}\nu_{x\theta}D_\theta\kappa_\theta}{\sinh\lambda w + \sin\lambda w}\left\{\begin{array}{l}\sinh\lambda x\cos\lambda(w-x)+\cosh\lambda x\sin\lambda(w-x)\\ +\sinh\lambda(w-x)\cos\lambda x+\cosh\lambda(w-x)\sin\lambda x\end{array}\right\}$$

$$= D_\theta\kappa_\theta\left[1-\frac{\nu_{x\theta}\nu_{\theta x}}{\sinh\lambda w+\sin\lambda w}\left\{\begin{array}{l}\sinh\lambda x\cos\lambda(w-x)+\cosh\lambda x\sin\lambda(w-x)\\ +\sinh\lambda(w-x)\cos\lambda x+\cosh\lambda(w-x)\sin\lambda x\end{array}\right\}\right] \quad \text{(B.8)}$$

A simplified model of the situation is now introduced. It is assumed that the shell consists of three regions: two edge bands of width w_{edge} where no anticlastic restraint is present ($M_x = 0$), and the remainder of the shell where full restraint exists (Fig. B.2). w_{edge} is chosen so that the values of total bending moment applied to the true and simplified systems are equal for equal curvature change κ_θ.

The stiffness per unit width for the different regions of the simplified model are as follows:

$0 \le x \le w_{edge}$ and $(w-w_{edge}) \le x \le w$: $\quad M_\theta = D_\theta(1-\nu_{x\theta}\nu_{\theta x})\kappa_\theta$

$w_{edge} \le x \le (w-w_{edge})$: $\quad M_\theta = D_\theta\kappa_\theta$

M_θ is now integrated over the width of the ring for the two models and the results are equated:

$$\int_{x=0}^{w} M_\theta dx = \int_{x=0}^{w} D_\theta\kappa_\theta\left[1-\frac{\nu_{x\theta}\nu_{\theta x}}{\sinh\lambda w+\sin\lambda w}\left\{\begin{array}{l}\sinh\lambda x\cos\lambda(w-x)+\cosh\lambda x\sin\lambda(w-x)\\ +\sinh\lambda(w-x)\cos\lambda x+\cosh\lambda(w-x)\sin\lambda x\end{array}\right\}\right]dx$$

$$= \int_{x=0}^{w_{edge}} D_\theta(1-\nu_{x\theta}\nu_{\theta x})\kappa_\theta dx + \int_{x=w_{edge}}^{w-w_{edge}} D_\theta\kappa_\theta dx + \int_{x=w-w_{edge}}^{w} D_\theta(1-\nu_{x\theta}\nu_{\theta x})\kappa_\theta dx$$

$$= \int_{x=0}^{w} D_\theta\kappa_\theta dx - 2\int_{x=0}^{w_{edge}} D_\theta\nu_{\theta x}\nu_{x\theta}\kappa_\theta dx \quad \text{making use of symmetry} \quad \text{(B.9)}$$

Equation (B.9) is rearranged by subtracting the term $\int_{x=0}^{w} D_\theta \kappa_\theta dx = wD_\theta \kappa_\theta$ and dividing throughout by $D_\theta \nu_{x\theta} \nu_{\theta x} \kappa_\theta$:

$$\therefore \quad 2\int_{x=0}^{w_{edge}} dx = 2w_{edge}$$

$$= \int_{x=0}^{w} \frac{1}{\sinh\lambda w + \sin\lambda w} \left\{ \begin{array}{l} \sinh\lambda x \cos\lambda(w-x) + \cosh\lambda x \sin\lambda(w-x) \\ + \sinh\lambda(w-x)\cos\lambda x + \cosh\lambda(w-x)\sin\lambda x \end{array} \right\} dx$$

$$= \left[\frac{\cosh\lambda x \cos\lambda(w-x) - \cosh\lambda(w-x)\cos\lambda x}{\lambda(\sinh\lambda w + \sin\lambda w)} \right]_{x=0}^{w}$$

$$= \frac{2}{\lambda}\left[\frac{\cosh\lambda w - \cos\lambda w}{\sinh\lambda w + \sin\lambda w} \right] \qquad \text{(B.10)}$$

$$\text{Thus} \quad w_{edge} = \frac{1}{\lambda}\left[\frac{\cosh\lambda w - \cos\lambda w}{\sinh\lambda w + \sin\lambda w} \right] \qquad \text{(B.11)}$$

Total flexural rigidity (F.R.) of section:

$$\text{F.R.} = \frac{1}{\kappa_\theta}\int_{x=0}^{w} M_\theta dx = \int_{x=0}^{w_{edge}} D_\theta(1 - \nu_{x\theta}\nu_{\theta x})dx + \int_{x=w_{edge}}^{w-w_{edge}} D_\theta dx + \int_{x=w-w_{edge}}^{w} D_\theta(1 - \nu_{x\theta}\nu_{\theta x})dx$$

$$= 2E_\theta w_{edge}\frac{t^3}{12} + E_\theta(w - 2w_{edge})\frac{t^3}{12(1 - \nu_{x\theta}\nu_{\theta x})}$$

$$= E_\theta I_{eff} \quad \text{where} \quad I_{eff} = \left[2w_{edge} + \frac{w - 2w_{edge}}{1 - \nu_{x\theta}\nu_{\theta x}} \right] \qquad \text{(B.12)}$$

B.2 Transverse deflection of pinched ring with orthotropic material properties

Consider a quadrant of a ring with the above dimensions and section properties under loads $P/2$, Q and M_0 (Fig. B.3). At point X the bending moment M, tensile force N

and shear force V are:

$$\begin{aligned} M &= M_0 + \frac{PR}{2}(1-\cos\psi) + QR\sin\psi \\ N &= \frac{-P}{2}\cos\psi + Q\sin\psi \\ V &= \frac{-P}{2}\sin\psi - Q\cos\psi \end{aligned} \qquad \text{(B.13)(a-c)}$$

The conventional expression[149] for strain energy U in a curved beam under combined loading is extended to include the orthotropic situation. In this case the flexural rigidity F.R. = EI_{eff}. The shape factor F is a correction factor relating to the shear strain energy of the structure. It arises because simple theory assumes a uniform shear stress distribution in a beam whereas the true distribution has a parabolic profile. The value of F is assumed to be 6/5 as for an isotropic rectangular beam.

$$\begin{aligned} U &= \int_0^l \frac{M^2}{2\text{F.R.}}ds + \int_0^l \left(\frac{N^2}{2AE_\theta} - \frac{MN}{AE_\theta R}\right)ds + \int_0^l \frac{FV^2}{2AG_{\theta z}}ds \\ &= \frac{R}{2E_\theta I_{eff}}\int_0^{\frac{\pi}{2}} M^2 d\psi + \frac{R}{AE_\theta}\int_0^{\frac{\pi}{2}}\left(\frac{N^2}{2} - \frac{MN}{R}\right)d\psi + \frac{FR}{2AG_{\theta z}}\int_0^{\frac{\pi}{2}} V^2 d\psi \\ &= \frac{R}{E_\theta I_{eff}}\left[\frac{M_0^2\pi}{4} + \frac{M_0 PR}{2}\left(\frac{\pi}{2}-1\right) + M_0 QR + \frac{P^2R^2}{32}(3\pi-8) + \frac{PQR^2}{4} + \frac{Q^2R^2\pi}{8}\right] \\ &\quad + \frac{1}{AE_\theta}\left[\frac{-P^2\pi R}{32} - \frac{Q^2\pi R}{8} + \frac{P^2R}{4} + \frac{PM_0}{2} - M_0 Q - \frac{PQR}{4}\right] \\ &\quad + \frac{FR}{AG_{\theta z}}\left[\frac{P^2\pi}{32} + \frac{PQ}{4} + \frac{Q^2\pi}{8}\right] \end{aligned} \qquad \text{(B.14)}$$

If quadrant forms part of a symmetrical ring there is no rotation at either end, and Q becomes a dummy load of zero value. The restraint against end rotation is enforced using Castigliano's theorem by choosing M_0 so that $\frac{\partial U}{\partial M_0} = 0$.

$$M_0 = -PR\left(\frac{1}{2}-\frac{1}{\pi}\right) - \frac{2QR}{\pi} - \frac{PI_{eff}}{\pi AR} + \frac{2QI_{eff}}{\pi AR} \qquad \text{(B.15)}$$

The change in transverse diameter of the ring δ_h may then be calculated.

$$\begin{aligned}\delta_h &= 2\left.\frac{\partial U}{\partial Q}\right|_{Q=0} \\ &= \frac{PR^3}{E_\theta I_{eff}}\left(\frac{2}{\pi}-\frac{1}{2}\right) + \frac{PR}{2AE_\theta}\left(1-\frac{8}{\pi}\right) + \frac{2PI_{eff}}{\pi A^2 E_\theta R} + \frac{PFR}{2AG_{\theta z}}\end{aligned} \qquad \text{(B.16)}$$

B.3 Derivation of equivalent orthotropic material properties for a many-layered angle-ply laminate

Assume the laminate to be made up of a large number of plies in balanced pairs, i.e. each ply having an angle ϕ to the direction x of the load is rigidly constrained by a similar ply of orientation $-\phi$ to undergo zero shear strain when subjected to a tensile load. This constraint may be simulated by application of equal and opposite shear stresses τ_{xy} applied to the two plies. Since the laminate has many layers (Fig. 3.1) it is assumed that there is no freedom to twist so the shear constraint may be rigorously applied.

The off-axis behaviour of each ply is modelled by equation (3.3)(a) where the off-axis compliance matrix $[\bar{S}]$ is defined by equation (3.4)(a). As a result of a stress σ_x applied to the laminate, it undergoes longitudinal and transverse strains ε_x and ε_y. Since $\sigma_y=0$, a reduced version of (3.3)(a) may be written:

$$\begin{Bmatrix}\varepsilon_x \\ \gamma_{xy}\end{Bmatrix} = \begin{bmatrix}\bar{S}_{11} & \bar{S}_{16} \\ \bar{S}_{16} & \bar{S}_{66}\end{bmatrix}\begin{Bmatrix}\sigma_x \\ \tau_{xy}\end{Bmatrix} \Leftrightarrow \begin{Bmatrix}\sigma_x \\ \tau_{xy}\end{Bmatrix} = \frac{1}{\bar{S}_{11}\bar{S}_{66}-\bar{S}_{16}^2}\begin{bmatrix}\bar{S}_{66} & -\bar{S}_{16} \\ -\bar{S}_{16} & \bar{S}_{11}\end{bmatrix}\begin{Bmatrix}\varepsilon_x \\ \gamma_{xy}\end{Bmatrix} \qquad \text{(B.17)}$$

Setting $\gamma_{xy} = 0$ and rearranging gives: $$\frac{\sigma_x}{\varepsilon_x} = E_x = \frac{\bar{S}_{66}}{\bar{S}_{11}\bar{S}_{66} - \bar{S}_{16}^2} \quad \text{(B.18)}$$

By a similar process, another reduced version of (3.3)(a) may be written:

$$\begin{Bmatrix} \varepsilon_y \\ \gamma_{xy} \end{Bmatrix} = \begin{bmatrix} \bar{S}_{12} & \bar{S}_{26} \\ \bar{S}_{16} & \bar{S}_{66} \end{bmatrix} \begin{Bmatrix} \sigma_x \\ \tau_{xy} \end{Bmatrix} \Leftrightarrow \begin{Bmatrix} \sigma_x \\ \tau_{xy} \end{Bmatrix} = \frac{1}{\bar{S}_{12}\bar{S}_{66} - \bar{S}_{16}\bar{S}_{26}} \begin{bmatrix} \bar{S}_{66} & -\bar{S}_{26} \\ -\bar{S}_{16} & \bar{S}_{12} \end{bmatrix} \begin{Bmatrix} \varepsilon_y \\ \gamma_{xy} \end{Bmatrix} \quad \text{(B.19)}$$

Setting $\gamma_{xy} = 0$ and rearranging gives: $$\frac{\sigma_x}{\varepsilon_y} = \frac{\bar{S}_{66}}{\bar{S}_{12}\bar{S}_{66} - \bar{S}_{16}\bar{S}_{26}} \quad \text{(B.20)}$$

Hence: $$\nu_{xy} = -\frac{\varepsilon_y}{\varepsilon_x} = -\frac{\bar{S}_{12}\bar{S}_{66} - \bar{S}_{16}\bar{S}_{26}}{\bar{S}_{11}\bar{S}_{66} - \bar{S}_{16}^2} \quad \text{(B.21)}$$

Similarly: $$E_y = \frac{\bar{S}_{66}}{\bar{S}_{22}\bar{S}_{66} - \bar{S}_{26}^2} \quad \text{and} \quad \nu_{yx} = \frac{\bar{S}_{12}\bar{S}_{66} - \bar{S}_{16}\bar{S}_{26}}{\bar{S}_{22}\bar{S}_{66} - \bar{S}_{26}^2} \quad \text{(B.22) (a&b)}$$

Provided a consistent definition of ϕ is observed in the definition of $[\bar{S}]$ using equation (3.4)(a), this type of analysis can be applied to many-layered laminates defined in other axis systems to obtain (for example) E_θ, $\nu_{\theta x}$.

B.4 Derivation of flexural rigidities D_x and D_θ and decay parameter λ using classical lamination theory

The derivation of equation (B.7) giving λ for the homogeneous orthotropic cylinder is a simple extension of the derivation for isotropic cylinders. However, λ may also be derived from the section properties obtained using classical lamination theory.
It will be assumed that the antisymmetric angle-ply laminate may be described in terms of its compliance matrix defined as follows:

$$\begin{Bmatrix} \varepsilon_x^0 \\ \varepsilon_\theta^0 \\ \varepsilon_{x\theta}^0 \\ \kappa_x \\ \kappa_\theta \\ \kappa_{x\theta} \end{Bmatrix} = \begin{bmatrix} \alpha_{11} & \alpha_{12} & 0 & 0 & 0 & \beta_{16} \\ \alpha_{12} & \alpha_{22} & 0 & 0 & 0 & \beta_{26} \\ 0 & 0 & \alpha_{66} & \beta_{16} & \beta_{26} & 0 \\ 0 & 0 & \beta_{16} & \delta_{11} & \delta_{12} & 0 \\ 0 & 0 & \beta_{26} & \delta_{21} & \delta_{22} & 0 \\ \beta_{16} & \beta_{26} & 0 & 0 & 0 & \delta_{66} \end{bmatrix} \begin{Bmatrix} N_x \\ N_\theta \\ N_{x\theta} \\ M_x \\ M_y \\ M_{x\theta} \end{Bmatrix} \quad \text{or:} \quad \begin{Bmatrix} \{\varepsilon^0\} \\ \{\kappa\} \end{Bmatrix} = \begin{bmatrix} [\alpha] & [\beta] \\ [\beta]^T & [\delta] \end{bmatrix} \begin{Bmatrix} \{N\} \\ \{M\} \end{Bmatrix}$$

$$\text{where:} \quad \begin{bmatrix} [\alpha] & [\beta] \\ [\beta]^T & [\delta] \end{bmatrix} = \begin{bmatrix} [A] & [B] \\ [B] & [D] \end{bmatrix}^{-1} \qquad \text{(B.23)}$$

B.4.1 *Derivation of meridional and circumferential flexural rigidities D_x and D_θ*

It is assumed that under a distributed meridional stress couple M_x the cylindrical shell constrains itself to undergo zero circumferential (anticlastic) curvature by means of an unknown stress couple M_θ. The stress couple M_x required to cause unit meridional curvature is obtained by inverting a reduced laminate compliance matrix:

$$\begin{Bmatrix} \kappa_x \\ \kappa_\theta \end{Bmatrix} = \begin{bmatrix} \delta_{11} & \delta_{12} \\ \delta_{12} & \delta_{22} \end{bmatrix} \begin{Bmatrix} M_x \\ M_\theta \end{Bmatrix} \quad \Leftrightarrow \quad \begin{Bmatrix} M_x \\ M_\theta \end{Bmatrix} = \frac{1}{\delta_{11}\delta_{22} - \delta_{12}^2} \begin{bmatrix} \delta_{22} & -\delta_{12} \\ -\delta_{12} & \delta_{11} \end{bmatrix} \begin{Bmatrix} \kappa_x \\ \kappa_\theta \end{Bmatrix}$$

$$\therefore \text{ if } \kappa_\theta = 0 \quad \text{then} \quad \frac{M_x}{\kappa_x} = D_x = \frac{\delta_{22}}{\delta_{11}\delta_{22} - \delta_{12}^2} \qquad \text{(B.24)}$$

$$\text{similarly} \quad D_\theta = \frac{\delta_{11}}{\delta_{11}\delta_{22} - \delta_{12}^2} \qquad \text{(B.25)}$$

In the simpler case where no restraint against anticlastic curvature exists (at a free edge, for instance) the circumferential flexural rigidity is $D_\theta = 1/\delta_{22}$. Thus the medium width ring may be modelled as possessing the following flexural rigidity:

$$\text{Flexural rigidity (F.R.)} = \frac{2w_{edge}}{\delta_{22}} + (w - 2w_{edge}) \left[\frac{\delta_{11}}{\delta_{11}\delta_{22} - \delta_{12}^2} \right] \qquad \text{(B.26)}$$

To determine w_{edge} using equation (B.11) it is first necessary to calculate λ.

B.4.2 *Derivation of decay parameter* λ

This is calculated from $\lambda = (k/4D_x)^{1/4}$ where k is the radial stiffness of the shell per unit area and D_x is the flexural rigidity defined above. By axial symmetry it may assumed that the cylindrical shell constrains itself (by means of an unknown twisting couple $M_{x\theta}$) so that the twist $\kappa_{x\theta}$ of the shell surface is zero if the shell is subjected to internal pressure, despite the tendency of an antisymmetric laminate to twist under direct loading. This constraint may be applied by inverting a reduced compliance matrix for the laminate:

$$\begin{Bmatrix} \varepsilon_\theta^0 \\ \kappa_{x\theta} \end{Bmatrix} = \begin{bmatrix} \alpha_{22} & \beta_{26} \\ \beta_{26} & \delta_{66} \end{bmatrix} \begin{Bmatrix} N_\theta \\ M_{x\theta} \end{Bmatrix} \Leftrightarrow \begin{Bmatrix} N_\theta \\ M_{x\theta} \end{Bmatrix} = \frac{1}{\alpha_{22}\delta_{66} - \beta_{26}^2} \begin{bmatrix} \delta_{66} & -\beta_{26} \\ -\beta_{26} & \alpha_{22} \end{bmatrix} \begin{Bmatrix} \varepsilon_\theta^0 \\ \kappa_{x\theta} \end{Bmatrix} \quad \text{(B.27)}$$

The radial deflection δ_r may be expressed as $\varepsilon_\theta^0 R$ and the internal pressure p as N_θ/R. Hence if $\kappa_{x\theta}$ is set to zero in equation (B.27) the radial stiffness k per unit area is:

$$k = \frac{p}{\delta_r} = \frac{N_\theta}{\varepsilon_\theta^0 R^2} = \frac{\delta_{66}}{R^2(\alpha_{22}\delta_{66} - \beta_{26}^2)} \quad \text{(B.28)}$$

The decay parameter λ may now be calculated:

$$\lambda = \sqrt[4]{\frac{k}{4D_x}} = \sqrt[4]{\frac{\delta_{66}(\delta_{11}\delta_{22} - \delta_{12}^2)}{4R^2\delta_{22}(\alpha_{22}\delta_{66} - \beta_{26}^2)}} \quad \text{(B.29)}$$

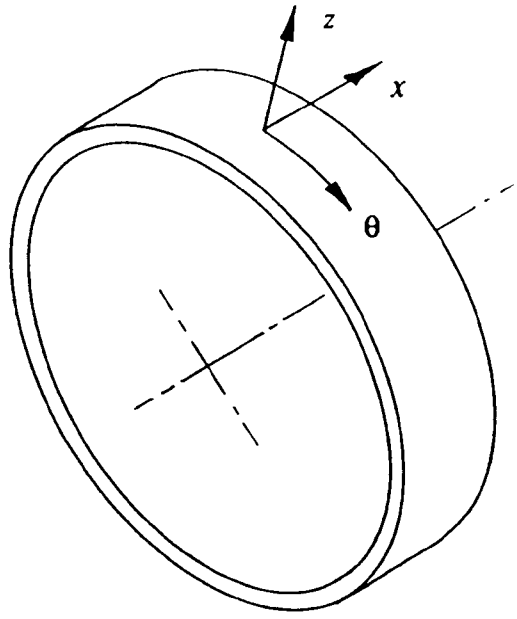

Fig. B.1. Co-ordinate system for analysis of medium-width pinched ring

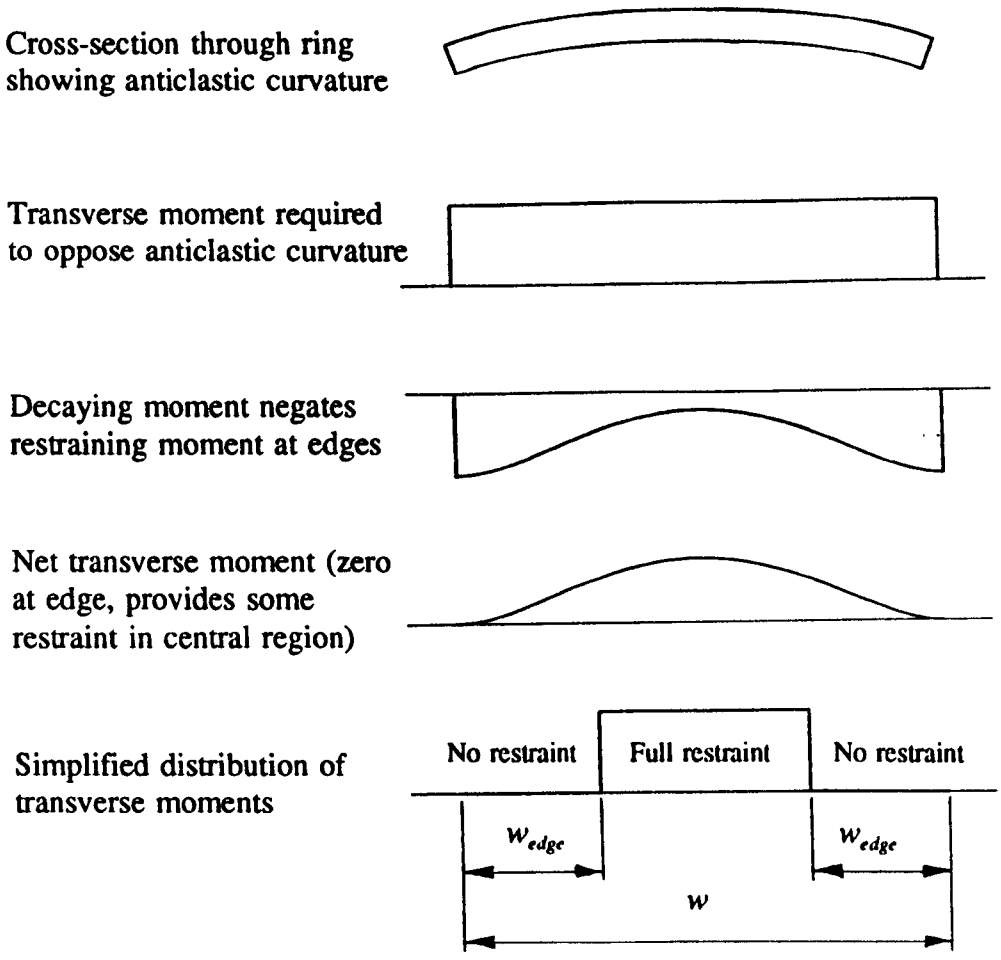

Fig. B.2. Transverse moments present in a medium-width ring in flexure

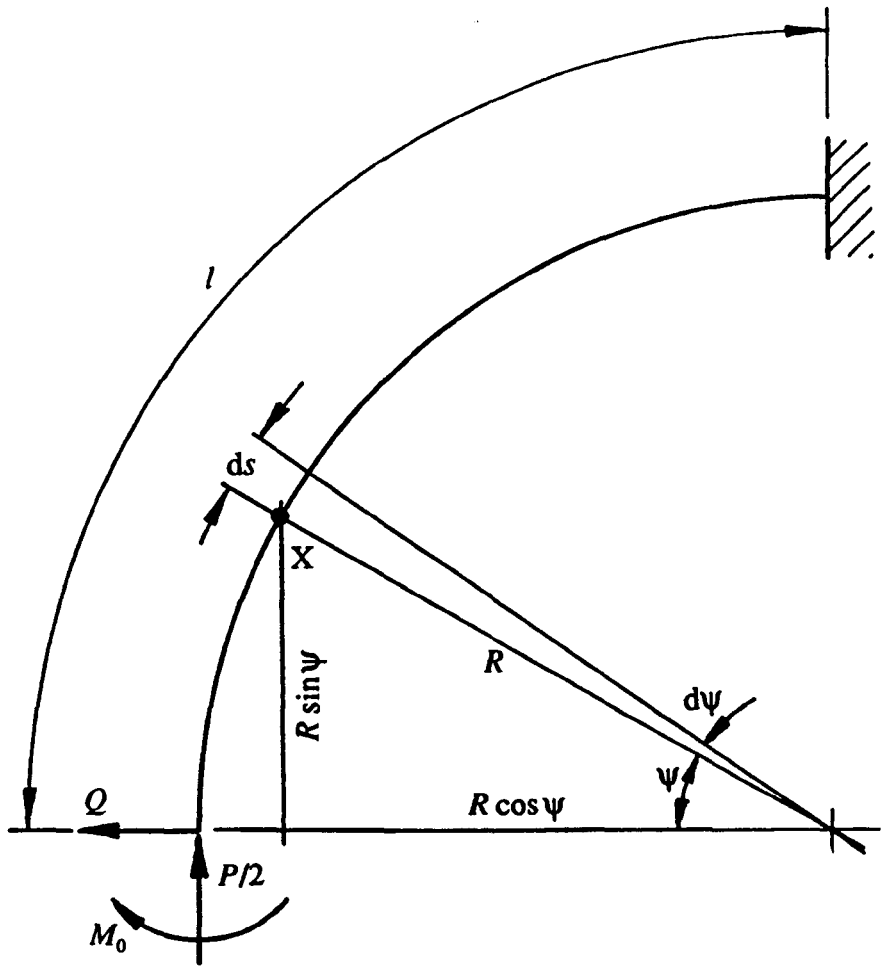

Fig. B.3: One quadrant of ring showing loads and dimensions

APPENDIX C: DATA ANALYSIS SOFTWARE FOR MATERIALS TESTING

C.1 Introduction

It is well known that the properties of composite materials are subject to considerable scatter. In order to increase confidence in the results obtained it was necessary to test a substantial number of specimens, and the corresponding quantity of experimental data justified the writing of a considerable amount of data analysis software. The main programs used for processing a typical set of experimental results (the pinched ring test results) will be described in some detail and illustrated with flowcharts. Variations upon these programs were used for processing the results from the split disc, axial compression and open-ended pressure tests and these modified programs will be described largely in terms of any significant variations from the "parent" programs.

C.2 Data analysis software for pinched ring test results

C.2.1 *Program MEASUR* (Fig. C.1)

This program performs calculations relating to the measured dimensions and masses of the rings. It includes a number of calculations relating to the theory of filament winding. These are based either on simple geometry or basic physics and have been extended by the author from formulae in common use at Crescent Consultants Ltd[8,22].

The fibre and matrix material properties are read from a material data file; these properties are used in the fibre mass ratio calculations.

The input data for MEASUR is read from a data file, and begins with a description of the set of rings together with data (including winding process data from CADFIL I) which is common to these rings. The width measurements, a

sample of thickness measurements (both for peak and trough thickness), the burnoff results (fibre content by mass) and the masses of each ring are then read in succession.

The mean peak and trough thicknesses are calculated, along with the standard deviations of each. The average thickness of the ring, as used in all subsequent calculations, is the mean of the mean peak and trough thicknesses.

It must be realised that the values of winding angle θ and bandwidth b read from the CADFIL I package are those assumed before the application of the progression factor, and it is therefore necessary to correct for this modification (and for any deviations from the assumed values of diameter).

$$\theta_{actual} = \tan^{-1}\left[\tan\theta_{raw} \times \text{P.F.} \times \frac{d_{mid}}{d_{nominal}}\right] \qquad \text{(C.1)}$$

$$b = \frac{\pi\, d_{actual} \cos\theta_{actual}}{N_{cycles}} \qquad \text{(C.2)}$$

where: θ_{raw} = winding angle assumed during fibre path generation
θ_{actual} = winding angle corrected for mandrel diameter and progression factor
P.F. = progression factor calculated by post-processor
$d_{nominal}$ = diameter of fibre generation mesh
d_{mid} = mid-surface diameter of rings
b = actual bandwidth
N_{cycles} = number of bands per repeated cycle

For the specimens wound in a nominally circumferential (hoop) direction the bandwidth is accurately known and is equal to the helix pitch of the winding and a different formula is used to determine the winding angle:

$$\theta_{actual} = \tan^{-1}\left(\frac{\pi\, d_{actual}}{b}\right) \qquad \text{(C.3)}$$

Although the fibre content by mass was measured for each set of rings using a burnoff procedure based upon BS2782: Part 10: Method 1002[114], an alternative

method of calculating this value is to estimate the amount of glass fibre contained within an individual ring and compare this with the measured mass. For an angle-wound specimen the calculation is as follows:

$$\text{F.M.R.} = 2N_{\text{total}} \times \frac{\text{TEX}}{K_1} \times \frac{w}{\cos\theta_{\text{actual}}} \times \frac{1}{m_{\text{ring}}}$$

where: F.M.R. = fibre mass ratio (fibre content of composite by mass)
TEX = mass per unit length of dry fibre (g/km)
w = width of ring (mm)
m_{ring} = mass of ring (g)
K_1 = constant = 10^6 for units as given
N_{total} = total number of bands wound onto specimen (C.4)

The corresponding formula for hoop-wound specimens is:

$$\text{F.M.R} = \frac{\pi w d_{\text{actual}} N_{\text{layers}}}{b m_{ring}} \times \frac{\text{TEX}}{K_1} \qquad \text{(C.5)}$$

where N_{layers} = number of layers in laminate

The fibre content may also be estimated from the measured thickness of the laminate; the cross-sectional area of the impregnated tow is calculated and then used to calculated the proportion of fibre by volume, and hence (knowing the densities of fibre and matrix) the proportion by mass.

$$A = \frac{bt}{N_{\text{layers}}} \qquad \text{(C.6)}$$

$$\text{F.M.R.} = \left[1 + \rho_m \times \left(\frac{K_2 A}{\text{TEX}} - \frac{1}{\rho_f}\right)\right]^{-1} \qquad \text{(C.7)}$$

where: A = cross-sectional area of impregnated tow
ρ_f = density of fibre material (g/cm^3)
ρ_m = density of matrix material (g/cm^3)
K_2 = constant = 10^3 for given set of units

The constants K_1 and K_2 arise because the experimental measurements are normally taken in a set of units which are not dimensionally consistent.

Two output files are produced: one contains details of the means and standard deviations for the thicknesses, and the other contains the various estimates of fibre content and summarises the dimensional data for the specimens (length, mean thickness, winding angle and mid-surface diameter).

C.2.2 *Program CORREL* (Fig. C.2)

This program takes the manually-recorded data relating ring deflections to applied load and performs a least-squares linear regression analysis, giving the estimated value (and the 95% confidence limits) of the deflection per unit load of the ring. In addition, it re-tabulates in neater form the input data, and plots the data graphically for on-screen examination or hard-copy output.

This program and its derivatives make use of well-known linear regression methods described in a variety of texts such as those by Chatfield[150] and Chou[151]. This theory is presented in the conventional notation relating to a dependent variable y expressed in terms of an independent variable x. Throughout the data processing exercise the load was chosen as the independent variable x. The decision to choose this convention was based upon the fact that linear regression minimises the sum of squares of errors in y and neglects errors in x. It is the author's belief that random errors in the measured values of load are likely to be less significant than the strain readings obtained from strain gauges since the latter are particularly sensitive to thermal effects and electrical interference. For consistency this convention has been applied also to the analysis of the pinched ring data although the dial indicator readings are not sensitive to these sources of error.

The data relating to each ring is read from the appropriate file and for each of the N values of load the total diametral deflection is calculated. The appropriate summations are performed to give Σx, Σx^2, Σy, Σy^2 and Σxy, and the mean values of x and y are calculated:

$$\bar{x} = \frac{\Sigma x}{N} \quad \text{(a)} \qquad \bar{y} = \frac{\Sigma y}{N} \quad \text{(b)} \qquad \text{(C.8)}$$

The constants S_{xx}, S_{yy} and S_{xy}, and hence the gradient and intercept, are calculated.

$$\Delta = \frac{S_{xy}}{S_{xx}} \qquad \text{(C.8)}$$

$$c = \bar{y} - \bar{x}\Delta \qquad \text{(C.9)}$$

where $S_{xy} = \Sigma xy - N\bar{x}\bar{y}$
$S_{xx} = \Sigma x^2 - N\bar{x}^2$
Δ = gradient of best straight line
(= diametral deflection per unit load)
c = y-intercept of line

A measure of the proportionality of the two variables is given by the correlation coefficient r:

$$r = \frac{S_{xy}}{\sqrt{S_{xx} S_{yy}}} \qquad \text{(C.11)}$$

where $S_{yy} = \Sigma y^2 - N\bar{y}^2$, S_{xx} and S_{xy} as above

To find the 95% confidence limits on the gradient, it is first necessary to evaluate the residual standard deviation $\hat{\sigma}$:

$$\hat{\sigma} = \sqrt{\frac{S_{yy} - \Delta S_{xy}}{N-2}} \qquad \text{(C.12)}$$

The Student's t statistic for a 2-tailed 95% confidence band is found using the NAG[122] FORTRAN function G01CAF for a 1-tailed probability of 0.975 and N-2 degrees of freedom. This value is then used to calculate the confidence limits on the gradient:

$$\Delta_{\text{upper, lower}} = \Delta \pm \frac{t_{0.975, N-2}\,\hat{\sigma}}{\sqrt{S_{xx}}} \qquad \text{(C.13)}$$

The data points, best straight line and lines representing the upper and lower confidence limits on gradient passing through $(\bar{x},\bar{y})$ are all plotted on a graph which is written to a data file for viewing or hard plotting. This is achieved using the SIMPLEPLOT library[152] available on the University's ICL VME

system. For the purpose of this thesis, simplified graphs were plotted using the UNIRAS library[153] available on the ICL DRS 6000 (Unicorn) system.

C.2.3 *Program ORTHPROV* (Fig. C.3.)

This program calculates the circumferential Young's modulus E_θ of the angle-ply laminated composite using the theory outlined in sections 5.3.1 and 5.3.2 and derived in sections B.1 and B.2 of Appendix B.

Before E_θ can be calculated from the experimental data it is necessary first to have estimates of E_x, E_θ, $\nu_{\theta x}$ and $\nu_{x\theta}$ for use in equation (5.8). These values were calculated using equations (3.4)(a) and (5.9)(a-d) making use of typical estimates of material properties (such as those obtained from Weatherby[106]).

w_{edge}, the distance over which the edge effects are considered, is calculated using equation (5.4) and hence the effective second moment of area I_{eff} of the ring section is calculated using equation (5.7). Finally, the circumferential Young's modulus may be calculated from the experimental data using equation (5.14). This is performed using both the best estimate of the deflection per unit load and the 95% confidence limits on this value.

C.2.4 *Program NORMAL* (Fig. C.4)

This program is used to normalise the calculated values of Young's modulus with respect to the fibre content of the composite. The normalisation process is carried out on the best estimate of Young's modulus obtained from the program ORTHPROV and also on the 95% confidence limits on the Young's modulus.

The Halpin-Tsai equations[3] (equation (5.1) (a-d)) and equations (3.4)(a) and (5.9)(a-d) are used to calculate estimated values of E_θ both for the measured value of fibre content by mass of each specimen (as obtained from the burnoff tests[114]) and for the nominal value of 78% (typical of the fibre content of the hoop-wound specimens). The measured values of E_θ are then scaled by the ratio of these calculated values. It is accepted that the Halpin-Tsai equations do not give a

precise representation of material properties but they were used for simplicity and because it was felt to be essential to make some effort towards normalisation. Various values of the constant ξ were tried in calculating E_2 but the difference in normalised values was quite insignificant, being approximately $1 MNm^{-2}$.

C.2.5 *Program TRANSFIT* (Fig. C.5.)

This program optimises the values of on-axis properties describing a unidirectional composite so that the theoretical variation of Young's modulus with ply angle (for a many-layered angle-ply laminate) is fitted to experimentally-measured properties of the laminated specimens. The theoretical relationship consists of an equation of similar form to equation (B.18). The curve-fitting is achieved using the NAG FORTRAN library[122] subroutine E04GEF which is designed to solve a set of N non-linear simultaneous equations. In this case the variables are the values of on-axis compliance S_{11}, S_{12}, S_{22} and S_{66} of the unidirectional composite, and the constants in the ith equation depend upon the measured value of Young's modulus of the ith laminated specimen ($(E_\theta)_i$ for the pinched rings) and its ply angle ϕ_i. The equations may be stated as:

$$\frac{\bar{S}_{66}}{\bar{S}_{11}\bar{S}_{66} - \bar{S}_{16}^2} - (E_\theta)_i = 0 \quad \text{where } \bar{S}_{11}, \bar{S}_{12}, \bar{S}_{22} \text{ and } \bar{S}_{66} \text{ are functions of } S_{11}, S_{12}, S_{22}, S_{66} \text{ and } \phi_i, \text{ and } i = 1 \ldots N. \tag{C.14}$$

The first stage in solving these equations is to set up the constants required in each of the simultaneous equations, and to store them in COMMON memory so that they may be accessed repeatedly. This is achieved in the subroutine COMFIL which reads the measured circumferential Young's modulus and the winding angle for each ring i from the edited output of the program ORTHPROV, and stores the powers of $(\sin\theta)_i$ and $(\cos\theta)_i$ along with the circumferential Young's modulus $(E_\theta)_i$. The constant π and the chosen value of Poisson's ratio ν_{12} are also stored in COMMON memory.

A set of functions $f_i(S_{11}, S_{12}, S_{22}, S_{66})$ is defined in equations (5.15) and (5.16). It is necessary when using E04GEF to define a subroutine LSFUN2 which calculates the value of the each of the functions f_i for any given set of values of

compliances. It should be noted that to avoid ill-conditioning it was necessary to express f_i as a function of only 3 independent variables, S_{12} being treated as $-\nu_{12}S_{11}$ for calculating both f_i and its derivatives. In detail, the functions f_i are calculated using the following equations:

$$f_i(S_{11}, S_{22}, S_{66}) = \frac{\bar{S}_{66}}{\bar{S}_{11}\bar{S}_{66} - \bar{S}_{16}^2} - (E_\phi)_i \qquad \text{(C.15)}$$

$\bar{S}_{11}$ etc. are obtained by substituting $-\nu_{12}S_{11}$ for S_{12} and expanding equation (3.4)(a):

$$\begin{aligned}
\bar{S}_{11} &= S_{11}\cos^4\phi - 2\nu_{12}S_{11}\sin^2\phi\cos^2\phi + S_{66}\sin^2\phi\cos^2\phi + S_{22}\sin^4\phi \qquad \text{(C.16)}\\
\bar{S}_{16} &= 2S_{11}\sin\phi\cos^3\phi - S_{66}(\sin\phi\cos^3\phi - \sin^3\phi\cos\phi) \qquad \text{(a-c)}\\
\bar{S}_{66} &= 4(1+2\nu_{12})S_{11}\sin^2\phi\cos^2\phi + 4S_{22}\sin^2\phi\cos^2\phi + S_{66}(\sin^4\phi + \cos^4\phi - 2\sin^2\phi\cos^2\phi)
\end{aligned}$$

The Jacobian matrix is also required. This is the matrix of partial derivatives of the functions f_i with respect to each of the variables. The components of the Jacobian matrix are:

$$\frac{\partial f_i}{\partial S_{jk}} = \frac{(\bar{S}_{11}\bar{S}_{66} - \bar{S}_{16}^2)\dfrac{\partial \bar{S}_{66}}{\partial S_{jk}} - \bar{S}_{66}\left(\dfrac{\partial \bar{S}_{11}}{\partial S_{jk}}\bar{S}_{66} + \dfrac{\partial \bar{S}_{66}}{\partial S_{jk}}\bar{S}_{11} - 2\bar{S}_{16}\dfrac{\partial \bar{S}_{16}}{\partial S_{jk}}\right)}{(\bar{S}_{11}\bar{S}_{66} - \bar{S}_{12}^2)^2} \qquad \text{(C.17)}$$

where $j, k = 1, 2, 6$ and:

$$\begin{aligned}
&\frac{\partial \bar{S}_{11}}{\partial S_{11}} = \cos^4\phi - 2\nu_{12}\sin^2\phi\cos^2\phi \qquad \frac{\partial \bar{S}_{11}}{\partial S_{22}} = \sin^4\phi \qquad \frac{\partial \bar{S}_{11}}{\partial S_{66}} = \sin^2\phi\cos^2\phi\\
&\frac{\partial \bar{S}_{16}}{\partial S_{11}} = 2\sin\phi\cos^3\phi + 2\nu_{12}(\sin\phi\cos^3\phi - \sin^3\phi\cos\phi) \qquad \frac{\partial \bar{S}_{16}}{\partial S_{22}} = -2\sin^3\phi\cos\phi \qquad \frac{\partial \bar{S}_{16}}{\partial S_{66}} = \sin^3\phi\cos\phi - \sin\phi\cos^3\phi\\
&\frac{\partial \bar{S}_{66}}{\partial S_{11}} = 4\sin^2\phi\cos^2\phi(1+2\nu_{12}) \qquad \frac{\partial \bar{S}_{66}}{\partial S_{22}} = 4\sin^2\phi\cos^2\phi \qquad \frac{\partial \bar{S}_{66}}{\partial S_{66}} = \sin^4\phi + \cos^4\phi - 2\sin^2\phi\cos^2\phi
\end{aligned}$$

(C.18)
(a-c)
(d-f)
(g-i)

The NAG subroutine E04GEF, when called by the main program TRANSFIT, makes repeated calls to LSFUN2 and optimises the independent variables so that the sum of the squares of f_i is minimised. If the optimisation is successful, the resulting values of compliance are used to calculate the moduli E_1, E_2 and G_{12}. If the optimisation is unsuccessful (for instance, if the solution to the simultaneous equations has not converged after a reasonable number of iterations) a diagnostic message is printed.

One of the problems encountered in using the E04GEF subroutine was that it was incapable of correctly optimising against variables with very small numerical values (e.g. compliance, with values such as 2×10^{-5}). This problem was overcome by scaling the whole problem by a factor of 10^6 so that the numerical values are in a more reasonable range.

C.3 Data processing software for split disc test results

The programs used for processing these results follow closely the structure of those used for processing the pinched ring results although varying degrees of modification were required. Since the specimens were the identical ones used for the pinched ring tests, the output from program MEASUR is used without alteration.

C.3.1 *Program CORRELSG* (Fig. C.2)

This program closely follows the program CORREL. The only significant alteration is that it includes the facility to confine the linear regression to points lying within a certain band of loads. The rejected points are marked on the graphs with a different type of symbol from those accepted for the linear regression. The linear regression gives values of strain per unit load for each individual gauge. Differences from CORREL also exist in the details of the output file format.

C.3.2 *Program YOUNGMOD*

This program replaces ORTHRING as the program in which the values of Young's modulus are calculated from the flexibility data and the ring dimensions. The Young's modulus is estimated from the strain per unit load for each ring:

$$E_\theta = \left[2\times 10^{-9}\, w\, t \frac{d\varepsilon_\theta}{dP} \right]^{-1} \qquad \text{(C.19)}$$

where: E_θ = circumferential Young's modulus (MNm^{-2})
w = width of ring (mm)
t = mean thickness of ring (mm)
$\frac{d\varepsilon_\theta}{dP}$ = gradient of strain-force graph ($\mu\varepsilon\, kN^{-1}$)

C.3.3 *Program NORMALSG*

This program is identical to NORMAL except for minor alterations to the output file headings.

C.3.4 *Program POISNORM*

This program is similar in concept to NORMAL etc. but is aimed at normalising the values of Poisson's ratio. An equation of similar form to equation (B.21) is used as for calculating the theoretical values of Poisson's ratio from the estimated unidirectional properties.

C.4 Data processing software for axial compression specimens

This closely follows that used for the split disc specimens. The following modified programs are used.

C.4.1 *Program YOUNGCOMP*

This is identical to YOUNGMOD except for the formula used for calculating Young's modulus:

$$E_x = \left(10^{-9}\,\pi\, d\, t \frac{d\varepsilon_x}{dP}\right)^{-1}$$

where: E_x = meridional (axial) Young's modulus (MNm^{-2}) (C.20)
d = mid-surface diameter of tube (mm)
t = thickness of tube (mm)
$\frac{d\varepsilon_x}{dP}$ = meridional (axial) strain per unit load ($\mu\varepsilon N^{-1}$)

C.4.2 *Program NORMALSGC*

This differs from NORMAL only in the fact that the laminate ply angles are measured with respect to the meridional (axial) direction rather than the circumferential (hoop) direction. The ply angle convention for the axial compression specimen data was manually altered when the output data from NORMALSGC was combined with the split disc data for curve-fitting.

C.5 Data processing software for open-ended pressure specimens

This follows closely the software used for the pinched ring and split disc tests, the main difference being that no attempt was made to calculate the fibre content of the specimen using the specimen mass, and therefore all sections of the program and data structure relating to specimen mass are omitted from the corresponding programs MEASURPT, YOUNGPT and NORMALPT and TRNSFTPT. Program CORRELPT differs from CORREL only in the printout headings. The only significant change in the software is the formula used in YOUNGPT for the calculation of Young's modulus:

$$E_\theta = \frac{10^5 d_{inner}}{2t\frac{d\varepsilon_\theta}{dp}}$$

where: E_θ = circumferential Young's modulus (MNm^{-2})
d_{inner} = inner diameter of tube
t = thickness of tube
$\frac{d\varepsilon_\theta}{dp}$ = gradient of strain-pressure graph ($\mu\varepsilon\ bar^{-1}$)

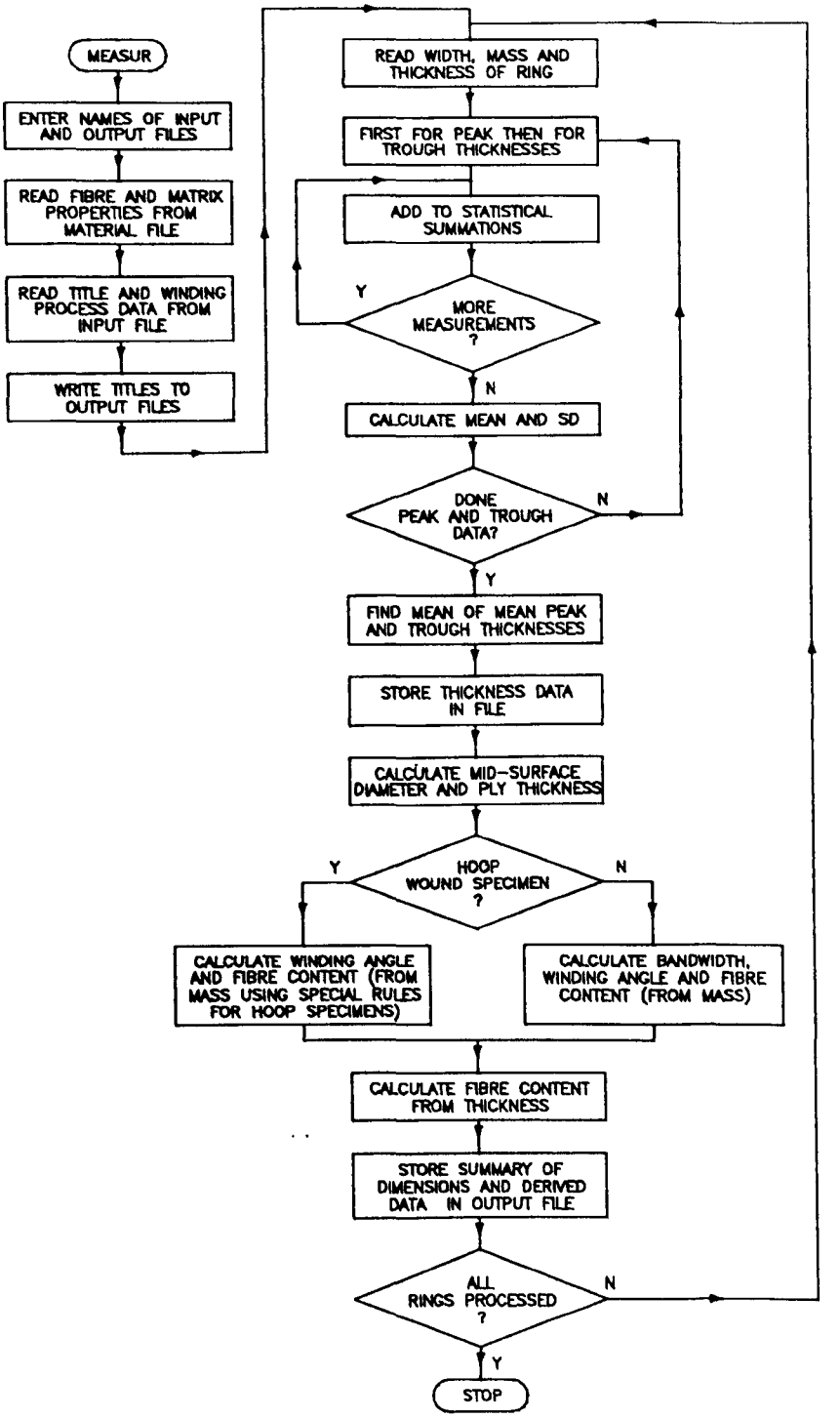

Fig. C.1.: Structure of programs MEASUR etc. for processing specimen dimensions

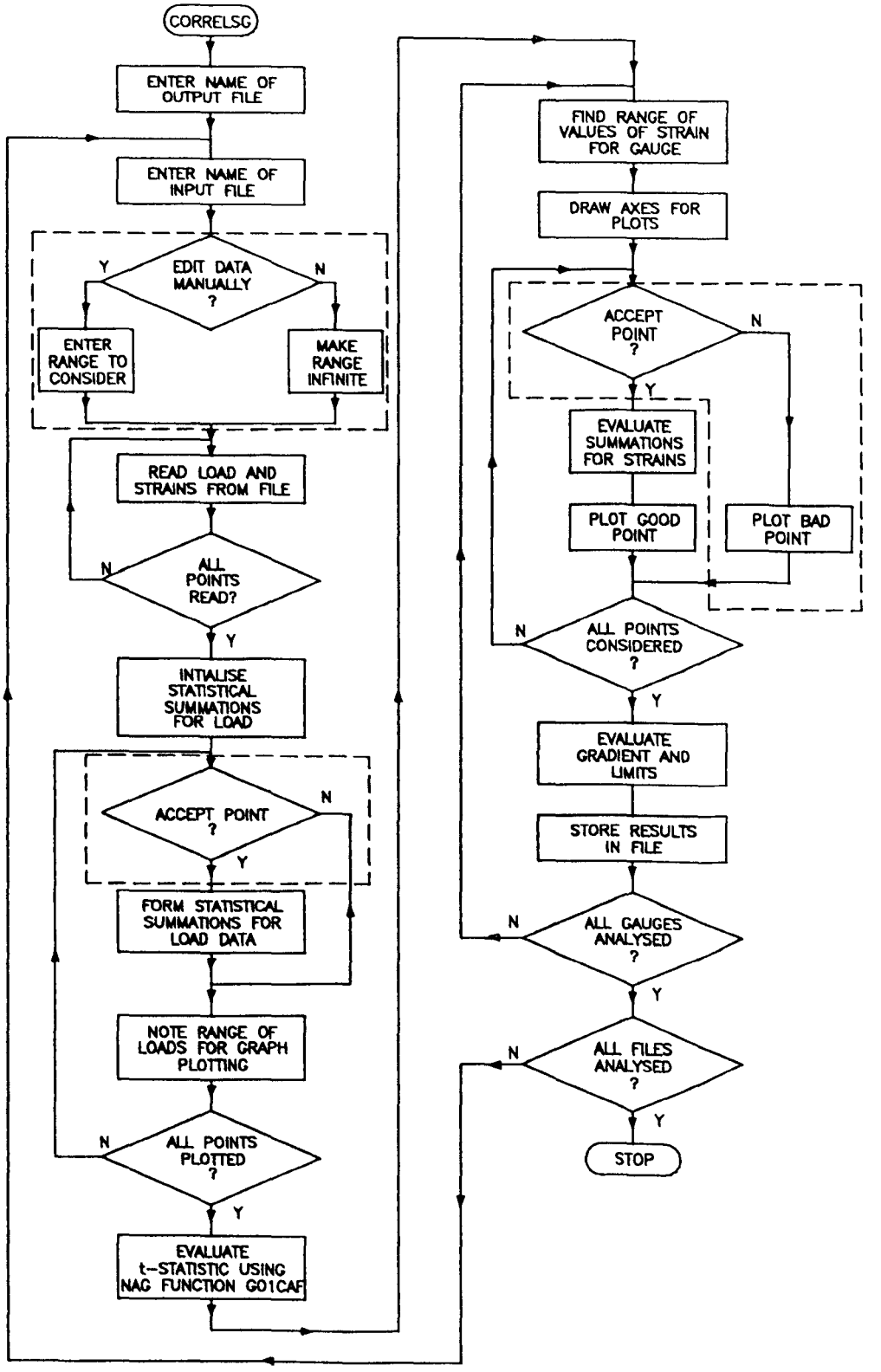

Fig. C.2.: Structure of programs CORREL, CORRELSG etc. performing linear regression on deflection/strain data (dotted regions omitted from program CORREL)

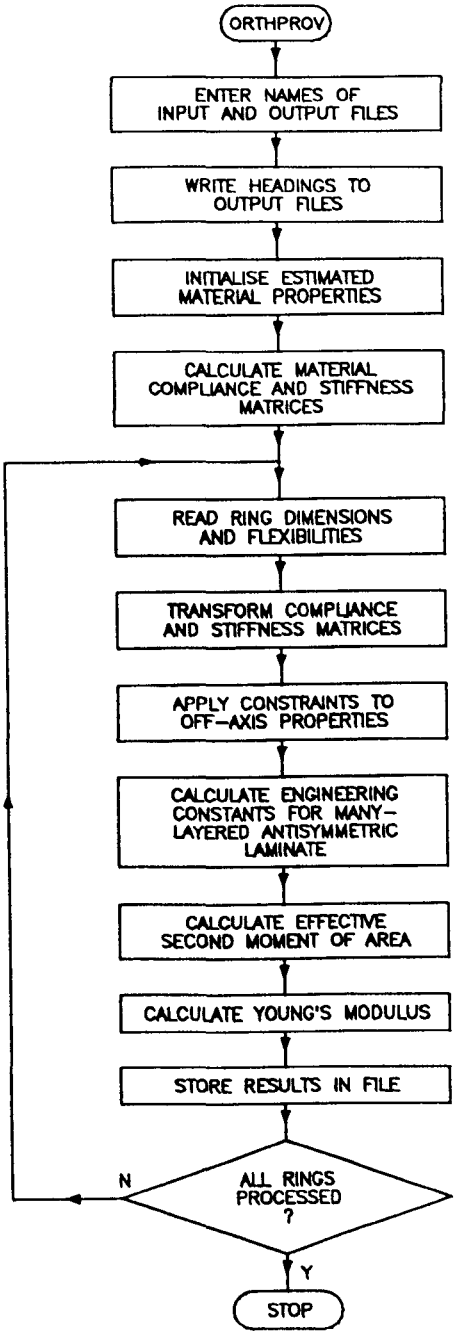

Fig. C.3.: Structure of program ORTHPROV for estimating the circumferential Young's modulus of a pinched ring from deflection/load gradient

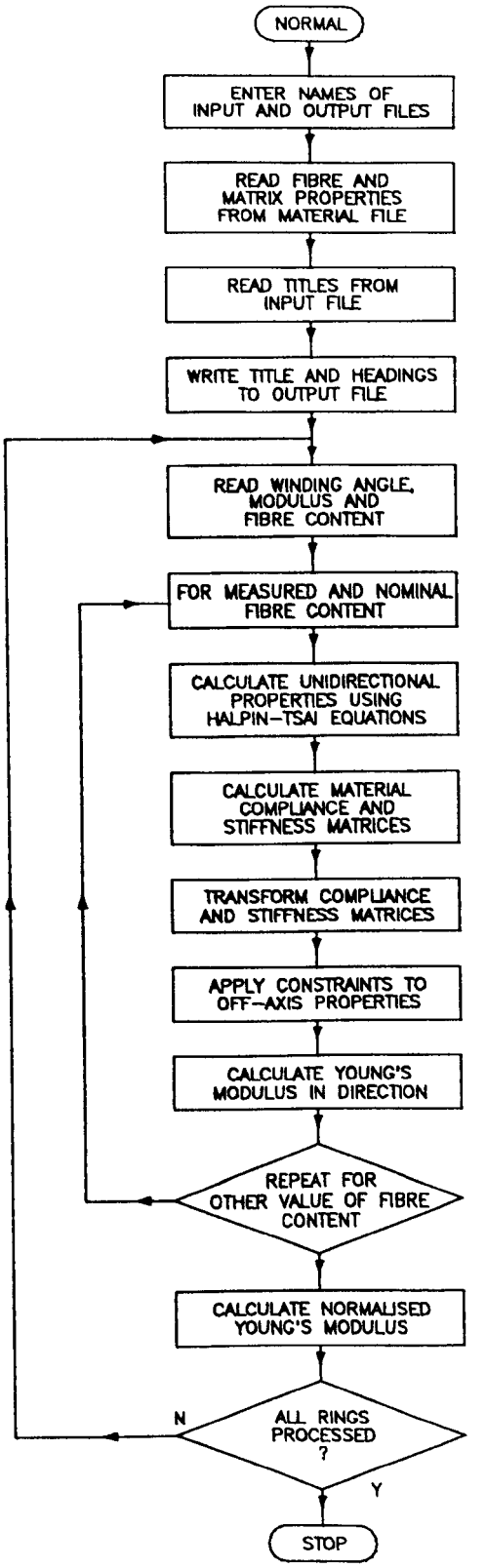

Fig. C.4.: Structure of programs NORMAL etc. for normalising material properties to a refer to a standard percentage of fibre.

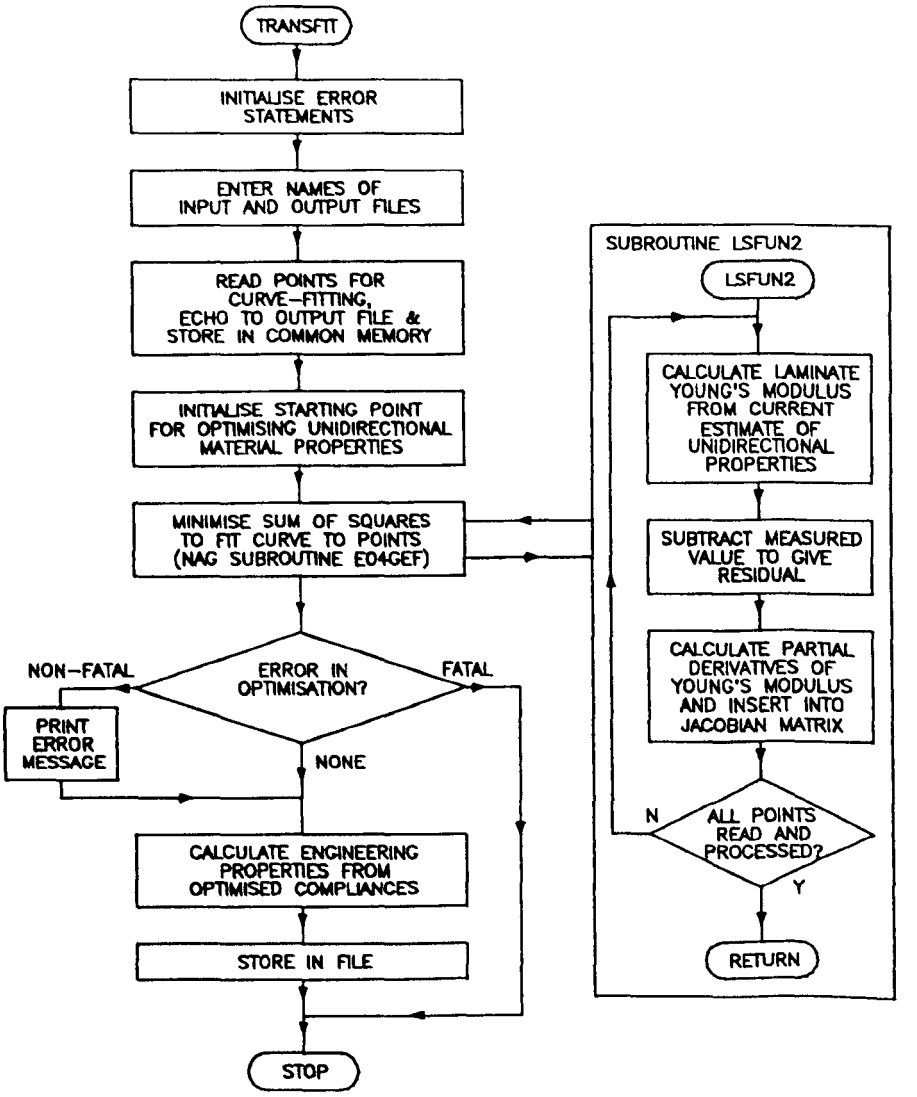

Fig. C.5.: Structure of programs TRANSFIT etc. for estimating unidirectional material properties from angle-ply laminate data.

APPENDIX D: TYPICAL OBSERVATIONS FROM TESTS OF MATERIAL PROPERTIES, SUMMARISED IN GRAPHICAL FORM

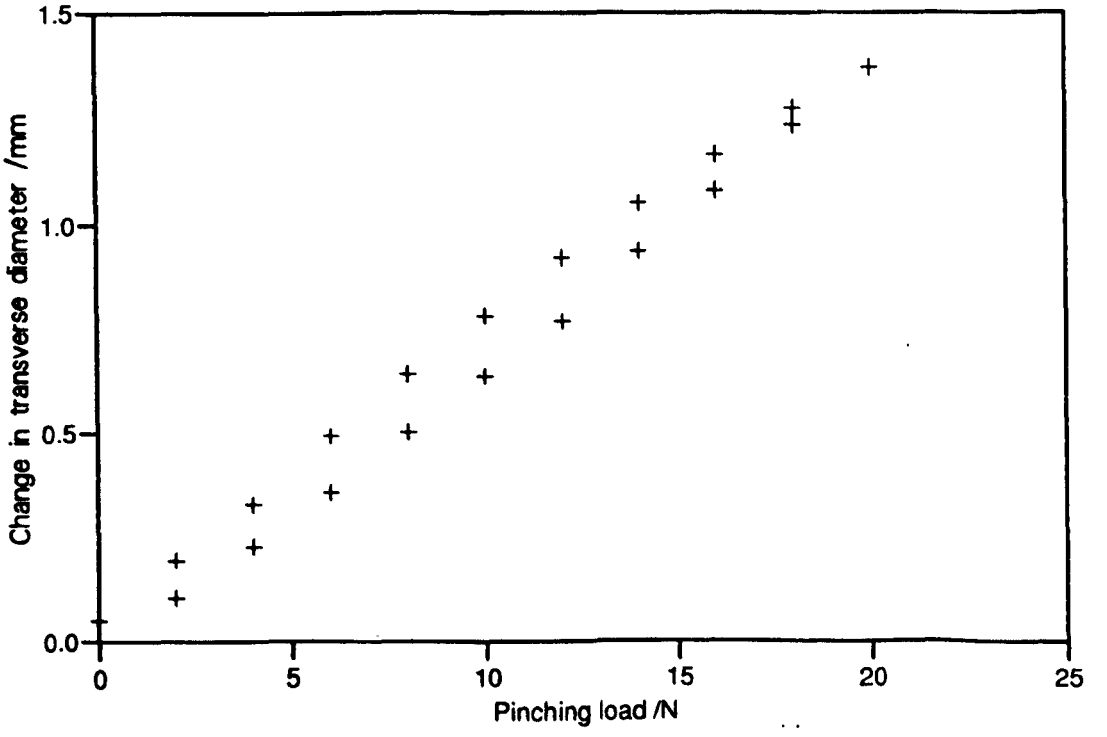

Fig. D.1: Variation of measured transverse diameter with load for pinched ring specimen with ±30° winding (plies ±60° to direction of bending stress): specimen 2 ring 6

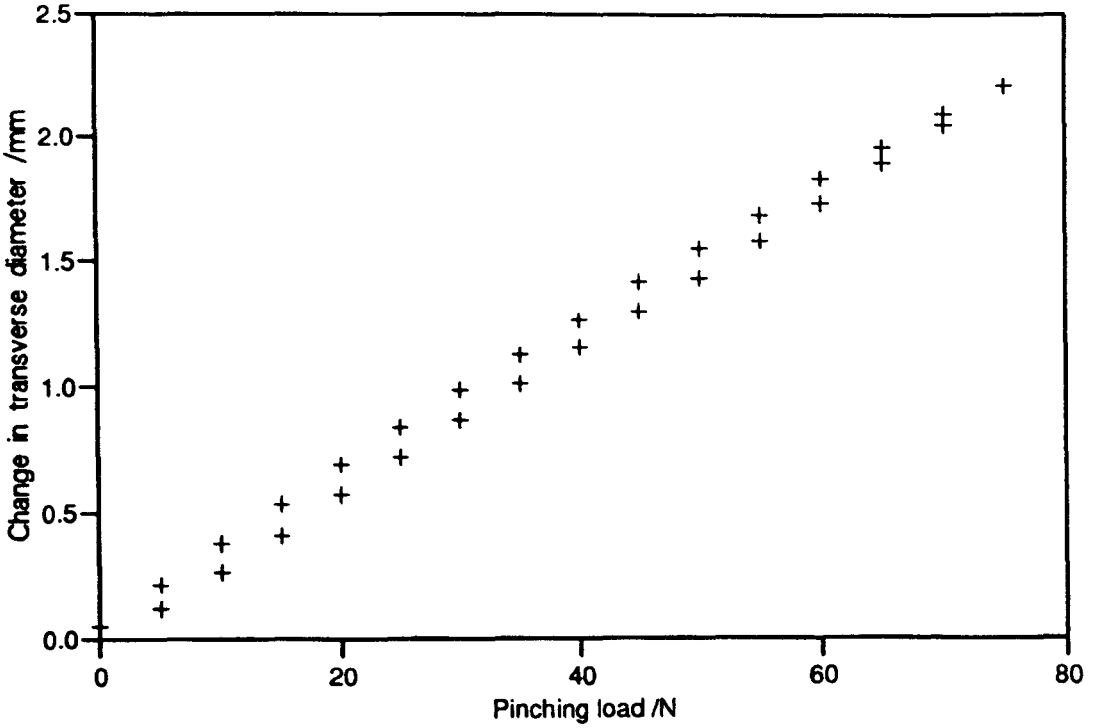

Fig. D.2: Variation of measured transverse diameter with load for pinched ring specimen with ±45° winding (plies ±45° to direction of bending stress): specimen 2 ring 5

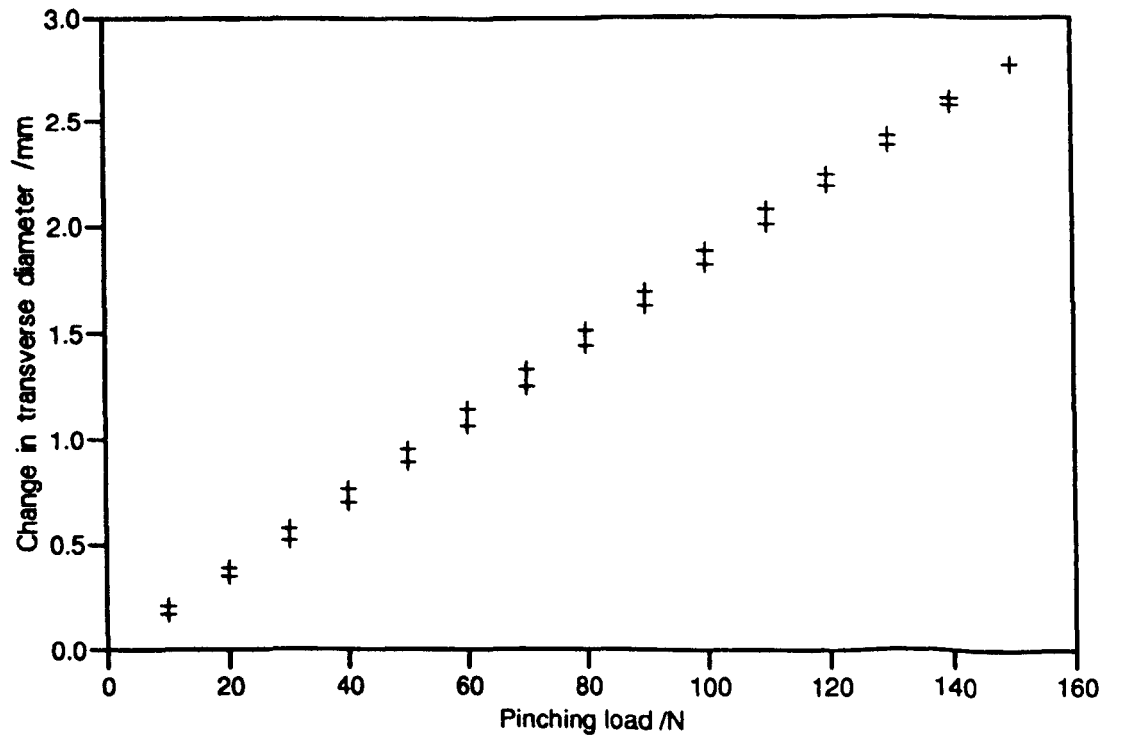

Fig. D.3: Variation of measured transverse diameter with load for pinched ring specimen with ±60° winding (plies ±30° to direction of bending stress): specimen 7 ring 4

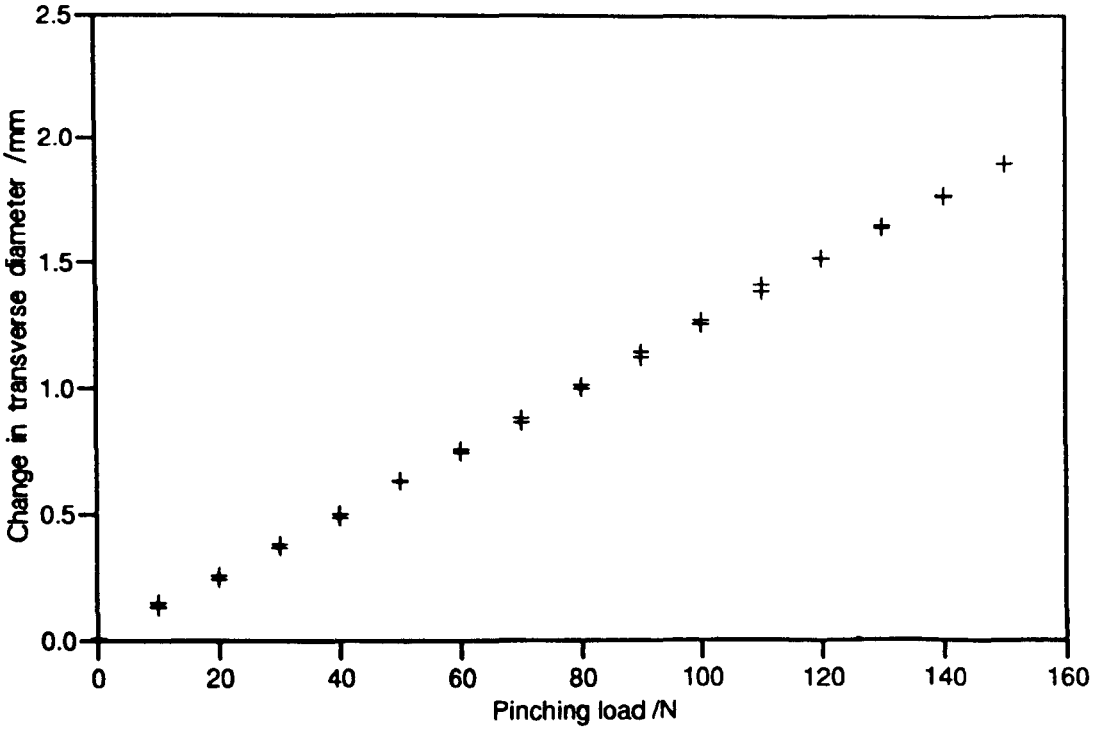

Fig. D.4: Variation of measured transverse diameter with load for pinched ring specimen with ±75° winding (plies ±15° to direction of bending stress): specimen 2 ring 3

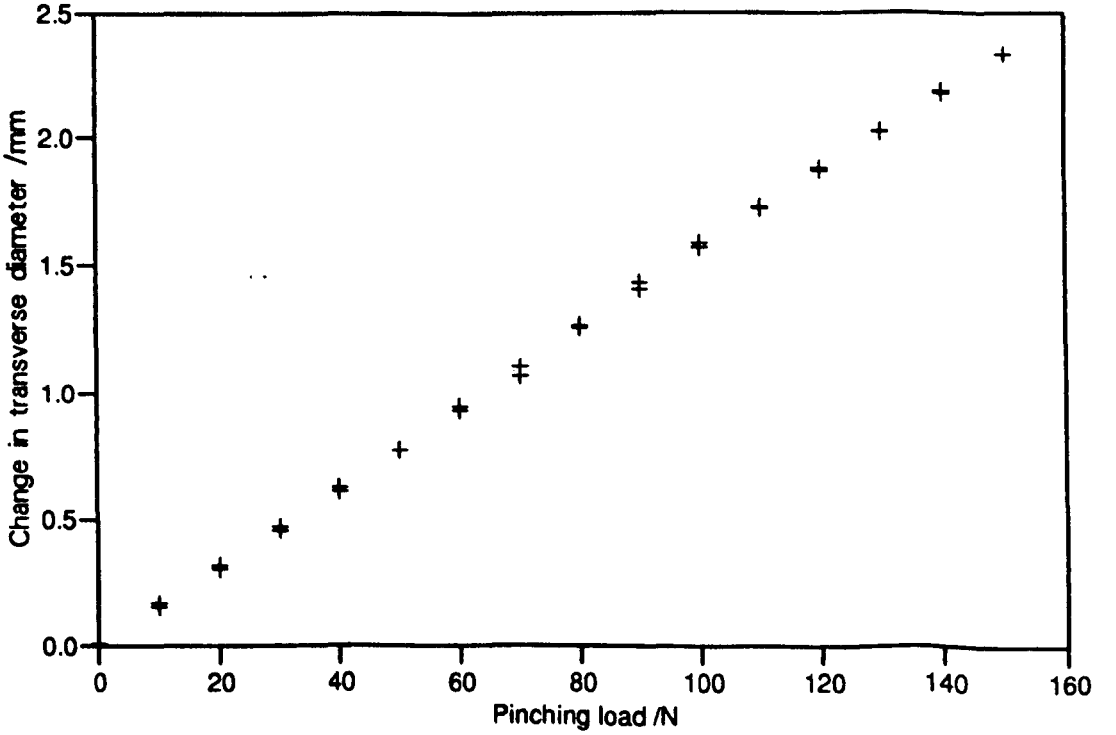

Fig. D.5: Variation of measured transverse diameter with load for pinched ring specimen with 90° (hoop) winding (fibres parallel to direction of bending stress): specimen 7 ring 5

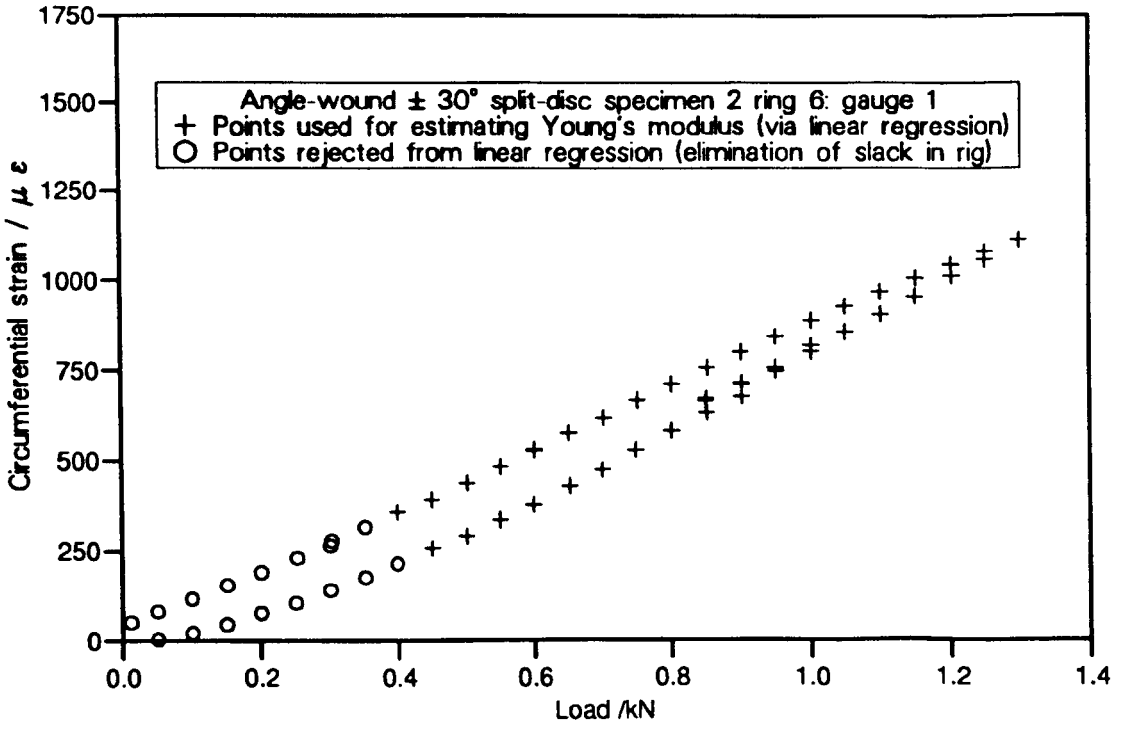

(a) Strain measured in direction of stress

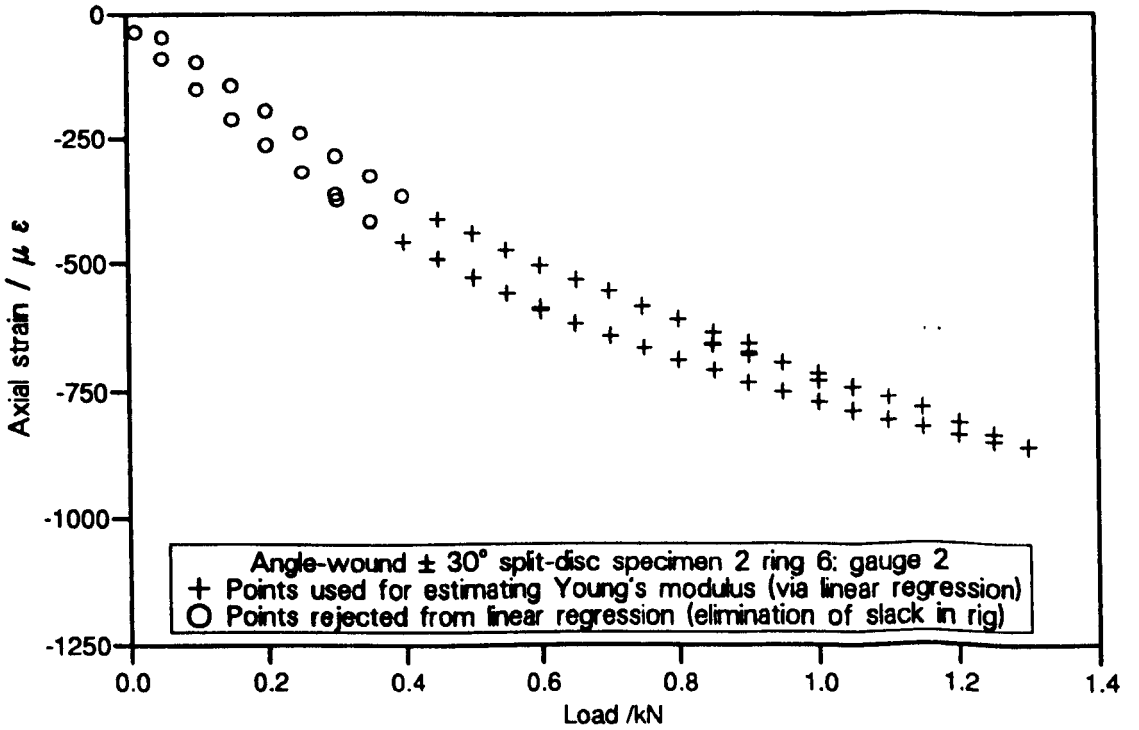

(b) Strain measured perpendicular to direction of stress

Fig. D.6: Variation of strain with load for split-disc specimen with ±30° winding angle (ply angle of ±60° with respect to applied stress): specimen 2 ring 6

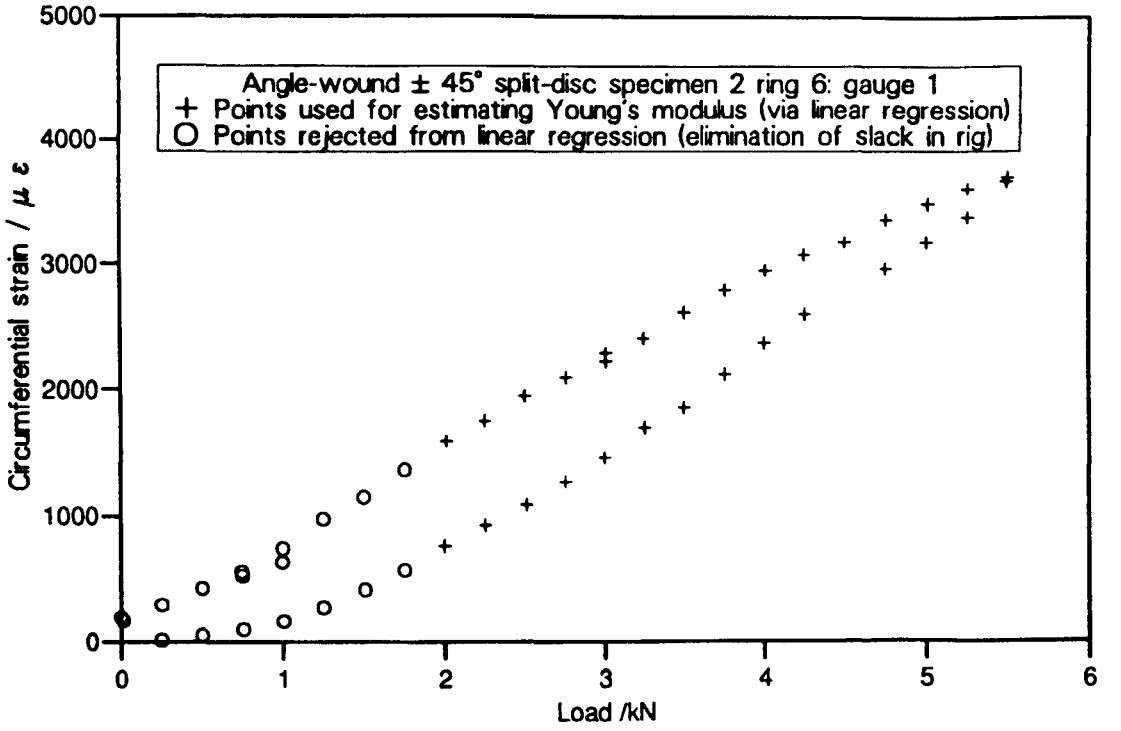

(a) Strain measured in direction of stress

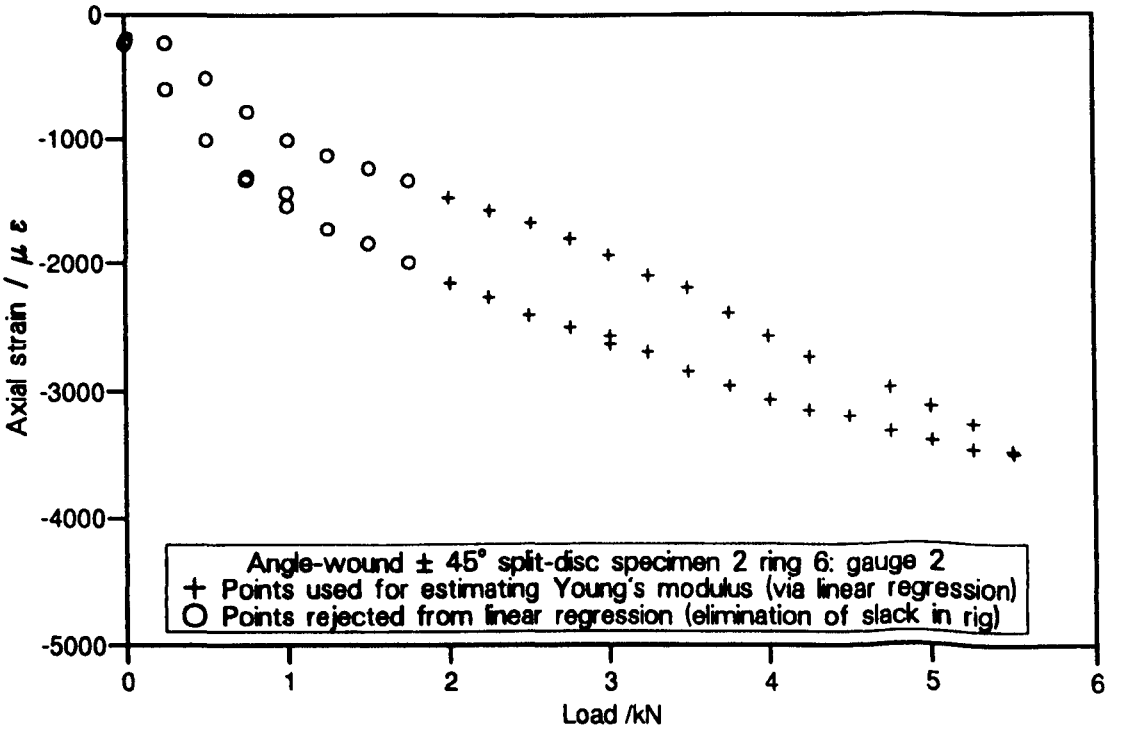

(b) Strain measured perpendicular to direction of stress

Fig. D.7: Variation of strain with load for split-disc specimen with ±45° winding angle (ply angle of ±45° with respect to applied stress): specimen 2 ring 6

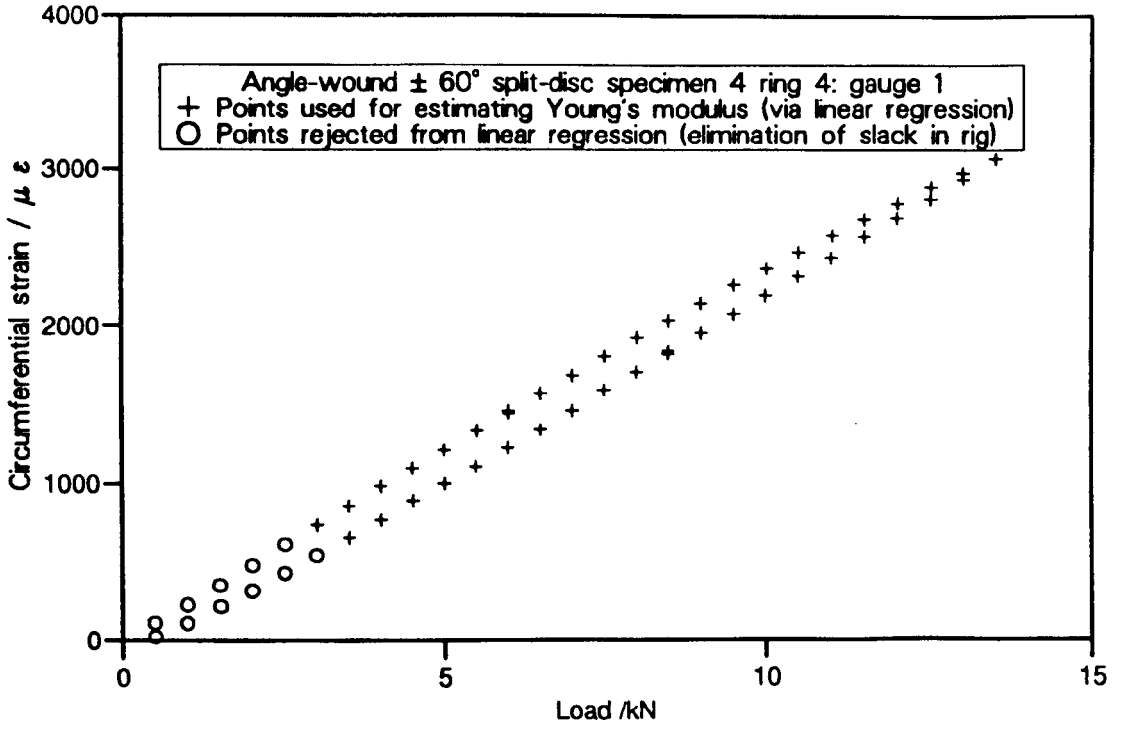

(a) Strain measured in direction of stress

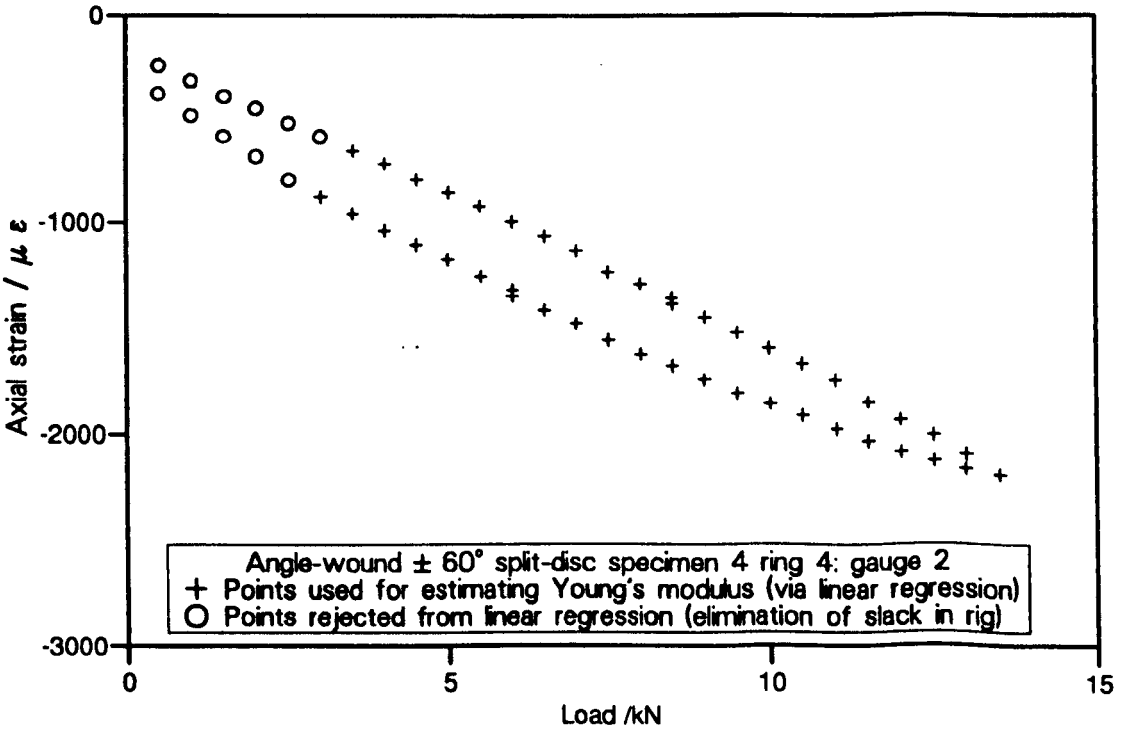

(b) Strain measured perpendicular to direction of stress

Fig. D.8: Variation of strain with load for split-disc specimen with ±60° winding angle (ply angle of ±30° with respect to applied stress): specimen 4 ring 4

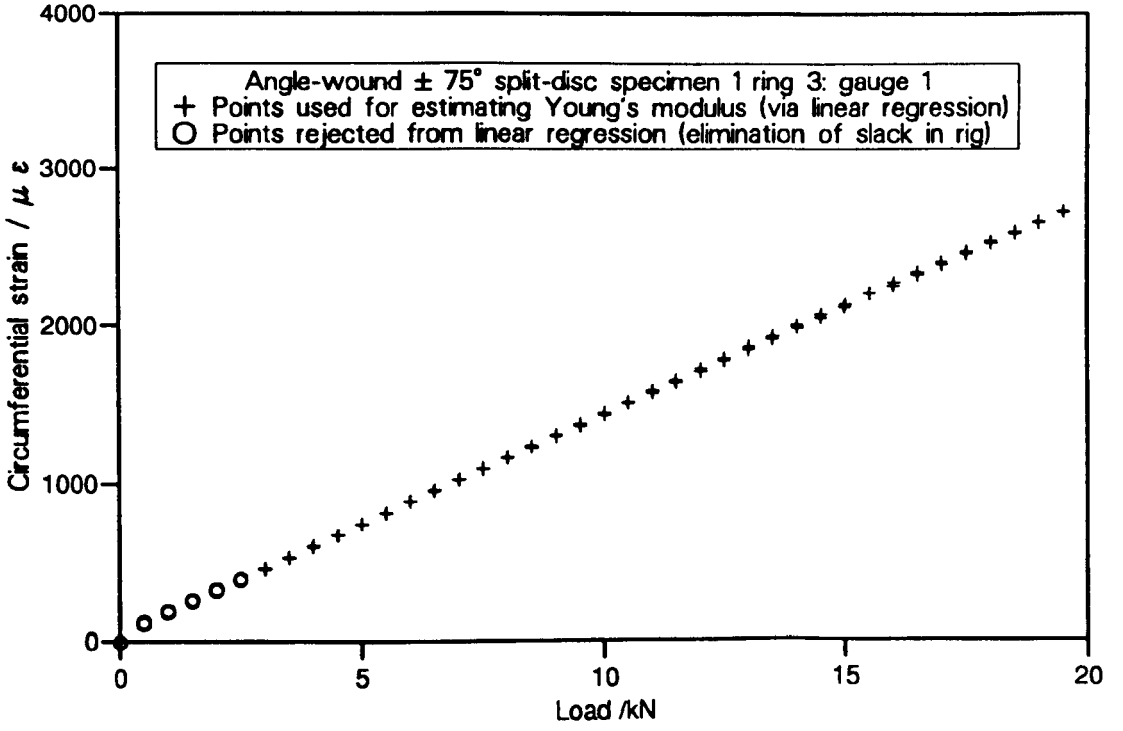

(a) Strain measured in direction of stress

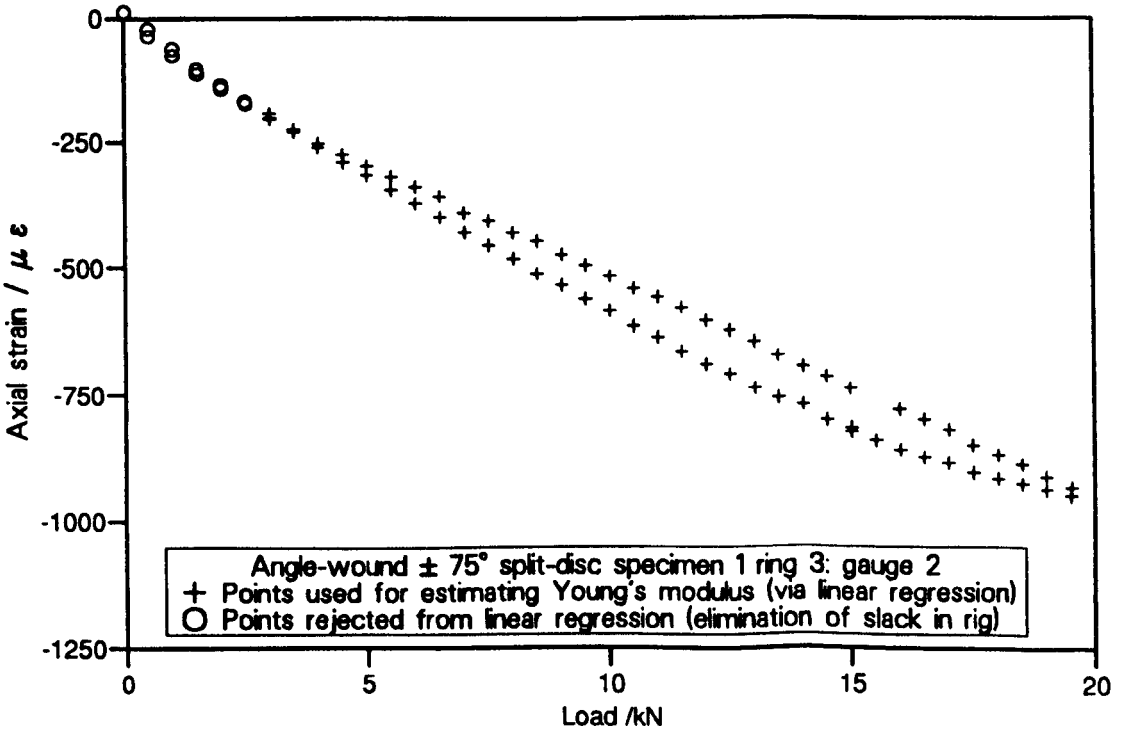

(b) Strain measured perpendicular to direction of stress

Fig. D.9: Variation of strain with load for split-disc specimen with ±75° winding angle (ply angle of ±75° with respect to applied stress): specimen 1 ring 3

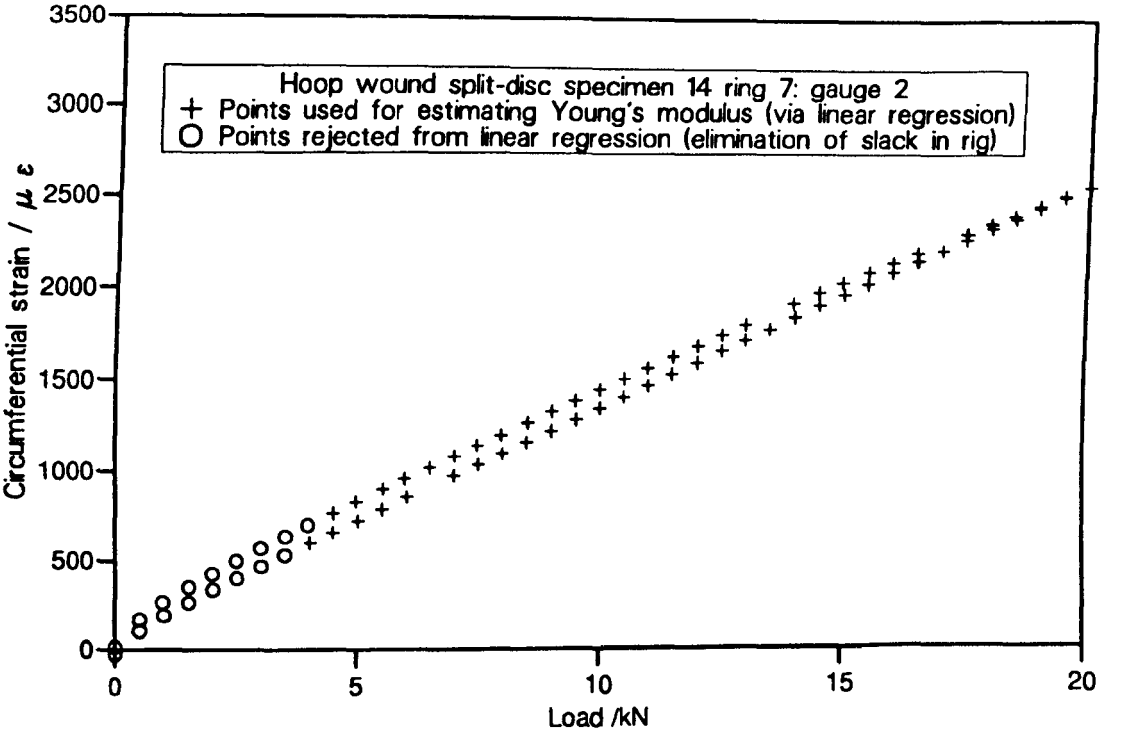

(a) Strain measured in direction of stress

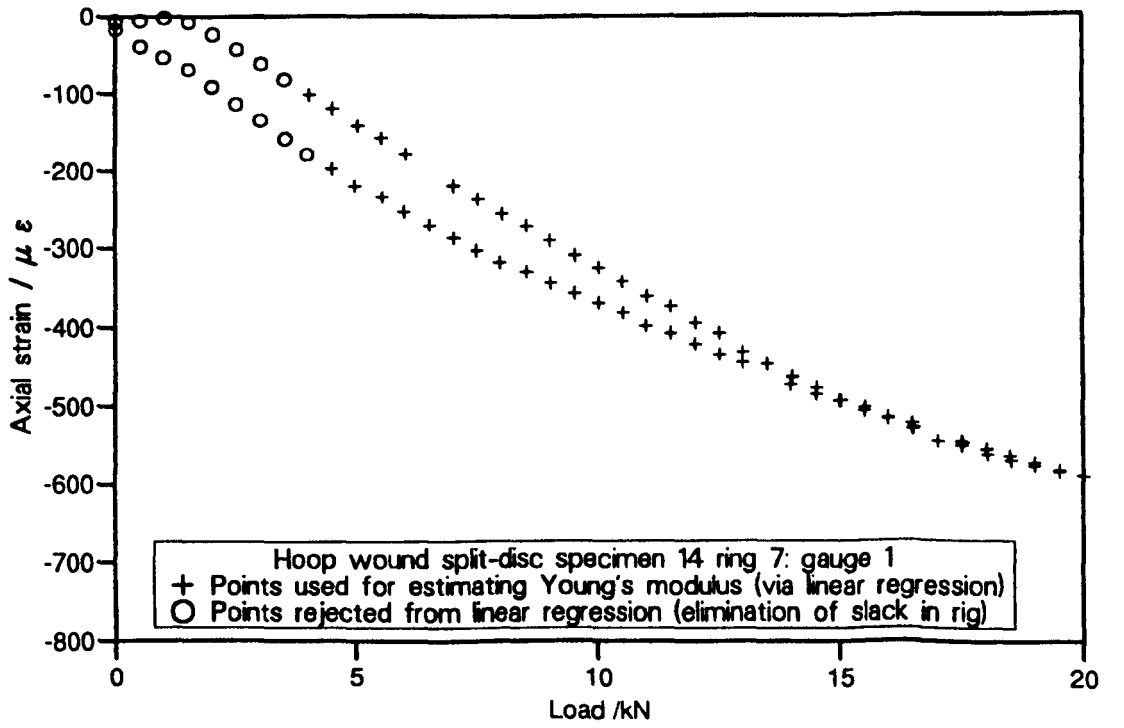

(b) Strain measured perpendicular to direction of stress

Fig. D.10: Variation of strain with load for split-disc specimen with 90° (hoop) winding (fibres parallel to direction of applied stress): specimen 14 ring 7

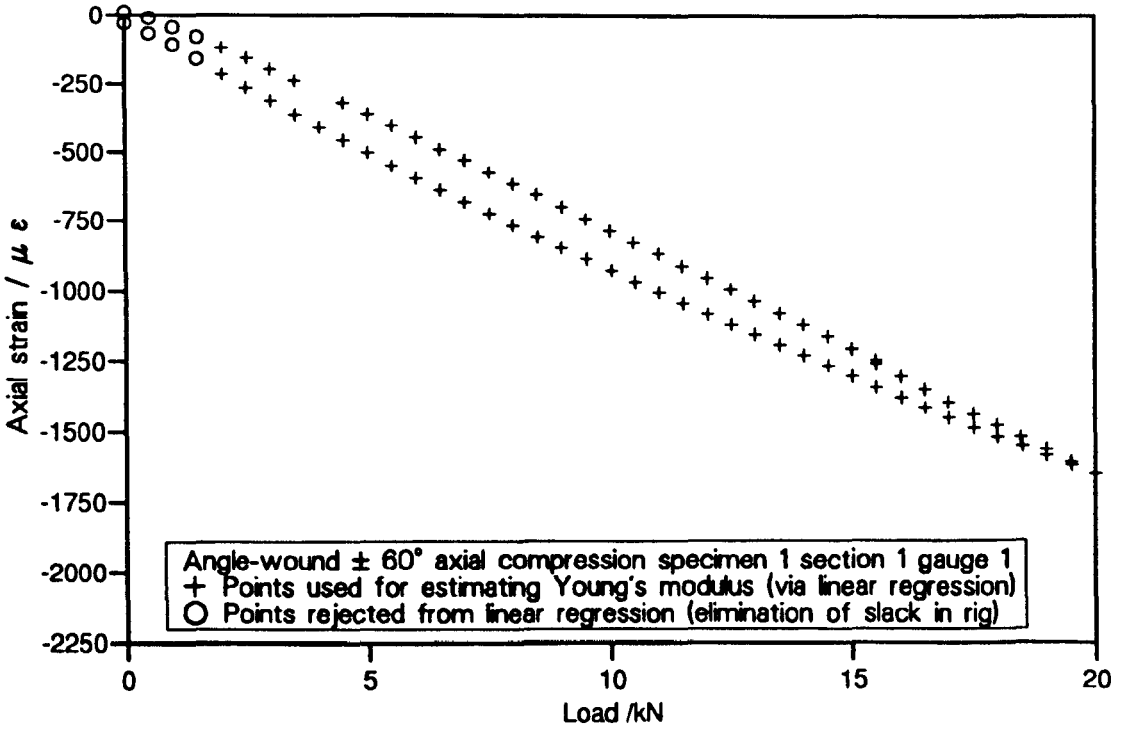

Fig. D.11: Variation of strain (in direction of stress) with load for axial compression specimen with ±60° winding (plies ±60° to direction of applied stress): specimen 1 tube 1.

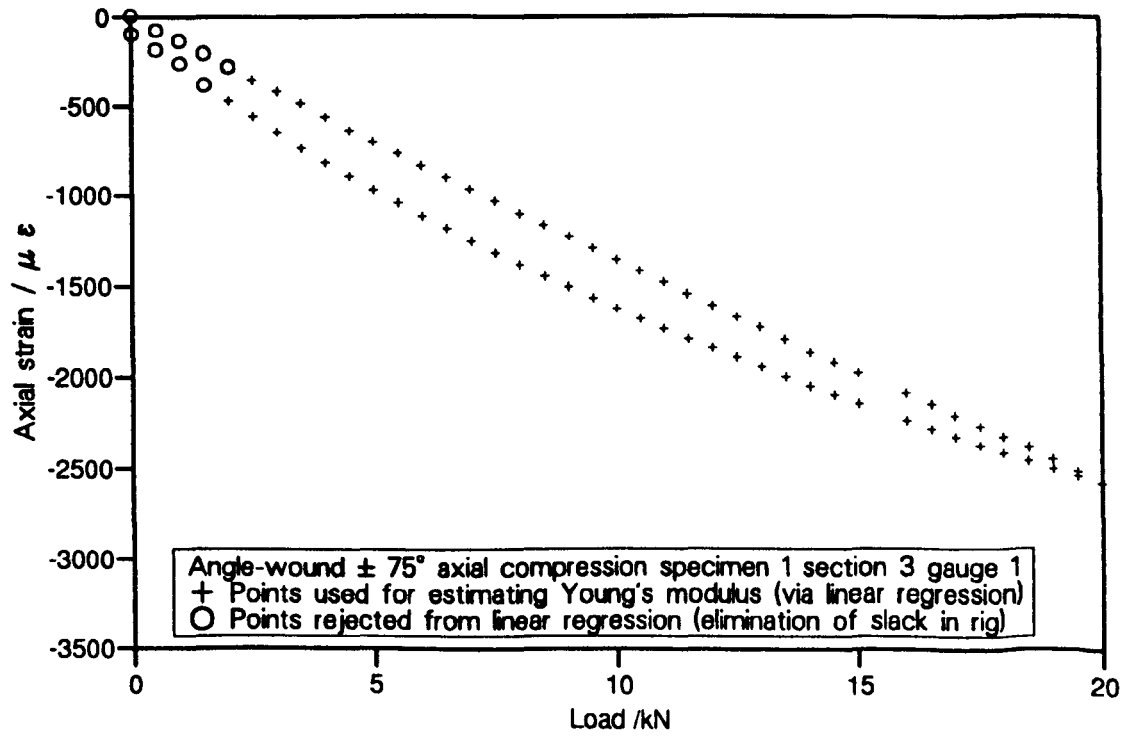

Fig. D.12: Variation of strain (in direction of stress) with load for axial compression specimen with ±75° winding (plies ±75° to direction of applied stress): specimen 1 tube 3.

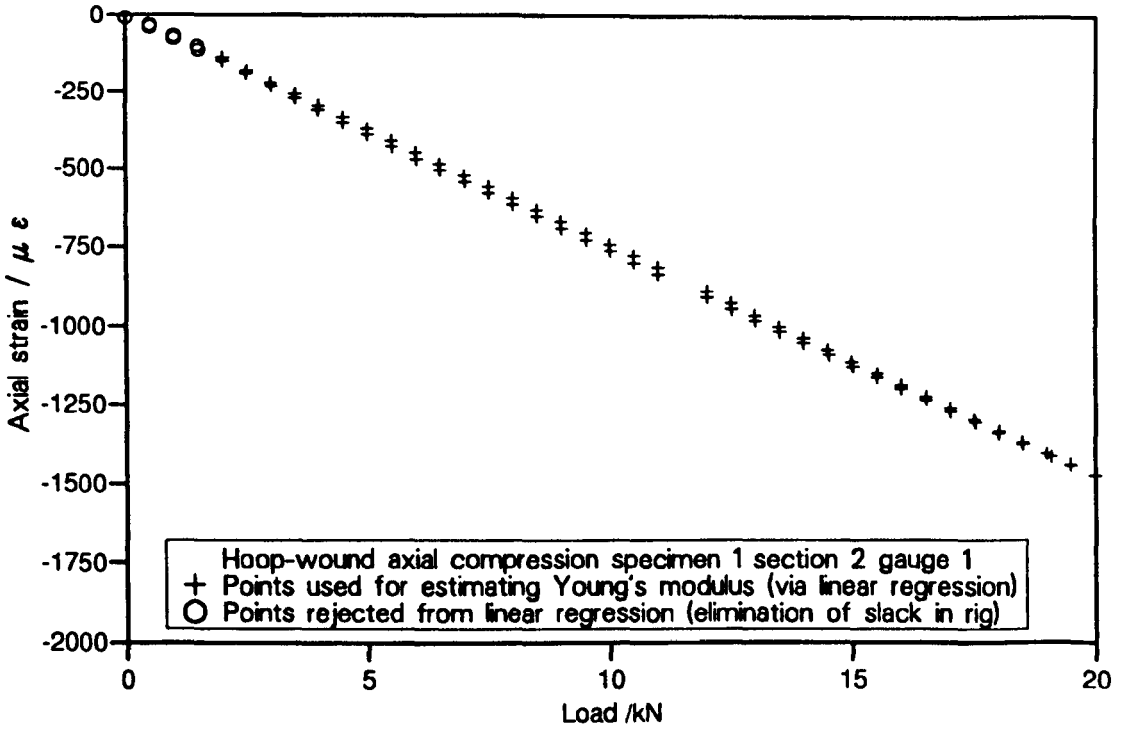

(a) Strain measured in direction of stress

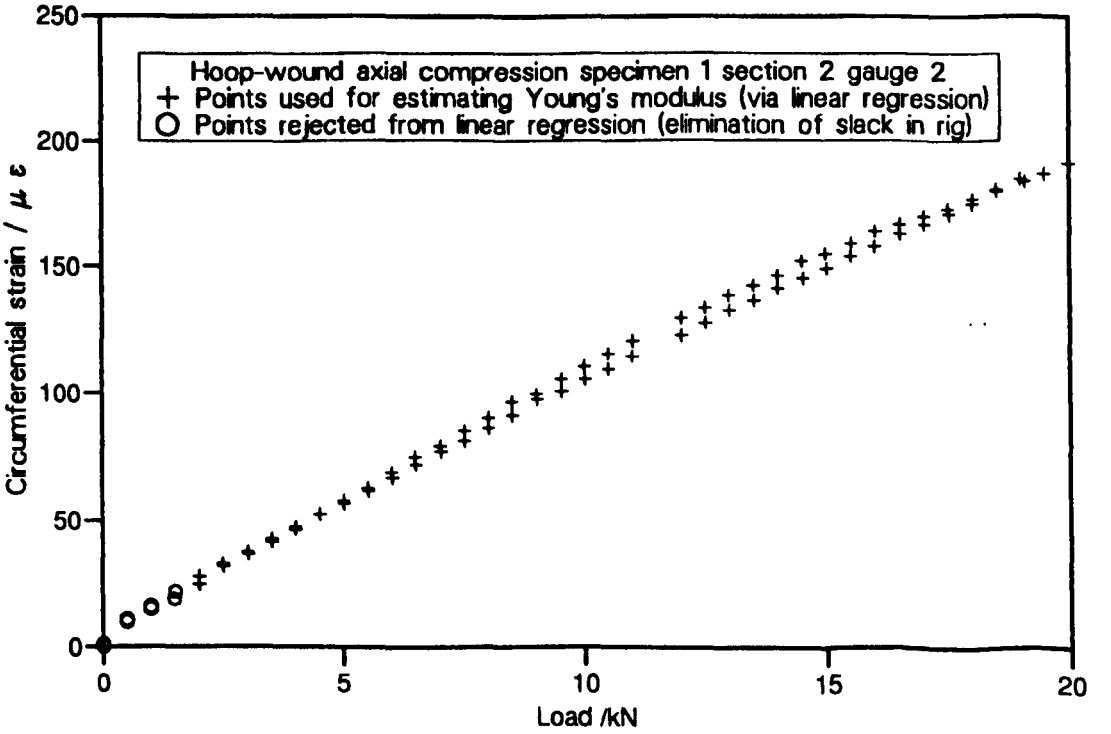

(b) Strain measured perpendicular to direction of stress

Fig. D.13: Variation of strain with load for axial compression specimen with 90° winding (fibres perpendicular to direction of applied stress): specimen 1 tube 2.

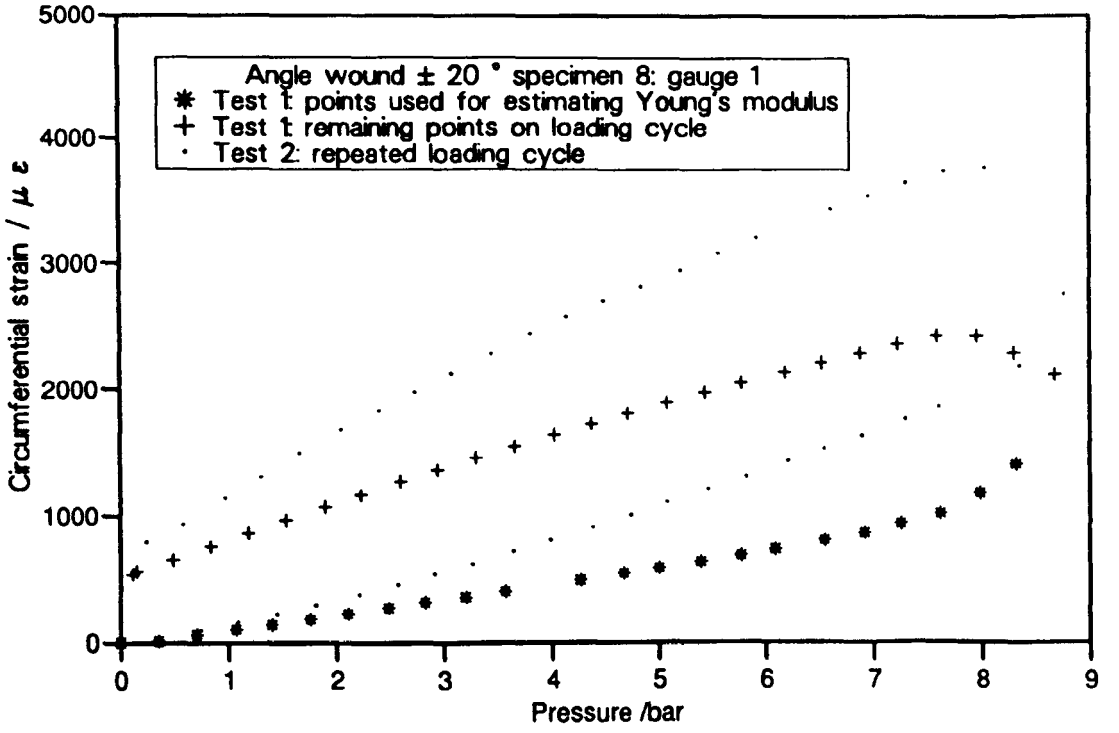

(a) Strain measured in direction of stress

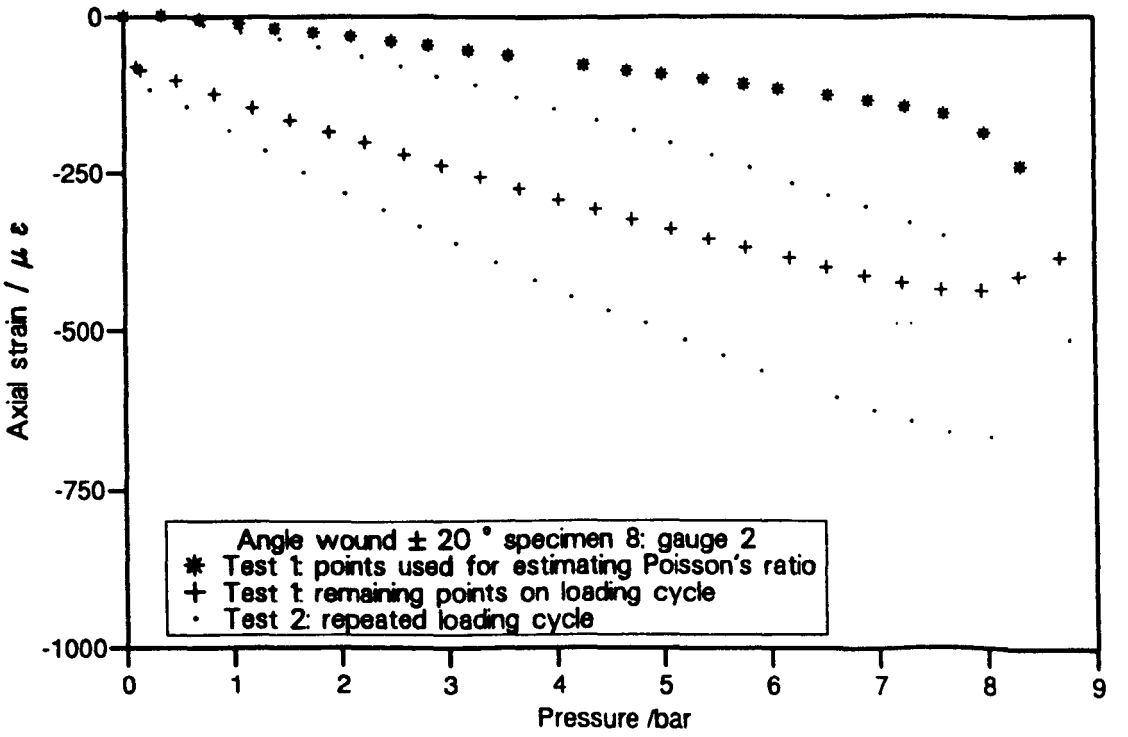

(b) Strain measured perpendicular to direction of stress

Fig. D.14: Variation of strain with pressure for open-ended pressure specimen 8 with ±20° winding angle (ply angle of ±70° with respect to applied stress)

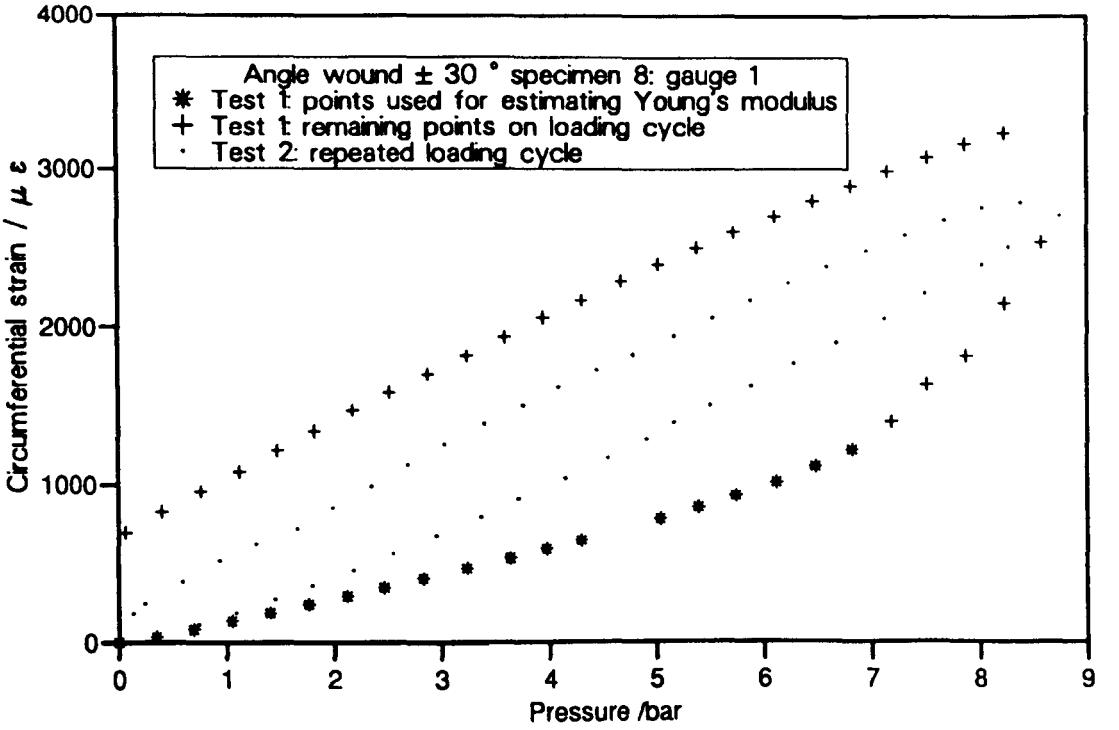

(a) Strain measured in direction of stress

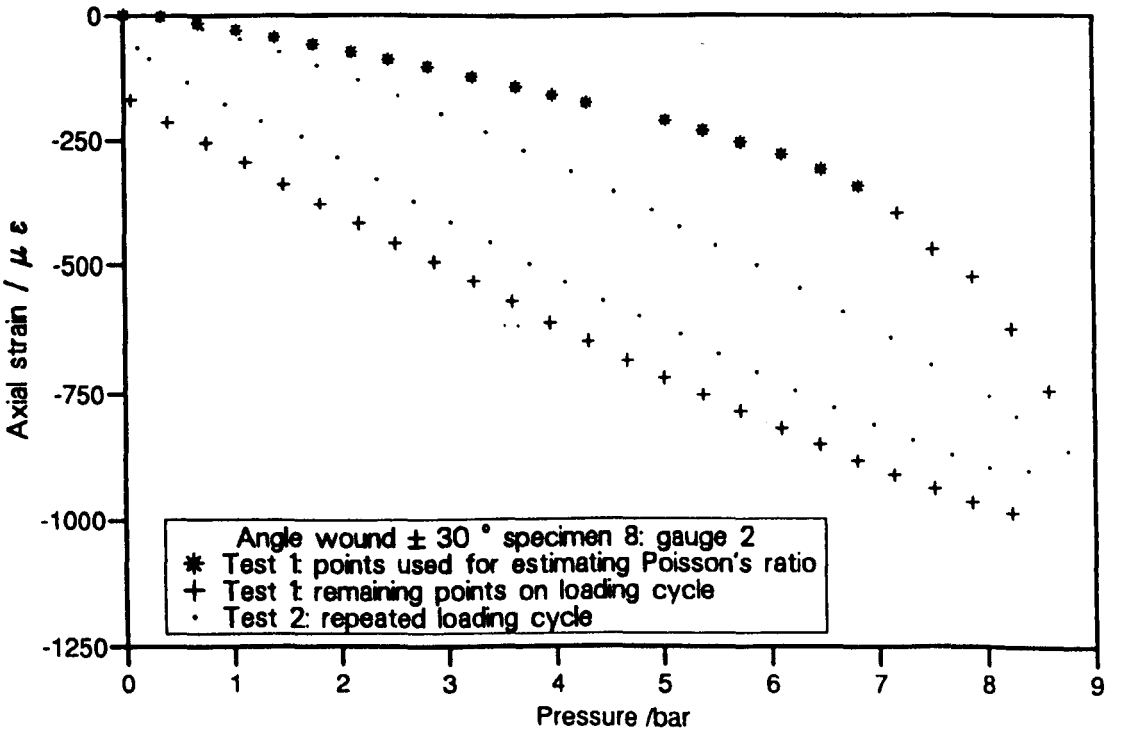

(b) Strain measured perpendicular to direction of stress

Fig. D.15: Variation of strain with pressure for open-ended pressure specimen 8 with ±30° winding angle (ply angle of ±60° with respect to applied stress)

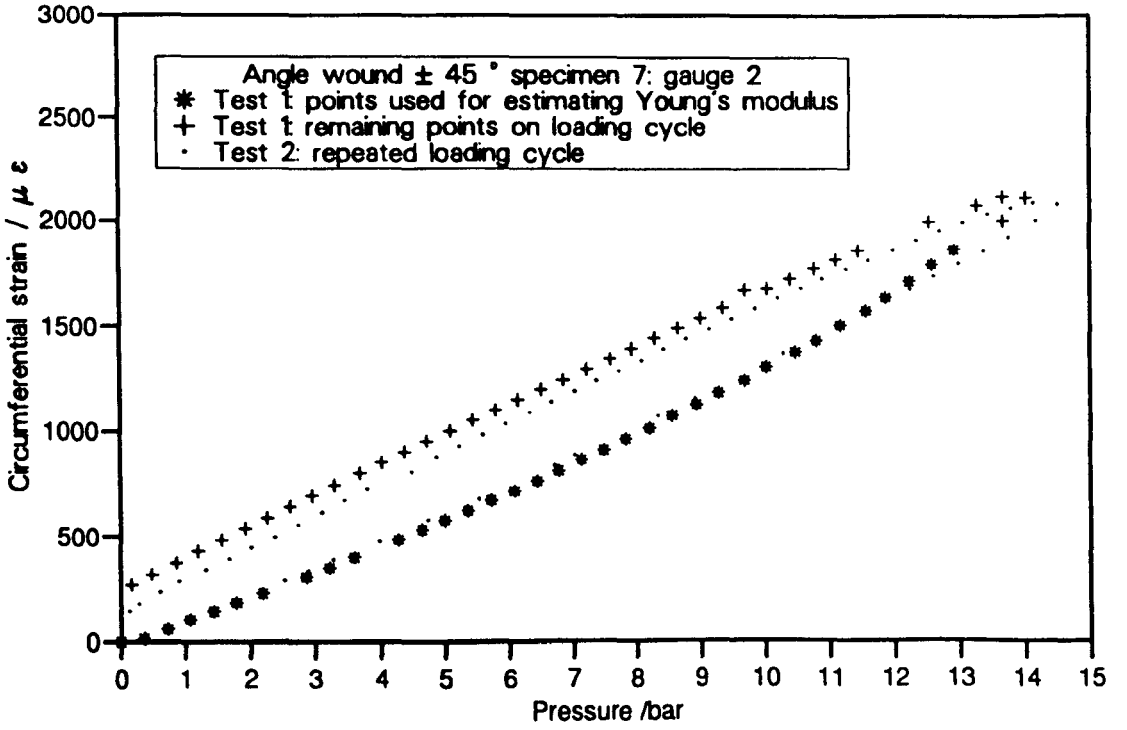

(a) Strain measured in direction of stress

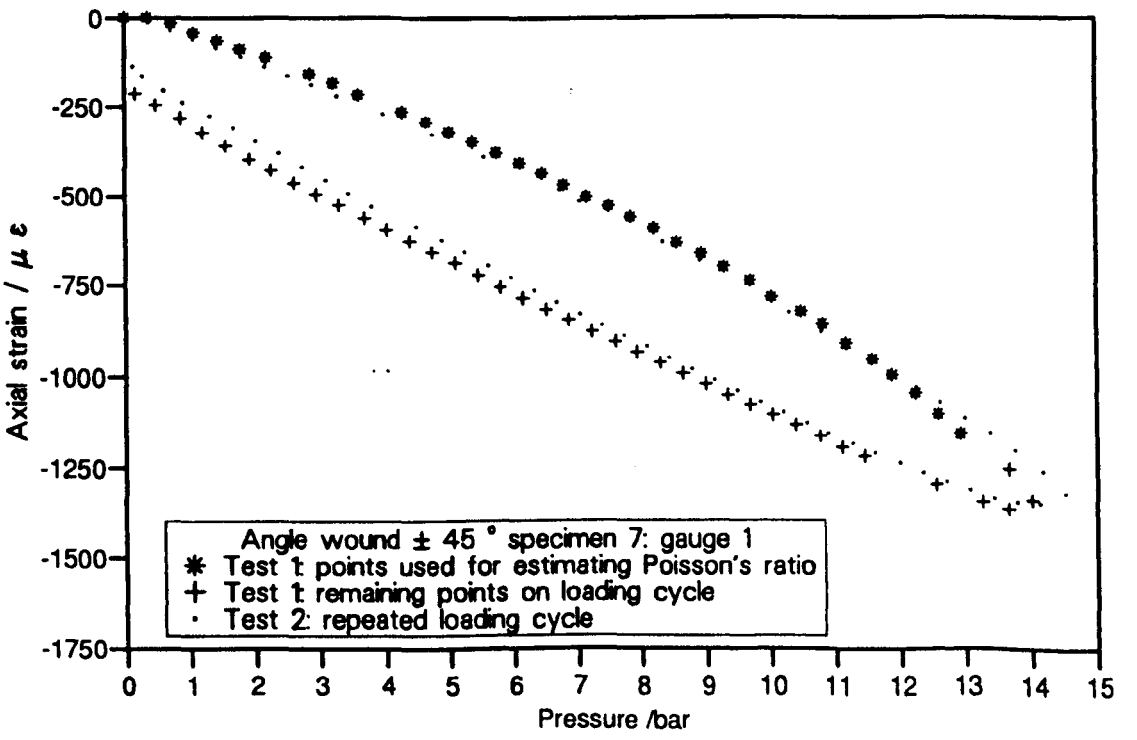

(b) Strain measured perpendicular to direction of stress

Fig. D.16: Variation of strain with pressure for open-ended pressure specimen 7 with ±45° winding angle (ply angle of ±45° with respect to applied stress)

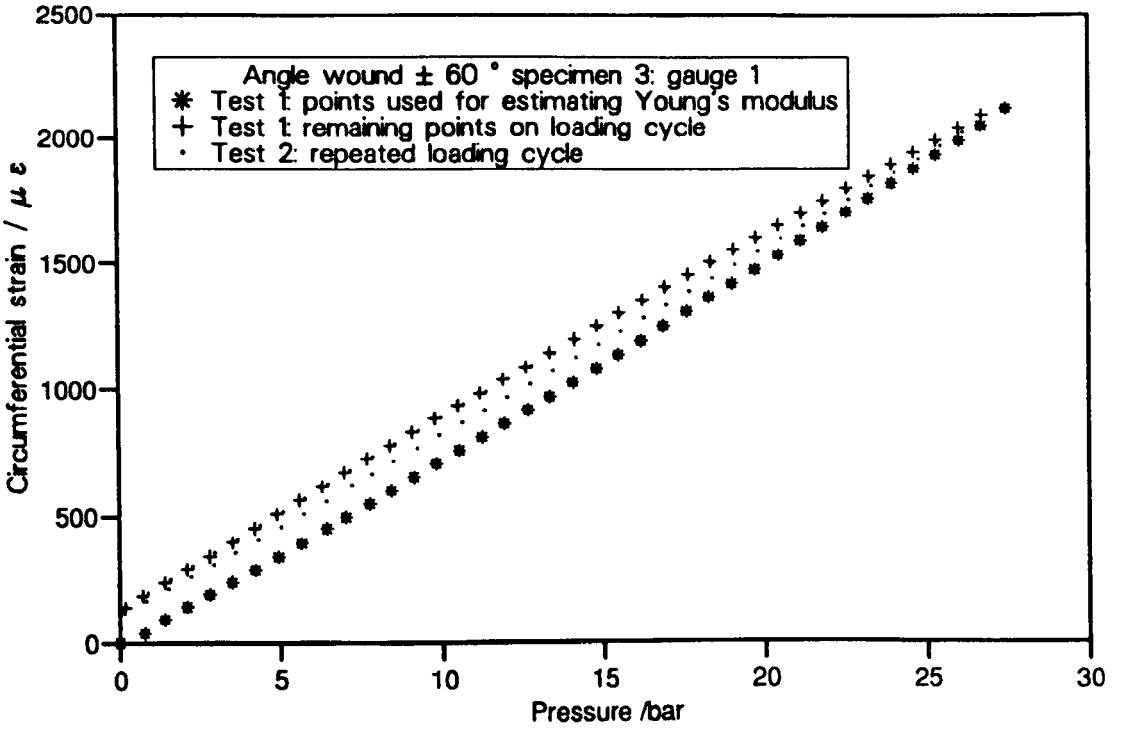

(a) Strain measured in direction of stress

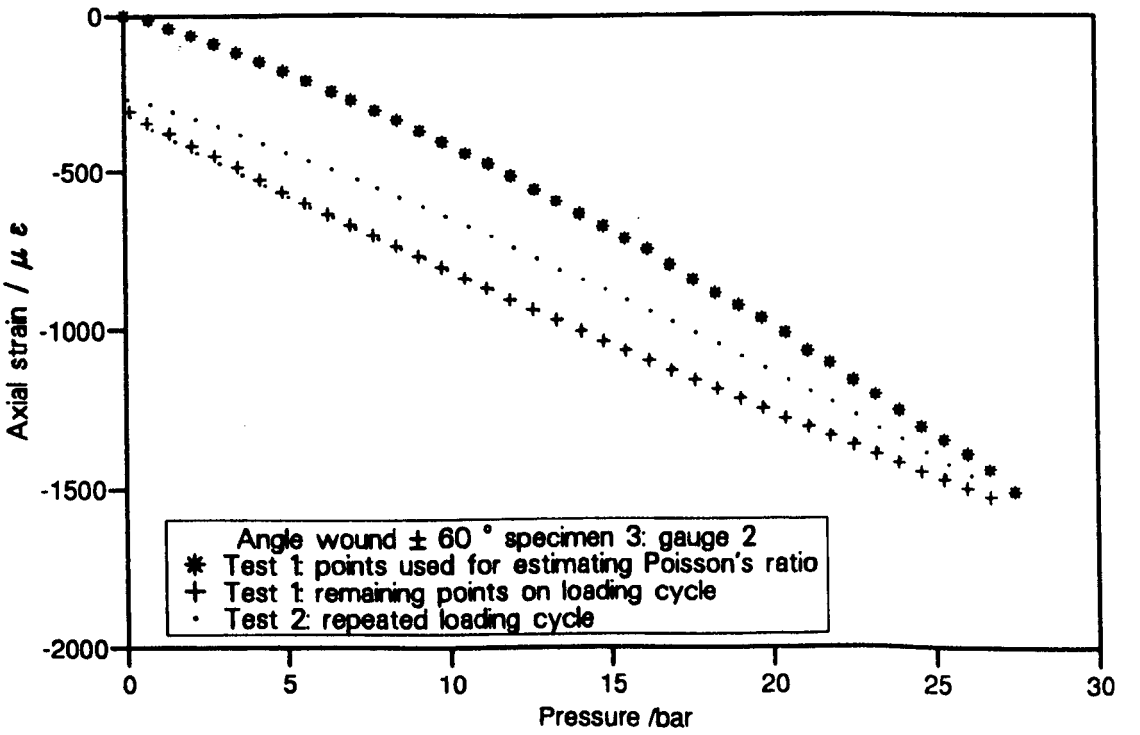

(b) Strain measured perpendicular to direction of stress

Fig. D.17: Variation of strain with pressure for open-ended pressure specimen 7 with ±60° winding angle (ply angle of ±30° with respect to applied stress)

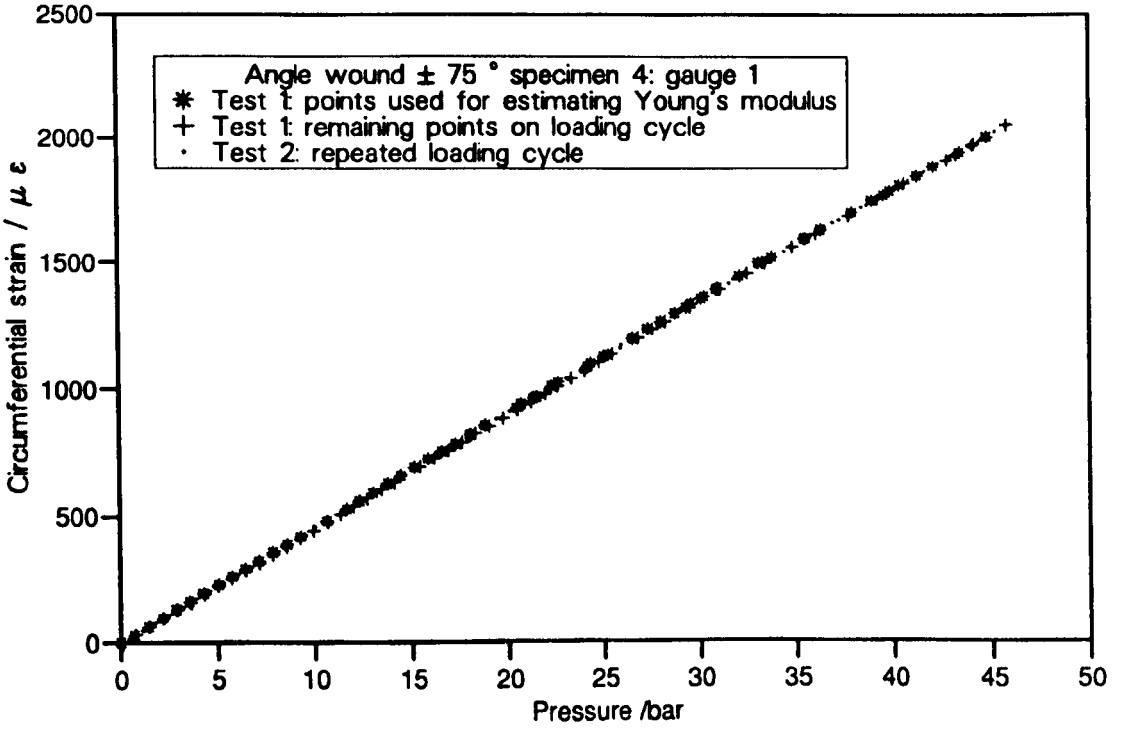

(a) Strain measured in direction of stress

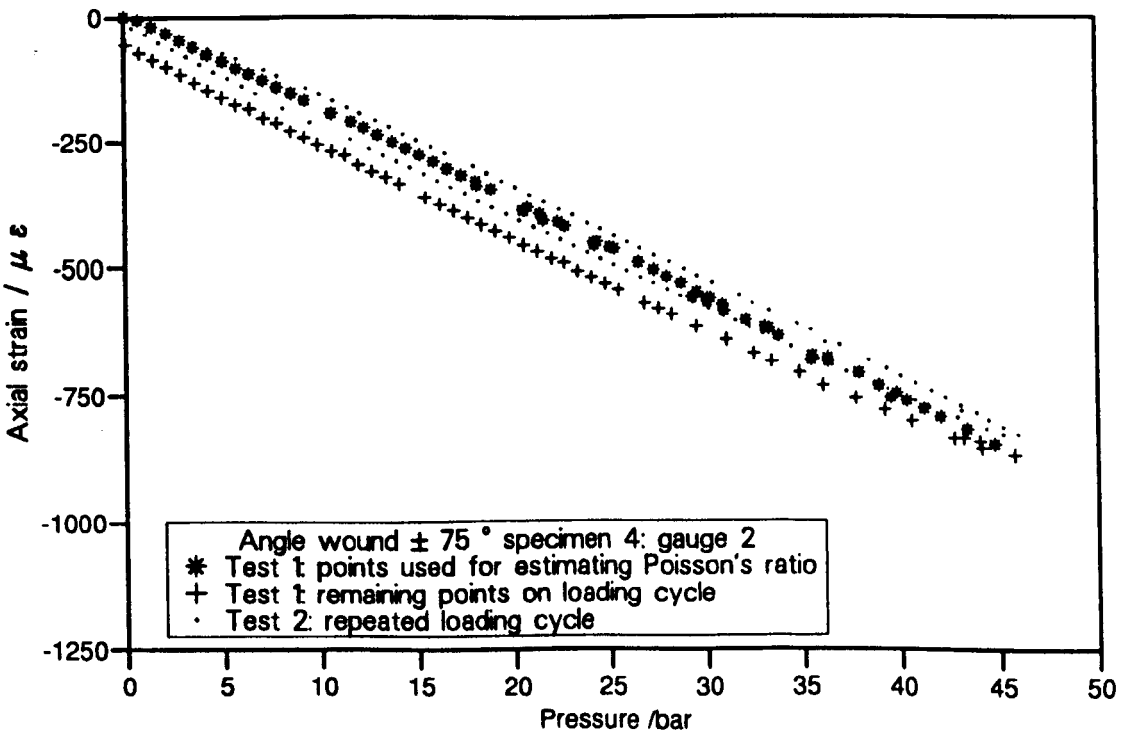

(b) Strain measured perpendicular to direction of stress

Fig. D.18: Variation of strain with pressure for open-ended pressure specimen 4 with ±75° winding angle (ply angle of ±15° with respect to applied stress)

APPENDIX E: STRAIN DISTRIBUTIONS IN OPEN-ENDED PRESSURE SPECIMENS AND ROLLER-ASSISTED SPLIT DISC SPECIMENS

E.1 Strain distribution in an open-ended pressure specimen

It is assumed that tube expands radially by a distance δ with negligible change in thickness (Fig. E.1). Typical inner and outer radii of the tube are r_i = 56 mm, r_o = 58.8 mm. The ratio of internal to external strains is calculated:

$$(\varepsilon_\theta)_i = \frac{\delta}{r_i} \quad \text{and} \quad (\varepsilon_\theta)_o = \frac{\delta}{r_o} \quad \therefore \quad \frac{(\varepsilon_\theta)_i}{(\varepsilon_\theta)_o} = \frac{r_o}{r_i} = \frac{58.8}{56} = 1.05 \qquad \text{(E.1)}$$

i.e. there is a 5% variation in strain from the inside to the outside of the cylinder.

E.2 Strain distribution in roller-assisted split disc specimen

It is assumed that the change in thickness of the specimen is negligible, and that a portion of the specimen subtends an angle θ around the dee (Fig. E.2). As the ring is stretched to subtend an angle $\theta + \delta\theta$, the inner and outer radii remain constant. The inner and outer surfaces increase in length by $r_i\delta\theta$ and $r_o\delta\theta$ respectively, hence the strains at the inner and outer surfaces are equal:

$$(\varepsilon_\theta)_i = \frac{r_i\delta\theta}{r_i\theta} = \frac{\delta\theta}{\theta} \quad \text{and} \quad (\varepsilon_\theta)_o = \frac{r_o\delta\theta}{r_o\theta} = \frac{\delta\theta}{\theta} \qquad \text{(E.2)}$$

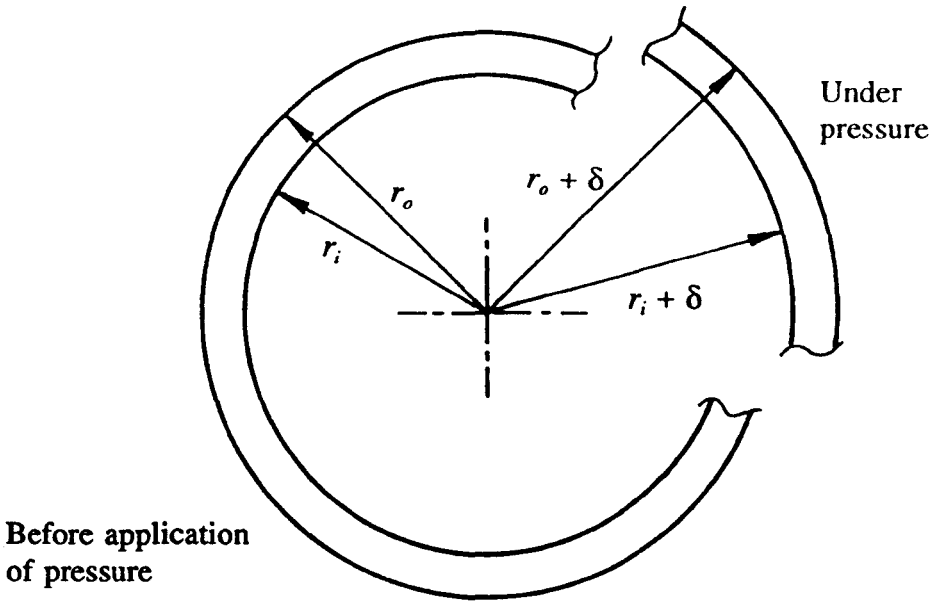

Fig. E.1: Cylindrical shell under internal pressure, assuming change in thickness to be negligible compared with radial movement

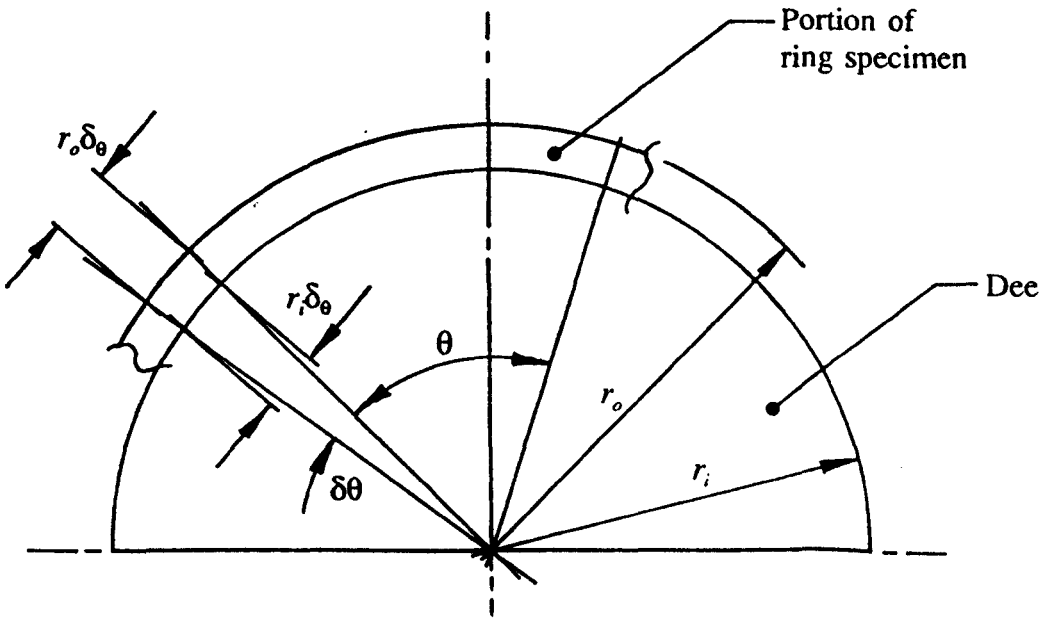

Fig. E.2: Portion of ring specimen being stretched around dee in roller-assisted split disc experiment (rollers omitted for clarity, change in thickness assumed to be negligible)

APPENDIX F: ESTIMATION OF ERRORS DUE TO LOCALISED BENDING OF ROLLER-ASSISTED SPLIT DISC SPECIMENS

F.1 Nomenclature for analysis of split disc specimen

For the purpose of this analysis, the following nomenclature is defined; some of the symbols take a different meaning from that which is used elsewhere in the thesis because of the specialised nature of the analysis. The nomenclature is categorised according to its main area of application in the following analysis. Commonly-used symbols (E, I etc.) take their usual meanings.

F.1.1 *Symbols used primarily in contact mechanics calculations*

a_i half-width of contact region i

d diameter of roller (equal to roller spacing)

p contact load per unit length of contact region

t thickness of ring

w width of ring

E_i^* equivalent modulus of contact region i between (in general) dissimilar materials under plane-strain conditions

P total contact load on each roller

R_d radius of a contacting surface (e.g. dee) identified by subscript

R_i equivalent radius of contacting surfaces at contact region i

T circumferential tension in ring

Δ relative movement between reference points on structure or dimensional change of a component due to contact effects

F.1.2 *Subscripts used primarily in contact mechanics calculations*

d relating to dee

p relating to ring, especially to transverse compressive properties of GRP (assumed to be isotropic for contact mechanics calculations)

r relating to roller

s relating to properties of steel

1 relating to roller/ring interface

2 relating to roller/dee interface

F.1.3 *Symbols used primarily in beam-on-elastic-foundation analysis*

x position along "beam" from loading point

A cross-sectional area of ring

M bending moment in "beam" consisting of ring cross-section

R_{ring} mid-surface radius of ring

α decay factor (degree of localisation of bending effects)

β periodicity of oscillations of bending effects

θ an angle; slope of "beam" due to applied load

F.1.4 *Subscripts used primarily in beam-on-elastic-foundation analysis*

x, θ relating to meridional and circumferential orthotropic properties of GRP ring (used for evaluation of flexural rigidity)

0 relating to end of "beam" (x=0).

Other subscripts in the form of text are assumed to be self-explanatory.

F.2 Problem definition

When the ring specimen in the roller-assisted split disc rig undergoes strain, the "inner race" (formed by the dees) ceases to be circular as the dees move apart. Localised bending effects therefore occur in the region of the split line (Fig. F.1) and it is necessary to establish the severity and extent of these effects.

F.3 Approach to solution

The ring is treated as a beam on an elastic foundation composed of the needle rollers (Fig. F.2). The foundation modulus of the bed of needle rollers (linearised to consider only small perturbations of loading under the maximum-load conditions) is found using a contact mechanics approach. The "elastic foundation" is considered as a

continuum, although the periodicity of the deflections of the ring is found to be of the same order of magnitude as the roller spacing and hence the results of this calculation can only be considered as very approximate.

F.4 Assumptions and simplification

F.4.1. In order to utilise existing solutions, and because this calculation is intended as no more than a first approximation to the true situation, it was decided to treat the filament-wound ring as being isotropic for the purpose of the contact calculations. The Young's modulus is assumed to be approximately equal to its transverse Young's modulus, and a Poisson's ration of 0.3 is also assumed.

F.4.2 The reference points (between which the relative movement of beam and foundation is defined) were chosen as the mid-surface of the ring and the centre of the dee. The deformation of the dee contributes very little to the total movement and the latter reference point was chosen to simplify the analysis.

F.4.3 The beam (i.e. the ring) is assumed to be thin and no shear deformation is considered. This makes the analysis manageable but is likely to lead to significant inaccuracies since the periodicity of the deformations is of similar magnitude to the beam thickness.

F.4.4 The ring is treated (in the contact analysis) as an elastic half-space since its thickness is approximately 45 times greater than the width of its contact with the roller.

F.4.5 The rollers, ring and dee are assumed to be sufficiently deep that plane strain conditions apply in the analysis of contact.

F.4.6. The circumferential tension is assumed to maintain contact forces between the ring, rollers and dee which are sufficiently large to prevent the ring from lifting clear of the rollers. It should be noted that the rollers cannot

provide a net inward force on the ring, and the beam-on-elastic-foundation analysis considers small perturbations of the contact forces about their nominal value.

F.5 Data

Inner radius of ring	$= R_p$	= -56.05 mm (negative ⇔ concave surface)
Radius of roller	$= R_r$	= 1.525 mm
Radius of dee	$= R_d$	= 54.525 mm
Thickness of ring	$= t$	= 2.8 mm
Width of ring	$= w$	= 30 mm

Assume transverse (meridional) Young's modulus of ring = $E_x = E_p$ = 10000 MNm^{-2}

Circumferential Young's modulus of ring = E_θ = 50000 MNm^{-2}

Assume major Poisson's ratio of ring = $\nu_{\theta x} = \nu_p = 0.3$

Young's modulus of steel = E_s = 207000 MNm^{-2}

Poisson's ratio of steel = $\nu_s = 0.3$

Maximum load applied to apparatus = 20 kN.

F.6 Analysis

F.6.1 *Equivalent moduli and radii*

Using conventional contact mechanics notation[117], equivalent values of plane-strain modulus and surface radius are defined (Fig. F.3).

Roller/ring interface:

$$E_1^* = \frac{1}{\frac{1-\nu_p^2}{E_p} + \frac{1-\nu_s^2}{E_s}} = 10.483\times10^3 MNm^{-2} \qquad (C.1)$$

$$R_1 = \frac{1}{\frac{1}{R_p} + \frac{1}{R_r}} = 1.5676\,mm \qquad (C.2)$$

Roller/dee interface: $$E_2^* = \frac{1}{\left(\frac{2(1-\nu_s^2)}{E_s}\right)}$$

$$= \frac{E_s}{2(1-\nu_s^2)} = 113.74\times10^3\,\text{MN/m}^2 \quad \text{(C.3)}$$

$$R_2 = \frac{1}{\frac{1}{R_r}+\frac{1}{R_d}} = 1.4823\,\text{mm} \quad \text{(C.4)}$$

F.6.2 *Contact force per unit length of roller*

Refer to Fig. F.4.

T = 10000N if total load on apparatus is 20kN.

$$P = 2T\sin\frac{\theta}{2} \approx 2T\frac{R_r}{R_d+R_r} = 2\times10000\times\frac{1.525}{53+1.525} \quad \text{(C.5)}$$

$$= 559.38\,\text{N}$$

$$\therefore\ p = \text{load per unit length of contact} = \frac{P}{w} = \frac{559.38}{30} \quad \text{(C.6)}$$

$$= 18.646\,\text{N/mm}$$

F.6.3 *Widths of contact areas*

Refer to Fig. F.5.

$$a_1 = \sqrt{\frac{4pR_1}{\pi E_1^*}} = 0.05958\,\text{mm};\quad a_2 = \sqrt{\frac{4pR_2}{\pi E_2^*}} = 0.01759\,\text{mm} \quad \text{(C.7) (a\&b)}$$

F.6.4 *Relative movement of components under load*

Refer to Fig. F.6. Movement between mid-thickness of ring and centre of dee under load per unit length p is given by:

$$\Delta_{total} = \Delta_{roller} + \Delta_{dee} + \Delta_{ring} \quad \text{where:} \tag{C.8}$$

Δ_{roller} = change in diameter of roller across contacting surfaces

$$= \frac{2p(1-\nu_s^2)}{\pi E_s}\left[\ln\left(\frac{4R_r}{a_1}\right) + \ln\left(\frac{4R_r}{a_2}\right) - 1\right] \tag{C.9}$$

$$= \frac{2p(1-\nu_s^2)}{\pi E_s}\left[\ln\left(2R_r\sqrt{\frac{\pi E_1^*}{R_1}}\right) + \ln\left(2R_r\sqrt{\frac{\pi E_2^*}{R_2}}\right) - \ln p - 1\right]$$

Δ_{dee} = change in radius of dee at contacting surface

$$= \frac{p(1-\nu_s^2)}{\pi E_s}\left[2\ln\left(\frac{4R_d}{a_2}\right) - 1\right] \tag{C.10}$$

$$= \frac{p(1-\nu_s^2)}{\pi E_s}\left[2\ln\left(2R_d\sqrt{\frac{\pi E_2^*}{R_2}}\right) - \ln p - 1\right]$$

Δ_{ring} = change in half-thickness of ring from contacting surface to mid-surface

$$= \frac{p(1-\nu_p^2)}{\pi E_p}\left[2\ln\left(\frac{2\frac{t}{2}}{a_1}\right) - \frac{\nu_p}{1-\nu_p}\right] \tag{C.11}$$

$$= \frac{p(1-\nu_p^2)}{\pi E_p}\left[2\ln\left(t\sqrt{\frac{\pi E_1^*}{4R_1}}\right) - \ln p - \frac{\nu_p}{1-\nu_p}\right]$$

$$\left.\frac{d\Delta_{total}}{dp}\right|_p = \left.\frac{d\Delta_{roller}}{dp}\right|_p + \left.\frac{d\Delta_{dee}}{dp}\right|_p + \left.\frac{d\Delta_{ring}}{dp}\right|_p = \text{linearised flexibility of system}$$

$$= \frac{2(1-\nu_s^2)}{\pi E_s}\left[\ln\left(2R_r\sqrt{\frac{\pi E_1^*}{R_1}}\right) + \ln\left(2R_r\sqrt{\frac{\pi E_2^*}{R_2}}\right) - \ln p - 2\right]$$

$$+ \frac{(1-\nu_s^2)}{\pi E_s}\left[2\ln\left(2R_d\sqrt{\frac{\pi E_2^*}{R_2}}\right) - \ln p - 2\right]$$

$$+ \frac{(1-\nu_p)}{\pi E_p}\left[2\ln\left(t\sqrt{\frac{\pi E_1^*}{4R_1}}\right) - \ln p - \frac{\nu_p}{1-\nu_p} - 1\right]$$

$$= 2.290\times10^{-4}\ \text{mm}^2/\text{N} \quad \text{for given numerical values} \qquad \text{(C.12)}$$

$$\therefore \text{ for 30 mm wide rollers and ring: } \frac{d\Delta_{total}}{dP} = \frac{2.290\times10^{-4}}{30} = 7.63\times10^{-6}\ \text{mm/N} \qquad \text{(C.13)}$$

F.6.5 *Modelling of ring as beam on elastic foundation*[118]

The foundation modulus of the "bed" of rollers is calculated, treating the structure as a continuum:

$$k = \frac{dP}{d\Delta_{total}} \times \frac{1}{d_r} = \frac{1}{7.63\times10^{-6}\times3.05} = 42959\ \text{Nmm}^{-2} \qquad \text{(C.14)}$$

Flexural rigidity of beam is calculated assuming full restraint against anticlastic curvature is provided by the rollers:

$$\text{F.R.} = \frac{E_\theta w t^3}{12(1-\nu_{\theta x}\nu_{x\theta})} = \frac{50\times10^3 \times 30 \times 2.8^3}{12\left(1-0.3\times\frac{0.3\times10\times10^3}{50\times10^3}\right)} = 2.794\times10^6\ \text{N mm}^2 \qquad \text{(C.15)}$$

Hetenyi[118] shows that, for a tensioned beam on an elastic foundation with an end moment M_0, the moment M at a distance x from the end is given by:

$$M = M_0 \frac{1}{3\alpha^2 - \beta^2} \frac{1}{\beta} e^{-\alpha x}\left[(3\alpha^2 - \beta)\beta\cos\beta x - (\alpha^2 - 3\beta^2)\alpha\sin\beta x\right] \quad \text{(C.16)}$$

Substituting F.R. for *EI* in original equations[118] for α and β:

$$\alpha = \sqrt{\sqrt{\frac{k}{4\text{F.R.}}} + \frac{T}{4\text{F.R}}} \quad \text{and} \quad \beta = \sqrt{\sqrt{\frac{k}{4\text{F.R.}}} - \frac{T}{4\text{F.R.}}} \quad \text{(C.17) (a\&b)}$$

$$= 0.2507\,\text{mm}^{-1} \qquad = 0.2471\,\text{mm}^{-1}$$

In this example M can be found to decay to 1% of M_0 over a distance of x = 18.4mm, and not to exceed 5% of M_0 beyond x = 8.3 mm.

F.6.6 *End slope and moment*

Under a total load of 20kN, the ring specimen will undergo a strain of:

$$\varepsilon_\theta = \frac{T}{AE_\theta} = \frac{10000}{30 \times 2.8 \times 50 \times 10^3} = 2.381 \times 10^{-3} = 2381\,\mu\varepsilon \quad \text{(C.18)}$$

and hence the dees will move apart by $\pi R_{ring} \varepsilon_\theta = \pi \times 57.45 \times 2.381 \times 10^{-3} =$ 0.429mm.

Because of symmetry, the ring must retain zero slope at the original split line even though the dees (and their centres of curvature) have moved away from this. It is assumed that contact with the dees extends as far as the original location of split line (Fig. F.7); the slope θ_0 of the ring at this point (with respect to the dee) must be 3.727 x 10^{-3} rad. Hetenyi[118] shows that the slope θ of a tensioned beam on an elastic foundation (under an end moment M_0) is given by:

$$\theta = \frac{M_0}{EI} \frac{1}{3\alpha^2 - \beta^2} \frac{1}{\beta} e^{-\alpha x}\left[2\alpha\beta\cos\beta x - (\alpha^2 - \beta^2)\sin\beta x\right] \quad \text{(C.19)}$$

Substituting F.R. for *EI* and setting $x = 0$ and $\theta = \theta_0$ yields:

$$M_0 = \frac{\text{F.R.}(3\alpha^2 - \beta^2)\theta_0}{2\alpha} = 2648\,\text{N mm} \quad \text{(C.20)}$$

F.6.7 *Stresses and strains due to localised bending moment*

At the edge of the dee the maximum bending stress is given by:

$$\hat{\sigma} = \pm\frac{6M_0}{wt^2} = \pm\frac{6\times 2648}{30\times 2.8^2} = \pm 67.55\ \text{Nmm}^{-2} \qquad \text{(C.21)}$$

Hence the maximum bending strain (assuming zero anticlastic curvature and therefore plane strain) is:

$$\hat{\varepsilon} = \frac{\sigma_\theta(1-\nu_{r\theta}\nu_{\theta r})}{E_\theta} = 1.327\times 10^{-3} = 1327\,\mu\varepsilon \qquad \text{(C.22)}$$

This corresponds to an error of 55.7% on strain due to circumferential tension alone; it can be shown that this error due to localised bending will decay to 2% at 14.4mm from the edge of the dee and becomes negligible (<0.5%) beyond 19mm from the edge.

F.7 Conclusions

It will have been observed that the periodicity of "ripples" around the ring caused by the localised bending at the split line is comparable with the spacing of the rollers and hence the above analysis is indeed only a very crude approximation to the real situation. However, the results obtained suggest that the effects of this bending are sufficiently localised that the accuracy of the strain gauge readings will not be significantly affected provided the specimens are positioned with the gauges at a reasonable distance (say 20mm or more) from the split line.

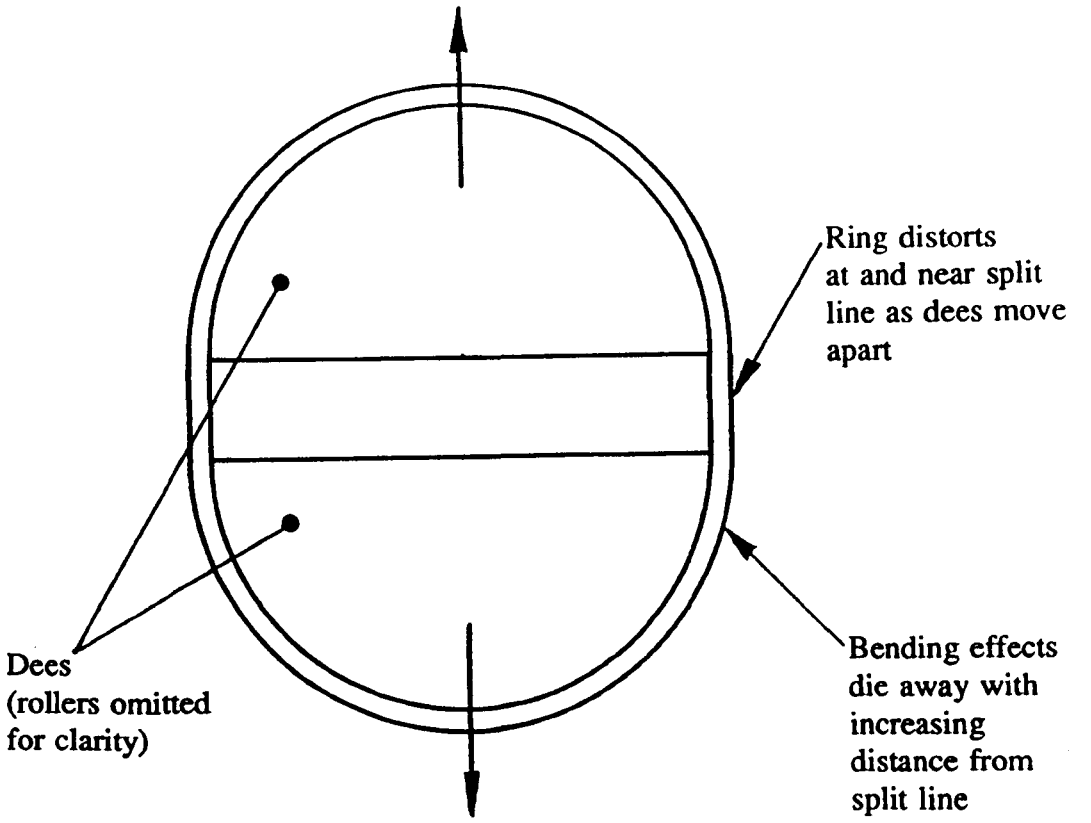

Fig. F.1: Localised distortion of ring on split disc apparatus

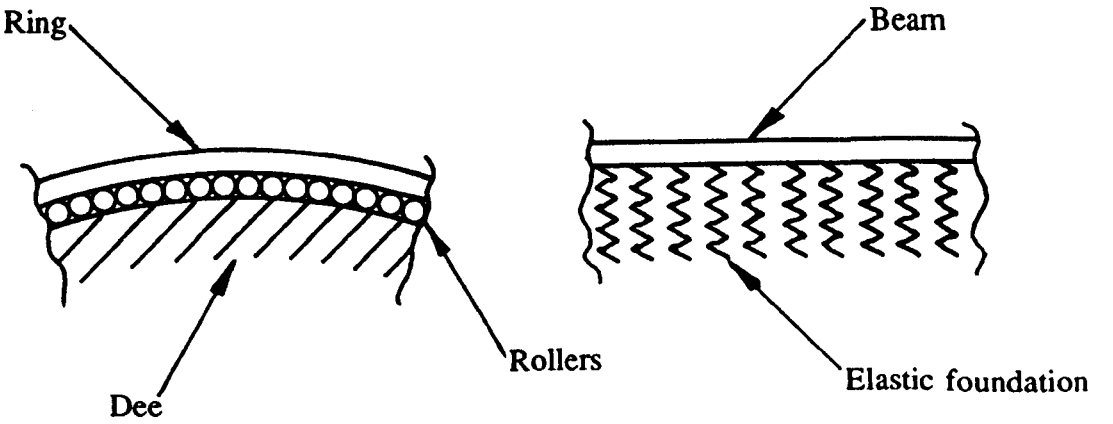

Fig. F.2: Ring supported on closely-spaced rollers is modelled as an elastically-mounted beam; contact mechanics is used to determine foundation modulus

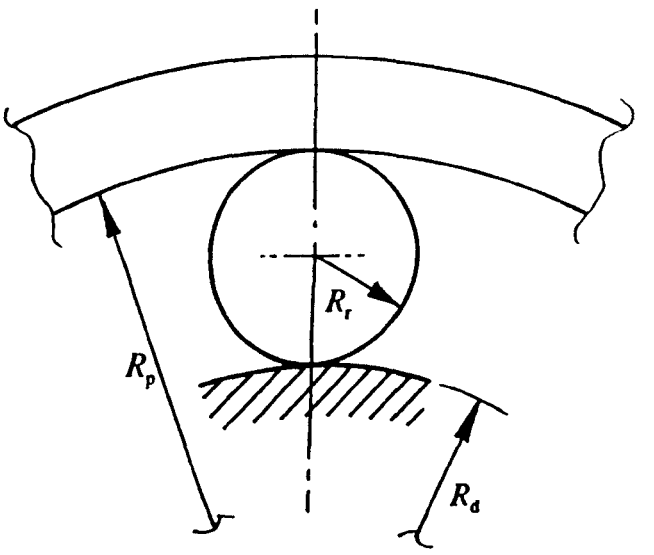

Fig. F.3: Radii of contacting surfaces

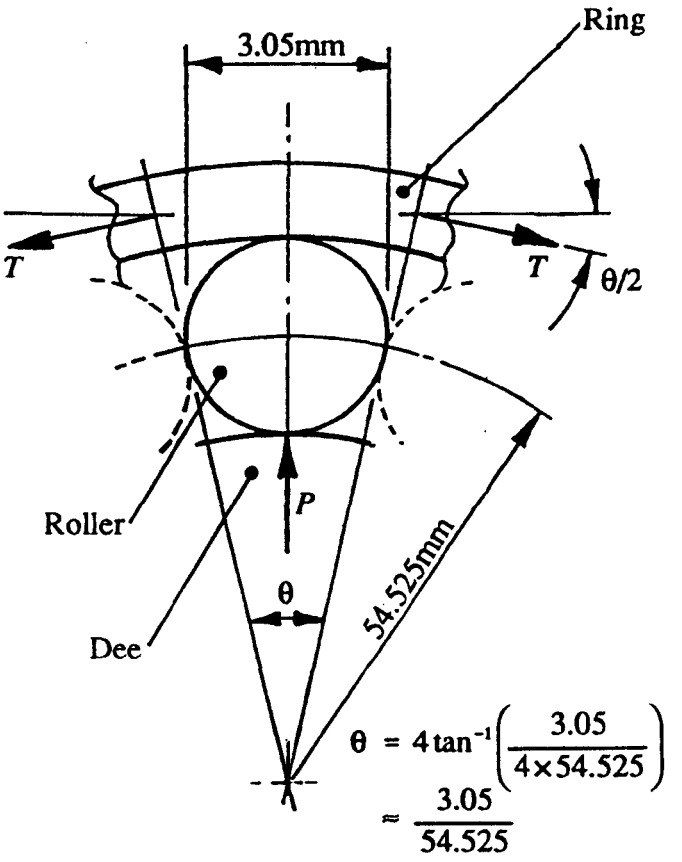

Fig. F.4: Calculation of contact force *P*

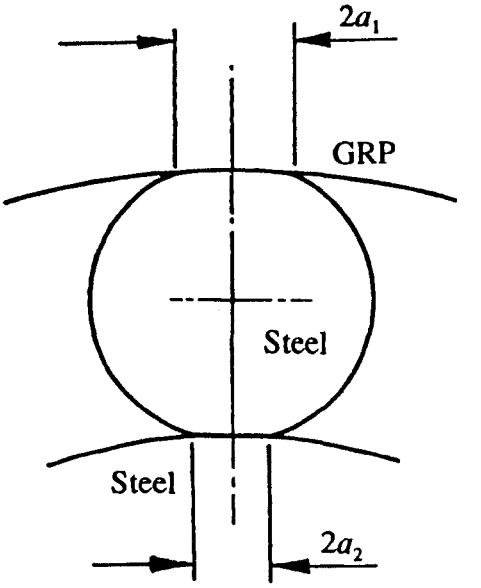

Fig. F.5: Widths of contact regions

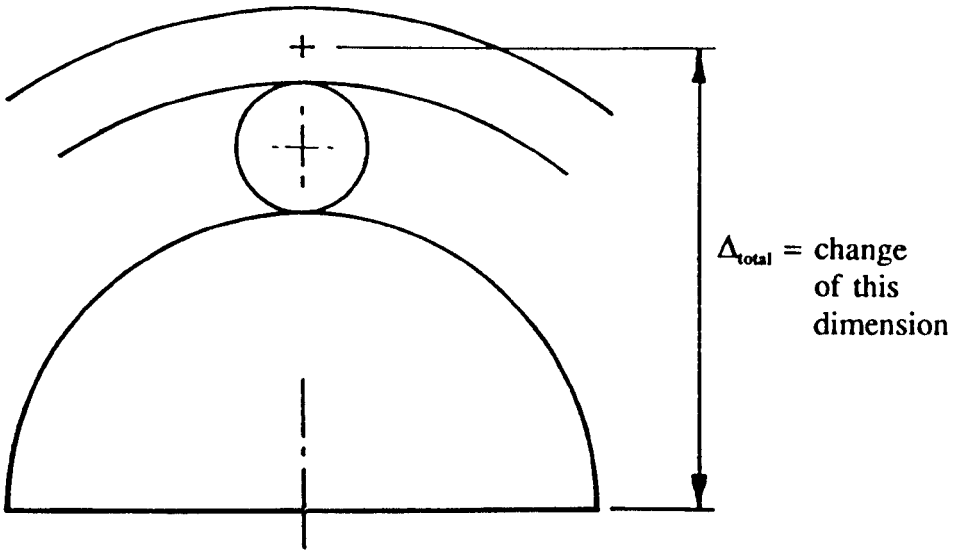

Fig. F.6: Reference distance for total deflection of ring/roller/dee system

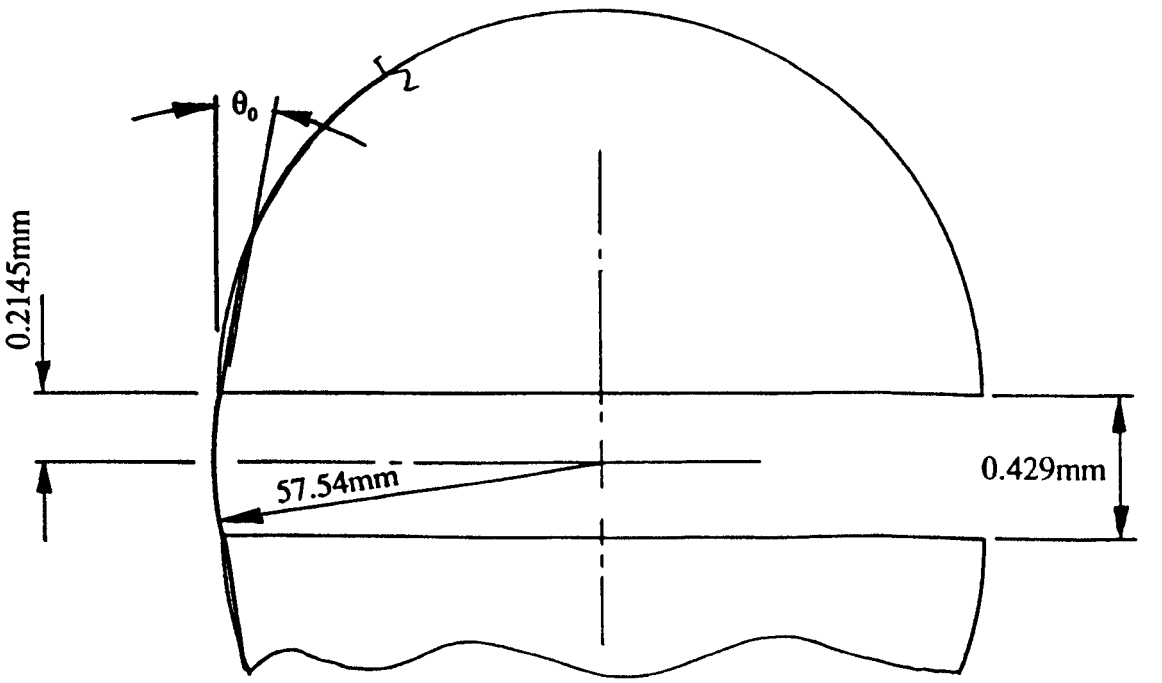

Fig. F.7: End slope θ_0 of ring at split line (separation of dees greatly exaggerated)

APPENDIX G: DATA FILE FOR INPUT TO PROGRAM MESHGEN

*R.ELBOWMESH	*File name for output of mesh*
90.0	*Angle change of elbow*
76.2	*Diameter of duct*
112.5	*Rad of curvature of centreline*
158.15	*Length of first parallel section*
158.15	*Length of second parallel section*
79.099	*Offset of centreline intersection from axis*
16	*Number of elements around duct*
6	*No. of "elements" along 1st parallel section*
6	*No. of "elements" along 2nd parallel section*
8	*No. of "elements" along curve*

Reference may be made to Fig. 8.1 which specifies the elbow dimensions.

APPENDIX H: MESH DEFINITION FILE PRODUCED BY MESHGEN FOR INPUT TO MODELGEN

```
 1312              Number of nodes
   1       -164.438     139.220       0.000       0.707107   0.707107   0.000000
   2       -164.955     138.703       7.433       0.693520   0.693520   0.195090
   3       -166.488     137.169      14.580       0.653281   0.653281   0.382683
   4       -168.978     134.680      21.167       0.587938   0.587938   0.555570
   5       -172.328     131.329      26.941       0.500000   0.500000   0.707107
.................
 Node no.            Co-ordinates                          Normal vectors
.................
1310        168.978     134.680     -21.167      -0.587938   0.587938  -0.555570
1311        166.488     137.169     -14.580      -0.653281   0.653281  -0.382683
1312        164.955     138.703      -7.433      -0.693520   0.693520  -0.195090
   320    Number of elements
         1         8         1     3     67    65     2     35    66    33
         2         8         3     5     69    67     4     37    68    35
         3         8         5     7     71    69     6     39    70    37
         4         8         7     9     73    71     8     41    72    39
.................
Element          No. of                    Element topology
 number          nodes
.................
       316         8     1239   1241   1305   1303   1240   1273   1304   1271
       317         8     1241   1243   1307   1305   1242   1275   1306   1273
       318         8     1243   1245   1309   1307   1244   1277   1308   1275
       319         8     1245   1247   1311   1309   1246   1279   1310   1277
       320         8     1247   1217   1281   1311   1248   1249   1312   1279
 1312    Number of nodes
    1     2        1     16
    2     1        1
    3     2        1      2
    4     1        2
.................
Node    No. of      Element numbers
number  elements
        attached
.................
 1308     1      318
 1309     2      318    319
 1310     1      319
 1311     2      319    320
 1312     1      320
```

APPENDIX I: NEUTRAL FILE CREATED BY MODELGEN FOR USE BY FEDATGEN

```
 1312   Number of nodes
    1      -162.684     140.974       0.000       0.70711    0.70711    0.00000
    2      -163.234     140.424       7.917       0.69352    0.69352    0.19509
    3      -164.805     138.852      15.566       0.65328    0.65328    0.38268
    4      -167.407     136.251      22.651       0.58794    0.58794    0.55557
    5      -170.960     132.697      28.876       0.50000    0.50000    0.70711
..............
Node              Co-ordinates                          Normal vector
number
..............
 1307       180.296     123.362    -37.838      -0.27060    0.27060   -0.92388
 1308       175.310     128.348    -34.009      -0.39285    0.39285   -0.83147
 1309       170.960     132.697    -28.876      -0.50000    0.50000   -0.70711
 1310       167.407     136.251    -22.651      -0.58794    0.58794   -0.55557
 1311       164.805     138.852    -15.566      -0.65328    0.65328   -0.38268
 1312       163.234     140.424     -7.917      -0.69352    0.69352   -0.19509
  320   Number of elements
    1        8        4        8     1    3   67   65    2   35   66   33      0.69352 0.69352   0.19507
    1      0.338745      0.05059    -0.31698     0.94708   1
    2      0.000300     -0.40388     0.15005     0.90242   2
    3      0.341089      0.31694    -0.05054    -0.94710   3
    4      0.083914     -0.18192     0.43058    -0.88403   4
    5      0.115814      0.06910    -0.33355     0.94020   5
    6      0.198653     -0.38935     0.13299     0.91144   6
    7      0.048310      0.37529    -0.11665    -0.91954   7
    8      0.113703     -0.13167     0.38822    -0.91211   8
```

```
    2       6       4       8     3     5    69    67     4   37    68    35      0.58795     0.58795    0.55555
    1      0.318681      -0.19503    -0.56351     0.80276    1
    2      0.348323       0.56326     0.19536    -0.80285    3
    3      0.186368       0.11748     0.61745    -0.77779    4
    4      0.169800      -0.17336    -0.57926     0.79650    5
.........
  Layer     Layer          Direction cosines of fibre  Fibre
  number    thickness                                  family

Element  Number  Times   Number              Topology                                  Element normal vector
number   of      to      of nodes
         layers  repeat
.............
  319       6       4       8  1245 1247 1311 1309 1246 1279 1310 1277     -0.58795     0.58795  -0.55555
    1      0.186368      -0.11748     0.61745     0.77779    1
    2      0.348323      -0.56326     0.19536     0.80285    2
    3      0.318681       0.19503    -0.56351    -0.80276    4
    4      0.039233      -0.10373     0.62633     0.77263    5
    5      0.273326       0.62733    -0.10216    -0.77202    7
    6      0.169800       0.17336    -0.57926    -0.79650    8
  320       8       4       8  1247 1217 1281 1311 1248 1249 1312 1279     -0.69352     0.69352  -0.19507
    1      0.083914       0.18192     0.43058     0.88403    1
    2      0.341089      -0.31694    -0.05054     0.94710    2
    3      0.000300       0.40388     0.15005    -0.90242    3
    4      0.338745      -0.05059    -0.31698    -0.94708    4
    5      0.113703       0.13167     0.38822     0.91211    5
    6      0.048310      -0.37529    -0.11665     0.91954    6
    7      0.198653       0.38935     0.13299    -0.91144    7
    8      0.115814      -0.06910    -0.33355    -0.94020    8
```

APPENDIX J: ANALYTICAL SOLUTION TO PROBLEM OF PINCHED ORTHOTROPIC CYLINDRICAL TUBE

J.1 Introduction to orthotropic solution to the pinched cylinder problem

The theory underlying this solution closely follows Calladine's approach[137] to the traditional problem of the isotropic pinched cylinder. No originality is claimed for the orthotropic extension to this theory; indeed, Calladine mentions the ease with which it is achieved but does not present any results or derivation. However, no evidence has been found that Calladine's solution has been applied to filament-wound cylinders with varying winding angle. The derivation of the isotropic version of the theory is presented by Calladine in a very complete form and duplication of much of the background theory is considered unnecessary in this context.

The basis of the solution is Rayleigh's method. This relies upon the estimation of a suitable deflected shape from which the strain energy and hence the total potential energy are calculated. In this case the expression for potential energy is found to be of identical form to that relating to a beam on an elastic foundation. This analogy is between these situations is exploited so as to apply standard solutions to the problem under consideration.

J.2 Derivation of orthotropic extension to Calladine's solution

A thin cylindrical shell of radius a and wall thickness t is assumed to be made from a specially orthotropic material. Under a general state of membrane stresses, the strain energy per unit area is given by:

$$\begin{aligned} U_{\text{membrane}} &= \frac{1}{2}t\sigma_x\varepsilon_x^0 + \frac{1}{2}t\sigma_\theta\varepsilon_\theta^0 + \frac{1}{2}t\tau_{x\theta}\gamma_{x\theta}^0 \\ &= \frac{1}{2}\frac{E_x t}{1-\nu_{x\theta}\nu_{\theta x}}(\varepsilon_x^0+\nu_{\theta x}\varepsilon_\theta^0)\varepsilon_x^0 + \frac{1}{2}\frac{E_\theta t}{1-\nu_{x\theta}\nu_{\theta x}}(\varepsilon_\theta^0+\nu_{x\theta}\varepsilon_x^0)\varepsilon_\theta^0 + \frac{1}{2}G_{x\theta}t(\gamma_{x\theta}^0)^2 \\ &= \frac{t}{2(1-\nu_{x\theta}\nu_{\theta x})}\left[E_x(\varepsilon_x^0)^2 + E_\theta(\varepsilon_\theta^0)^2 + 2\nu_{\theta x}E_x\varepsilon_x^0\varepsilon_\theta^0\right] + \frac{1}{2}tG_{x\theta}(\gamma_{x\theta}^0)^2 \end{aligned} \qquad \text{(J.1)}$$

where x and θ are defined as the axial and circumferential directions respectively. Similarly, the strain energy per unit area due to bending and twisting is given by:

$$\begin{aligned} U_{\text{bending}} &= \frac{1}{2}M_x\kappa_x + \frac{1}{2}M_\theta\kappa_\theta + \frac{1}{2}M_{x\theta}\kappa_{x\theta} \\ &= \frac{1}{2}\frac{E_x t^3}{12(1-\nu_{x\theta}\nu_{\theta x})}(\kappa_x + \nu_{\theta x}\kappa_\theta)\kappa_x + \frac{1}{2}\frac{E_\theta t^3}{12(1-\nu_{x\theta}\nu_{\theta x})}(\kappa_\theta + \nu_{x\theta}\kappa_x)\kappa_\theta + \frac{1}{2}\frac{G_{x\theta}t^3}{12}\kappa_{x\theta}^2 \\ &= \frac{t^3}{24(1-\nu_{x\theta}\nu_{\theta x})}\left[E_x\kappa_x^2 + E_\theta\kappa_\theta^2 + 2E_x\nu_{\theta x}\kappa_x\kappa_\theta\right] + \frac{G_{x\theta}t^3}{24}\kappa_{x\theta}^2 \end{aligned} \qquad \text{(J.2)}$$

Calladine makes the assumption that only ε_x^0 and κ_θ contribute significantly to the strain energy except in the case of high harmonics of the deformation. He shows that if a trial function for the nth harmonic of radial deformation w is $w_n(x)\cos n\theta$ then the significant components of strain and change of curvature are:

$$\varepsilon_x^0 = \frac{a}{n^2}w_n''(x)\cos n\theta \quad \text{and} \quad \kappa_\theta = \frac{(n^2-1)}{a^2}w_n(x)\cos n\theta \qquad \text{(J.3) (a) and (b)}$$

Inserting these into the equations (J.1) and (J.2) yields an approximate expression for the strain energy per unit area of the shell:

$$\begin{aligned} U_{\text{total}} &\approx \frac{E_x t}{2(1-\nu_{x\theta}\nu_{\theta x})}\frac{a^2}{n^4}\cos^2 n\theta\,(w_n''(x))^2 \\ &\quad + \frac{E_\theta t^3}{24(1-\nu_{x\theta}\nu_{\theta x})}\frac{(n^2-1)^2}{a^4}\cos^2 n\theta(w_n(x))^2 \end{aligned} \qquad \text{(J.4)}$$

Calladine demonstrates for the case of the pinched cylinder that the assumption regarding the significant modes of deformation is valid except for high harmonics of the deformation, and that inaccuracies in equation (J.4) become significant for $n>(a/t)^{1/2}$ as the assumption ceases to be valid.

If a sinusoidally varying load per unit circumference $q_n \cos n\theta$ is applied at $x=0$ to a cylindrical shell with its ends at $x=L_1$ and $x=-L_2$, the potential energy (per unit circumference) due to the load is $-q_n w_n(0)\cos n\theta$ (where $q_n = 2P/\pi a$ for $n = 2, 4...$ for the pinched cylinder problem). The remainder of the potential energy is due to the

strain energy considered in equation (J.4). Integrating over the length and circumference of the cylinder, the total potential energy is:

$$\Pi = \frac{E_x t}{1 - \nu_{x\theta}\nu_{\theta x}} \frac{a^2}{n^4} \frac{\pi a}{2} \int_{-L_1}^{L_1} (w_n''(x)^2)\,dx + \frac{E_\theta t^3}{12(1 - \nu_{x\theta}\nu_{\theta x})} \frac{(n^2-1)^2}{a^4} \frac{\pi a}{2} \int_{-L_1}^{L_1} (w_n(x))^2\,dx - \pi a q_n w_n(0) \tag{J.5}$$

where the function $w_n(x)$ minimises the total potential energy of the system. This expression is analogous to that for a beam of flexural rigidity B on an elastic foundation of modulus k under a point load F at x=0:

$$\Pi = \frac{B}{2} \int_{-L_1}^{L_1} (w''(x))^2\,dx + \frac{k}{2} \int_{-L_1}^{L_1} (w(x))^2\,dx - Fw(0) \tag{J.6}$$

It is therefore possible to use existing results for beams on elastic foundations[52] to find the function $w_n(x)$ by making use of the following substitutions:

Quantity (referred to beam on elastic foundation problem)	Symbol		Equivalent quantity for pinched orthotropic cylinder problem
	Used in this appendix	Used by Hetenyi[52]	
Deflection	w	y	$w_n \cos n\theta$
Beam flexural rigidity	B	EI	$B_n = \dfrac{\pi E_x t a^3}{(1 - \nu_{x\theta}\nu_{\theta x}) n^4}$
Foundation modulus (force per unit length per unit deflection)	k	k	$k_n = \dfrac{\pi E_\theta t^3 (n^2-1)^2}{12(1 - \nu_{x\theta}\nu_{\theta x}) a^3}$
Concentrated load on beam	F	P	$F_n \cos n\theta = 2P \cos n\theta$ for even $n \geq 2$
Decay parameter (derived from k and B)	λ	λ	$\lambda_n = \sqrt[4]{\dfrac{k_n}{4B_n}} = \sqrt[4]{\dfrac{E_\theta t^2 n^4 (n^2-1)^2}{48 E_x a^6}}$

The general form of the solution to problems of this type is:

$$w_n(x) = A_n e^{\lambda_n x}\cos\lambda_n x + B_n e^{\lambda_n x}\sin\lambda_n x + C_n e^{-\lambda_n x}\cos\lambda_n x + D_n e^{-\lambda_n x}\sin\lambda_n x \quad (J.7)$$

where A_n ... D_n are found using boundary conditions. For instance, at the free ends of a cylinder $w_n''(x) = w_n'''(x) = 0$. The solution to the pinched cylinder problem is obtained by summing the Fourier series of deflection components and may be expressed in the form:

$$w(x,\theta) = \sum_{n=2,4...} w_n(x)\cos n\theta \quad (J.8)$$

J.3 Solution for pinched filament-wound cylinder with varying winding angle

This problem differs from the simple case of a pinched orthotropic cylinder with uniform properties. The main differences are as follows:

(a) The cylinder walls take the form of an antisymmetric laminate rather than a homogeneous orthotropic material. This is difficult to solve rigorously but can be simplified by assuming the laminate to have many layers (thus eliminating coupling effects between tension and twisting etc.). An approximate or intuitive approach to the problem of a laminated cylinder with few layers is suggested in Section J.4.

(b) Assuming the laminate to be many-layered, its axial and circumferential Young's moduli will change with axial position if the winding angle varies.

(c) The wall thickness, and hence the mid-surface radius of the cylinder, will vary with axial position if the winding angle varies.

The approach to this problem was outlined in Chapter 7, and consists of discretising the cylinder into a series of shorter cylindrical elements (Fig. 7.4(a) and (b)), each with different values of orthotropic material properties, radius and thickness. It is then a simple matter to treat each of these as a short elastically-mounted beam using

Calladine's analogy. These are considered to be rigidly fastened end-to-end ensuring continuity of deflection and slope (Fig. 7.4(c)) in the manner suggested by Hetenyi[138] for problems of this type. Working within the notation of the beam analogy, a flexibility matrix $[C]_e$ may be defined for each element. This relates the vector of end deflections and slopes $\{w\}_e$ to the vector of end forces and moments $\{F\}_e$, using conventions shown in Fig. J.1:

$$\begin{bmatrix} C_{11} & C_{12} & C_{13} & C_{14} \\ C_{21} & C_{22} & C_{23} & C_{24} \\ C_{31} & C_{32} & C_{33} & C_{34} \\ C_{41} & C_{42} & C_{43} & C_{44} \end{bmatrix}_e \begin{Bmatrix} F_1 \\ M_1 \\ F_2 \\ M_2 \end{Bmatrix}_e = \begin{Bmatrix} w_1 \\ \theta_1 \\ w_2 \\ \theta_2 \end{Bmatrix}_e \quad \text{or:} \quad [C]_e = \{F\}_e \{w\}_e \tag{J.9}$$

The components of $[C]_e$ are as follows[148]:

$$\begin{aligned}
C_{11} = C_{33} &= \frac{2\lambda}{k} \frac{\sinh\lambda l \cosh\lambda l - \sin\lambda l \cos\lambda l}{\sinh^2\lambda l - \sin^2\lambda l} \\
C_{34} = C_{43} = -C_{12} = -C_{21} &= \frac{2\lambda^2}{k} \frac{\sinh^2\lambda l + \sin^2\lambda l}{\sinh^2\lambda l - \sin^2\lambda l} \\
C_{22} = C_{44} &= \frac{4\lambda^3}{k} \frac{\sinh\lambda l \cosh\lambda l + \sin\lambda l \cos\lambda l}{\sinh^2\lambda l - \sin^2\lambda l} \\
C_{13} = C_{31} &= \frac{2\lambda}{k} \frac{\sinh\lambda l \cos\lambda l - \sin\lambda l \cosh\lambda l}{\sinh^2\lambda l - \sin^2\lambda l} \\
C_{24} = C_{42} &= \frac{4\lambda^3}{k} \frac{\sinh\lambda l \cos\lambda l + \sin\lambda l \cosh\lambda l}{\sinh^2\lambda l - \sin^2\lambda l} \\
C_{23} = C_{32} = -C_{14} = -C_{41} &= \frac{4\lambda^2}{k} \frac{\sinh\lambda l \sin\lambda l}{\sinh^2\lambda l - \sin^2\lambda l}
\end{aligned} \tag{J.10}$$

The flexibility matrix $[C]_e$ may be inverted to give the element stiffness matrix $[K]_e$:

$$[K]_e \{w\}_e = \{F\}_e \quad \text{where} \quad [K]_e = [C]_e^{-1} \tag{J.11}$$

The stiffness matrix for the whole system may now be assembled from the element stiffness matrices. This assembly process links the elemental beams so that continuity of deflection and slope exists at each junction or node, and enables the net force on each junction to be calculated for a given set of deflections and slopes. As an example (Fig. J.2) two elements may be assembled into a system represented by the following equation:

$$\begin{bmatrix} (K_{11})_1 & (K_{12})_1 & (K_{13})_1 & (K_{14})_1 & 0 & 0 \\ (K_{21})_1 & (K_{22})_1 & (K_{23})_1 & (K_{24})_1 & 0 & 0 \\ (K_{31})_1 & (K_{32})_1 & (K_{33})_1+(K_{11})_2 & (K_{34})_1+(K_{12})_2 & (K_{13})_2 & (K_{14})_2 \\ (K_{41})_1 & (K_{42})_1 & (K_{43})_1+(K_{21})_2 & (K_{44})_1+(K_{22})_2 & (K_{13})_2 & (K_{14})_2 \\ 0 & 0 & (K_{31})_2 & (K_{32})_2 & (K_{33})_2 & (K_{34})_2 \\ 0 & 0 & (K_{41})_2 & (K_{42})_2 & (K_{43})_2 & (K_{44})_2 \end{bmatrix} \begin{Bmatrix} w_1 \\ \theta_1 \\ w_2 \\ \theta_2 \\ w_3 \\ \theta_3 \end{Bmatrix} = \begin{Bmatrix} F_1 \\ M_1 \\ F_2 \\ M_2 \\ F_3 \\ M_3 \end{Bmatrix}$$

$$\text{or:} \quad [K]\{w\} = \{F\} \tag{J.12}$$

where $(K_{jk})_i$ $(j,k=1...4)$ represent the components of the stiffness matrix $[K]$ for the ith element. $(K_{jk})_i = (K_{kj})_i$, i.e. $[K]$ is symmetric, since $[C]_e$ and hence also $[K]_e$ are symmetric.

In practice, it is the force matrix which is known and the deflections and slopes which are required; equation (J.12) must therefore be solved using matrix inversion or otherwise:

$$\{w\} = [K]^{-1}\{F\} \tag{J.13}$$

Having solved the problem for the beam-on-elastic-foundation, the solution to the cylinder problem is solved by analogy for each of the Fourier components of the load. The deflections for each Fourier component are then summed to give the deflections when subjected to a pinching load.

J.4 Extensions to Calladine's solution

In the original solution to the problem of a pinched isotropic cylinder, the value of B_n is given as $\pi Et a^3/[(1-\nu^2)n^4]$. Calladine states, without presenting a detailed justification, that the solution can be improved by omission of the term $(1-\nu^2)$. This corresponds to a relaxation of the assumption that ε_θ is constrained to be zero. The author has noted that this modified result is equivalent to the solution due to Ting and Yuan[135]. Further work would be required to investigate whether a similar extension can be made to cover the case of the orthotropic cylinder.

Calladine's expressions for B_n and k_n for the isotropic problem include the terms $Et/(1-\nu^2)$ and $Et^3/[12(1-\nu^2)]$ respectively. These may be recognised as the section moduli of a plate or shell under tension (with a restraint against transverse strain) and under bending. Intuition suggests that is possible to substitute equivalent expressions for the behaviour of a laminated plate or shell if suitable assumptions are made regarding the freedom of the laminate to distort due to the effect of coupling. For example, it is necessary in calculating B_n to calculate the tensile stiffness of the laminate in the axial (x) direction and one possible assumption is that the structure of the cylinder restrains the laminate against twisting. In addition, Calladine assumes that transverse (circumferential) membrane strain is constrained to be zero. Defining the laminate behaviour in terms of equation (5.13), the term $Et/(1-\nu^2)$ may be replaced with A_{11}. A similar process may be applied to the calculation of k_n, when it is necessary to calculate the flexural rigidity of the laminated shell in the circumferential direction. Assuming that the shell experiences restraint against anticlastic curvature but is free to distort in shear, $Et^3/[12(1-\nu^2)]$ may be replaced with $\delta_{11}/(\delta_{11}\delta_{22}-\delta_{12}^2)$. These suggested substitutions are to be regarded as rules-of-thumb rather than as accurate theory, and it is likely that in reality no degree of freedom will be either fully restrained or completely free. Typical results from the homogeneous orthotropic and laminated orthotropic extensions to Calladine's theory will be presented in section J.7 and compared with relevant finite element solutions.

J.5 Implementation of solution using a FORTRAN program

Practical implementation of this solution requires the use of a computer to handle the matrix algebra, and a FORTRAN program has been written to achieve this. A flowchart of the program is shown in Fig. J.3. Two methods are used for calculating the deflected shape of the cylinder, namely the homogeneous orthotropic extension to Calladine's solution (derived in Sections J.2 and J.3), and the modifications to this methods based upon classical lamination theory (suggested in Section J.4). In both cases the Fourier series of deflections was summed to 10 terms (n=2...20). Although the terms of order 6 and above are inaccurate the effects of these terms (and hence any errors due to them) are confined to a region approximately 30 millimetres either

side of the point of loading. Omission of these higher-order terms leads to a spurious localised bulge or notch in the transverse (horizontal) diameter as well as a blunted pinching effect on the vertical diameter.

The linear algebra is implemented using the appropriate subroutines from the NAG library. Advantage is taken of the fact that all the matrices are symmetrical, and subroutine F01ACF is used to obtain the inverse of the laminate stiffness matrix and the element flexibility matrix as accurately as the machine precision will allow. Advantage is also taken of the banded nature of the system stiffness matrix, enabling subroutine F04ACF to be used for solving equation (J.12).

J.6 Comparison of approach with finite element method

This piecewise implementation of Calladine's solution has clear similarities with the finite element method, especially with regard to the assembly of element stiffness matrix components into a global stiffness matrix. It is an application of matrix displacement method[139] which is one of the techniques from which finite element analysis evolved. However, there are some important differences between this solution and the operation of typical finite element systems.

(a) The element formulation used in this solution inherently includes restraints in the form of the elastic foundation, in contrast with many types of finite element which require appropriate restraints to be applied to the system. For the problem under consideration, the boundary conditions are that both ends of the cylinder are free and hence no additional restraints need to be applied to the system.

(b) Most finite element formulations are approximate, being based upon linear or polynomial interpolation of displacements etc. within the element. However, Hetenyi's solutions to the beam-on-elastic-foundation problem may be assumed to be exact, and hence the formulation of each beam-on-elastic-foundation element is also exact. The accuracy of the solution to the problem of the contiguous elastically-mounted beam is therefore limited only by the numerical

accuracy of the computer and the equation-solving algorithms. However, the solution to the pinched cylinder problem as presented here is not exact; this is because Calladine's analogy is only approximate, and because discretisation of the continuously varying properties of the cylinder inevitably introduces errors. In principle it would be possible to re-formulate the elemental beams to consider continuously varying beam stiffness and foundation modulus[138]. However, problems of this kind are mathematically complex, and such work was not considered to be justified in this context.

J.7 Comparison of results with relevant FE results

Fig. J.4 shows comparison of the results from the computer program with the results of comparable finite element solutions. The FE solution chosen for comparison with the homogeneous orthotropic Calladine solution is the PAFEC model using axisymmetric Fourier elements, since both these solutions assume the laminate structure to have many layers and hence ignore the coupling effects. The FE solution chosen for comparison with the classical lamination theory extension to Calladine's solution is from the ABAQUS model with uniform lamination sequence. In all cases the unidirectional material properties assumed are those fitted to the flexural data; these are presented in Table 7.5. It is observed that the homogeneous orthotropic solution is in close agreement (typically within 2%) with the results from the axisymmetric PAFEC model. The results from the laminated extension to Calladine's theory yields results similarly close to those from the ABAQUS thin shell model.

J.8 Conclusions

The work presented in this appendix provides a useful comparison with the finite element solutions obtained via the FILFEM I automatic model-generation system, and close agreement has been obtained between the results of these two approaches. However, Calladine's solution (and solutions based upon it) relate primarily to a simple specimen and a loading situation which is of academic interest rather than common practical application. By contrast, FILFEM I can generate models for

complex axisymmetric structures, and capabilities of the available FE codes provide the main limitation upon the kinds of problems that can be solved for a given structure. Additional work is required to consider further extensions to Calladine's solution if more realistic assumptions are to be made in the derivation of analytical solutions to the pinched orthotropic cylinder and laminated cylinder problems. Should other test problems be tackled with FILFEM-generated models, it may be possible to follow a similar approach in deriving analytical solutions to provide comparison with the FE results obtained.

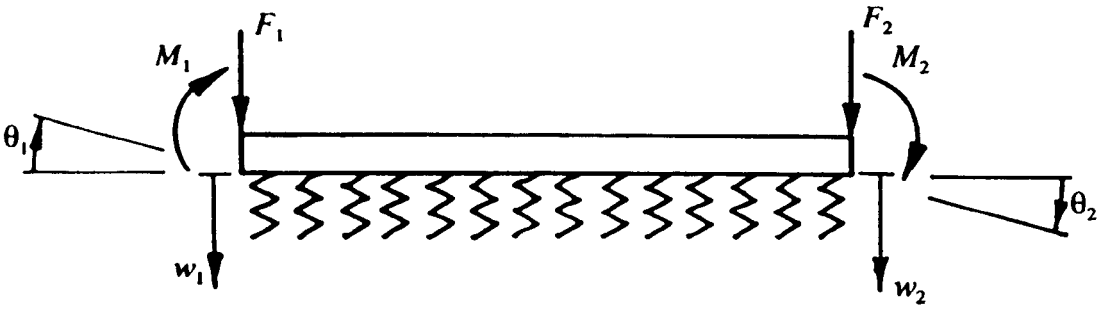

Fig. J.1: Sign convention used in definition of beam-on-elastic-foundation flexibility matrix

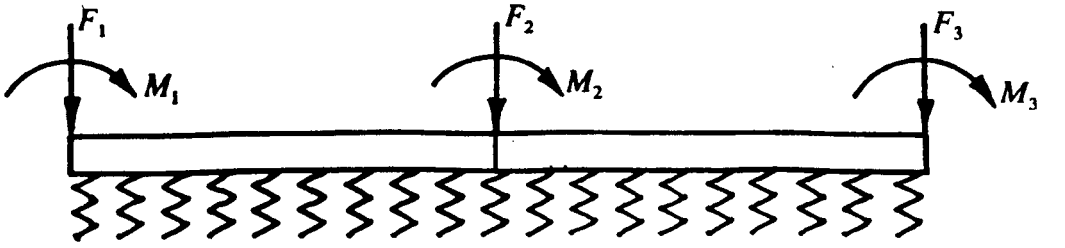

Fig. J.2: System of two beams on elastic foundations rigidly joined end-to-end, showing loads applied to system

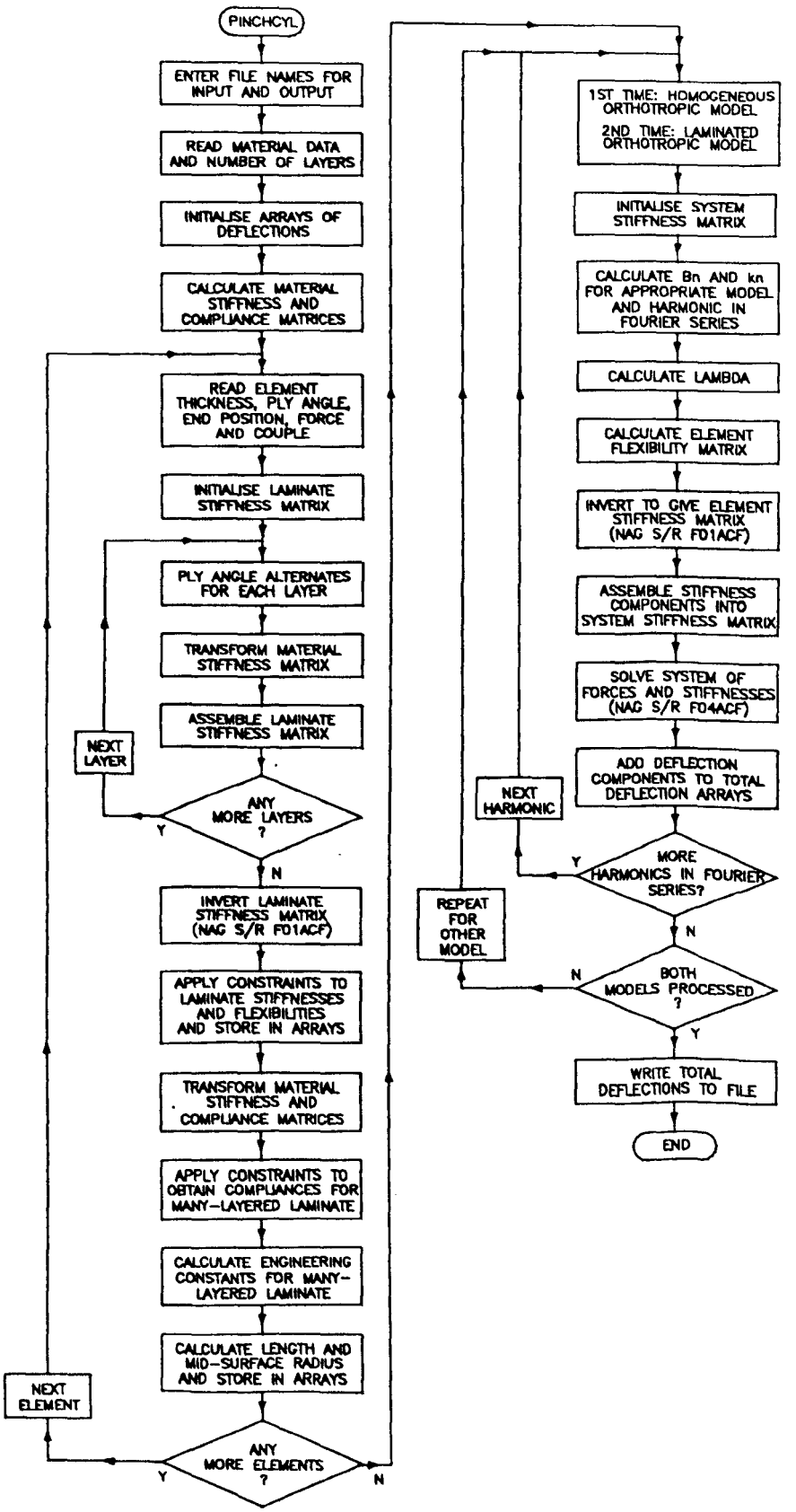

Fig. J.3: Flow chart showing operation of PINCYL program

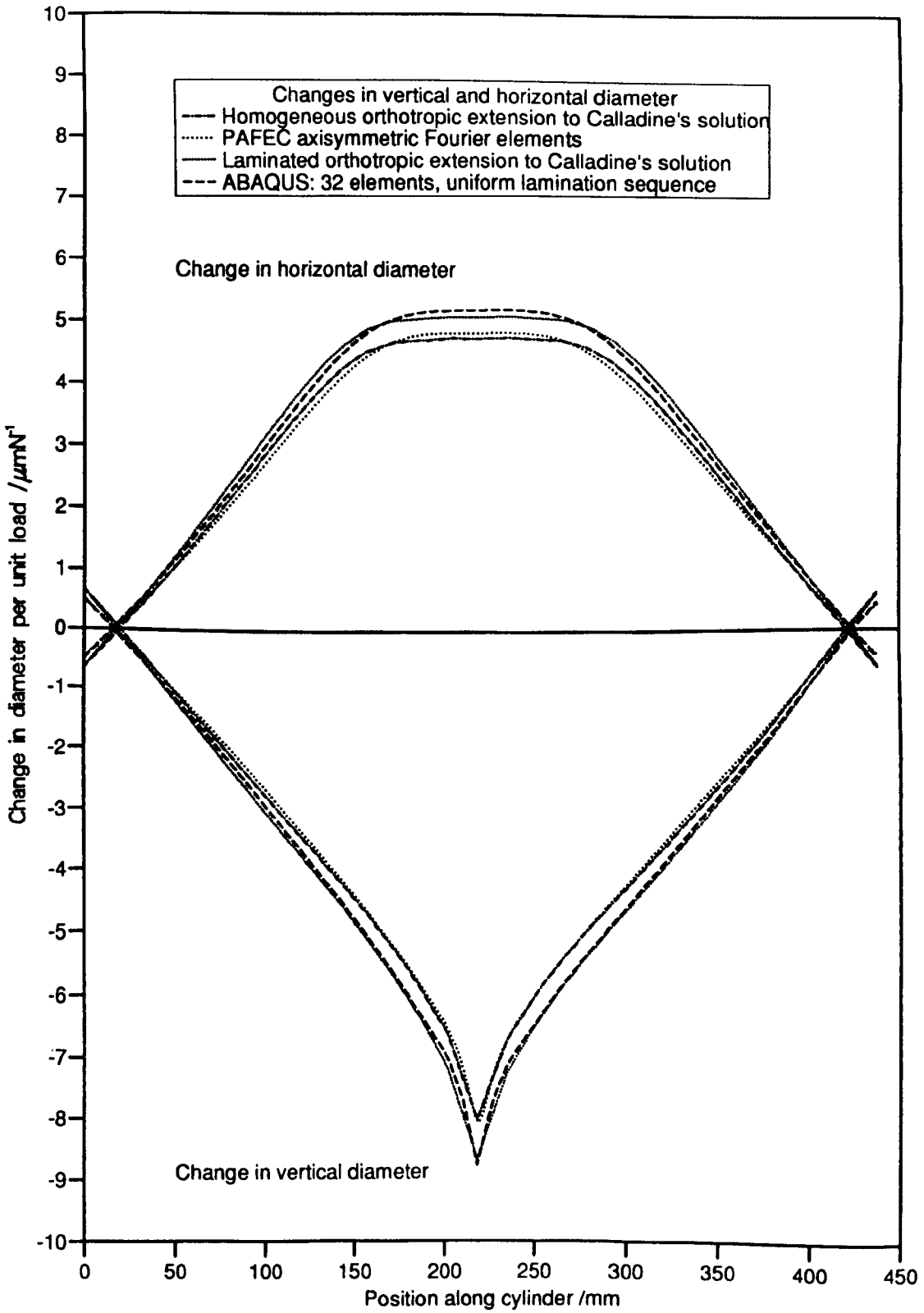

Fig. J.4: Comparison of results from PINCYL program compared with relevant finite element results